SEMICONDUCTOR ASSISTED PHOTODEGRADATION OF HUMIC ACID USING Fe DOPED TiO_2

by

HÜLYA AYKAÇ

B.S. in Environmental Engineering, Ondokuz Mayıs University, 2007

Submitted to the Institute of Environmental Sciences in partial fulfillment of the requirements for the degree of

Master of Science

in

Environmental Technology

Boğaziçi University

2011

SEMICONDUCTOR ASSISTED PHOTODEGRADATION OF HUMIC ACID USING Fe DOPED TiO_2

APPROVED BY:

Prof. Dr. Miray Bekbölet (Thesis Supervisor)	. . . . .
Prof. Dr. Zekiye Çınar	. . . . .
Prof. Dr. Ayşen Erdinçler	. . . . .

DATE OF APPROVAL (20/04/2011)

Dedicated to my family…

ACKNOWLEDGEMENT

I wish to express my sincere gratitude to my thesis supervisor. Prof. Dr. Miray Bekbölet for her scientific guidance, tremendous encouragement and valuable contribution throughout this study. Her wide knowledge and logical way of thinking have been of great value for me. Her understanding and personal guidance as well as her interest and support have provided a good basis for this thesis.

I am also highly thankful to Prof. Dr. Ayşen Erdinçler and Prof. Dr. Zekiye Çınar for their participation in my thesis jury, best reviews, invaluable comments and constructive critism.

I would also like to appreciate Assoc. Prof. Dr. Emre Burcu Güngör from Ondokuz Mayıs University, who encouraged me with her strong personality. She is a very important person that I will never forget throughout my life.

In addition, I would like to thank Dr. Ceyda Uyguner Demirel, research assistant Sibel Şen Kavurmacı and Esra İlhan Değirmenci share their best knowledge in order to complete this study.

I would express my special thanks to Ayşe Akyapı, Özlem Karataş, Sezin Sönmez, Nazlı Hande Güremek, Emel Akay and Hasan Ayaz for their never-ending support and friendship.

Last but not least, I am grateful to my family who believed in me and was always by my side with their patience, tremendous support, and constant encouragement during my educational life.

SEMICONDUCTOR ASSISTED PHOTODEGRADATION OF HUMIC ACID USING Fe DOPED TiO_2

The main objective of this research is to investigate the effect of Fe doping on TiO_2 on the photocatalytic degradation of humic acid and its molecular size fractions in aqueous medium in comparison to the use of bare TiO_2. The photocatalytic oxidation of humic acid was carried out using bare TiO_2 and Fe doped TiO_2 as the photocatalyst. The degradation kinetics was assessed based on pseudo first order. Adsorption experiments were conducted to elucidate the surface interactions of the molecular size fractions of humic acid solutions onto oxide surfaces. Bare TiO_2 and Fe doped TiO_2 in the range of 0.1-1.0 mg mL^{-1} were used as adsorbents. The adsorption experiments were also evaluated by using appropriate adsorption isotherms. The photocatalytic and adsorption experiments were carried out using various molecular size fractions, namely raw, 0.45 μm filtered fraction, 100 kDa fraction, and 30 kDa fraction of humic acid solution in the presence of bare TiO_2 and Fe doped TiO_2. The results of adsorption experiments were evaluated using appropriate adsorption isotherms. The spectroscopic properties of each size fraction were characterized and compared by UV-vis spectroscopy and fluorescence spectroscopy in emission and synchronous scan modes.

UV-vis spectra recorded for all of the samples displayed a consistent basic declining pattern irrespective of the irradiation period and photocatalyst type. On the other hand, fluorescence spectral profiles exhibited different patterns with respect to both irradiation time and photocatalyst type. Therefore, UV-vis parameters could be used for kinetic evaluation of the photocatalytic degradation of the humic acid and its molecular size fractions whereas fluorescence spectra could only bring a qualitative basis for comparison.

HÜMİK ASİDİN Fe BAĞLI TiO_2 KULLANILARAK YARIİLETKENLE DESTEKLENMİŞ FOTOBOZUNMASI

Bu araştırmanın temel amacı, sulu ortamda, hümik asit ve hümik asidin moleküler boyut fraksiyonlarının fotokatalitik bozunma üzerinde TiO_2 ye bağlı demirin etkisini, yalın TiO_2'nin kullanımına kıyasla incelemektir. Hümik asidin fotokatalitik oksidasyonu, fotokatalist olarak yalın TiO_2 ve Fe bağlı TiO_2 kullanılarak gerçekleştirilmiştir. Bozunma kinetiği birinci dereceden reaksiyon kinetik modelleri üzerinden değerlendirilmiştir. Adsorpsiyon deneyleri, humik asit çözeltilerin oksit yüzeylerde moleküler boyut fraksiyonlarının yüzeysel etkileşimini açığa çıkarmak için yürütülmüştür. Adsorbent olarak, 0.1-1.0 mg mL^{-1} aralığında yalın TiO_2 ve Fe bağlı TiO_2 kullanılmıştır. Adsorpsiyon deneylerinin sonuçları uygun adsorpsiyon izotermleri kullanarak değerlendirilmiştir. Fotokatalitik ve adsorpsiyon deneyleri yalın TiO_2 ve Fe bağlı TiO_2 varlığında, hümik asit çözeltisinin ham, 0.45 μm filtre edilmiş fraksiyonu, 100 kDa ve 30 kDa fraksiyonu gibi farklı moleküler boyut fraksiyonları ile yapılmıştır. Her fraksiyonun spektroskopik özellikleri, UV-vis spektroskopisiyle ve emisyon ve eş zamanlı tarama modları içeren floresans spektroskopisiyle nitelendirilmiş ve kıyaslanmıştır.

Tüm örnekler için kaydedilen UV-vis spektra, fotokatalist tipine ve ışınlama süresine bakılmaksızın tutarlı bir temel azalan model sergilemiştir. Diğer bir taraftan, floresans spektral profiller fotokatalist tipi ve ışınlama süresi bakımından farklı modeller göstermiştir. Bu yüzden, karşılaştırma için floresans spektra sadece niteliksel bir temel getirirken, UV-vis parametreleri hümik asit ve onun moleküler boyut fraksiyonlarının fotokatalitik bozunmasının kinetik değerlendirmesi için kullanılabilir.

TABLE OF CONTENTS

LIST OF FIGURES

LIST OF TABLES

LIST OF SYMBOLS/ABBREVIATIONS

Symbol	Explanation	Units Used
A	Related UV-vis parameter or	m^{-1} (UV-vis)
	NPOC content of HA	mg L^{-1} (NPOC)
AHA	Aldrich humic acid	
AOPs	Advanced oxidation processes	
BLF	Black Light Fluorescent Lamp	
C	Concentration	mg L^{-1}
C_e	Equilibrium concentration of adsorbate	mg L^{-1} (NPOC)
		m^{-1} (UV-vis)
C_i	Initial concentration of adsorbate	mg L^{-1} (NPOC)
		m^{-1} (UV-vis)
C_s	Amount of adsorbate adsorbed on adsorbent	mg L^{-1} (NPOC)
		m^{-1} (UV-vis)
$Color_{436}$	Absorbance at 436 nm	cm^{-1} or m^{-1}
Da	Dalton	
DBPs	Disinfection By-products	
DOC	Dissolved organic carbon	
DOM	Dissolved organic matter	
FI	Fluorescence intensity	
FI_{emiss}	Emission fluorescence intensity	
FI_{syn}	Synchronous fluorescence intensity	
FA	Fulvic acid	
HA	Humic acid	
HS	Humic substances	
K	Langmuir adsorption constant	m^{-1} (UV-vis)
NOM	Natural organic matter	

1. INTRODUCTION

Natural organic matter (NOM) is a complex mixture of organic compounds, which interact with many inorganic and organic pollutants and may decrease toxicities of these pollutants in water chemistry (Cabaniss and Shuman, 1988; Ma et al., 1999). NOM is present in all water sources and the majority of the water soluble NOM exists as aquatic humic substances (HSs). Humic substances are a ubiquitous constituent of the natural organic matter (NOM) found in the environment (Aiken et al., 1985). The general term ‘‘humic substances’’ encompasses a variety of fractions identified on the basis of their solubility in alkali and acid. Humic acids are soluble in dilute alkaline solution but precipitate from an acidified solution (pH < 2). Fulvic acids are the portion that remains in the aqueous acidified solution (soluble in both acid and base). The remainder is humin, which cannot be extracted by dilute base and acid (Choudhry, 1981).

Humic acids (HAs) are macromolecular yellow-to-black colored natural organic matter derived from the degradation of plant, algal, and microbial material (Thurman et al., 1982). Although their formation mechanism and chemical structures are not well understood, they are known to be high in carbon content (50–60%) of both aliphatic and aromatic character and rich in oxygen-containing functionalities such as carboxyl, phenolic, alcoholic, and quinoid groups. Humic materials may be specifically targeted for removal from potable water supplies because they can adversely affect appearance and taste, and they can react with chlorine to form potentially carcinogenic chlorinated organic compounds. Further, the presence of macromolecular dissolved organic matter may reduce the effectiveness of water treatment processes that employ membranes or microporous adsorbents. The removal of (or the reduction in concentration of) such organic matter is therefore an important factor in water treatment.

Molecular weight and molecular size distributions are important properties for an understanding of the physical and chemical characteristics of humic substances. Also, UV-visible spectroscopy has its own very essential function in the study of humic acid. Determination of molecular weights for aquatic humic substances is not a simple task, since humic substances are a very complex mixture of organic heterogeneous structures

with a wide range of molecular sizes. Methods often used for determining molecular weights and sizes of humic substances include ultracentrifugation, viscosimetry, small-angle X-ray scattering, size exclusion chromatography (SEC), ultrafiltration (UF), and colligative property measurements, such as vapour-pressure osmometry (VPO) and freezing-point depression.

Photocatalytic oxidation is a potential method for the treatment of organic contaminants and has received significant interest and research. The heterogeneous photocatalysis can be an effective alternative solution for the elimination of the HA from aqueous solution. With this process it is possible to degrade the majority of the organic molecules, without adding of additional chemicals except the photocatalyst (e.g. titanium dioxide). Titania (TiO_2) as a photocatalyst is widely used for decomposition of toxic organic compounds both in the aqueous and in the gas phase. Titania is efficient for these purification purposes, photostable, environmentally friendly and inexpensive. Although, heterogeneous photocatalysis using TiO_2 has been considered as an effective technology for treating refractory organic compound in water, the efficiency of the photocatalytic degradation reaction is limited by the high recombination rate of photoinduced electrons and holes. Much effort has been contributed to improve the photocatalytic efficiency of TiO_2 by doping with transition metal ions. Among various metal ions, Fe^{3+} is considered an interesting dopant due to its half-filed electronic configuration.

The main objective of this research is to investigate the effect of Fe doping on TiO_2 on the photocatalytic degradation of humic acid and its molecular fractions in aqueous medium in comparison to the use of bare TiO_2. The adsorption experiments were conducted to determine the effects of molecular size dependent fractions of humic acid solution on TiO_2 surface. The results of batch adsorption experiments were evaluated using appropriate adsorption isotherms. The spectroscopic properties of each size fraction were characterized and compared by UV-vis spectroscopy and fluorescence spectroscopy in emission and synchronous scan modes. UV–vis parameters were described in terms of the absorbance values measured at the selected wavelengths as follows: absorbance values at 436 nm as $Color_{436}$, 365 nm as UV_{365}, 280 nm as UV_{280} and 254 nm as UV_{254} and the emission scan fluorescence spectra was scanned in the range of 360-600 nm and 380-600 nm at excitation wavelength of 350 and 370 nm, respectively.

2. THEORETICAL BACKGROUND

2.1. Natural Organic Matter and Humic Substances

Natural organic matter is widely distributed in soil, natural water, and sediments and consists of a mixture of the decomposition products of plant and animal residues and of substances synthesized biologically and/or chemically from decomposed products or intermediate products (Aiken et al., 1985; Suffet and MacCarthy, 1989). The size, chemical composition, structure, and functional groups, and polyelectrolytic characteristics of NOM may vary greatly, depending on the origin and age of the material (Aiken et al., 1985; Chin et al., 1994; Gu et al., 1995; Chin et al., 1998). NOM is known to play important roles in the fate and transport of many toxic organic or inorganic chemicals and in nutrient cycling throughout the environment. NOM acts as important precursor of disinfection by-products (DBPs) and enables the microorganisms to grow in the treatment unit or distribution system (Khan et al., 1998; Siddiqui et al., 1997). It is generally known that formation of DBPs highly depends on the concentration of NOM as a main contributor, but there are many other factors such as NOM composition and water treatment methods (Kim and Yu, 2005).

Various methods have been used to isolate NOM from natural water. XAD resin method has been reported in many applications for fractionation of NOM. After fractionation of NOM by resin adsorption, characterization of NOM is carried out to gather the information on chemical composition by various spectroscopic techniques and on molecular size by high performance size exclusion chromatography (HP-SEC). In use of HPSEC, however, it is not effective for the analyses of small molecular weight compounds including organic carboxylic acids. Spectroscopic techniques such as ultraviolet- visible (UV/Vis), Fourier-transform infrared (FTIR), nuclear magnetic resonance (NMR), and fluorescence have been previously applied for both quantitative and qualitative characterization of NOM (Hautala et al., 2000; Davis et al., 1999; Thomsen et al., 2002; Peuravuori et al., 2002). The method measuring the spectrum of NOM using FT-IR and NMR analyzers has been accepted as an adequate way to estimate the NOM characterization (Maurice et al., 2002; Ma et al., 2001).

Natural organic matter in the environment can be divided into two classes of compounds that are Humic Substances (HSs) (mainly humic and fulvic acids) and Non-Humic Substances including hydrocarbons, carbonhydrates, aminoacid etc. Humic substances, described to be composed of chemically complex, non-biochemical organic components, which are largely hydrophilic, amorphous, dark colored and resistant to chemical and biological degradation are among the most widely distributed organic materials on the planet (Stevenson, 1982).

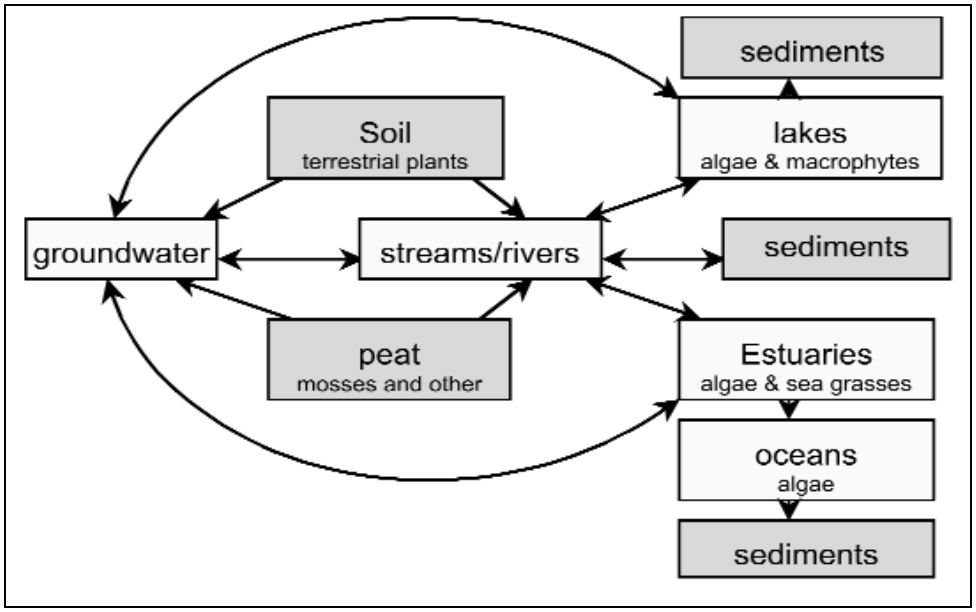

Figure 2.1. Diagram of the occurrence and possible environmental flow paths of humic substances (Kopal et al., 2001).

Humic substances are formed in both terrestrial and aquatic systems. They can be insoluble components that are parts of soil and/or sediment, or be dissolved in ground or surface water. The soluble humics can also be bound to the other soil/sediment components. The humic matter composition of ecosystems is mainly controlled by a net balance of formation, degradation, and transfer (Schnitzer and Khan, 1972; Buffle, 1988; Aiken et al., 1985). The diagram in Figure 2.1 shows the occurrence and flow paths of dissolved humic substances in the natural environment.

Humic substances can generally be divided into three fractions according to their solubility, namely: humic acid (HA), fulvic acid (FA) and humin (Suffet and MacCarthy, 1989). Humic acid is the fraction of humic substances that are not soluble in water under acid conditions (below pH 2) but become soluble at greater pH. They are often referred to as being the high molecular weight fraction, with weights being estimated to range from 1500 to 5000 Daltons in streams and from 50000 to 500000 Daltons in soils. Fulvic acid is the fraction of humic substances that are soluble under all pH conditions and are referred to as moderate molecular weight substances ranging from 600 to 1000 Daltons in streams and 1000 to 5000 Daltons in soils. The third fraction, Humin, is defined as the fraction that is not soluble in water at any pH value.

2.1.1. Chemical Properties of Humic Substances

Humic substances are heterogeneous mixtures of high molecular weight organic compounds, both aromatic and aliphatic, that are rich in oxygen-containing functional groups (e.g., COOH, phenolic and/or enolic OH, alcoholic OH, and quinolic CdO)(Stevenson, 1994).They comprise approximately 60-70% of the total organic carbon in soils and 40-60% of dissolved organic carbon in natural waters (Senesi,1993). The vast diversity in structural components of humic substances is a result of the random polymerization of a variety of decomposed materials. Moreover, the composition of humic substances varies according to their source and method of extraction. It is this structural heterogeneity that has made the structural and conformational characterization of humic substances extremely challenging. The chemical properties of humic substances are presented in Figure 2.2.

Humic acids contain hydrogen, carbon, nitrogen, sulfur, phosphorus and oxygen. The range of elemental composition of humic materials is approximately 40-60% carbon, 30-50% oxygen, 4-5% hydrogen, 1-4% nitrogen, 1-2% sulfur and 0-0.3 % phosphorus. Studies on humins have shown that they are similar to humic acids except that they are strongly bound to metals and clays, rendering them insoluble (Gaffney et al., 1996).

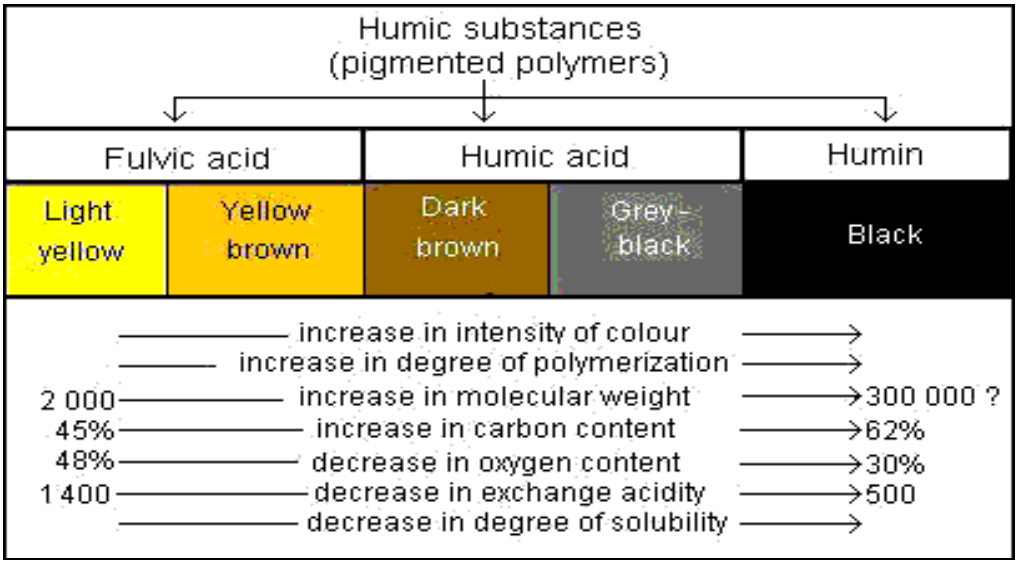

Figure 2.2. Chemical properties of humic substances (Stevenson, 1982)

Although the composition of humic substances is complex, there are some general characteristics. Humic acids consist of phenolic (Ar–OH) or quinone (ArMO) aromatic rings bridged by –O–, $–CH_2–$, –NH–, –NM, –S–, and other groups (Stevenson, 1982). Attached to the aromatic backbone are functional groups that include carboxyls, enols, alcohols, ethers, ketones, aldehydes, esters, amines and amides. Amino acids, amino sugars, peptides and aliphatic compounds may also be present (Stevenson, 1982). In 1993, Schulten and co-workers proposed a tentative structure for humic substances. They reported a flexible network of aromatic chains bonded by long-chain alkyl structures.

Table 2.1. Elemental analysis of humic acid (Schnitzer and Khan, 1972).

Element	Humic acid (wt %)
C	53.6-58.7
H	3.2-6.2
N	0.8-5.5
O	32.8-38.3
S	0.1-1.5

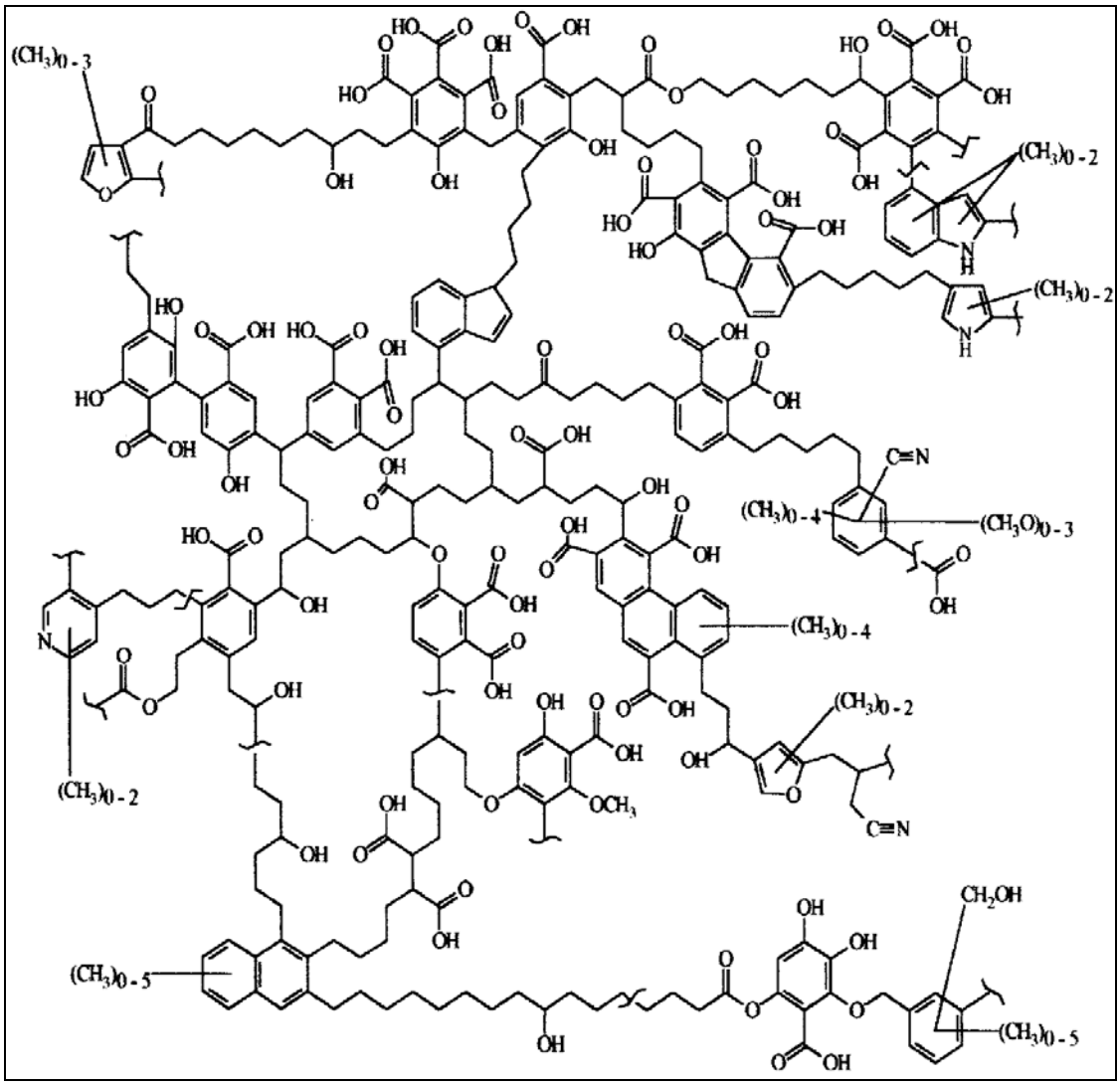

Figure 2.3. The structural concept of a humic acid (Schulten et al, 1993).

Humic material contains high amount of radicals. These radicals can exist as permanent components or as transient species, generated by pH changes, chemical reduction or solar irradiation. They generally play important roles in polymerization or oxidation-reduction reactions (Gaffney et al., 1996).

2.1.2. Influences of Aquatic Humic Substances on Treatment Processes

Humic substances in drinking water may pose a problem because they impart a color to the water that is not aesthetically pleasing to domestic consumers. The color also renders it unsuitable for the paper, beverage and textile industries. Besides, they have adverse effect because of their fouling potential of membranes and ion exchange resins. However it is also well established that humic substances upon chlorination (used for disinfection purposes) form mutagenic halogenated compounds. Numerous reports have demonstrated the formation of trihalomethanes, haloacetonitriles, haloacetic acids, and MX (3-chloro-4-(dichloromethyl)-5-hydroxy-2(H)-furanone) a highly reactive and unstable furanone derivative. (Palmer et al, 2002). Therefore, it is desirable to minimize the presence of humic substances in drinkable and industrial waters. The presence of humic acids (HA), as part of natural organic matters, has been a problem in the water due to their water-soluble formation, a wide range of distribution in molecular weight and size, and their non-biodegradability.

Removing of humic acid in water treatment has attracted much of environmental and health considerations. It is hence necessary to remove the humic substances content in water below a safety threshold. HAs have received much attention particularly in relation with water treatment since they are precursors of the disinfection byproducts (DBPs) (e.g., trihalomethanes (THMs)) in chlorination process. Activated carbon adsorption (Hesse et al., 1999), coagulation, precipitation (Ødegaard et al., 1999; O'melia et al., 1999), adsorption/ion exchange (Fettig, 1999; Heijman, 1999), biofiltration (Graham, 1999; Huck, 1999), ozonation (Ohlenbusch, 1998), and ultrafiltration have been widely studied as the humic removal process. However, conventional coagulation and flocculation process followed by filtration methods are unable to remove TOC by more than 10–50% (Wang et al., 2000). Maintenance of residual sludge containing high aluminum concentration generated by this coagulation/flocculation process poses additional concerns. Humic acid biodegradation (Wang, 2000) and surface activated carbon adsorption are relatively slow processes and hence inefficient. Heterogeneous photocatalysis is an effective alternative solution for elimination of HA from aqueous solution.

2.2. Photocatalytic Degradation

Heterogeneous photocatalysis is a process in which the illumination of an oxide semiconductor produces photo excited electrons (e^-) and holes (h^+). These can migrate to the oxide surface and participate in half-cell reactions that are part of a closed, catalytic cycle. In the aqueous phase, the illuminated surface is widely regarded as a producer of hydroxyl radicals and these and other highly oxidizing initial products of this indirect photochemistry go on to attack oxidizable contaminants (Ollis et al. 1991).

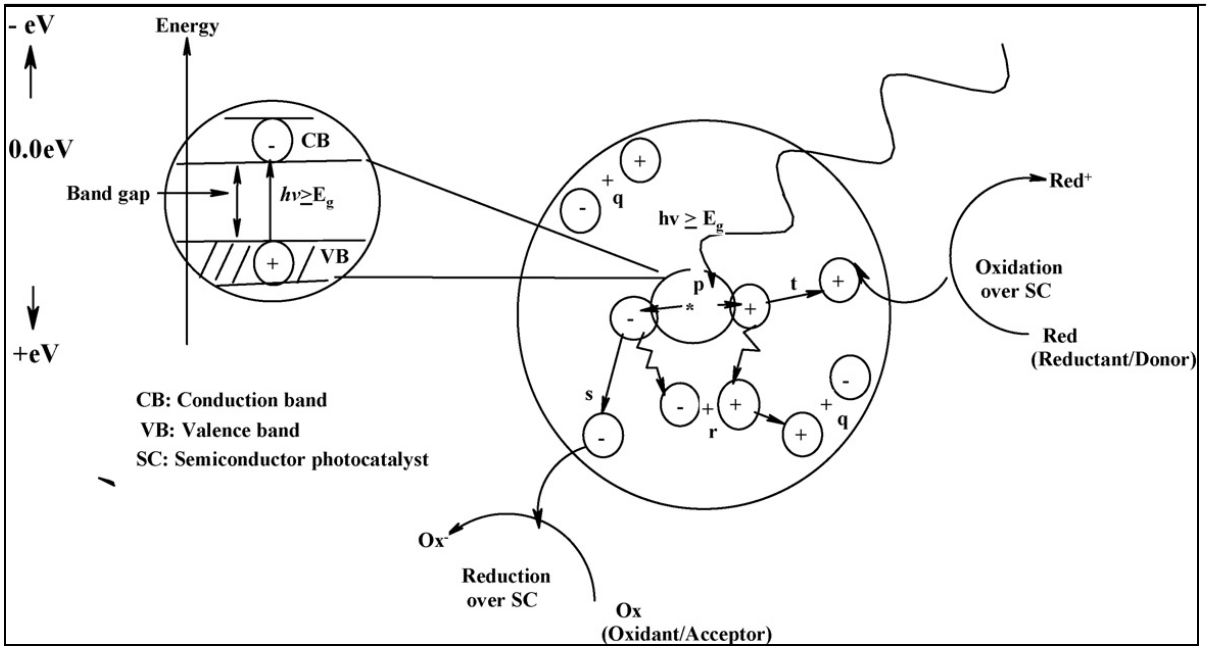

Figure 2.4. Schematic photophysical and photochemical processes over photon activated semiconductor cluster (p) photogeneration of electron/hole pair, (q) surface recombination, (r) recombination in the bulk, (s) diffusion of acceptor and reduction on the surface of semiconductor (SC), and (t) oxidation of donor on the surface of SC particle (Carp et al. 2004).

The basic principles of heterogeneous photocatalysis can be summarized shortly as follows. A semiconductor (SC) is characterized by an electronic band structure in which the highest occupied energy band, called valence band (VB), and the lowest empty band, called conduction band (CB), are separated by a bandgap, i.e. a region of forbidden

energies in a perfect crystal. When a photon of energy higher or equal to the band gap energy is absorbed by a semiconductor particle, an electron from the VB is promoted to the CB with simultaneous generation of a hole (h^+) in the VB. The e_{CB}^- and the h_{VB}^+ can recombine on the surface or in the bulk of the particle in a few nanoseconds (and the energy dissipated as heat) or can be trapped in surface states where they can react with donor or acceptor species adsorbed or close to the surface of the particle. Thereby, subsequent anodic and cathodic redox reactions can be initiated (Figure 1). The energy level at the bottom of the CB is actually the reduction potential of photoelectrons and the energy level at the top of the VB determines the oxidizing ability of photoholes, each value reflecting the ability of the system to promote reductions and oxidations.

The following chain reactions have been widely postulated.

$$TiO_2 + h\nu\ (UV) \rightarrow TiO_2\,(e^-_{CB} + h^+_{VB}) \quad (2.1)$$

Photogenerated holes (h^+_{VB}) may directly oxidize the organic substrate, S anchored to the oxide surface.

$$h^+_{VB} + S \rightarrow S^{\bullet+} \quad (2.2)$$

$$h^+_{VB} + H_2O \rightarrow HO^\bullet + H^+ \quad (2.3)$$

$$h^+_{VB} + OH^- \rightarrow HO^\bullet \quad (2.4)$$

$$HO^\bullet + HO^\bullet \rightarrow H_2O_2 \quad (2.5)$$

On the other hand, in the presence of electron scavengers (i.e. O_2) reduction reactions may take place leading to the following sequence of the reactions.

$$e^-_{CB} + O_2 \rightarrow O_2^{\bullet-} \quad (2.6)$$

$$e^-_{CB} + H_2O_2 \rightarrow OH^- + HO^\bullet \quad (2.7)$$

$$O_2^{\bullet-} + H^+ \rightarrow HO_2^\bullet \quad (2.8)$$

$$O_2^{\bullet-} + HO_2^\bullet \rightarrow HO_2^- + O_2 \quad (2.9)$$

$$HO_2^\bullet + HO_2^\bullet \rightarrow O_2 + H_2O_2 \quad (2.10)$$

$$H_2O_2 \leftrightarrow HO_2^- + H^+ \quad (2.11)$$

$$HO^\bullet + HO_2^\bullet \rightarrow H_2O + O_2 \quad (2.12)$$

The formed reactive oxygen species ($O_2^{\bullet-}$, $HO_2^{\bullet}$ and $HO^{\bullet}$) reacts with the adsorbed substrate leading to oxidation and under appropriate irradiation periods even to complete mineralization.

Photocatalyst concentration; The rate of photocatalytic reaction is strongly influenced by concentration of the photocatalyst. It is observed that rate of reaction increases with increase in catalyst concentration and becomes constant above at a certain level. Generally, in any given photocatalytic application, the optimum catalyst concentration must be determined in order to avoid excess catalyst and ensure total absorption of efficient photons (Chun et al., 2000).

Oxygen pressure; Oxygen was found to be essential for semiconductor photocatalytic degradation of organic compounds. Dissolved molecular oxygen is strongly electrophilic and thus an increase of its content probably reduces unfavourable electron–hole recombination routes (Ollis et al., 1991). But higher concentrations lead to a downturn of the reaction rate, which could be attributed to the fact that the TiO_2 surface becomes highly hydroxylated to the extent of inhibiting the adsorption of pollutant at active sites (Braun and Oliveros, 1997).

Reaction temperature; Generally, the increase in temperature enhances recombination of charge carriers and desorption process of adsorbed reactant species, resulting in decrease of photocatalytic activity. This is in conformity with Arrhenius equation, for which the apparent first order rate constant K_{app} should increase linearly with exp $(-1/T)$ (Gaya and Abdullah, 2008).

pH; An important parameter in the photocatalytic reactions taking place on particulate surfaces is the pH of the solution, since it dictates the surface charge properties of the photocatalyst and size of aggregates it forms (Haque and Muneer, 2007). Acid-base properties of TiO_2 govern the adsorption process since the main functional groups residing on the humic molecule express pH dependent deprotonation capabilities. Therefore, if natural water conditions are considered as the main focus of the photocatalytic degradation of natural organic matter, the following probable surface reactions in terms of electrostatic attractions should be taken into account at neutral pH conditions (pH: 6-7).

1. Deprotonation of carboxylic groups resulting in partially-negatively charged humic moieties and almost equally distributed positive and negatively charged TiO_2 surface reveals an electrostatic attraction between the negatively charged humic molecule and positively charged TiO_2 surface and a probable repulsive force between the negatively charged surface and humic moieties. The overcoming force facilitates the surface adsorption of humics onto TiO_2 as explained by several studies (Uyguner and Bekbolet, 2004b, Bekbolet et al., 2002).
2. The hydrophobic fractions of humic moieties express van der Waals forces on the charge distribution of TiO_2 particles resulting in conformational changes in humic molecules.
3. pH conditions induce structural changes in humic molecules ranging from compact structures (low pH) to almost linear structures (high pH). The net result could also be explained as trains and loops structure directly related to the origin of humic acids.

Photocatalytic technology has major advantages. Photocatalysis offers a good substitute for the energy-intensive conventional treatment methods with the capacity for using renewable and pollution-free solar energy. Besides, unlike conventional treatment measures, which transfer pollutants from one medium to another, photocatalysis leads to the formation of innocuous products. This process can be used to destroy a variety of hazardous compounds in different wastewater streams. Also, It can be applied to aqueous and gaseous-phase treatments, as well as solid (soil) phase treatments to some extent.

Heterogeneous photocatalysis allows the treatment of water or air streams containing, simultaneously, organic, biological or inorganic pollutants. The technique has been applied successfully to air purification, e.g., destruction of volatile organic compounds (VOCs) in the gas phase. In the case of water purification or remediation, the technique offers several advantages such as the use of oxygen as the only oxidant, the capability for simultaneous oxidative and reductive reactions, low costs and use of solar light. Furthermore, chemical photosynthesis, fuel production or photographic processes, color removal and the destruction of dyes (Davis et al.,1994); reduction of COD (chemical oxygen demand) (Chen and Rulkens, 1997); mineralization of hazardous organics (Suri et al.,1993); destruction of hazardous inorganics such as cyanides (Kim et al.,1998);

degradation of harmful fungicides, herbicides, and pesticides (Muneer and Bahnemann, 2001) destruction of malodorous compounds (Canela et al.,1999) decontamination of soil (Hamerski, 1999); purification and decontamination of indoor air and destruction of cancer cells and viruses are other important applications of heterogeneous photocatalytic systems.

2.2.1. Photocatalyst

A photocatalyst is characterized by its capability to adsorb simultaneously two reactants, which can be reduced and oxidized by a photonic activation through an efficient absorption. The ability of a semiconductor to undergo photoinduced electron transfer to an adsorbed particle is governed by the band energy positions of the semiconductor and the redox potential of the adsorbates. The energy level at the bottom of conduction band is actually the reduction potential of photoelectrons. The energy level at the top of valence band determines the oxidizing ability of photoholes, each value reflecting the ability of the system to promote reductions and oxidations. The flatband potential, V_{fb}, locates the energy of both charge carriers at the semiconductor–electrolyte interface, depending on the nature of the material and system equilibrium (Serpone, 1997). From the thermodynamic point of view, adsorbed couples can be reduced photocatalytically by conduction band electrons if they have more positive redox potentials than V_{fb} of the conduction band, and can be oxidized by valence band holes if they have more negative redox potentials than the V_{fb} of the valence band (Rajeshwar, 1995).

Many chalcogenide semiconductors such as TiO_2, ZnO, ZrO_2, CdS, MoS_2, Fe_2O_3 and WO_3 have been examined and used as photocatalysts for the degradation of organic contaminants. The band gaps properties of some semiconductors used in photocatalysis are reported in Table 2.2.

An ideal photocatalyst for photocatalytic oxidation is characterized by photo-stability, chemically and biologically inert nature, availability and low cost and capability to adsorb reactants under efficient photonic activation.

Table 2.2. Band-gap energies of semiconductors used for photocatalytic processes (Thakur et al., 2010).

Photocatalyst	**Band-gap energy(eV)**
Si	1.1
WSe_2	1.2
WO_3	2.8
Fe_2O_3	2.2
V_2O_5	2.7
SiC	3.0
$BaTiO_3$	3.3
CdO	2.1
CdS	2.4
CdSe	1.7
Fe_2O_3	3.1
TiO_2 rutile	3.02
TiO_2 anatase	3.23
Sr TiO_3	3.4
SnO_2	3.5
GaP	2.3
GaAs	1.4
$SrTiO_3$	3.4
TiO_2	3.0
ZnS	3.7

In spite of the constant vigorous research activities over two decades in search for an ideal photocatalyst, titania has remained a benchmark against which any emerging material candidate will be measured (Rajeshwar et al., 2001). TiO_2 is the most widely used photocatalyst because of its good activity, high chemical stability, high ultraviolet adsorption, commercial availability, and inexpensiveness. Both crystal structures, anatase, and rutile are commonly used, with anatase showing a greater photocatalytic activity for

most of the reactions. Some studies showed that a mixture of anatase (70%–75%) and rutile (30%– 25%) is more active than pure anatase (Malato et al., 2003; Carp et al., 2004). Besides, Zhang and Maggard (2007) reported the preparation of hydrated form of amorphous titania with wider band energy gap than anatase and significant photocatalytic activity. A study on the photo electrochemical activities of nanocrystalline TiO_2 film electrodes showed that the photocurrent (or photoactivity) for anatase-type TiO_2 was higher than that of rutile-type TiO_2 at longer wavelength and increased with decreasing wavelength (around 300 nm) (Shiga et al., 1998).

2.2.2. Titanium dioxide

Titanium, the world's fourth most abundant metal (exceed only by aluminum, iron, and magnesium) and the ninth most abundant element (constituting about 0.63 per cent of the Earth's crust), was discovered in 1791 in England by Reverend William Gregor.

TiO_2 contains not less than 99 per cent and not more than 100 per cent O_2 calculated on the dry basis. The theoretical composition of the oxide is: Titanium 60 per cent, Oxygen 40 per cent. It contains iron, columbion and tantalum in important amounts; tin, chromium and vanadium have also been reported (Rakhshandeh, 1993). Titanium dioxide (TiO_2) belongs to the family of transition metal oxides (Greenwood and Earnshaw, 1997). In the beginning of the 20th century, industrial production started with titanium dioxide replacing toxic lead oxides as pigments for white paint. It is used as a white pigment in paints (51% of total production), plastic (19%), and paper (17%), which represent the major end-use sectors of TiO_2.

Besides the four polymorphs of TiO_2 found in nature (i.e., anatase (tetragonal), brookite (orthorhombic), rutile (tetragonal), and TiO2 (B) (monoclinic)), two additional high-pressure forms have been synthesized starting from rutile: TiO_2 (II), which has the PbO_2 structure and TiO_2 (H) with the hollandite structure. The structures of rutile, anatase and brookite can be discussed in terms of (TiO_2^{6-}) octahedrals. The three crystal structures differ by the distortion of each octahedral and by the assembly patterns of the octahedral chains. Anatase can be regarded to be built up from octahedrals that are connected by their

vertices, in rutile, the edges are connected, and in brookite, both vertices and edges are connected.

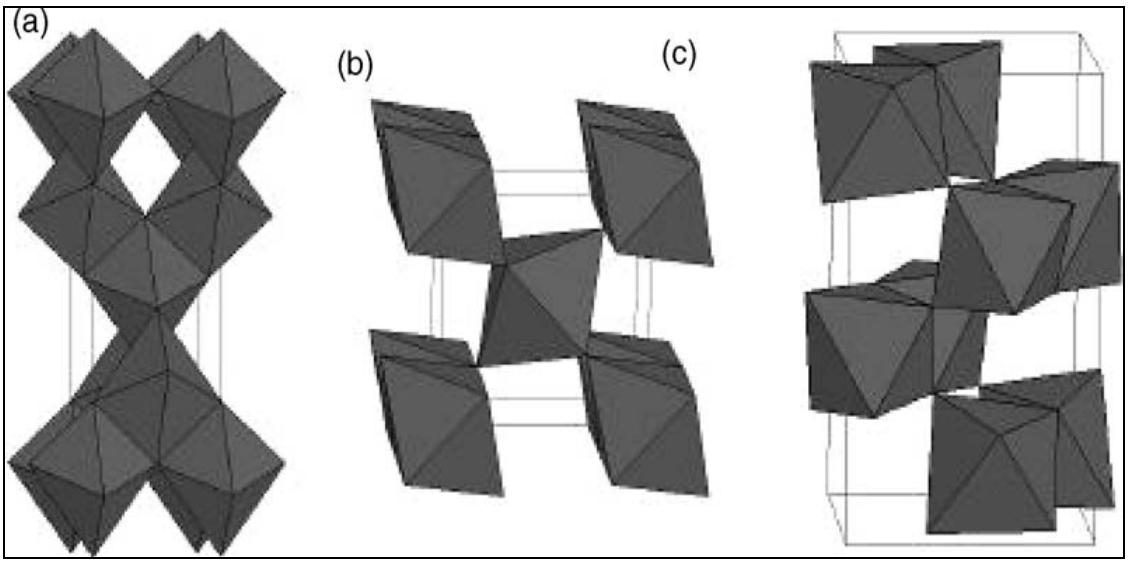

Figure 2. 5. Crystal structures of anatase (a), rutile (b), and brookite (c) (Carp et al., 2004).

The enthalpy of the anatase-rutile phase transformation is low (ranging from–1.3 to– 6.0 kJ/mol) (Daßler, 1988). Kinetically, anatase is stable, i.e., its transformation into rutile at room temperature is so slow that the transformation practically does not occur. At macroscopic scale, the transformation reaches a measurable speed for bulk TiO_2 at T > 600ºC (So et al., 2001).

2.2.2.1. Doped photocatalyst. The titanium dioxide (TiO_2) is an effective photocatalyst owing to its inertness, strong oxidizing power, non-toxicity and stability within a wide range of pH, and inexpensive photosensitized material (Hoffman et al., 1995). However, its large scale application is still limited because the band gap of photocatalytically more active titania phase (anatase) is 3.2 eV, which requires UV irradiation ($\lambda \leq 387$ nm). The ultimate goal is the direct utilization of solar energy, but the solar spectrum is relatively poor in UV light at the surface on Earth. The other difficulty with TiO_2 is the high recombination rate of the photoexcited electron–hole pairs in the irradiated particles. The fast recombination is in competition with the reactions decomposing the pollutants (Ambrus et al., 2008).

A number of studies have recently tried to overcome this problem, focusing on the surface modifications of photocatalysts. The surface modification of TiO_2 can be achieved by metal doping into TiO_2. To increase the visible light absorption of TiO_2 materials, it has been reported that the addition of transition metals to TiO_2 can improve the photocatalytic activity by decreasing the energy band gap or preventing (e^-/h^+) pair recombination by electron/hole trapping (Carneiro et al., 2007). The effect of metal ion dopants on the photocatalytic activity is reported to be a complex problem comprised of several operating factors (Carp et al, 2004). The total induced alteration of the photocatalytic activity is made from the sum of changes which occurs in: *i.* the light absorption capability of the TiO_2 photocatalyst, *ii.*adsorption capacity of the substrate molecules at the catalyst's surface, *iii.* Interfacial charge transfer rate. Doping ions generally act as trapping sites influencing the life-time of charge carriers. Dopant ions have a stable half-filled electronic configuration (d^5 and f^7). When these metallic ions trap electrons, the half-filled electronic configuration is destroyed thereby a decrease in stability is attained. The trapped electrons can easily be transferred to oxygen adsorbed on the surface of the titania and the dopant ions return to the original stable electronic configuration. This might promote electron charge transfer and efficient separation of the electrons and holes by shallow trapped electrons. Since surface sites can be occupied by dopants, the surface properties as well as the point of charge (pH_{zpc}) may be changed. Consequently the expected adsorption behavior of the substrate may also be altered.

Amongst a variety of transitional metals, iron has been considered to be an appropriate candidate due to the fact that the radium of Fe^{3+} (0.69 A) is similar to that of Ti^{4+} (0.745 A), so Fe^{3+} can be easily incorporated into the crystal lattice of TiO_2 (Choi et al., 1994). Fe^{3+} can provide a shallow trap for photo-generated electron and hole because the energy level of Fe^{2+}/Fe^{3+} lies close to that of Ti^{3+}/Ti^{4+} favoring the separation of photo-generated electron-hole pair, and consequently resulting in the improvement of quantum yield (Yamashita et al., 2003; Choi et al.,1994). Moreover, Fe doping could induce batho-chromic effect. An enhancement of the intrinsic absorption edge of TiO_2 from 380 nm to higher wavelengths *i.e.,* to 400-650 nm compared to bare titania has been reported (Carp et al, 2004).

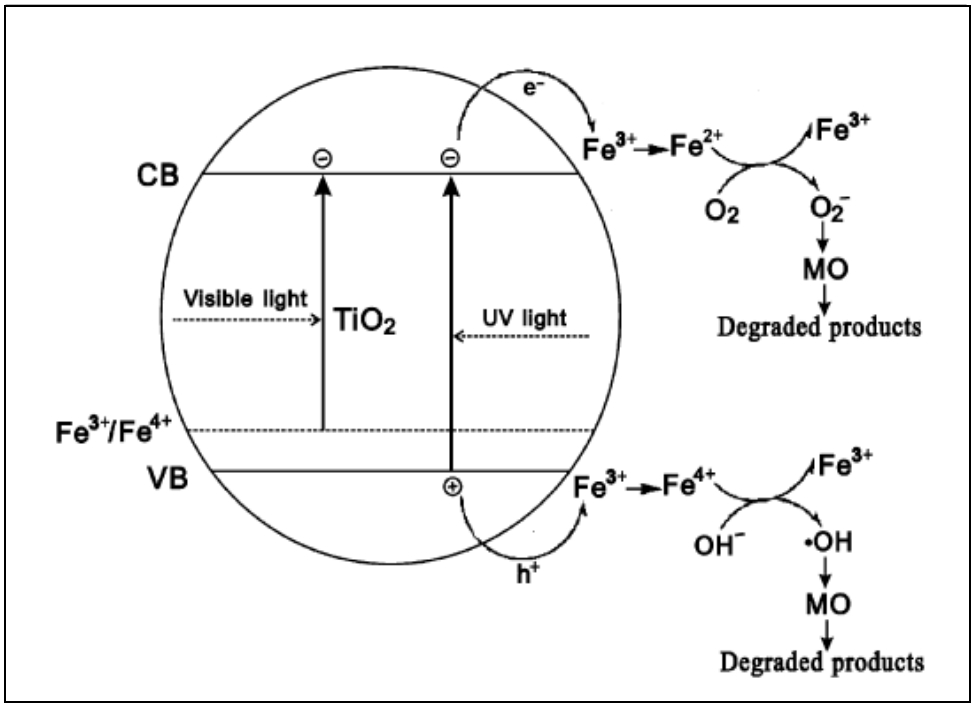

Figure 2.6. Proposed mechanism for methyl orange (MO) degradation under UV and visible light irradiation.

The following reaction scheme was also introduced by Tong et al, 2008.

$$TiO_2 + h\nu \rightarrow e^- + h^+ \quad (2.13)$$

$$Fe^{3+} + h^+ \rightarrow Fe^{4+} \quad (2.14)$$

$$Fe^{3+} + e^- \rightarrow Fe^{2+} \quad (2.15)$$

$$Fe^{2+} + O_2\,(ads) \rightarrow Fe^{3+} + O_2^- \quad (2.16)$$

$$Fe^{2+} + Ti^{4+} \rightarrow Fe^{3+} + Ti^{3+} \quad (2.17)$$

$$Ti^{3+} + O_2\,(ads) \rightarrow Ti^{4+} + O_2^- \quad (2.18)$$

$$Fe^{4+} + OH^-\,(ads) \rightarrow Fe^{3+} + OH^{\bullet}\,(ads) \quad (2.19)$$

However, when the concentration of Fe^{3+} ions becomes too large, Fe^{3+} ions can act as the recombination centers for the photo-generated electrons and holes and resulting in the decrease of photocatalytic activity. Above 0.1% concentration, Fe^{3+} ions steadily become recombination centers and the photocatalytic activity gradually decreases:

$$Fe^{4+} + e^- \rightarrow Fe^{3+} \quad (2.20)$$

$$Fe^{2+} + h^+ \rightarrow Fe^{3+} \quad (2.21)$$

$$Fe^{2+} + OH^{\bullet} \rightarrow Fe^{3+} + OH^- \quad (2.22)$$

Different with the intrinsic excitation of TiO_2 under UV irradiation, the excitation behavior of Fe TiO_2 under visible irradiation arises from the electronic transition from the dopant energy level (Fe^{3+} / Fe^{4+}) to the conduction band of TiO_2. Due to the fact that the t_{2g} level of 3d orbital of Fe^{+3} ions is above the valence band of TiO_2, Fe^{+3} ion can absorb a photon with a wavelength exceeding 400 nm to produce a Fe^{4+} ion and a TiO_2 conductive band electron. The conductive band electron further reacts with adsorbed O_2 to form O_2^-, while Fe^{4+} reacts with surface hydroxyl group to produce hydroxyl radical. Thus, MO was photodegraded even under the visible light irradiation

$$Fe^{3+} + h\nu \rightarrow Fe^{4+} + e^- \quad (2.23)$$

$$e^- + O_2\,(ads) \rightarrow O_2^- \quad (2.24)$$

Choi and co-workers (1994) reported the highest chloroform degradation efficiency under UV irradiation for a sample containing 0.5 (at. %) Fe^{3+} and the substitution of Ti^{4+} ions in the titania lattice by Fe^{3+} ions was favored. Zhu et al. (2006) recently used a sol–gel method to prepare Fe-TiO_2 and studied the effect of Fe^{3+} doping concentration on the photoactivity of yellow XRG dye. Cong et al. (2007) studied the co-doping effect of N and Fe on TiO_2, which improved the activity under both visible and UV lights irradiation. It was commonly reported that the improvement of photocatalysts was attributed to the Fe^{3+} dopants which can help the separation of photo-generated electrons and holes, and also can absorb and utilize the visible light to photocatalyze the degradation of pollutants (Wei et al., 2007). Stir et al. (2003) characterized the structures of Fe doped TiO_2 samples prepared under different conditions.

Tong and co-workers (2008) examined preparation of Fe^{3+} doped TiO_2 catalysts by controlled hydrolysis of titanium alkoxide and studied on their photocatalytic activity for methyl orange degradation. The samples were characterized by X-ray diffraction (XRD), transmission electron microscopy (TEM), atomic absorption flame emission spectroscopy (AAS), electron paramagnetic resonance (EPR) spectrum, X-ray photoelectron

spectroscopy (XPS), UV–vis diffuse reflectance spectroscopy (DRS), and nitrogen adsorption–desorption methods. The photocatalytic activity of Fe doped TiO_2 catalysts was evaluated from the photodegradation of methyl orange (MO) aqueous solution both under UV and visible light irradiation. Fe^{3+} doping effectively improved the photocatalytic activity under both UV light irradiation and visible light irradiation with an optimal doping concentration of 0.1 and 0.2%, respectively.

Yalcin and co-workers (2010) studied a combination of experimental structural methods and the density functional theory (DFT) calculations to characterize and describe the effect of Fe^{3+} dopant on the electronic structure, visible light and the photocatalytic activity of TiO_2. Fe^{3+} doped photocatalysts with different Fe^{3+} contents were prepared by an incipient wet impregnation method, in order to prevent penetration of the dopant cations into the bulk of TiO_2.The Fe^{3+} doped photocatalysts were characterized by FT-IR, XRD, Raman and XPS. The morphological structure of the photocatalysts was examined by SEM. A higher photocatalytic activity for the degradation of 4-nitrophenol was obtained for the Fe^{3+} doped TiO_2 compared to the undoped TiO_2. The results of the DFT calculations indicate that the origin of the visible light activity of the Fe^{3+} doped TiO_2 is due to the introduction of additional electronic states within the band-gap.

2.2.3. Summary of the Previous Studies Performed for the Assessment Photocatalytic Treatment

The requirement for the improvement of drinking water standards, and the related technological advances for the removal of natural organic matter bring about the need for the understanding of natural organic matter (NOM). The number of studies on aquatic humic substances has published because of the formation of potentially harmful disinfection by products. Bekbolet and co-workers have been studying about photocatalytic degradation and adsorption of humic substances since 1996.

Bekbolet and colleagues (1996) studied the effect of photocatalyzed oxidation on the degradation and decolourisation of humic acid. Further, adsorptive behavior of humic acid was studied. After the photocatalytic oxidation of humic acid, it was examined that with respect to a decrease in the content of organic matter and decolourisation an increase in

biodegradability was observed. Also, it was reported that when the irradiation time was increased the adsorption characteristic of humic acid showed a change.

Bekbolet and Ozkosemen (1996) investigated the effects of the photocatalyst concentration, pH, and humic acid concentration during photocatalytic degradation of humic acid. The optimum TiO_2 concentration was found as 1.0 mg mL^{-1} since further increase in TiO_2 concentration led to opacity of the solution and. It was reported that photocatalytic oxidation of humic acid could be effective pretreatment method to keep the trihalomethane levels below the limit of 100 μgL^{-1}.

Bekbolet and co-workers (2002) examined the photocatalytic efficiencies of TiO_2 powders on the decolorisation of humic acid. Photocatalytic efficiencies of two commercial titania brands, Degussa P-25 and Hombikat UV-100 were discussed in relation to the degradation of humic acid in aqueous solutions. Decolourisation rate of humic acid for Degussa P-25 was found to be higher than the rate achieved by using Hombikat UV-100 specimen. It was concluded that there was certain dependency between the adsorption characteristics and the photocatalytic decolorisation rates but no dependency onto the surface area of TiO_2 powders.

Zhu and co-workers (2004) investigated characterization of Fe–TiO_2 photocatalysts synthesized by hydrothermal method and their photocatalytic reactivity for photodegradation of XRG dye diluted in water. Iron-ion-doped anatase titanium (IV) dioxide (TiO_2) samples were prepared by hydrothermal hydrolysis and crystallization in octanol-water solution. The samples were characterized by X-ray diffraction, BET-specific surface area determination, UV-vis diffuse reflectance spectroscopy and electron paramagnetic resonance spectroscopy. UV-vis diffuse reflectance spectra showed a slight shift to longer wavelengths and an extension of the absorption in the visible region for almost all the ion-doped samples, compared to the non-doped sample. The Photocatalytic activity of those catalysts was investigated for the liquid phase photocatalytic degradation of active yellow XRG dye diluted in water under UV and visible light irradiation. It was found that the catalysts doped with $FeCl_3$ have better catalytic activity for photodegradation of XRG than those doped with $FeCl_2$. The amount of doped iron ion

plays a significant role in affecting its photocatalytic activity and iron doped with optimum content can enhance photocatalytic activity, especially under visible light irradiation.

Uyguner and Bekbolet (2005a) studied on the spectral changes of humic acids during oxidation processes and the effects of the molecular size distribution of photocatalytically treated humic acid samples. It was observed photocatalytic degradation of humic acid leads to the formation of lower molecular size (small fractions) and higher UV absorbing compounds. For fractions less than 10 kDa, UV_{254} absorbing moieties in treated humic acid samples become higher than that of raw humic acid designating the generation of new species during photocatalysis. UV–vis spectroscopic changes were also evaluated by the parameters relating to the concomitant removal of the total organic carbon as well as by the ratios using absorption values at discrete wavelengths.

Uyguner and Bekbolet (2005b) studied the photocatalytic removal of model humic and fulvic acids of different origins by using TiO_2 Degussa P-25 as the photocatalyst. It was reported that there were substantial differences in photocatalytic removal efficiencies of humic and fulvic acids on the basis of their diverse chemical and physical properties such as molecular weight, molecular size, elemental composition and source of origin.

Zhang and co-workers (2006), studied to enhance the absorption in the visible region for supported TiO_2, Fe doped TiO_2 coatings have been prepared in one step by a code position process of metal organic chemical vapor deposition method. The results indicated that iron exists as isolated octahedrally coordinated Fe^{3+} ions substituting Ti^{4+} in the TiO_2 lattice. UV–vis diffuse reflectance spectra show a slight shift to longer wavelengths and an enhancement of the absorption in the visible region (>400 nm) for the Fe doped TiO_2 coatings, compared to the non-doped sample. The Fe doped TiO_2 samples exhibited good photocatalytic activities for the degradation of methyl orange under visible light irradiation.

Uyguner and Bekbolet (2007) examined the impact of aqueous Cr (VI) and Mn (II) species on the photocatalytic oxidation of humic acids as a major component of natural organic matter in aquatic systems. The experiment results were evaluated in terms of Langmuir-Hinshelwood rate with respect to $Color_{436}$ because of the pseudo-first-order rate

constant explains the overall removal tendency covering all competitive and consecutive reactions. The presence of these ions affected the adsorptive properties of the photocatalyst and the photocatalytic oxidation rate of humic acids. The impact of manganese ion on the photocatalytic oxidation could be better explained in terms of L-H kinetics where 15% increase was observed with respect to $Color_{436}$ while 54% decrease observed in the presence of chromium.

Bouras and co-workers (2007) studied pure versus doped nanocrystalline titania for photocatalysis. Thin films of pure or doped nanocrystalline titania have been deposited on glass slides by using a sol–gel procedure $Fe^{3+,}$ Cr^{3+} and Co^{2+} were used as dopants while the doping extended in a broad domain from very low to very high levels. The photocatalytic efficiency of pure or doped titania was tested for discoloration of an aqueous solution of Basic Blue 41. Photosensitization by absorption of light by the dye itself loses its importance in the presence of the dopant. Thus the doped material is a visible-light photocatalyst but substantial photodegradation efficiency is achieved only at very high doping levels, for example, 20 at.% for Fe^{3+} doping. In any case, direct UV excitation of pure titania is a more efficient photocatalytic process than visible excitation of the doped semiconductor and also data suggest that pure nanocrystalline titania is a better photocatalyst than doped titania.

Hung and co-workers (2007) studied on photocatalytic degradation of gaseous dichloromethane using pure and iron ion-doped TiO_2. They found the optimum doping amount of iron ions was 0.005 mol %, and this can enhance the photocatalytic activity, while too great an amount would make the iron ions become recombination centers for the electron–hole pairs and reduce the photocatalytic activity. UV–vis diffuse reflectance spectra of Fe deoped TiO_2 show an increase in absorbency in the visible light region with the increase in iron ions doping concentration.

Selcuk and Bekbolet (2008) investigated the photocatalytic and photoelectrocatalytic treatment methods for removing humic acid under different experimental conditions. Photoelectrocatalytic system was performed for humic acid oxidation in the presence of chloride anion and humic acid to observe the selectivity of photoelectrocatalytic system. To investigate the inhibitory effect of carbonate species, the system was performed in the

presence and absence of carbonate species. It was reported that the attraction of humic acid to the surface of TiO_2 was stronger than that of chloride ions and carbonate ions retarded HA degradation at basic condition.

Uyguner and Bekbolet (2010) investigated the removal efficiency of aqueous humic acid solutions by TiO_2 photocatalytic degradation in the presence of Cu (II) species. The photocatalytic oxidation studies of the molecular size fractions of humic acid were also performed. The photocatalytic removal of humic acid decreased when the system contained both humic acid and Cu (II) compared to humic acid alone. Both in the presence and absence of copper ions the removal rate constants of the size fractions displayed an increasing trend as Raw < 0.45μm filtered fraction, 100 kDa fraction, 30 kDa fraction. Batch equilibrium adsorption experiments were also evaluated for probable binary and ternary systems. Even though the presence of Cu (II) species significantly altered the isotherm shape irrespective of the spectral parameters, no significant difference was attained for TOC. K_f values displayed an inconsistent effect of Cu (II) species, while adsorption intensity factor 1/n, 1 denoted a prevailing favorable type of adsorption for UV_{254} and $Color_{436}$. TOC adsorption profile showed a rather linear-type adsorption as expressed by $1/n < 1$ both in the absence and presence of Cu (II) species.

Liu and Chen (2009) investigated that two series of iron (III) doped TiO_2 powders were prepared by even doping and uneven doping methods. The photocatalytic activities of TiO_2 based nanoparticles were evaluated by the photocatalytic rate of methyl orange oxidation. TiO_2 photocatalysts doped by Fe unevenly was shown to have a much higher photocatalytic destruction rate than that of TiO_2 photocatalysts doped by Fe evenly and undoped TiO_2.

2.3. Adsorption

Adsorption is the process by which ions or molecules present in one phase tend to condense and concentrate on the surface of another phase. The adsorbate is the substance that is being removed from the liquid phase at the interface. The absorbent is the solid, liquid or gas phase onto which the absorbate accumulates.

There are three general types of adsorption, physical, chemical and exchange adsorption.

- Physical adsorption is due to the operation of weak force of attraction or van der Waal's forces between molecules. Here, the adsorbed molecule is not affixed to a particular site on the solid surface but is free to move about over the surface. Physical adsorption is generally quite reversible; i.e., with a decrease in concentration the material is desorbed to the same extent that it was originally adsorbed.

- Chemical adsorption is result of much stronger forces, comparable with those leading to the formation of chemical compounds. Normally the adsorbed material forms a layer over the surface which is only one molecule thick and the molecules are not considered free to move from one surface site to another. Also, chemical adsorption is seldom reversible. The adsorbent must generally be heated to higher temperatures to remove the adsorbed materials.

- Exchange adsorption is used to describe adsorption characterized by electrical attraction between the adsorbate and the surface. Here, ions of a substrate concentrate at the surface as a result of electrostatic attraction to sites of opposite charge on the surface.

The sorption ability of different sorbents is strongly dependent on the available surface area, polarity, contact time, pH and the degree of hydrophobic nature of the adsorbent and adsorbate (Nadeem et al., 2006). Equilibrium condition is attained when the concentration of the solute remains constant, as a result of zero net transfer of solute adsorbed and desorbed from adsorbent surface.

2.3.1. Adsorption Isotherms

The constant-temperature equilibrium relationship between the quantity of adsorbate per unit of adsorbent q_A and its equilibrium solution concentration C_e is called the adsorption isotherm. Generally, q_A increases with C but not in direct proportion. The adsorption isotherms are equilibrium equations and apply to conditions resulting after the adsorbate-containing phase has been contact with the adsorbent for sufficient time to reach equilibrium.

Adsorption isotherms for solutes in dilute solution can be classified to according to initial slope. Adsorption isotherms can be termed according to their shapes resembling the letters, such as “S” type, “L” type, “H” type, “C” type (Giles et al., 1960). The four main classes are shown in Figure 2.7.

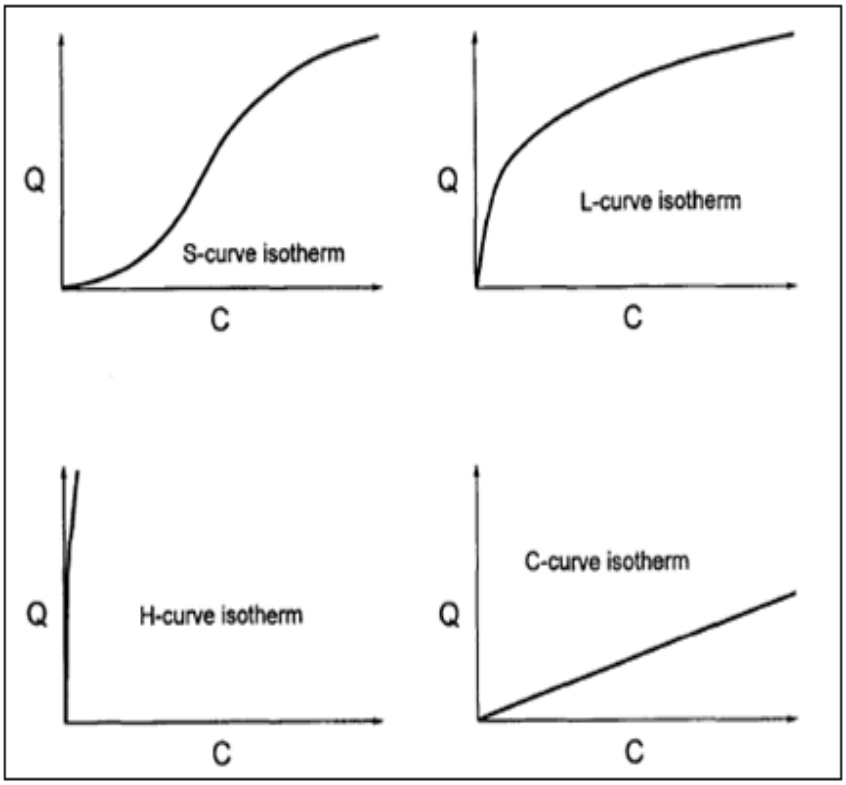

Figure 2.7. The four general categories of adsorption isotherm (Sposito, 1989).

The S-curve isotherm is characterized by initially small slope that increases with adsorptive concentration. This indicates that the affinity of the adsorbent for the adsorbate is less than that of the aqueous solution. The S-curve isotherm is the result of cooperative interactions among the adsorbed molecules. These interactions cause the adsorbate to become stabilized on a solid surface and, thus produce an enhanced affinity of the surface for the adsorbate as its concentration increases.

The C-curve isotherm shows an initial slope that remains independent of adsorptive concentration until the maximum possible adsorption is achieved. This type of isotherm is produced either by a constant partitioning of a substance between the interfacial region and the soil solution or by a proportionate increase in the amount of adsorbing surface as the concentration of an adsorbate increases.

L curve isotherm which typically concave to the concentration axis, is generally characterized by an initial slope that does not increase with the concentration of adsorbate in the solution. This type of isotherm is the resultant effect of a high relative affinity of the adsorbent particles for the adsorbate at low concentration. In addition, as the concentration of the adsorbate increases, the amount of the remaining adsorbing surface is decreased.

The H-curve isotherm is an extreme version of the L-curve isotherm. It is characterized by a large initial slope suggesting a very high relative affinity of the adsorbent for an adsorbate which is caused either by very specific interactions between the solid phases and the adsorbate (inner-sphere surface complexation) or by significant van der Waals interactions in the adsorption process. It is illustrate that the observed H-curve isotherm is the result of specific adsorption.

2.3.1.1. Langmuir isotherm. The Langmuir isotherm assumes that a single adsorbate binds to a single site on the adsorbent and that all surface sites on the adsorbent have the same affinity for the adsorbate.

Langmuir equation has the form,

$$q_A = \frac{q_m.K_a.C_e}{1 + K_a.C_e} \qquad (2.25)$$

Where, q_A stands for the mass of the contaminant adsorbed per unit weight of the adsorbent, K_a is a measure of affinity of adsorbate for adsorbent, C_e is the aqueous phase concentration of adsorbate and q_m is the maximum capacity of adsorbent for adsorbate. The Langmuir isotherm can be modified to account for competitive adsorption by more than one adsorbate and for adsorbents that have sites with different affinities for a given adsorbate. The equation is applicable to homogeneous adsorption when molecules are adsorbed at a fixed number of well-defined localized sites , each site can hold one adsorbate molecule, all sites are energetically equivalent and there is no interaction between molecules adsorbed on neighboring sites.

2.3.1.2. Freundlich isotherm. Freundlich isotherm can be derived from Langmuir isotherm by assuming that there exists a distribution of sites on the adsorbent that have different affinities for different adsorbates with each site behaving according to the Langmuir isotherm.

This equation has the form:

$$q_A = K_f C_e^{1/n} \tag{2.26}$$

where, C_e is the aqueous phase concentration of the adsorbate remaining in solution at equilibrium, q_A stands for the mass of contaminant adsorbed per unit weight of the adsorbent, 1/n is the constant for a given system and K_f is the constant in the Freundlich equation and it is related primarily to the capacity of the adsorbent for the adsorbate.

2.3.1.3. BET isotherm. BET isotherm was developed by Brunauer, Emet and Teller as an extension of the Langmiur isotherm to account for multilayer adsorption .This model assumes that a number of layers of adsorbate accumulate at the surface and that the Langmuir isotherm applies to each layer.

Adsorption process is very important to the fate and transport of contaminants in the environment and for the removal of contaminants in engineered reactors. One of the most important uses of adsorption in environmental practice has been for the removal of organic materials from waters, wastewaters and air. To illustrate; removal of taste and odor producing organic materials and other trace organic contaminants such as trihalomethanes,

pesticides and chlorinated organic compounds from drinking waters, removal of residual organic contaminants from treated wastewater effluents and treatment of leachates, industrial wastewater and hazardous wastes (Sawyer et al., 2003).

2.3.2. Summary of the Previous Studies Performed for the Assessment of Adsorptive Interactions of Humic Acids

Suphandag (1998) studied the adsorption capacity of natural organic matter on semiconductor powders. The adsorption capacity of humic acid was investigated under different pH conditions onto three different crystal structures of TiO_2 powders that the range changed from 0.1mg mL^{-1} to 1mg mL^{-1}. It was found that the adsorption capacity was higher at lower pH of humic acid solution, regardless of the crystal structures of TiO_2 powders used. Later, Suphandag (2006) examined the adsorption behavior of humic acid on the photocatalyst metal oxide. It was concluded that the adsorption of humic acids onto TiO_2 is affected by buildup of negative surface charge, limited size availability, and factors that control the size of humic acid molecules

Uyguner and Bekbolet (2004) investigated the effect of the chromium ion concentration on the adsorption of humic acid onto TiO_2. It was concluded that both $Color_{436}$ and UV_{254} was used as parameters in order to evaluate the adsorption effects of humic acid and chromium ions on the titanium dioxide surface. The presence of chromium ions was found to inhibit the adsorption capacity of humic acid onto TiO_2 powder.

Uyguner et al. (2007) reported the ozonation, photocatalysis and sequential oxidation systems followed by adsorption and coagulation characteristic of humic acids. They used two types of activated carbons in adsorption experiments (PAC and GAC) and aluminum sulfate ($Al_2 (SO_4)_3.18H_2O$), and ferric chloride ($FeCl_3 .6H_2O$) in coagulation experiments. It was found that $Color_{436}$ removal efficiencies for untreated, photocatalytically oxidized, ozonated, and sequentially oxidized humic acids increased for increasing PAC doses. $Color_{436}$ removal efficiencies for untreated, sequentially oxidized, photocatalytically oxidized, and ozonated humic acids also increased for GAC. On the other hand, UV_{254} removal efficiencies for untreated, photocatalytically oxidized, ozonated, and sequentially

oxidized humic acids decreased for increasing PAC and GAC doses. The adsorption capacities at $Color_{436}$ were higher than for the UV absorbing centers after treatment.

Ulker (2008) studied the effect of molecular size fractionation on the sorption properties of humic acid onto metal ion doped TiO_2 (Fe), and TiO_2 modified with an organic substance (ascorbic acid) samples in comparison to TiO_2 Degussa P-25. It was aimed to investigate the complex interactions between the surface properties of titanium dioxide and the molecular size dependent fractions of the humic acid in order to provide information in relation to the photocatalytic degradation of humic acids with surface modified TiO_2 powders. The adsorption profiles of the selected UV-vis parameters of humic acid and its molecular size fractions onto bare TiO_2 displayed various characteristics that were followed by fluorescence properties. The adsorption profiles of the $Color_{436}$ and UV_{254} of humic acid and its molecular size fractions and Fe doped TiO_2 exhibited distinct differences with respect to the conditions of the humic acid and bare TiO_2 system. The use of ascorbic acid modified TiO_2 expressed comparatively different adsorption patterns respect to bare TiO_2 as well as the Fe doped TiO_2. The observed differences in adsorption behavior of raw humic acid as well as the molecular size fractions could be explained by the probable diversity of the attraction sites on both of the organic moieties.

3. MATERIALS AND METHODS

3.1. Materials

3.1.1. Humic Acid

Commercially sourced humic acid used in all experiments was purchased from Aldrich (Aldrich Co. Ltd., USA). 1000 mg L^{-1} humic acid solutions was prepared by adding 1 g humic acid into distilled deionized water and dissolved using the ultrasonic sonication bath in order to provide homogenous dissolution. Stock solution of humic acid was stored in amber glass bottles and protected from sunlight. 20 mg L^{-1} humic acid were prepared from the stock solution by dilution then used in all the experiments.

3.1.2. Titanium Dioxide Powder

Commercial Degussa P25-TiO_2 with an average particle size of 20-30 nm and BET surface area of 50 ± 15 m^2 g^{-1} was used in the experiment. The crystal form of TiO_2 composed of 70% anatase and 30% rutile. Fe doped TiO_2 was prepared by Cinar and co-workers at Yildiz Technical University. Doping was performed by an incipient wet impregnation method in order to prevent penetration of the dopant cations into the bulk of TiO2. 8 g TiO_2 Degussa P25 and appropriate amount of $Fe(NO_3)_3 \cdot 9H_2O$ were mixed with definite volumes of doubly distilled water and stirred for 1 h. During this period, the mixture changed color into a light brownish beige depending upon the Fe^{3+} concentration. Prepared photocatalysts were washed with water three times, heat-treated at 373K for 24 h to eliminate water, calcined at 773K for 4 h, ground and sieved.

3.2. Laboratory Equipments

3.2.1. Specific Instruments

Perkin Elmer Lamda 35 UV-vis Double Beam Spectrophotometer was used to record UV-visible absorption spectra of humic acid employing Hellma cuvettes of 1.0 cm optical path length. Perkin Elmer LS 55 Luminescence Spectrophotometer was used to perform fluorescence spectra in the emission and synchronous scan modes were recorded on a Perkin Elmer LS 55 Luminescence Spectrometer equipped with a 150W Xenon arc lamp and a red sensitive photomultiplier tube using 1-cm path length quartz cell. Non-Purgeable Organic Carbon (NPOC) measurements of humic substances were performed on a Shimadzu TOC-V WP Total Organic Carbon Analyzer. Humic acid solutions were fractionated using Amicon Model 8050 Ultrafiltration Stirred Cell System into appropriate molecular sizes.

3.2.2. General Laboratory Instruments and Materials

Elma D-78224 Singen Sonication was used to obtain homogeneous suspension. Hettich EBA 20 Centrifuge was used for the removal of TiO_2 from suspension. Memmert Water Bath Shaker Model WB/OB 7-45 was used for adsorption experiments for mixing humic acid- TiO_2 suspensions for 24 hours. To dry the glassware Memmert Oven was

used. Scaltec SBA 31 Balance was used for weighing amounts of titanium dioxide. To remove residual catalyst from suspension, 0.45 μm diameter Sterile Millex-HA Millipore Filters were used.

3.3. Methodology

3.3.1. Photocatalytic Degradation

3.3.1.1. Experimental Set-Up. Photochemical experiments were carried out in a 50ml cylindrical Pyrex reaction vessel with a diameter of 7.5 cm and a height of 3.5 cm. Duration of the photocatalytic oxidation experiments, the reaction vessel was illuminated from the top and continuous stirring of the suspension was provided by means of a magnetic stirrer. The photoreactor was enclosed by a mirror casing and the whole system was placed in a box, the inner walls were covered with Al foil. As a light, 125W black light fluorescent (BLF) lamp emitting radiation between 300 and 420 nm with a maximum at 350 nm was used. The lamp exhibited a maximum emission at 365 nm and no emission below 300 nm and above 500 nm. The intensity of incident light measured by potassium ferrioxalate actinometer (Hatchard and Parker, 1956) was 2.85×10^{16} quanta s^{-1}. The lamp was built into a lamp housing which provides a location of 10 cm above the surface of the solution.

3.3.1.2. Experimental Procedure. 0.25 mg mL^{-1} TiO_2 Degussa P-25 as the photocatalyst was used in all the experiments weighted using balance. 50 mL of 20 mg L^{-1} humic acid solution was measured and poured directly to the reaction vessel then 0.25 mg mL^{-1} of TiO_2 added to this vessel. The slurry was sonicated for three minutes to provide a homogenous mixture. After that, reaction vessel placed on a magnetic stirrer to be irradiated for certain reaction periods (0, 10, 20, 30, 40, 50, 60 minutes). Because of the evaporation of water at longer irradiation periods, volume corrections were made with deionized water to prevent evaporation loss. At the beginning of each run, TiO_2 was removed from the suspension by filtering through 0.45 μm filters.

3.3.2. Adsorption

3.3.2.1. Experimental Procedure. Batch adsorption experiments were carried out using 100 mL Erlenmeyer Flasks. Each flask was filled with 50 mL humic acid solution. Increased amounts of TiO_2 were added into each Erlenmeyer flask in the range of 0.1 mg mL^{-1} to 1.0 mg mL^{-1}. One extra flask was filled with raw humic acid solution to compare with other sets. Each sample was sonicated before being placed to the shaker for evenly distribution of TiO_2 in the slurry. The samples were immersed in the water-bath at room temperature (± 25 °C) which is equipped with shaking device. The flasks were kept shaking for 24 hours. Then, the samples were centrifuged for 10 minutes at 5000 cycles min^{1}. The supernatant was filtered by the 0.45µm Millipore syringe filter.

3.3.3. Molecular Size Fractionation with Ultrafiltration

Humic acid solutions were fractionated using a 50 mL Amicon Model 8050 ultrafiltration stirred cells into appropriate molecular sizes and subjected batch adsorption experiments using TiO_2 as the adsorbent.

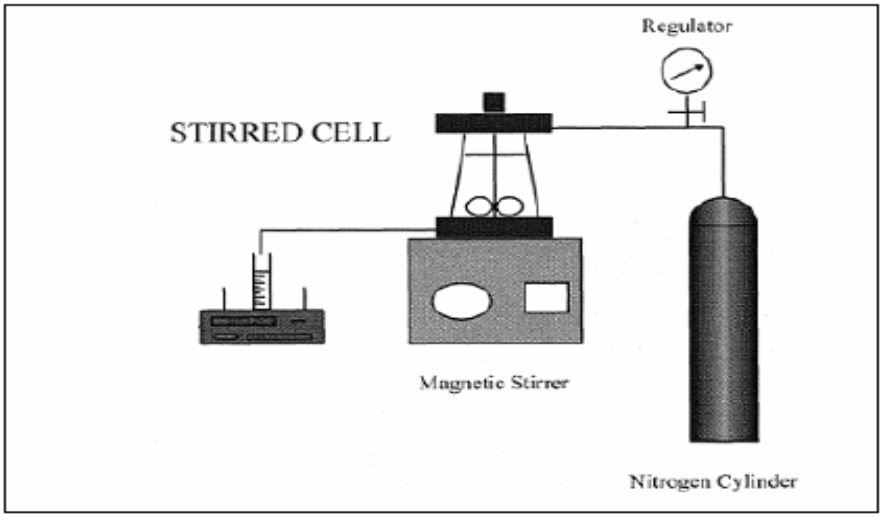

Figure 3.1. Schematic diagram of stirred cell system.

Molecular size fractions were in the range of 30kDa and 100kDa. Firstly, the samples were filtered by 0.45 µm Millipore cellulose acetate membrane filters. Then, samples were

fractionated into different molecular size fraction such as 100 kDa and 30 kDa by using ultrafiltration stirred cell system and Millipore YM series cellulose membranes. The cell was run on a magnetic stirrer with 50 mL samples. A nitrogen gas tube equipped with a pressure control valve was attached to the stirrer reactor to provide the operating pressure inside the cell. Millipore YM series cellulose membrane filters with 25 mm diameter and with nominal molecular weight cutoffs 100 kDa and 30 kDa were used within stirred cell. At the beginning of each run, the membranes were kept in distilled deionized water for 15 minutes and then the cell was operated on a magnetic stirrer and run with 50 mL distilled deionized water. After use prior to storage YM membranes were washed with 0.1 M NaOH solution and stored in 10% ethanol/water solution at refrigerator. Fractionated humic acid solutions were stored in dark glass bottles at cold rooms.

3.3.4. Analytical Methods

3.3.4.1. UV-vis Spectroscopic Measurements. UV-vis absorption spectra were recorded on a Perkin Elmer Lamda 35 UV-vis double beam spectrophotometer employing Hellma quartz cuvettes of 1.0 cm optical path length. Humic acid samples will be characterized by UV-vis spectra. Absorbance values at 436 nm ($Color_{436}$), 365 nm (UV_{365}), 280 nm (UV_{280}), and 254 nm (UV_{254}) will be recorded for the evaluation of UV-vis parameters.

3.34.2. Fluorescence Measurements. Fluorescence spectra in the emission and synchronous scan modes were recorded on a Perkin Elmer LS 55 Luminescence Spectrometer equipped with a 150W Xenon arc lamp and a red sensitive photomultiplier tube using 1-cm path length quartz cells were used. A scan speed of 400 nm min^{-1} will be used with a slit width opening of 10 nm. Synchronous scan spectra was recorded in the excitation wavelength range of 200-600 nm excitation wavelength range using the bandwidth of $\Delta\lambda$=18 nm between the excitation and emission monochromators. The emission spectra was scanned over the range of 360-600 nm and 380-600 nm at excitation wavelength of 350 and 370 nm, respectively.

3.3.4.3. Non-Purgeable Organic Carbon (NPOC Analysis). Non-Purgeable Organic Carbon (NPOC) measurements of humic substances were performed on a Shimadzu TOC Vwp Total Organic Carbon Analyser. Calibration of the instrument was done using potassium hydrogen phthalate in the concentration range of 0-25 mg L^{-1}.

4. RESULTS AND DISCUSSIONS

In this study, the effect of Fe doping on TiO_2 on the photocatalytic degradation of humic acid in aqueous medium was investigated in comparison to the use of bare TiO_2. Batch adsorption experiments were also conducted to follow the surface interactions of molecular size fractions of humic acid onto TiO_2 surface, the results of which were evaluated using appropriate adsorption isotherms. The discussion part was based on the explanations of the complex interactions among the surface properties of titanium dioxide and the molecular size fractions of the humic acid.

Following material specification part, preliminary experiments were performed using humic acid solution under dark conditions and in the absence of photocatalyst. The dark experiments were performed in the presence of 0.25 mg mL^{-1} TiO_2 dose with raw humic acid (20 mg L^{-1}). After each run, UV-vis spectroscopy and fluorescence spectroscopy in emission and synchronous scan modes were used to analyze the humic acid samples. UV–vis parameters were described in terms of the absorbance values measured at the selected wavelengths as follows: absorbance values at 436 nm as $Color_{436}$, at 365 nm as UV_{365}, at 280 nm as UV_{280} and at 254 nm as UV_{254}. Emission scan fluorescence spectra was scanned in the range of 360-600 nm and 380-600 nm at excitation wavelength of 350 and 370 nm, respectively, Moreover, synchronous scan fluorescence spectra was recorded in the range of 200-600 nm excitation wavelength region.

In the second part, photocatalytic degradation of humic acid was performed with 0.25 mg mL^{-1} TiO_2 as the photocatalyst and experiments were conducted with different molecular size fractions such as 0.45 μm filtered fraction, 100 kDa fraction and 30 kDa fraction of humic acid solution. The humic acid fractions were photocatalytically degraded for certain reaction periods up to 60 minutes. The spectroscopic properties of each size fraction were characterized and compared with each other by UV-vis spectroscopy and fluorescence spectroscopy, the specified UV-vis and fluorescence parameters and DOC.

In the third part, batch adsorption experiments were conducted to determine the effects of molecular size dependent fractions of humic acid solution with various molecular size fractions of, namely 0.45 μm filtered fraction 100 kDa, and 30 kDa of 20 mg L^{-1} humic acid solution. Bare TiO_2 and Fe doped TiO_2 in the range of 0.1-1.0 mg mL^{-1} were used as adsorbents. After each run, humic acid samples were analyzed by UV-vis spectra and fluorescence spectra as well as by the specified UV-vis and fluorescence parameters and DOC.

In the last section, the effects of molecular size fractionation on the sorption properties and photodegradation of humic acid onto Fe doped TiO_2 in comparison to bare TiO_2 Degussa P-25 were evaluated.

4.1. Material Specification

4.1.1. Spectroscopic Analysis of Humic Acid and Its Molecular Size Fractions

The spectroscopic properties of humic acid and its molecular size fractions were characterized and compared by UV-vis spectroscopy and fluorescence spectroscopy in emission and synchronous scan modes.

4.1.1.1. UV-vis Spectroscopic Evaluation of Humic Acid and Its Molecular Size Fractions. UV-vis spectra of humic substances are commonly broad; they do not exhibit any obvious features and monotonously decrease with increasing wavelength (Schnitzer and Khan, 1972; Traina et al., 1990; Chen et al., 2002; Uyguner and Bekbölet, 2005a). UV-vis spectra of raw, 0.45μm filtered fraction, 100 kDa fraction and 30 kDa fraction of humic acid were presented in Figure 4.1.

Any wavelength within the range of λ = 220-280 nm has been considered as an appropriate region for humic acid quantification. Therefore, examination of the UV-vis spectral features both in the above specified region as well as in the 280-600 nm region holds importance (Matilanian et al., 2011). In general, the molar absorptivities could vary due to the presence of different ranges of chromophores present in the humic structure.

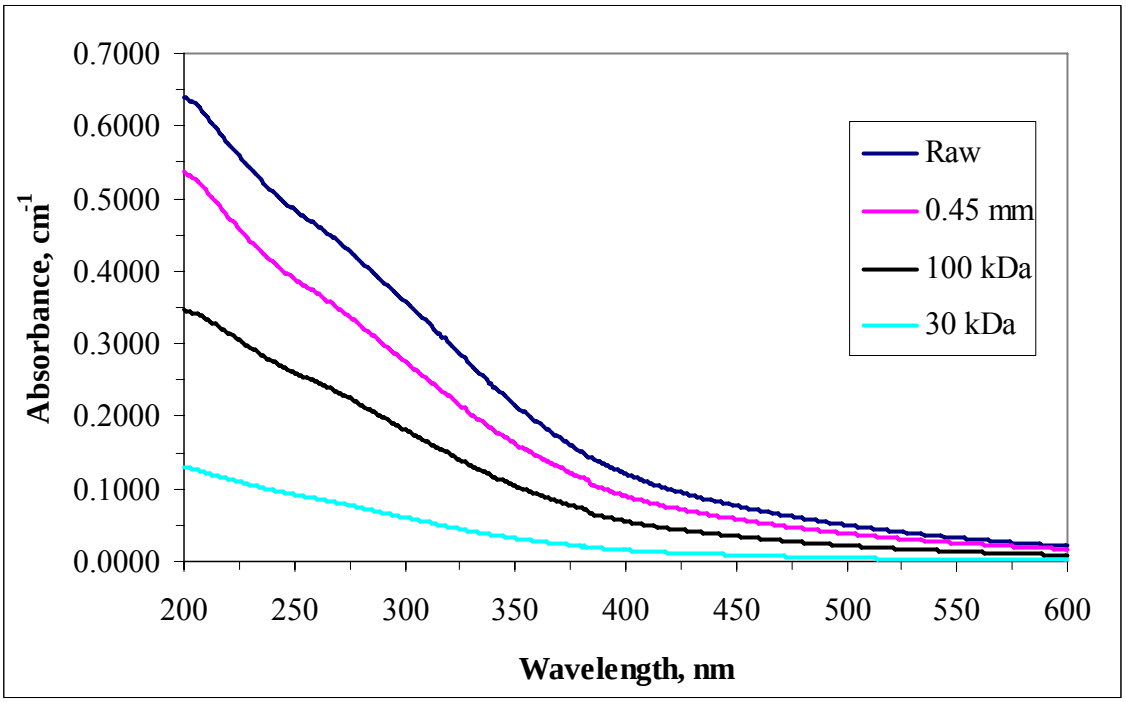

Figure 4.1. UV-vis spectra of raw, 0.45µm filtered fraction, 100 kDa fraction and 30 kDa fraction of humic acid.

UV-vis absorbance values of raw, 0.45µm filtered fraction, 100 kDa fraction and 30 kDa fraction of humic acid were measured between 200-600 nm wavelength region. As can be seen from Figure 4.1, UV-vis spectra of humic substances monotonously decrease with increasing wavelength. Also Figure 4.1 showed that raw humic acid had the highest absorbance values and 30 kDa fraction of humic acid had the lowest absorbance values for the spectral wavelength region. UV-vis absorbance values of different fractions of humic acids were followed an order as Raw > 0.45µm filtered fraction > 100 kDa fraction > 30 kDa fraction. The presented UV-vis profiles significantly express the molecular size differentiation of humic fractions by the observed decreasing trends in absorptivities.

It is known that the molecular size distribution profiles of the humic substances exhibit a general decreasing trend from high molecular size fractions to the lower molecular size fractions irrespective of the origin and source of the organic matter (Alberts et al., 2002). Similar results attained by other studies. Ülker (2008) and Degirmenci (2010) presented a gradually decreasing trend with decreasing molecular size fraction and examined that the absorbance values of 30 kDa fraction of humic acid recorded to be

significantly lower than other molecular size fractions at all wavelengths. Uyguner and Bekbolet (2005b) indicated that the decrease of the UV absorbing properties of each humic acid fraction could be a consequence of the distribution of the humic moieties with respect to the molecular size fractions. A similar trend could also be verified by the DOC contents of the raw and lower molecular size fractions.

4.1.1.2. Fluorescence Spectroscopic Evaluation of Humic Acid and Its Molecular Size Fractions. In this section fluorescence spectral changes of humic substances were analyzed. As a representative to the studied humic substances, both the emission and synchronous scan spectra of Aldrich humic acid were investigated in detail. Considering the complexity of the situation and to simplify the comparison of humic substances based on fluorescence properties, the use of emission wavelength at 350 and 370 nm were preferred throughout the study. This excitation wavelength at 350 nm has been widely used for similar studies in literature (Senesi, 1990; Hautala et al., 2000; Cho and Choi, 2002). Previous work, in the field of fluorescence spectroscopy for characterization of humic substances has established that they typically fluoresce in the excitation range of 300–400 nm and the emission range of 400–500 nm (Goslan et al., 2004).

Emission scan fluorescence spectra were scanned in the range of 360-600 nm and 380-600 nm at excitation wavelength of 350 and 370 nm, respectively. In Figure 4.2, it could be also easily observed that the emission scan spectra gave decreasing emission fluorescence intensity with decreasing molecular size fractions. The emission spectra for raw humic acid, 0.45μm filtered fraction, 100 kDa fraction and 30 kDa fraction of humic acid displayed a peak fluorescence emission intensity of irrespective of the excitation wavelength. On the other hand, the lowest emission fluorescence intensity is observed for 30 kDa fraction of humic acid. Similar results were obtained for the excitation wavelength of 370 nm as displayed in Figure 4.3. Comparatively lower intensities were recorded for the fluorescence spectra recorded by 370 nm excitation wavelength. The fluorescence spectra could also be considered as more broad and lacking a well defined peak profile. On the other hand, the fluorescence peaks for raw and 30 kDa fractions displayed the same difference of $\Delta FI = 40$ for the same emission wavelength of 450 nm.

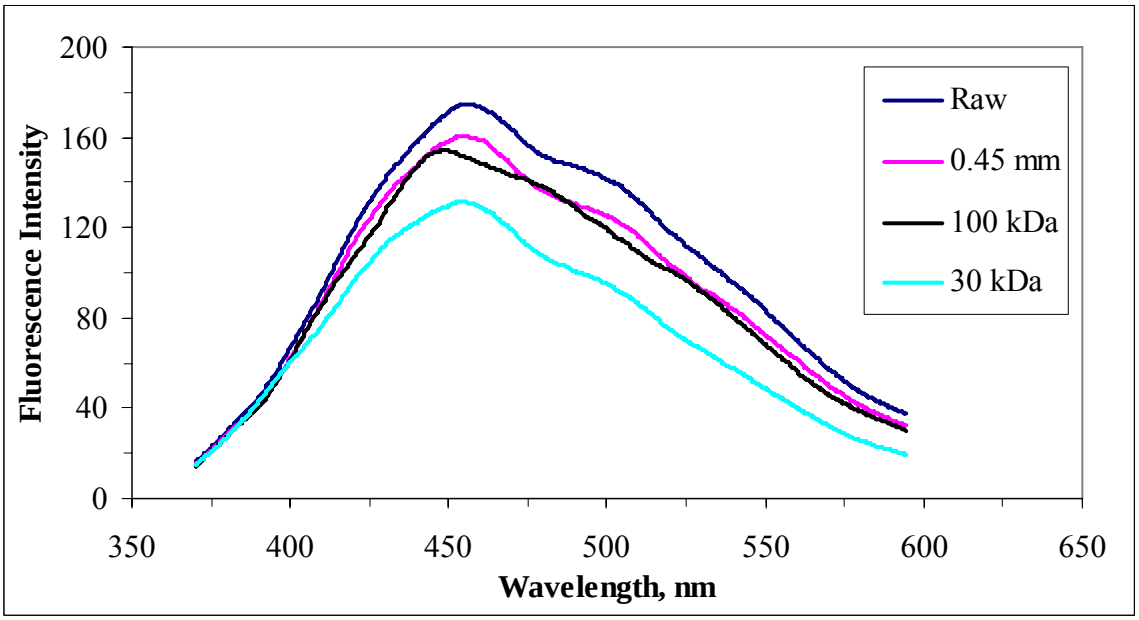

Figure 4.2. Emission scan fluorescence spectra ($FI_{emis\ 350}$) of raw, 0.45µm filtered fraction, 100 kDa fraction and 30 kDa fraction of humic acid.

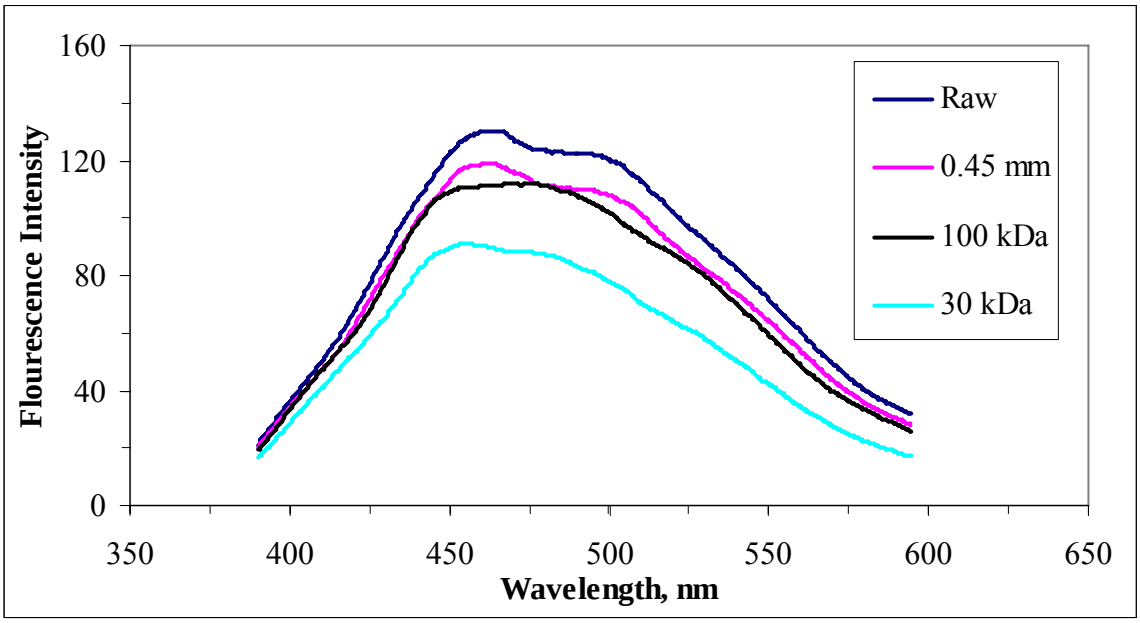

Figure 4.3. Emission scan fluorescence spectra ($FI_{emis\ 370}$) of raw, 0.45µm filtered fraction, 100 kDa fraction and 30 kDa fraction of humic acid.

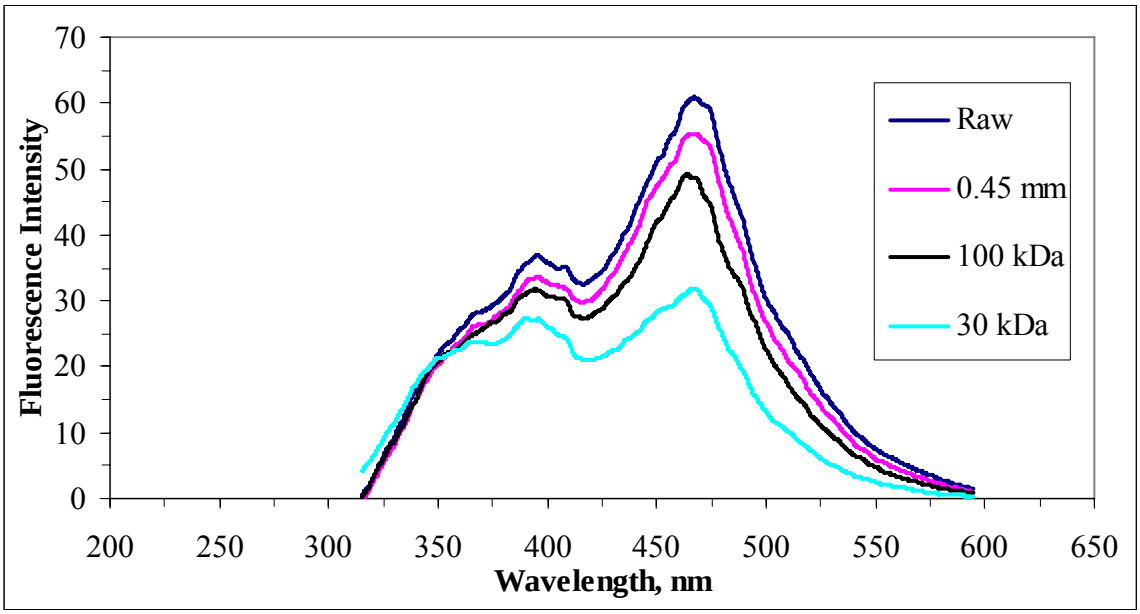

Figure 4.4. Synchronous scan fluorescence spectra of raw, 0.45µm filtered fraction, 100 kDa fraction and 30 kDa fraction of humic acid.

Synchronous scan fluorescence spectra were recorded in the excitation wavelength range of 320-600 nm excitation wavelength range as seen in Figure 4.4. In order to be comparable with literature results, $\Delta\lambda$ was chosen as 18 nm throughout this study (Senesi, 1990; Rivero et al., 1998; D'Orazio et al., 1999; Peuravuori et al., 2002). The fluorescence spectra of raw humic acid, 0.45µm filtered fraction, 100 kDa fraction and 30 kDa fraction of humic acid recorded by using synchronous scan mode displayed two peak regions at around 400 nm and 470 nm. Another study supported to this study examined by Degirmenci, (2010) that explained same result in terms of peak region. Further, the synchronous scan fluorescence spectra gave decreasing fluorescence intensities with respect to the decreasing molecular size fraction.

4.1.1.3. Specific Parameters of Humic Acid. UV–vis parameters were described in terms of the absorbance values measured at the selected wavelengths as follows: absorbance values at 436 nm as $Color_{436}$, at 365 nm as UV_{365}, at 280 nm as UV_{280} and at 254 nm as UV_{254}. The absorbance values measured at 254 nm (UV_{254}) and 280 nm (UV_{280}) are known to explain aromaticity removal, whereas absorbance measurement at 436 nm is used to monitor decolorization. Furthermore, specific UV absorbance ($SUVA_{254}$, m^{-1} $mg^{-1}L$) was

used to represent DOC normalized aromatic moieties and specific color absorbance ($SCoA_{436}$, m^{-1} $mg^{-1}L$) was defined as $Color_{436}$/DOC to signify organic carbon normalized color forming moieties. $SUVA_{365}$ was also calculated in a similar fashion as the ratio of the UV_{365} absorbing species to DOC. All of the specific parameters for raw, 0.45 μm filtered fraction, 100 kDa fraction and 30 kDa fraction of humic acid were presented in Table 4.1

Table 4.1. Specific parameters of raw, 0.45μm filtered fraction, 100 kDa fraction and 30 kDa fraction of humic acid.

Humic Acid	Raw	0.45μm f.f.*	100kDa f**	30kDa f**
UV-vis spectral parameters				
$Color_{436}$, m^{-1}	8.61	6.56	3.94	1.03
UV_{365}, m^{-1}	18.10	13.71	8.70	2.61
UV_{280}, m^{-1}	41.40	32.47	21.59	7.40
UV_{254}, m^{-1}	47.59	38.12	25.48	8.99
Fluorescence spectral parameters				
$FI_{emis\ 350}$	174.96	160.37	151.37	131.55
$FI_{emis\ 370}$	129.92	118.70	111.06	90.19
FI_{syn}	59.17	53.53	44.90	29.42
Dissolved organic carbon				
DOC, mg L^{-1}	6.039	5.739	2.925	1.005
Derived parameters : $SCoA_{436}$, $SUVA_{365}$, $SUVA_{280}$, $SUVA_{254}$ (m^{-1} mg^{-1} L) SFI_{emiss}, SFI_{syn} (cm^{-1} mg^{-1} L)				
$SCoA_{436}$	1.426	1.143	1.347	1.025
$SUVA_{365}$	2.997	2.389	2.974	2.597
$SUVA_{280}$	6.855	5.657	7.381	7.363
$SUVA_{254}$	7.880	6.642	8.711	8.945
$SFI_{emis\ 350}$	28.97	27.94	51.75	130.9
$SFI_{emis\ 370}$	21.51	20.68	37.97	89.74
SFI_{syn}	9.798	9.327	15.35	29.27

***** filtered fraction, ** fraction

The order of $Color_{436}$ was shown as; Raw > 0.45 μm filtered fraction > 100 kDa fraction > 30 kDa fraction as expected. The same order was also observed for other UV-vis spectral parameters, such as; UV_{365}, UV_{280} and UV_{254}. $SCoA_{436}$, $SUVA_{365}$, $SUVA_{280}$ and $SUVA_{254}$ values for raw humic acid were found to be 1.426, 2.997, 6.855, 7.880, respectively. The specific UV absorbance ($SUVA_{254}$) parameter can be used to describe the composition of humic material in terms of hydrophobicity and hydrophilicity, $SUVA_{254}$ >4 indicates mainly hydrophobic and especially aromatic moieties while a $SUVA_{254}$ <4 represents a hydrophilic organic fraction (Edzwald et al, 1985). In table 4.1, the calculated $SUVA_{254}$ was found greater than 4. Furthermore, 30 kDa fraction of humic acid acquired the highest $SUVA_{254}$ value whereas 0.45 μm filtered fraciton of humic acid had lowest $SUVA_{254}$ value. For SFI_{emis} parameters, the order was 30 kDa fraction > 100 kDa fraction> Raw > 0.45 μm filtered fraction. Same order was observed in terms of SFI_{syn}.

4.2. Photocatalytic Degradation of Humic Acid

4.2.1. Preliminary Experiments

Preliminary experiments were performed under dark conditions and in the absence of the photocatalyst in order to evaluate the interactions between humic acid-UV radiation and humic acid-TiO_2 as photocatalyst.

4.2.1.1. Experiments Carried Out Under Dark Conditions. The experiment was carried out using 20 mg L^{-1} humic acid solution in the presence of 0.25 mg mL^{-1} bare TiO_2 and 0.25 mg mL^{-1} Fe doped TiO_2 under dark conditions**.** Removal of humic acid was followed for certain reaction periods ranging from the start of the experiment to 60 minutes. UV-vis spectra of the samples attained by preliminary experiments using raw humic acid and TiO_2 binary system in the absence of light were shown in Figures 4.5 and 4.6

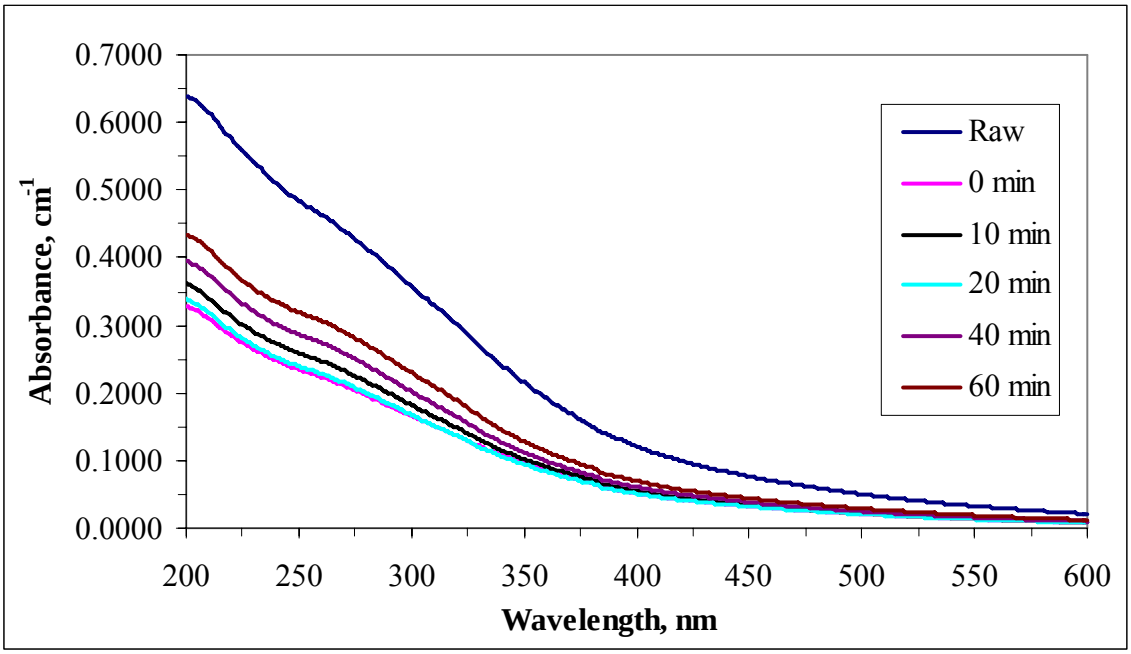

Figure 4.5. UV-vis spectra of preliminary experiments of raw humic acid under dark conditions in the presence of bare TiO_2.

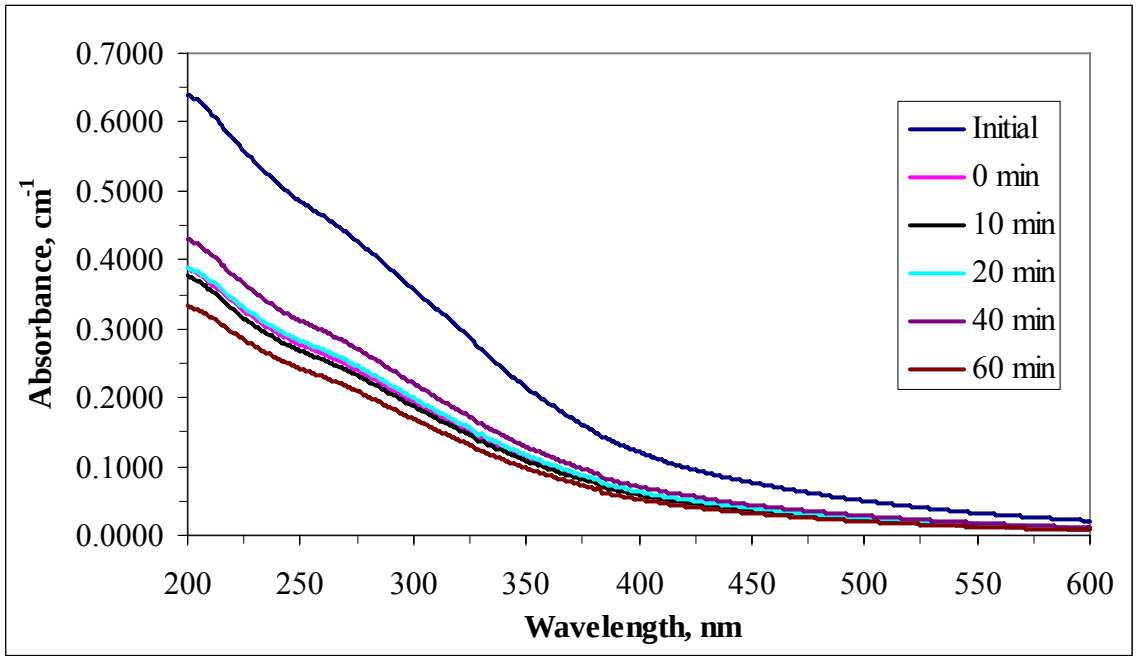

Figure 4.6. UV-vis spectra of preliminary experiments of raw humic acid under dark conditions in the presence of Fe doped TiO_2.

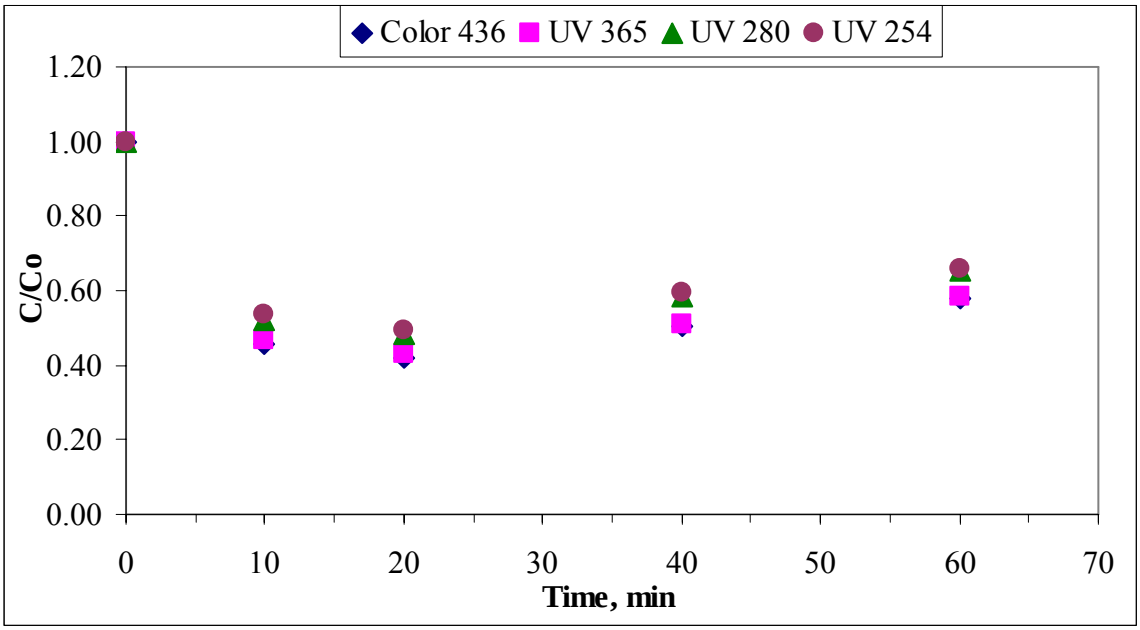

Figure 4.7. Normalized $Color_{436}$, UV_{365}, UV_{280} and UV_{254} values with respect to time in the presence of bare TiO_2.

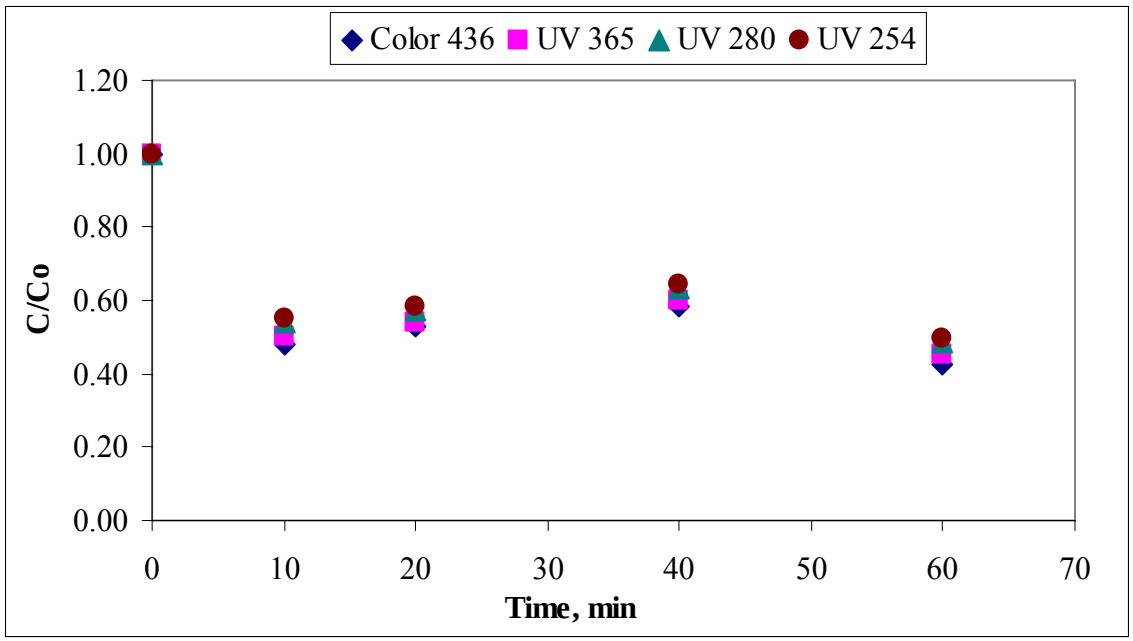

Figure 4.8. Normalized $Color_{436}$, UV_{365}, UV_{280} and UV_{254} values with respect to time in the presence of Fe doped TiO_2.

UV-vis absorbance values were measured between 200-600 nm wavelength region. It was observed that UV-vis spectra of humic acids monotonously decreased with increasing wavelength in a broad and featureless trend. However, no significant trend could be observed with respect to time (Figure 4.5 and 4.6).

As illustrated in Figures 4.7 and 4.8, normalized fractions of the UV-vis parameters as $Color_{436}$ and UV_{254} were found to be significantly lower for the initial stages of reaction periods. Under irradiation period of 40 min, an increasing trend in the normalized fraction of the UV-vis parameters was observed. The overall phenomena could be explained by the prevailing time dependent adsorption-desorption process throughout the whole duration of the reaction. The mechanism could also be explained by the interaction oxide surface and color forming moieties as well as the UV absorbing centers. The removal trend followed the sequence of $Color_{436}>UV_{365}>UV_{280}>UV_{254}$ irrespective of the reaction period. The removal percentages for $Color_{436}$ and UV_{254} obtained from dark reactions of humic acid in the presence of 0.25 mg mL^{-1} bare TiO_2 were resulted with 42% and 34%, respectively at the end of 60 minutes.

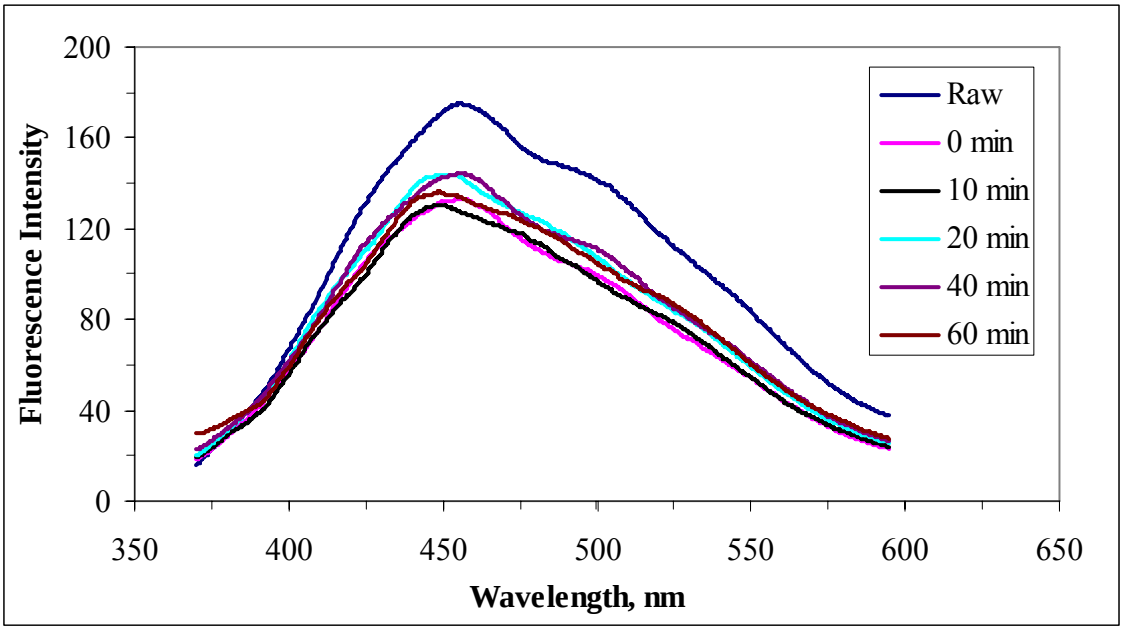

Figure 4.9. Emission scan fluorescence spectra ($FI_{emis\ 350}$) of raw humic acid during preliminary experiments conducted under dark conditions in the presence of bare TiO_2.

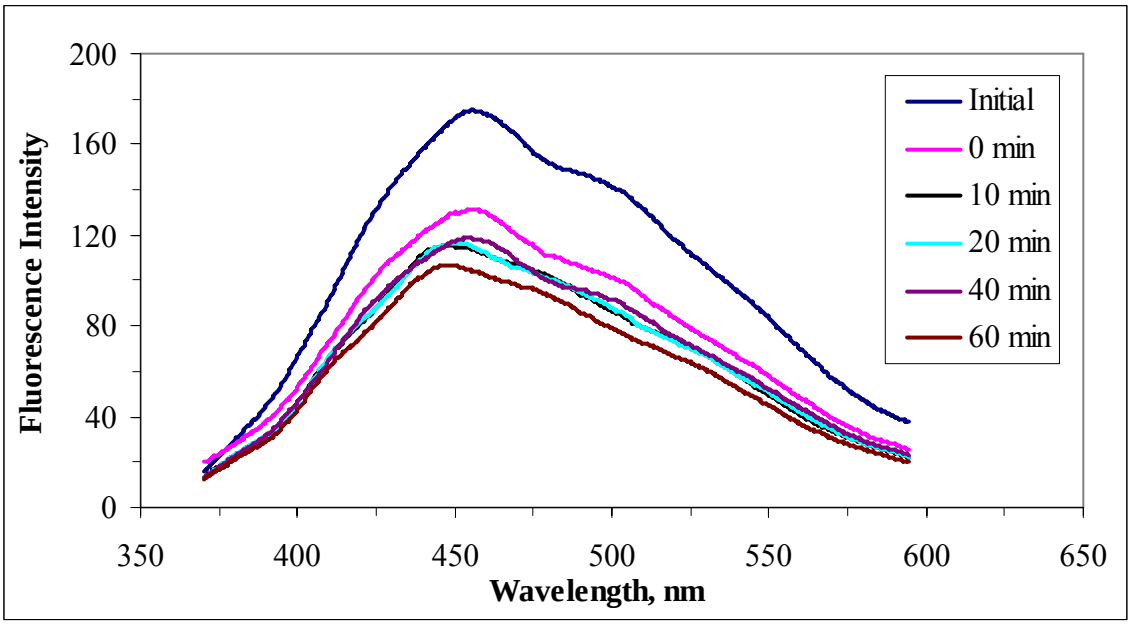

Figure 4.10. Emission scan fluorescence spectra ($FI_{emis\ 350}$) of raw humic acid during preliminary experiments conducted under dark conditions in the presence of Fe doped TiO_2.

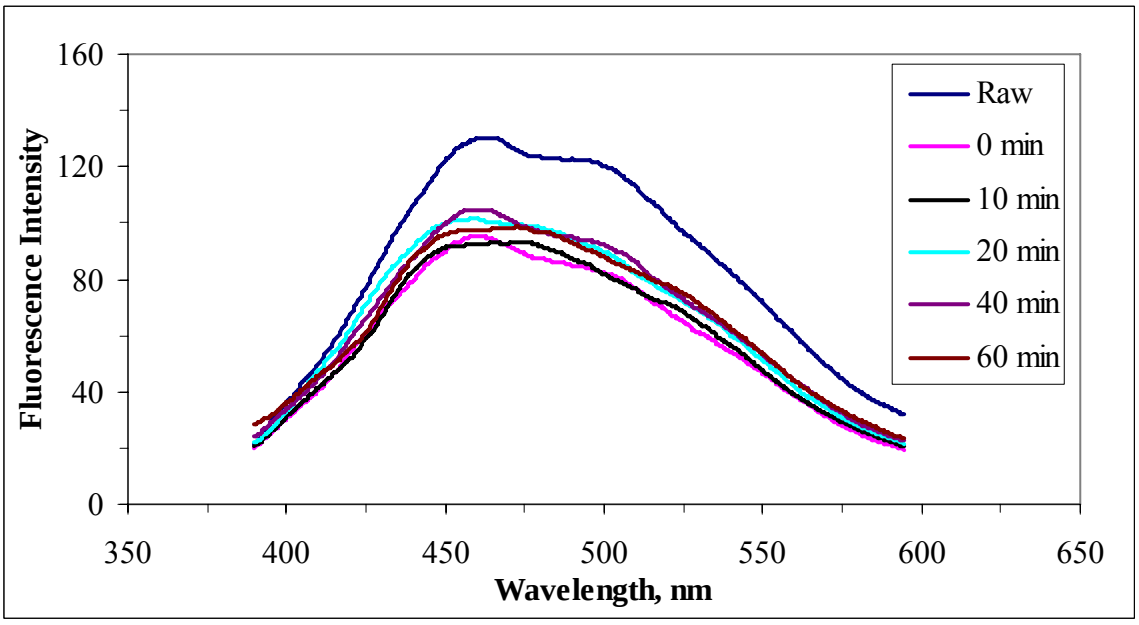

Figure 4.11. Emission scan fluorescence spectra ($FI_{emis\ 370}$) of raw humic acid during preliminary experiments conducted under dark conditions in the presence of bare TiO_2.

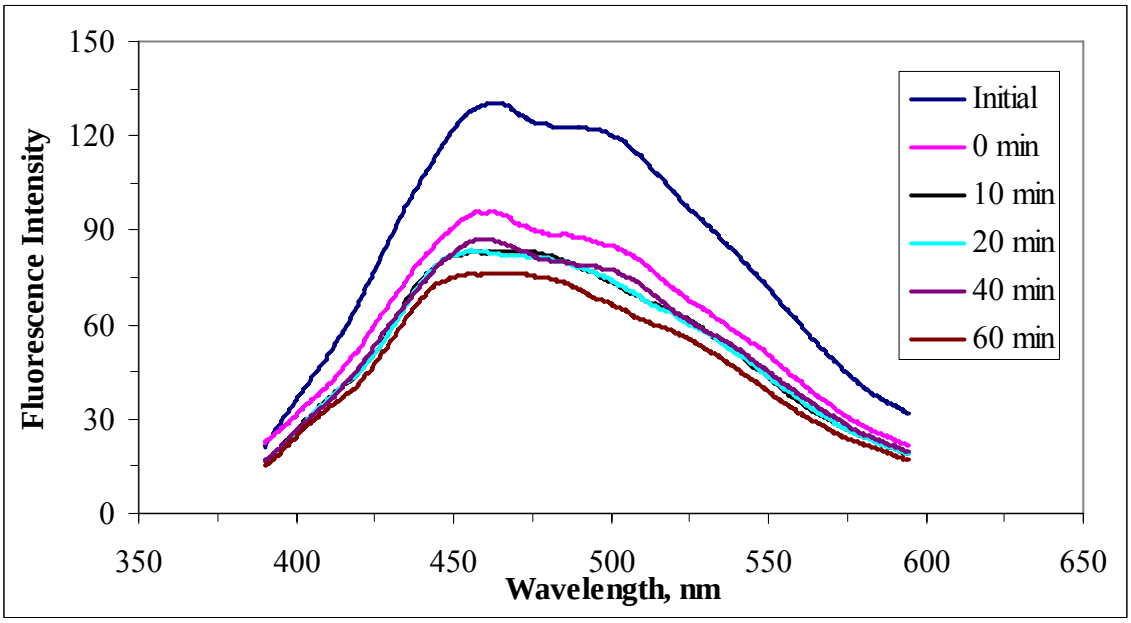

Figure 4.12. Emission scan fluorescence spectra ($FI_{emis\ 370}$) of raw humic acid during preliminary experiments conducted under dark conditions in the presence of Fe doped TiO_2.

The removal percentages for $Color_{436}$ and UV_{254} obtained from dark reactions of humic acid in the presence of 0.25 mg mL^{-1} Fe doped TiO_2 were resulted with 57 % and 50 %, respectively at the end of 60 minutes.

Emission scan fluorescence spectra were recorded in the range of 360-600 nm and 380-600 nm at excitation wavelengths of 350 and 370 nm, respectively, for fluorescence spectroscopic evaluation of raw humic acid in the presence bare TiO_2 and Fe doped TiO_2 (Figure 4.9, Figure 4.10, Figure 4.11 and Figure 4.12). From a broader perspective the emission scan fluorescence spectra displayed a similar trend irrespective of any reaction period and photocatalyst type. A major peak was observed at 450 nm wavelength under all conditions. It can be concluded that at all time periods, spectral trends were found to be nearly overlapping and exhibiting almost the same fluorescence intensity values during 60 minutes except raw humic acid solution. In a similar manner to the UV-vis spectral evaluation, an average decrease in fluorescence intensity due to adsorption could be expressed irrespective of the reaction period. More specifically, the role of the photocatalyst type could be visualized by the recorded different fluorescence intensities

with respect to irradiation time irrespective of the excitation wavelength (350 nm or 30 nm).

Synchronous scan fluorescence spectra recorded for the preliminary experiments of humic acid were shown in Figures 4.13 and 4.14. Synchronous scan spectra were recorded in the range of 300-600 nm excitation wavelength region. The synchronous scan fluorescence spectra for raw humic acid displayed a sharp peak around wavelength of 470 nm. Except for the spectra recorded for raw humic acid, the synchronous fluorescence spectra displayed an overlapping trend irrespective of the reaction period. However in the presence of Fe doped TiO_2, the recorded fluorescence intensities displayed time dependent differences. At the end of the 60 min reaction period, comparatively lower F.I. was recorded upon employment of Fe doped TiO_2.

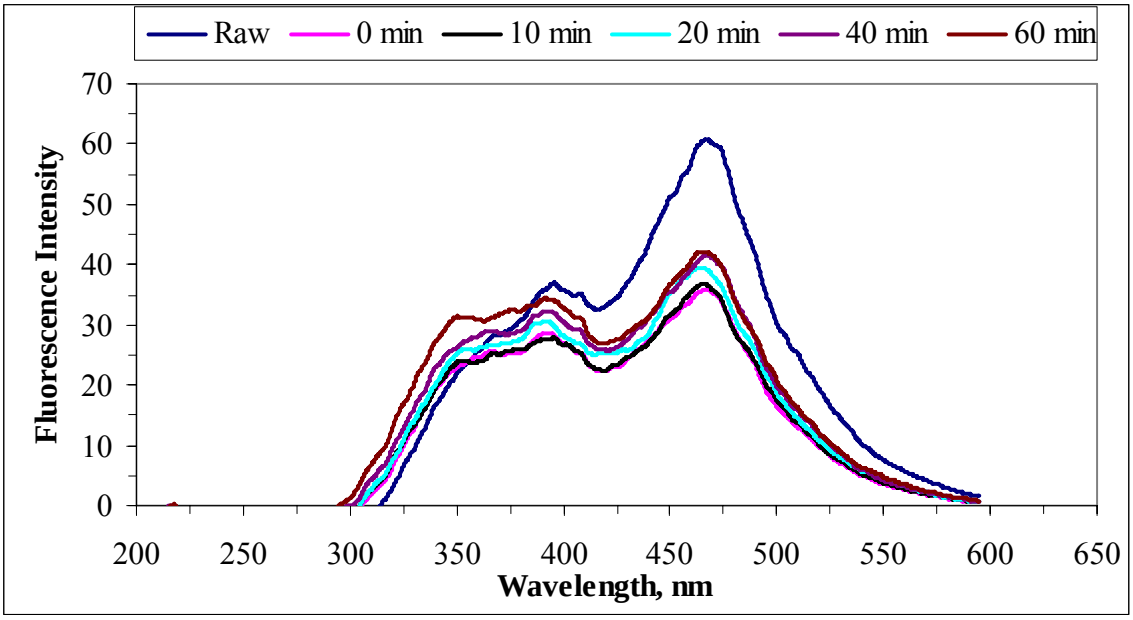

Figure 4.13. Synchronous scan fluorescence spectra of raw humic acids during preliminary experiments conducted under dark conditions in the presence of bare TiO_2.

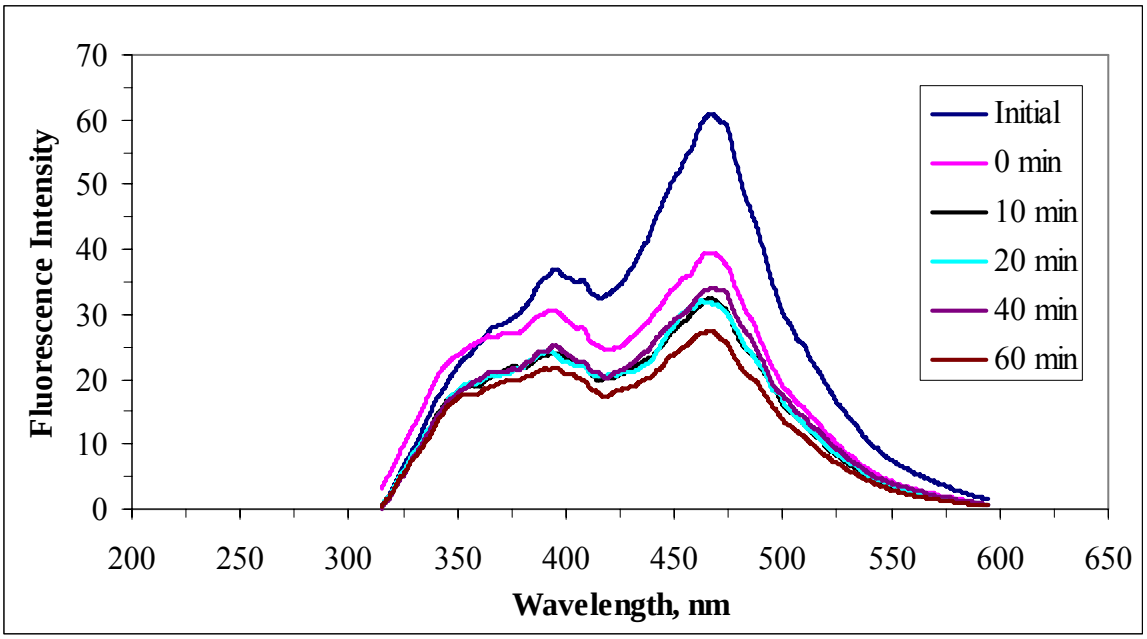

Figure 4.14. Synchronous scan fluorescence spectra of raw humic acids during preliminary experiments conducted under dark conditions in the presence of Fe doped TiO_2.

4.2.1.2. Experiments Carried Out in the Absence of TiO_2. The experiments were performed using 20 mg L^{-1} humic acid solutions in the absence of TiO_2 to evaluate the effect of light intensity on humic acid. Experiments were carried out for certain reaction periods ranging from the start of the experiment (t=0) to 60 minutes.

The UV-vis spectra were recorded between 200-600 nm wavelength regions for UV-vis spectroscopic evaluation of raw humic acid during preliminary experiments in the absence of TiO_2. It can be seen from Figure 4.15 that there was no significant absorbance difference with increasing time and all trends were found to be in an overlapping trend ($\leq$ 5 %).

The emission wavelength region of the BLF lamp is reported as 300-400 nm. Therefore, the light intensity active on humic acid solution could be considered as non-reactive as could also be verified by the recorded UV-vis spectra (Figure 4.15). The observed non-reactivity basically explained the exclusion of the photolytic degradation of humic moieties.

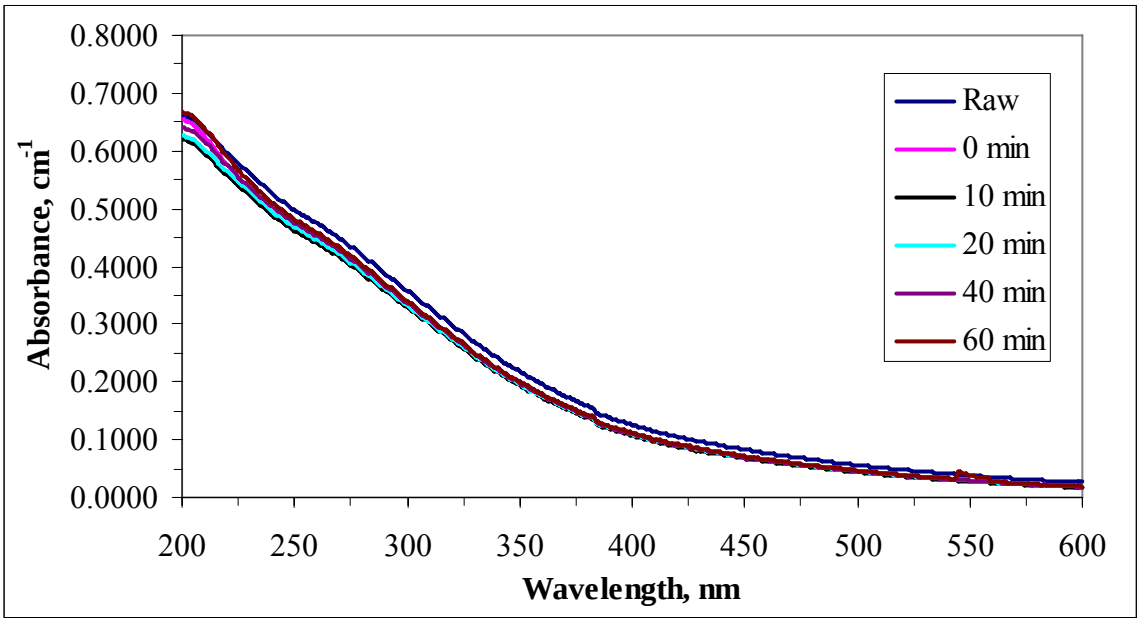

Figure 4.15. UV-vis spectra of preliminary experiments of raw humic acid in the absence of TiO_2.

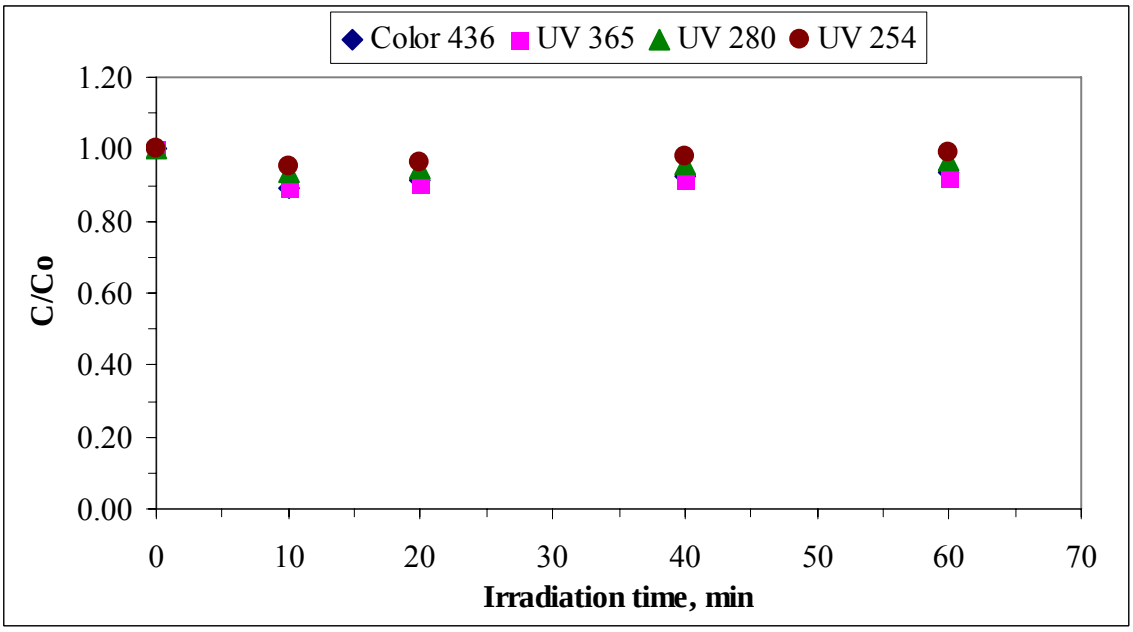

Figure 4.16. Normalized $Color_{436}$, UV_{365}, UV_{280} and UV_{254} values with respect to time in the absence of TiO_2.

As illustrated in Figure 4.16, normalized fractions of $Color_{436}$ and UV_{254} were found to be nearly the same. The removals of $Color_{436}$, UV_{365}, UV_{280} and UV_{254} obtained through light absorption of humic acid solution in the absence of TiO_2 were found to be with 7%, 8%, 3% and 1%, respectively at the end of 60 minutes as shown in Figure 4.16. Değirmenci (2010) reported similar removal results with respect to the irradiation time in the absence of TiO_2. The observed non reactivity of humic acid under BLF irradiation forms the basis of degradation mechanism taking place through solely photocatalytic pathway and contribution of photolysis could be regarded as insignificant as previously stated.

Emission scan fluorescence spectra were scanned in the range of 360-600 nm and 380-600 nm at excitation wavelength of 350 and 370 nm, respectively, for fluorescence spectroscopic evaluation of raw humic acid in the absence of TiO_2 (Figure 4.17 and Figure 4.18).

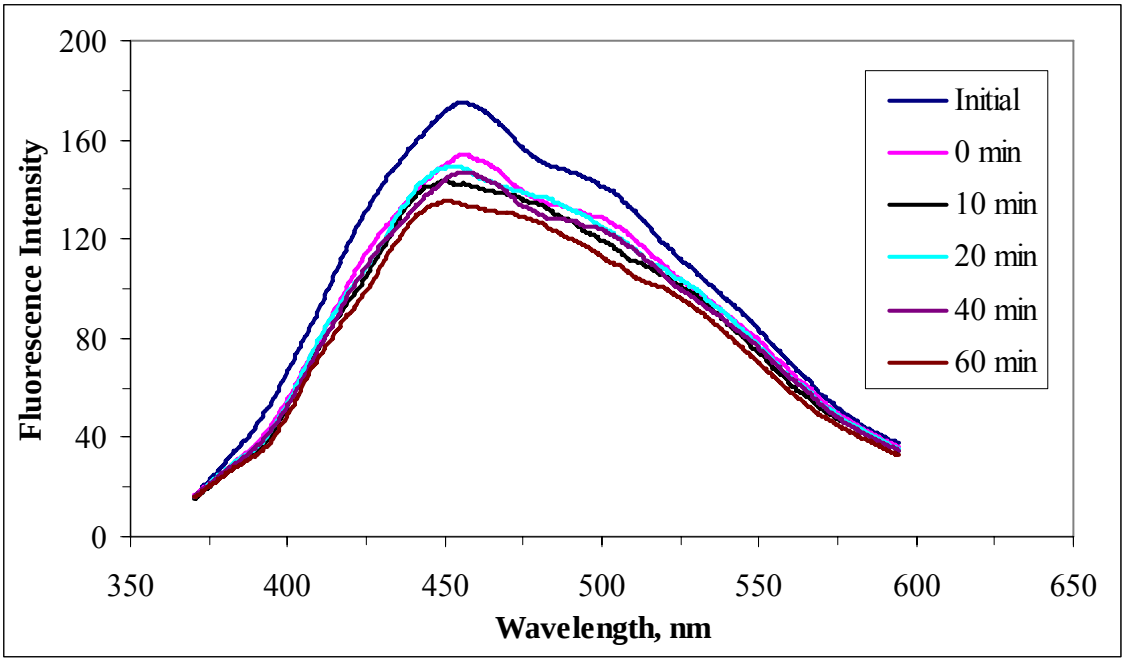

Figure 4.17. Emission scan fluorescence spectra ($FI_{emis\ 350}$) of preliminary experiments conducted in the absence of TiO_2.

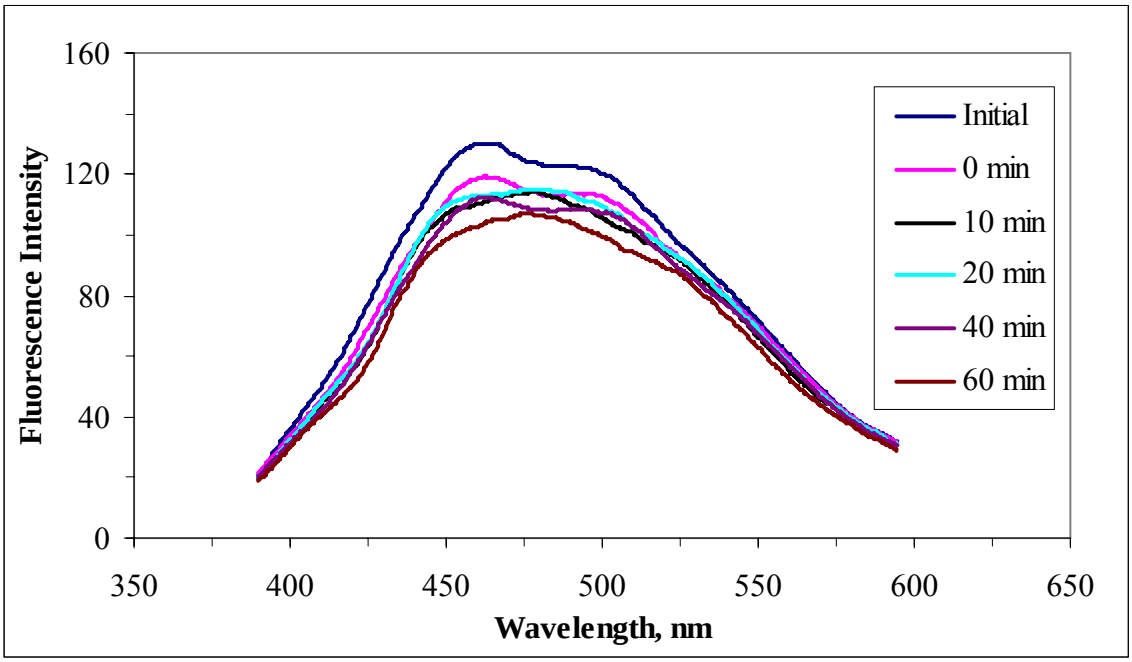

Figure 4.18. Emission scan fluorescence spectra ($FI_{emis\ 370}$) of preliminary experiments conducted in the absence of TiO_2.

Emission fluorescence spectra of humic acid samples recorded by using fluorescence scan mode displayed a peak irrespective of irradiation period. Peuravuori and co-workers ascribe the maximum around 460 nm to polycyclic aromatics consisting of seven fused benzene rings (Peuravuori et al, 2002). The observed differences in fluorescence intensity could be explained by the possible rearrangement of the fluorophoric groups upon excitation.

Synchronous scan fluorescence scan spectra of raw humic acid during preliminary experiments conducted in the absence of TiO_2 shown in Figure 4.19. The characteristic sharp peak in the region of 470 nm of raw humic acid and the moderate peak around 400 nm displayed an insignificant decrease in fluorescence intensity with respect to the irradiation time. It could be stated that no significant change in the trend of synchronous scan fluorescence spectra of humic acid could be attained upon preliminary experiments conducted in the presence of light intensity and in the absence of TiO_2.

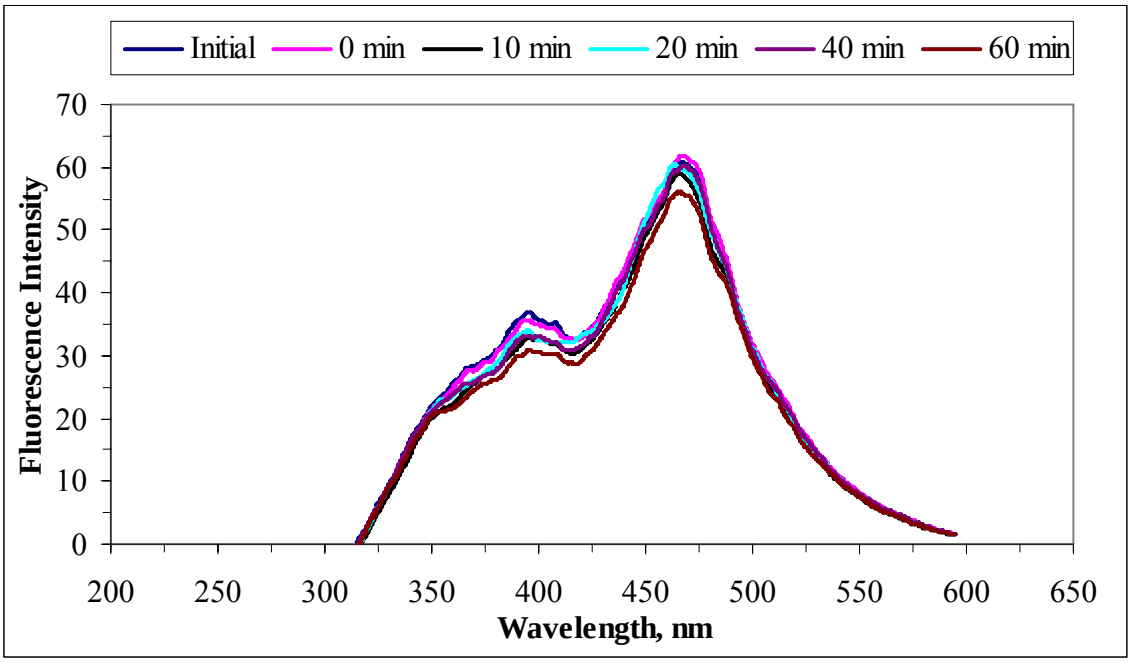

Figure 4.19. Synchronous scan fluorescence spectra of preliminary experiments conducted in the absence of TiO_2.

4.3. Photocatalytic Degradation of Humic Acid and its Molecular Size Fractions in the Presence of Bare TiO_2

Photocatalytic degradation of humic acid was conducted in the presence of 0.25 mg mL^{-1} bare TiO_2. Post oxidation characterization of the humic acid and its molecular size fractions *i.e.* 0.45 µm filtered fraction, 100 kDa fraction and 30 kDa fractions were assessed with respect to their UV-vis spectroscopic and fluorescence spectroscopic properties.

4.3.1. Photocatalytic Degradation of Raw Humic Acid in the Presence of Bare TiO_2

Spectroscopic properties of raw humic acid was characterized and compared by UV-vis spectroscopy and selected absorbance values at 436 nm as $Color_{436}$, 365 nm as UV_{365}, 280 nm as UV_{280}, 254 nm as UV_{254} and fluorescence spectroscopy in emission and synchronous scan modes in the range of 360-600 nm and 380-600 nm at excitation wavelength of 350 and 370 nm, respectively.

4.3.1.1. UV-vis Spectroscopic Evaluation of Raw Humic Acid During Photocatalytic Degradation. UV-vis absorbance values were measured between 200-600 nm wavelength region. As already mentioned previously, following photocatalytic treatment, UV-vis spectra of all of the humic acid samples displayed a broad, featureless and monotonously decreasing trend with respect to increasing wavelength. A representative example of the time dependent UV-visible spectra was given for the photocatalytic degradation of humic acid (Figure 4.20). It can be seen that the absorbance values showed decreasing trend with increasing irradiation time. Also, it could be easily noticed that, there were no significantly characteristic absorbance recordings after 500 nm wavelength as observed by the decolorization of the humic solutions. The significant decrease recorded for t=0 condition could be explained by the initial-adsorptive removal as was also verified by the preliminary experiments performed under dark conditions.

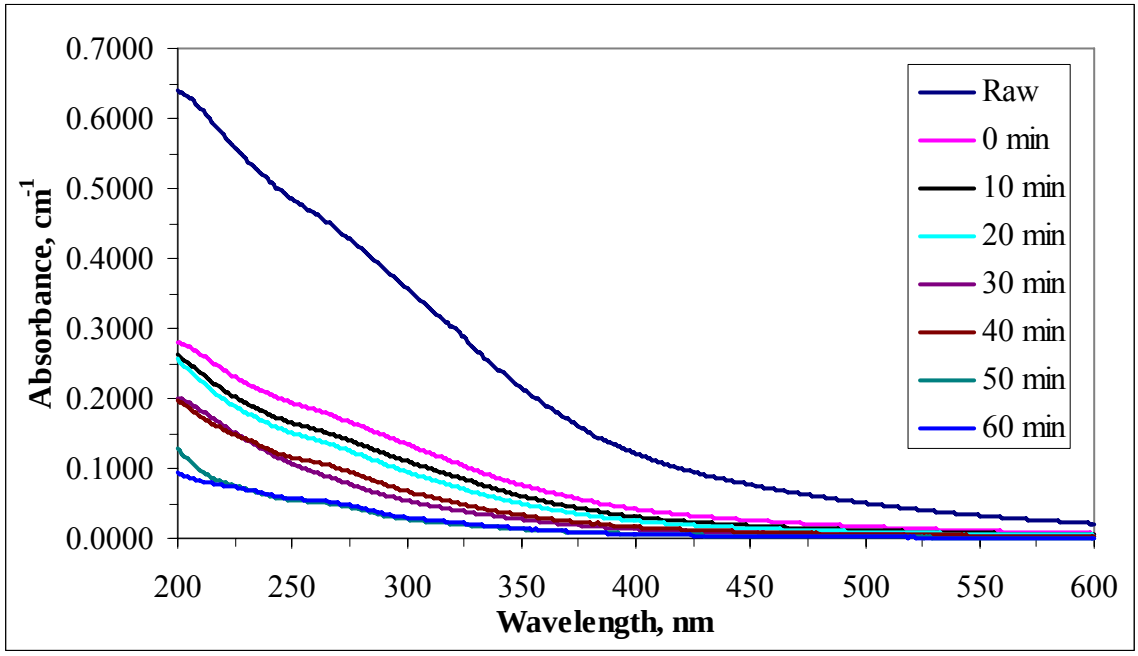

Figure 4.20. UV-vis spectra of raw humic acid during photocatalytic degradation in the presence of bare TiO_2.

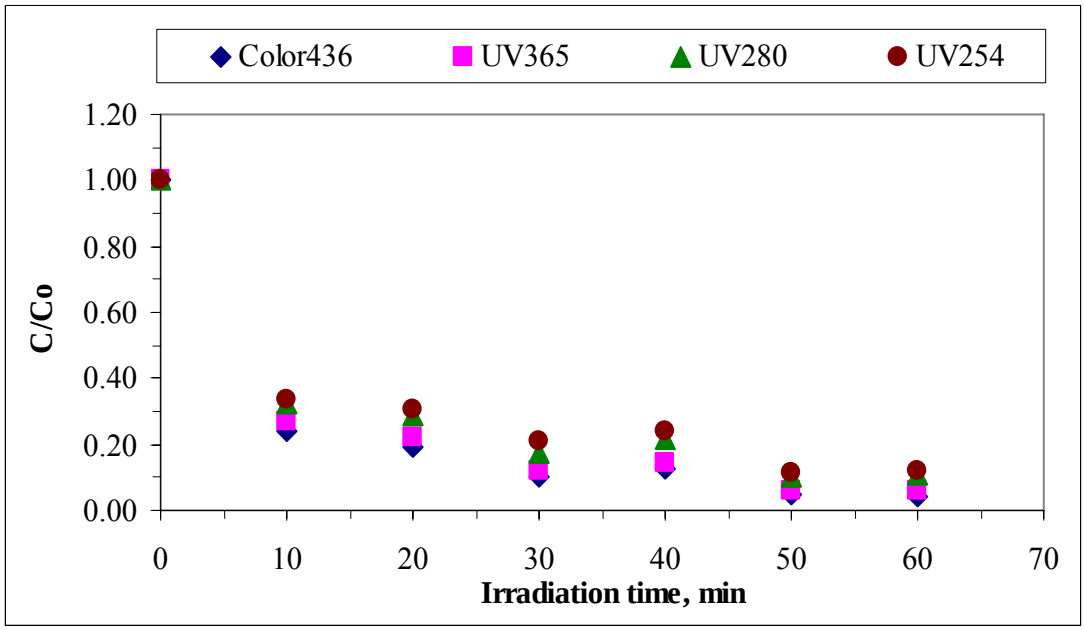

Figure 4.21. Normalized $Color_{436}$, UV_{365}, UV_{280}, UV_{254} values of raw humic acid with respect to irradiation time in the presence of bare TiO_2.

Photocatalytic degradation of raw humic acid in the presence of bare TiO_2 were also evaluated in terms of UV-vis parameters as expressed by $Color_{436}$, UV_{365}, UV_{280} and UV_{254} (Figure 4.21). Initial adsorptive removal efficiencies of raw humic acid were 66%, 65%, 61% and 60% for $Color_{436}$, UV_{365}, UV_{280} and UV_{254}, respectively. The general decreasing trend detected for all of the UV-vis parameters as shown in Figure 4.20. While 76% of $Color_{436}$ was removed in 10 minutes of irradiation, 96% removal was achieved after 60 minutes. The removal efficiencies followed a basic trend of $Color_{436} > UV_{365} > UV_{280} > UV_{254}$ irrespective of the irradiation time.

4.3.1.2. Fluorescence Spectroscopic Evaluation of Raw Humic Acid During Photocatalytic Degradation. Fluorescence spectra of all of the studied humic acid samples were characterized by broad peaks the intensities of which relatively decrease with increasing photocatalytic irradiation time.

Emission scan fluorescence spectra of humic acid samples were displayed in Figures 4.22 and 4.23. The emission scan fluorescence spectra were scanned over the wavelength range of 360-600 nm and 380-600 nm at excitation wavelength of 350 and 370

nm, respectively. The effect of the excitation wavelength on the fluorescence intensity of raw humic acid could also be observed most significantly in the 450 nm under oxidative conditions. In general, it could be said that the emission scan spectra displayed decreasing emission fluorescence intensity with respect to the irradiation time. However, the maximum fluorescence intensity was observed for 20 minutes of irradiation time. This condition also was observed at excitation wavelength of 370 nm. Both of the fluorescence spectra revealed the significance of the emission wavelength of 450 nm by displaying a peak that could still be distinguishable for longer irradiation period of 60 min. However, a slight shift to shorter wavelengths (~5 nm) could also be visualized displaying an insignificant decrease in fluorescence intensity in comparison to the fluorescence intensity recorded for emission wavelength of 450 nm.

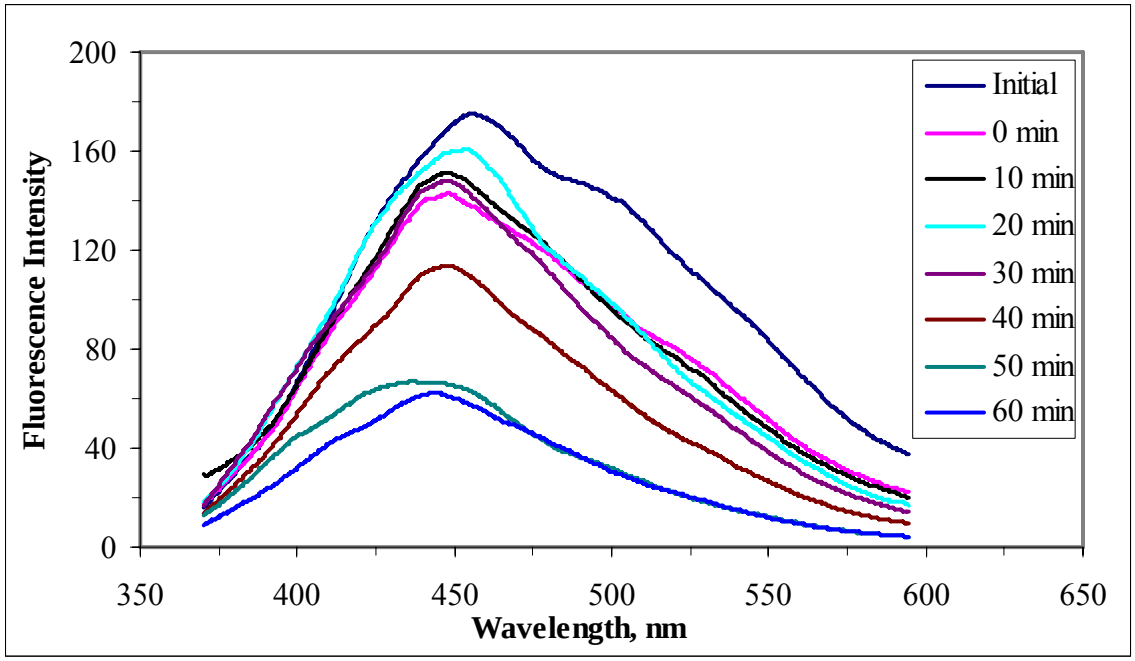

Figure 4.22. Emission scan fluorescence spectra ($FI_{emis\ 350}$) of raw humic acid during photocatalytic degradation (Initial represents raw humic acid).

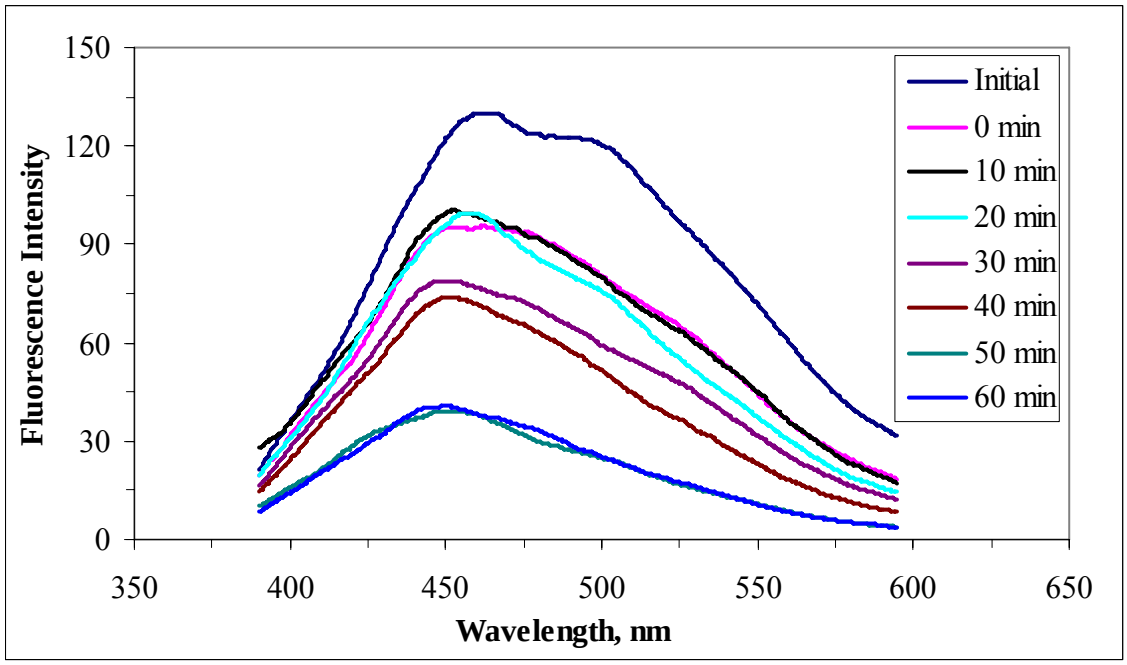

Figure 4.23. Emission scan fluorescence spectra ($FI_{emis\ 370}$) of raw humic acid during photocatalytic degradation (Initial represents raw humic acid).

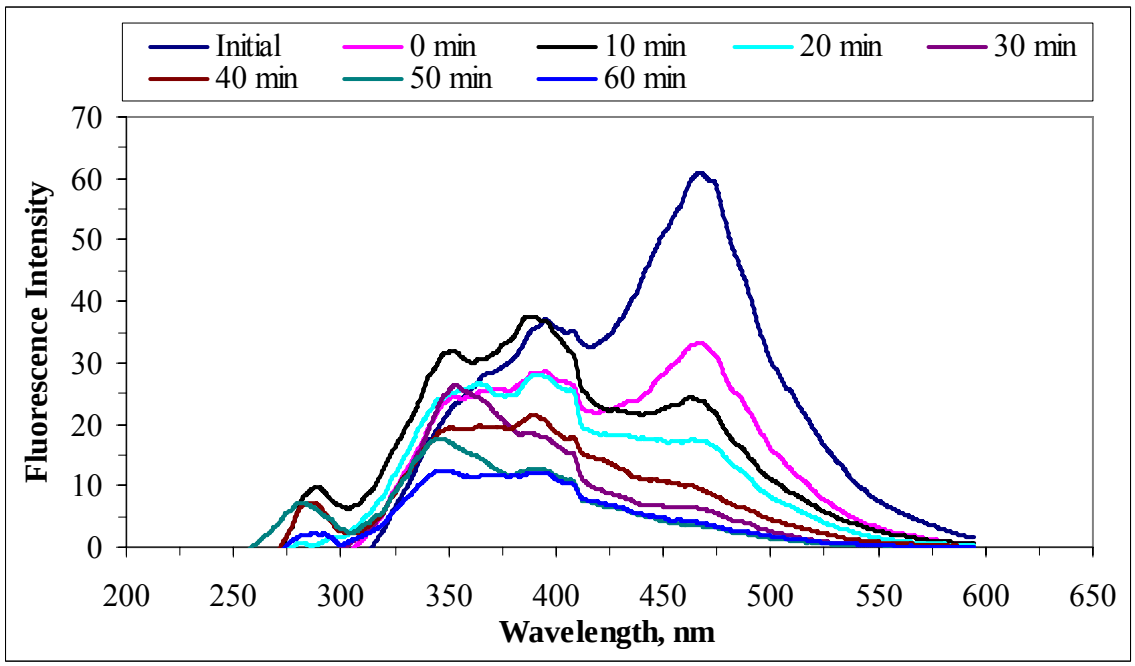

Figure 4.24. Synchronous scan fluorescence spectra of raw humic acid during photocatalytic degradation (Initial represents raw humic acid).

Synchronous scan fluorescence spectra for raw humic acid were shown in Figure 4.24. Two main fluorescence peaks were recorded at 350 nm and 470 nm wavelengths. Raw humic acid displayed a sharp peak around 470 nm for initial conditions of irradiation periods. The fluorescence intensity of the main peak recorded at 450 nm emission wavelength diminished after 20 min of irradiation time. Moreover, the synchronous scan fluorescence spectra displayed an inconsistent trend with respect to the irradiation periods. Upon irradiation period of 60 min, the shape of the fluorescence spectra could be visualized as representing an irregular area devoid of any significant peak.

4.3.2. Photocatalytic Degradation of 0.45µm Filtered Fraction of Humic Acid in the Presence of Bare TiO_2

Photocatalytic degradation of 0.45µm filtered fraction of humic acid samples were performed using bare TiO_2 and oxidative degradation of humic acid was followed by UV-vis spectra and fluorescence spectra recorded in emission scan and synchronous modes.

4.3.2.1. UV-vis Spectroscopic Evaluation of 0.45µm Filtered Fraction Humic Acid During Photocatalytic Degradation. UV-vis spectra of the oxidized 0.45µm filtered fraction of humic acid exhibited a decreasing trend with increasing wavelength. Displaying the same basic pattern of declining trend, a decrease in the absorbance values was observed with the increasing irradiation time during photocatalytic oxidation as presented in Figure 4.25. It is evident that the initial UV-vis spectra of humic acid expressed the higher absorbance values and humic sample attained after 60 minutes of irradiation time has the lowest absorbance value.

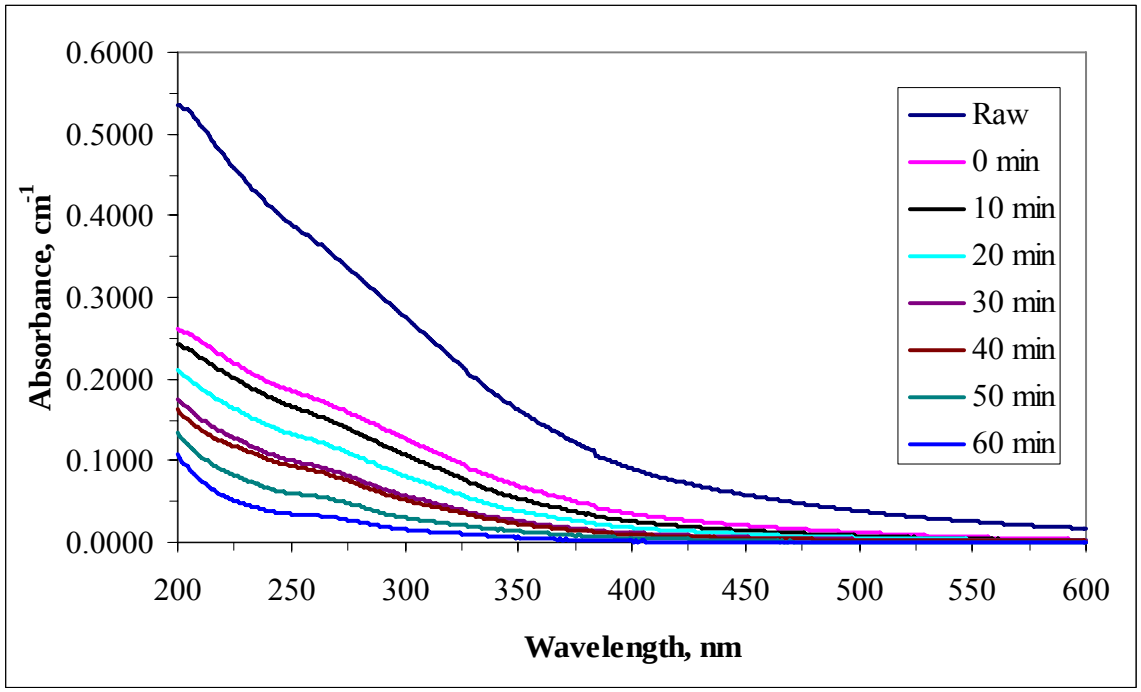

Figure 4.25. UV-vis spectra of 0.45µm filtered fraction of humic acid during photocatalytic degradation (Raw represents 0.45µm filtered fraction of humic acid).

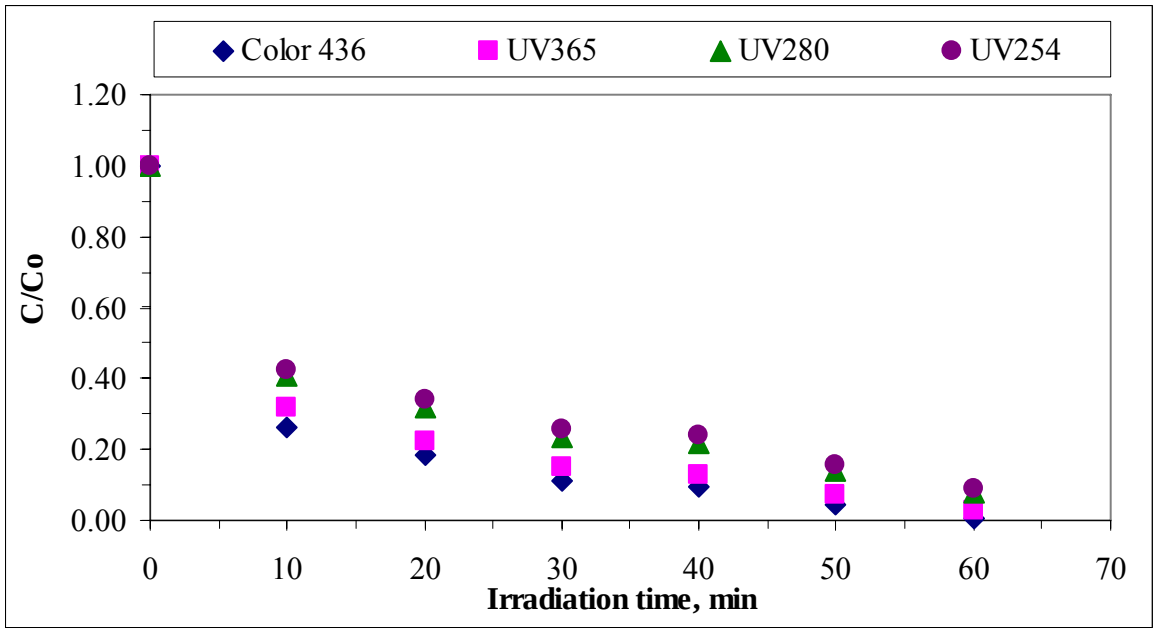

Figure 4.26. Normalized $Color_{436}$, UV_{365}, UV_{280}, UV_{254} values of 0.45 µm filtered fraction of humic acid with respect to irradiation time in the presence of bare TiO_2.

In a similar manner, the UV-vis spectral features were evaluated by using the specified parameters. The photocatalytic removal of the $Color_{436}$ and other specified UV parameters of humic acid as a function of the irradiation time were depicted in Figure 4.26. The most pronounced removal achieved was recorded upon irradiation period of 10 min. that could also be considered as an additive effect of pre-adsorption condition rather than a fast photocatalytic degradation regime.

Initial adsorptive removal of 0.45 μm filtered fraction of humic acid could also be assessed by the specified UV-vis parameters. The initial removal efficiencies were 63%, 58%, 53% and 52% for $Color_{436}$, UV_{365}, UV_{280} and UV_{254}, respectively. Further, 74% removal of $Color_{436}$ and 57% removal of UV_{254} were recorded at the end of 10 minutes of photocatalytic treatment. At the end of 60 minutes of irradiation time, the removal efficiencies followed a basic trend of $Color_{436}>UV_{365}>UV_{280}>UV_{254}$ irrespective of the irradiation time (Figure 4.26).

4.3.2.2. Fluorescence Spectroscopic Evaluation of 0.45μm Filtered Fraction of Humic Acid During Photocatalytic Degradation. Emission scan fluorescence spectra of 0.45μm filtered fraction of humic acid samples were displayed in Figure 4.27. Fluorescence spectra of the samples were recorded by excitation at 350 and 370 nm causing a major peak at the wavelength of 450 nm. As could be seen in Figure 4.27, a general decreasing trend was attained for the emission scan fluorescence with respect to irradiation period.

Synchronous scan fluorescence spectra of 0.45μm filtered fraction humic acid were shown in Figure 4.29. Synchronous scan fluorescence spectra were recorded in the range of 250-600 nm wavelength region. It can be said that the untreated humic acid displayed a sharp peak around wavelength of 470 nm. Uyguner and Bekbolet (2005b) found a similar result that the spectra of each size fraction exhibited a decreasing trend in terms of fluorescence intensity using fluorescence spectroscopic analysis. The gradual decrease of fluorescence intensity in synchronous scan fluorescence spectra might indicate the degradation of the high molecular weight components of humic acid and formation of lower molecular size fractions of humic acid during photocatalysis.

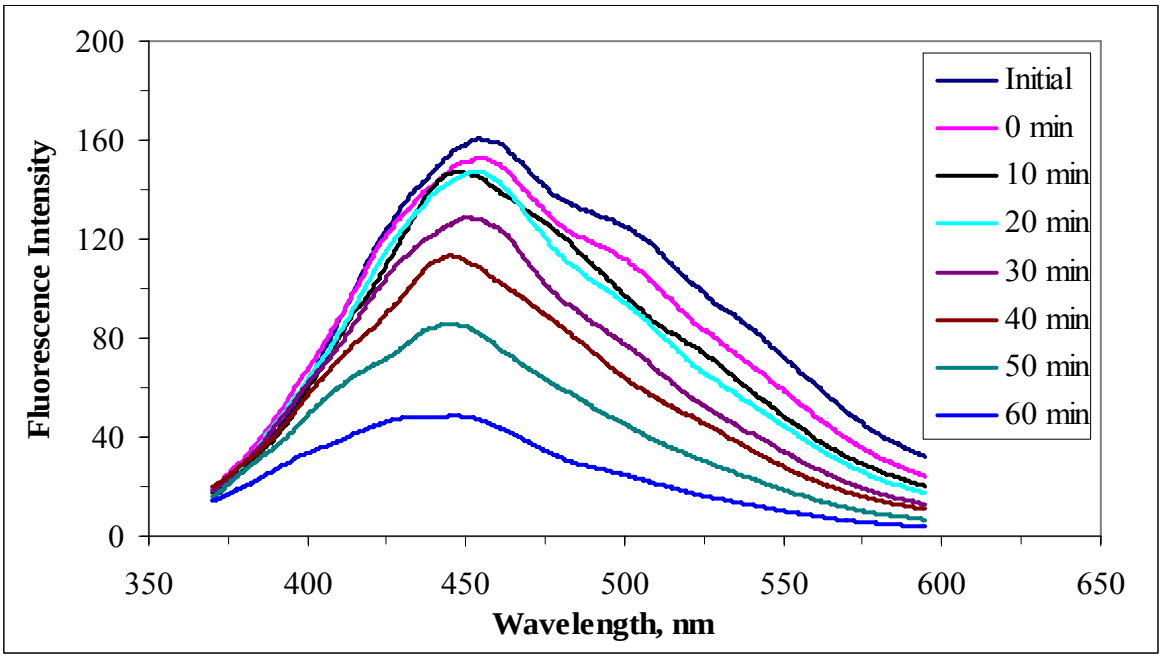

Figure 4.27. Emission scan fluorescence spectra ($FI_{emis\ 350}$) of 0.45µm filtered fraction humic acid during photocatalytic degradation (Initial represents 0.45µm filtered fraction of humic acid).

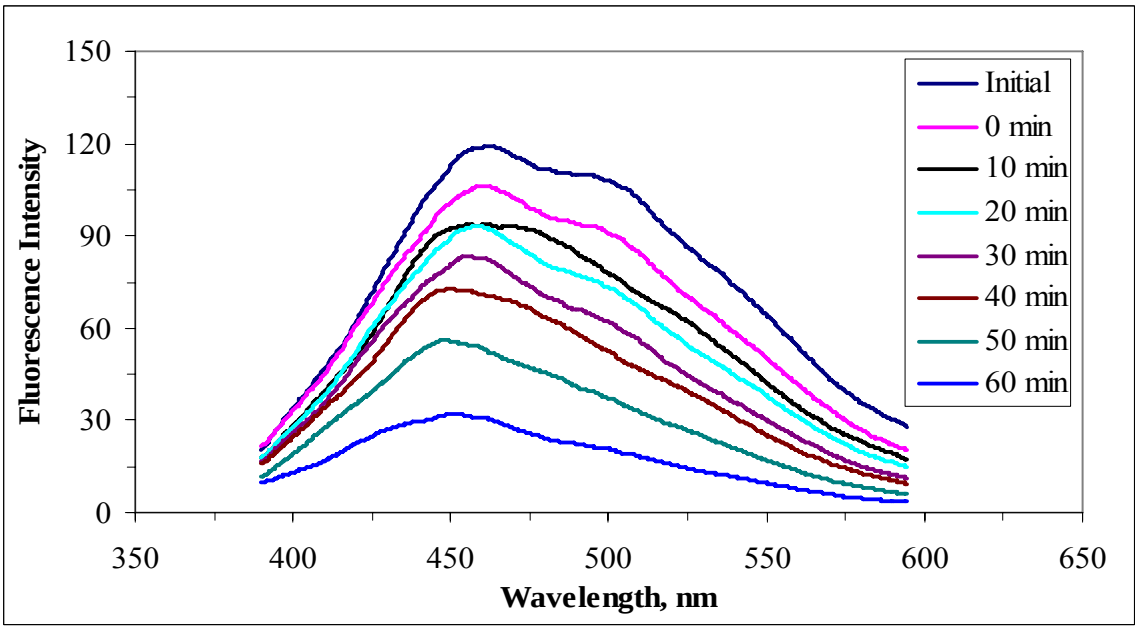

Figure 4.28. Emission scan fluorescence spectra ($FI_{emis\ 370}$) of 0.45µm filtered fraction humic acid during photocatalytic degradation (Initial represents 0.45µm filtered fraction of humic acid).

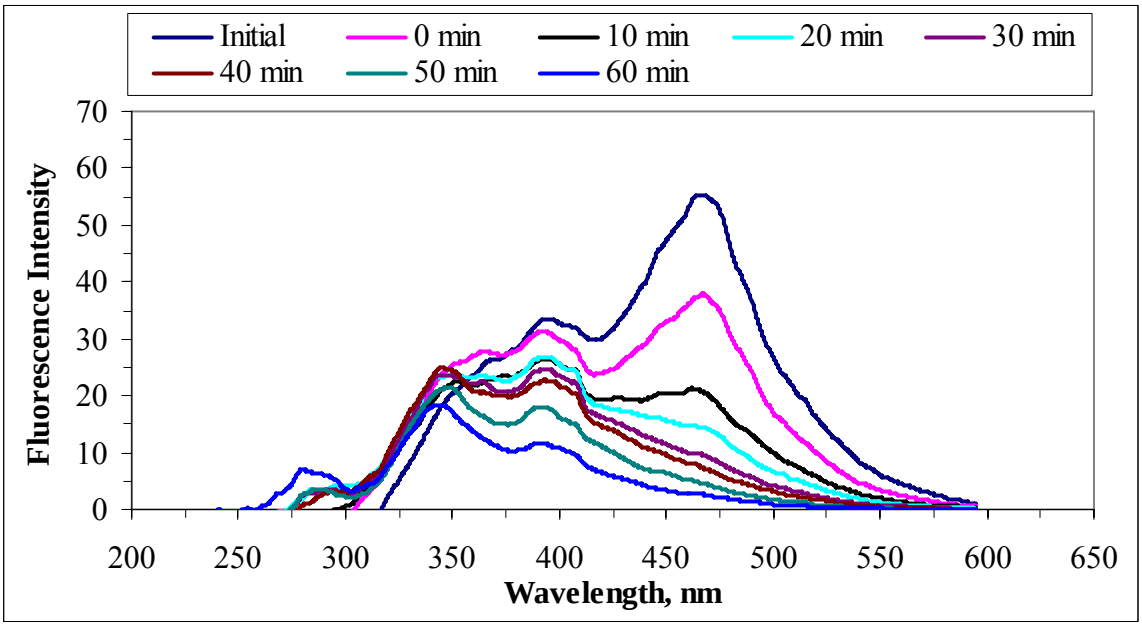

Figure 4.29. Synchronous scan fluorescence spectra of 0.45µm filtered fraction humic acid during photocatalytic degradation (Initial represents 0.45µm filtered fraction of humic acid)

4.3.3. Photocatalytic Degradation of 100 kDa Fraction of Humic Acid in the Presence of Bare TiO_2

Photocatalytic degradation of 100 kDa fraction of humic acid samples were evaluated by UV-vis spectra and fluorescence spectra as well as by the specified UV-vis and fluorescence parameters.

4.3.3.1. UV-vis Spectroscopic Evaluation of 100 kDa Fraction of Humic Acid During Photocatalytic Degradation. UV-vis spectra of 100 kDa fraction of humic acid during photocatalytic degradation were shown in Figure 4.30. It was observed that the UV-vis spectra of 100 kDa fraction of humic acid monotonously decreased with increasing wavelength in a broad and featureless trend. Furthermore, after 30 minutes of irradiation period, absorbance values became close to zero revealing insignificant absorptivity in the wavelength range of 220-600 nm. As a conclusion, 220-350 nm region can be considered as significant irrespective of the irradiation period. It should also be taken into account that the contribution of the inorganic species *i.e.* NO_3^- should also be considered.

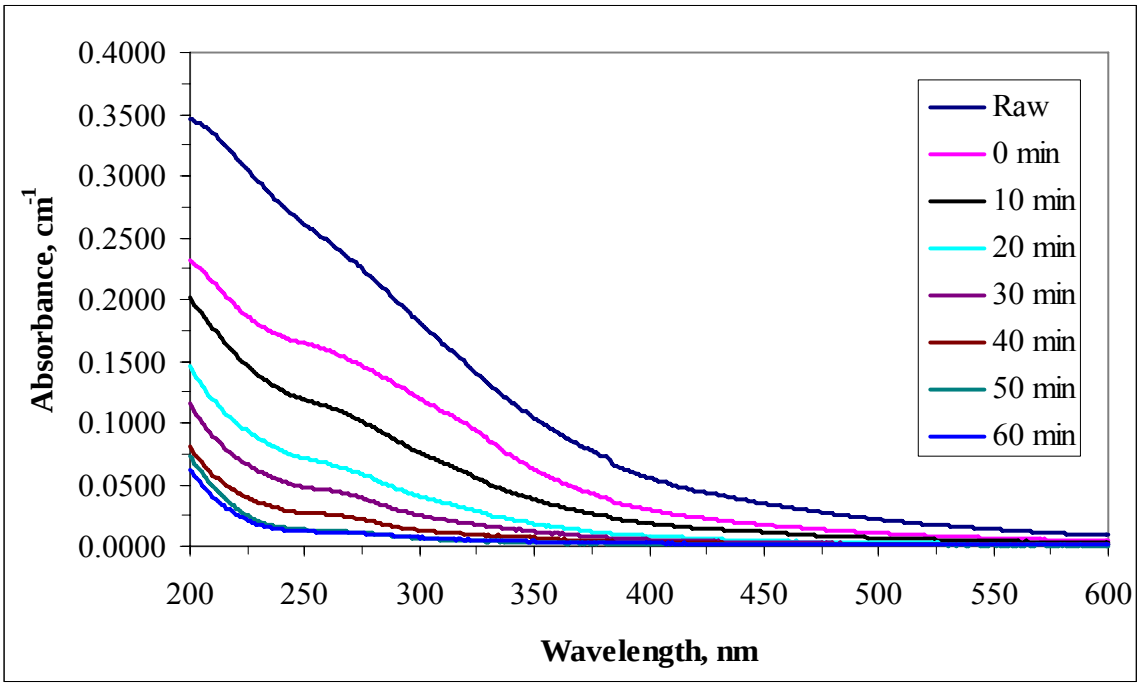

Figure 4.30. UV-vis spectra of 100 kDa fraction of humic acid during photocatalytic degradation (Raw represents 100 kDa fraction of humic acid).

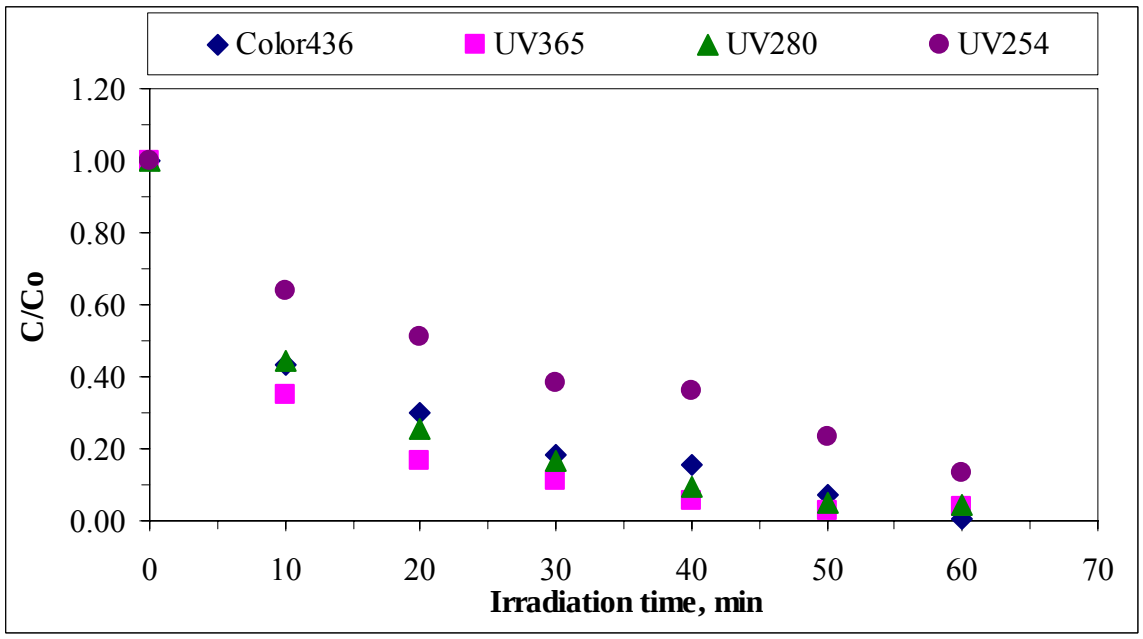

Figure 4.31. Normalized $Color_{436}$, UV_{365}, UV_{280}, UV_{254} values of 100 kDa fraction of humic acid with respect to irradiation time in the presence of bare TiO_2.

Photocatalytic degradation of 100 kDa fraction of humic acid was also evaluated in terms of UV-vis parameters as expressed by $Color_{436}$, UV_{365}, UV_{280} and UV_{254} (Figure 4.31). Initial adsorptive removal efficiencies of 100 kDa fraction of humic acid were 49%, 44%, 35% and 36% for $Color_{436}$, UV_{365}, UV_{280} and UV_{254}, respectively. Further, 57% removal of $Color_{436}$ and 36% removal of UV_{254} were recorded at the end of 10 minutes of photocatalytic treatment. As expected $Color_{436}$ removal displayed a faster degradation tendency in comparison to the other UV parameters. Almost complete removal of $Color_{436}$, UV_{365} and UV_{280} were attained after 50 min of irradiation period where as ≤ 25 % UV_{254} was also found to be present in the reaction medium. At the end of 60 minutes of irradiation time, almost complete removal was attained for all of the UV-vis parameters. The removal efficiencies followed a basic trend of $Color_{436}>UV_{365}>UV_{254}>UV_{280}$ irrespective of the irradiation time (Figure 4.31). It could be concluded that the UV absorbing centers displayed different removal tendencies with respect to the specified UV parameters depending on the selected wavelength of interest.

4.3.3.2. Fluorescence Spectroscopic Evaluation of 100 kDa Fraction Humic Acid during Photocatalytic Degradation. The emission scan fluorescence spectra of humic acid samples were displayed in Figures 4.32 and 4.33.

The effect of the excitation wavelength on the fluorescence intensity of 100 kDa fraction of humic acid could be observed most significantly at 450 nm for both excitation wavelengths of 350 and 370 nm. After 40 minutes of irradiation time, the peak at λ_{max} 450 nm started to disappear. After 60 minutes of irradiation, the characteristic sharp peak of raw humic acid completely disappears and the moderate peak around 400 nm decays in intensity. Since humic acid contains a variety of aromatic moieties and carboxylic groups, the molecular and structural characters within the molecule may be substantially changed as a result of HO• attack via photocatalytic oxidation. Comparison of the fluorescence spectra presented in Figures 4.32 and 4.33 displayed the importance of the excitation wavelength that could be regarded as significant for all of the molecular size fractions of the humic moieties.

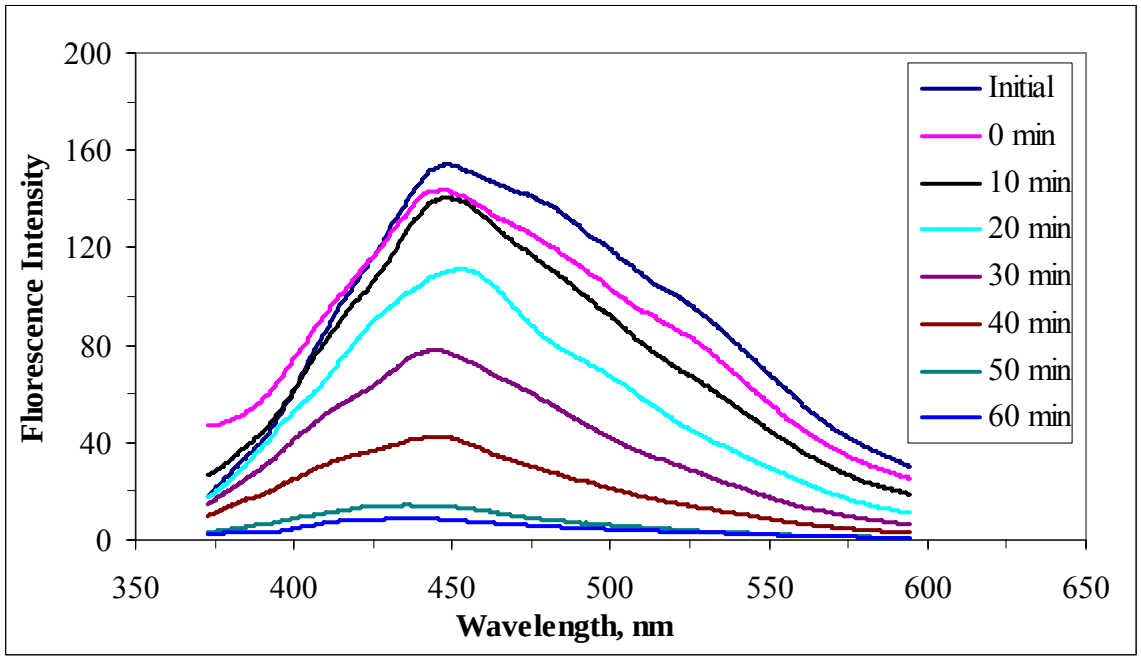

Figure 4.32. Emission scan fluorescence spectra ($FI_{emis\ 350}$) of 100 kDa fraction of humic acid during photocatalytic degradation (Initial represents 100 kDa fraction of humic acid).

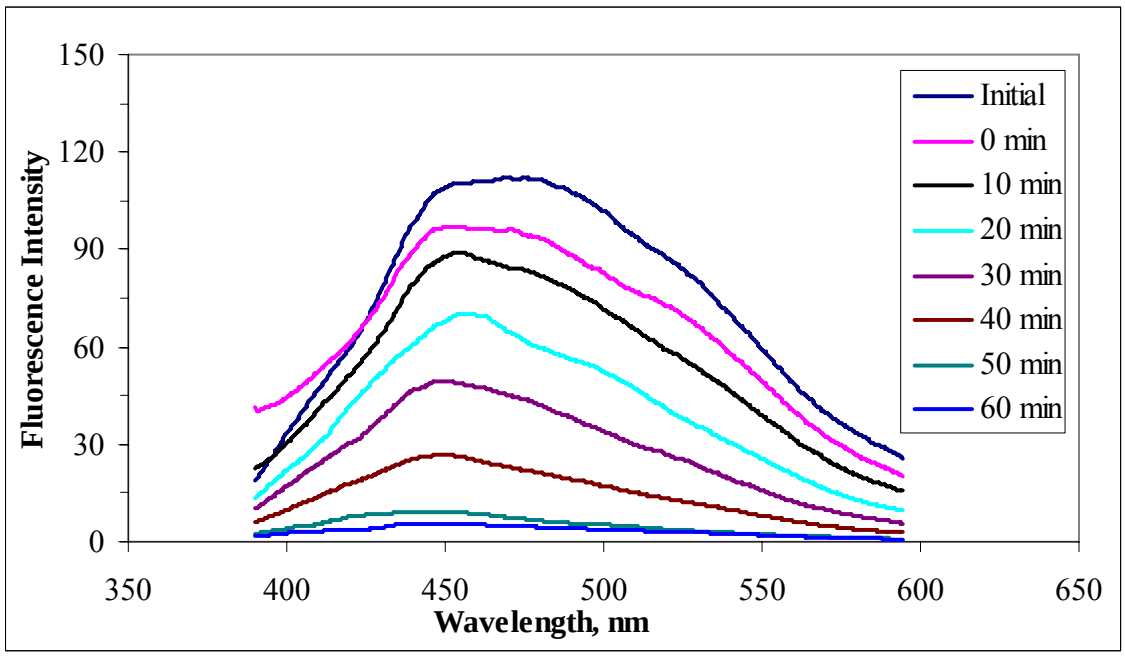

Figure 4.33. Emission scan fluorescence spectra ($FI_{emis\ 370}$) of 100 kDa fraction of humic acid during photocatalytic degradation (Initial represents 100 kDa fraction of humic acid).

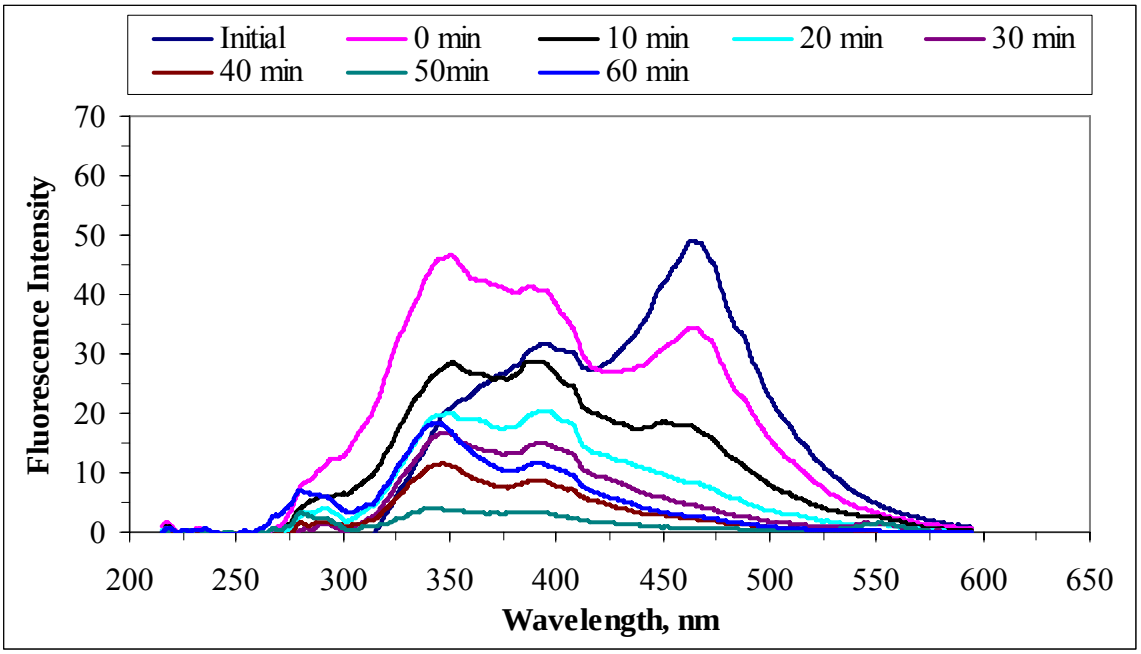

Figure 4.34. Synchronous scan fluorescence spectra of 100 kDa fraction of humic acid during photocatalytic degradation (Initial represents 100 kDa fraction of humic acid).

Synchronous scan spectra of 100 kDa fraction of humic acid, illustrated by Figure 4.34, gave a major peak around 350 nm except for the initial condition. It could be said that the synchronous scan spectra gave decreasing intensity with increasing radiation time. Besides, the peak at λ_{max} 350 nm started to disappear upon 50 minutes of irradiation time. As illustrated in Figure 4.34, the synchronous scan spectra of 100 kDa fraction of humic acid presented that the photocatalytic degradation also lead to a gradual decrease in fluorescence intensity. This might indicate the degradation of the comparatively higher molecular weight components of humic acid and formation of lower molecular size fractions of humic acid during photocatalysis. In general, electron withdrawing groups (*e.g.,* –COOH) decrease and electron donating groups (such as –OH, $–NH_2$) increase the intensity of fluorescence in aromatic compounds (Senesi, 1990). Therefore, the removal of the fluorescence intensity could also be regarded as the removal of the indicated moieties.

4.3.4. Photocatalytic Degradation of 30 kDa Fraction of Humic Acid in the Presence of Bare TiO_2

Photocatalytic degradation of 30 kDa fraction of humic acid samples were evaluated by UV-vis spectra and fluorescence spectra as well as by the specified UV-vis and fluorescence parameters.

4.3.4.1. UV-vis Spectroscopic Evaluation of 30 kDa Fraction Humic Acid during Photocatalytic Degradation. UV-vis spectra of 30 kDa fraction of humic acid during photocatalytic degradation were presented in Figure 4.35. UV-vis spectra of the 30 kDa fraction of the humic acid would also display the same monotonously decreasing trend with respect to increasing wavelength as expected. Moreover, displaying the same basic pattern of the declining trend, a decrease in the absorbance values was observed with the increasing irradiation time during photocatalytic oxidation. Also, Figure 4.35 indicated that the UV-vis absorption spectra approached to a phase of very low absortivities (< 0.040) for the wavelength region of 200- 250 nm after 20 minutes of irradiation time.

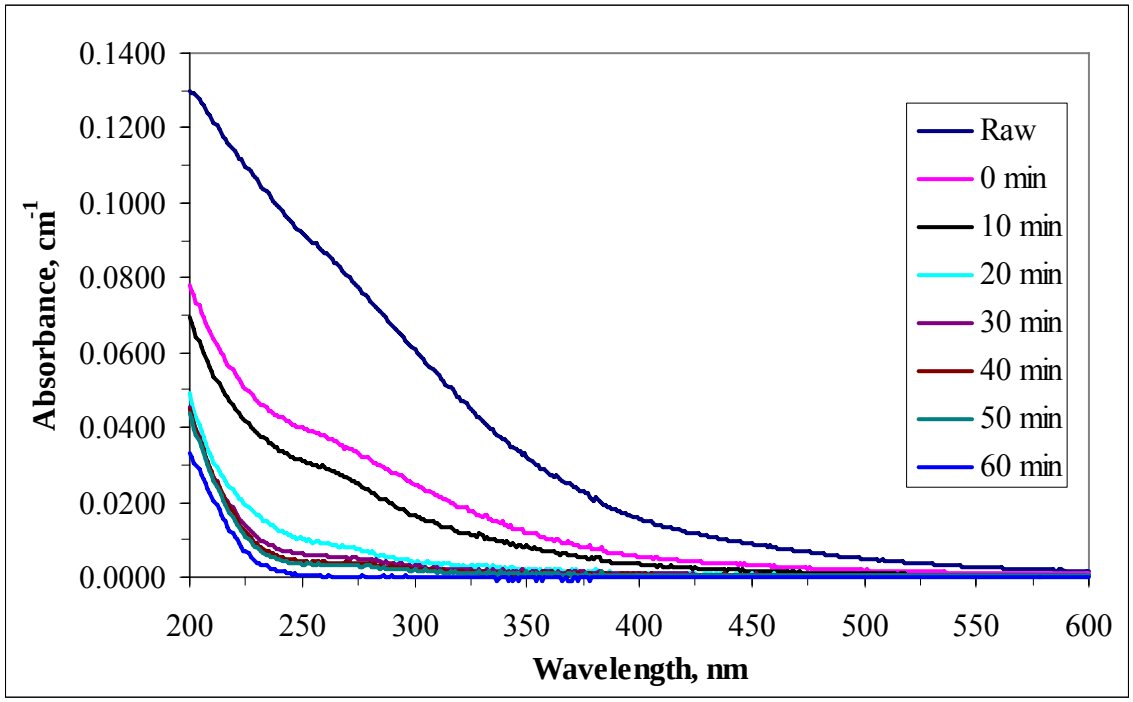

Figure 4.35. UV-vis spectra of 30 kDa fraction of humic acid during photocatalytic degradation (Raw represents 30 kDa fraction of humic acid).

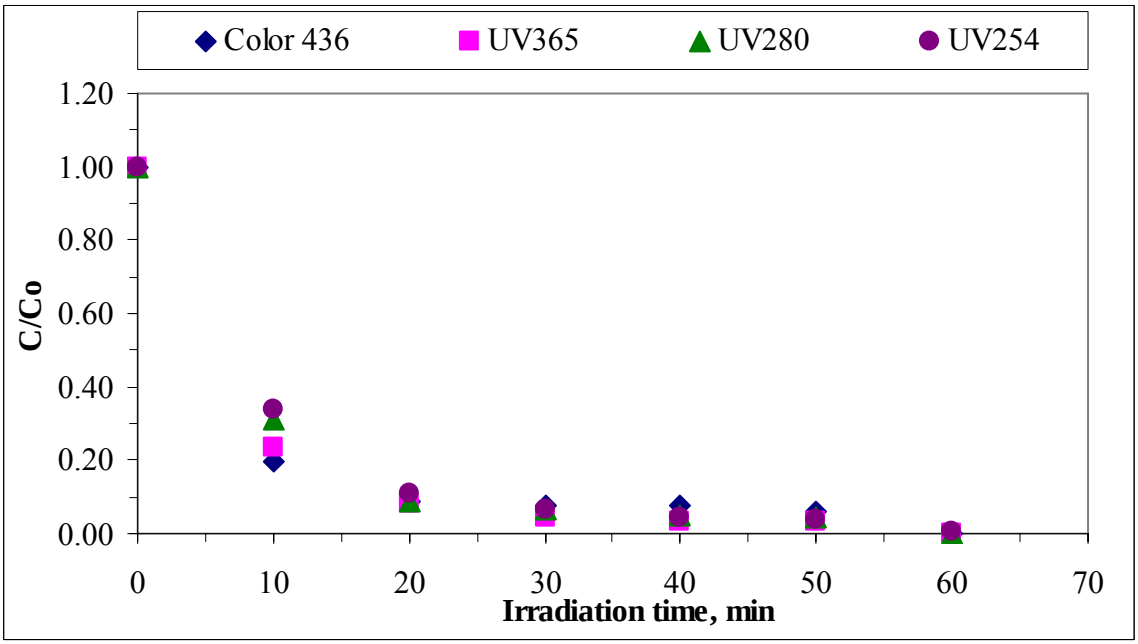

Figure 4.36. Normalized $Color_{436}$, UV_{365}, UV_{280} and UV_{254} values of 30 kDa fraction of humic acid with respect to irradiation time in the presence of bare TiO_2.

Photocatalytic degradation of 30 kDa fraction of humic acid was also evaluated in terms of UV-vis parameters as expressed by $Color_{436}$, UV_{365}, UV_{280} and UV_{254} (Figure 4.36). Initial adsorptive removal efficiencies of 30 kDa fraction of humic acid were found to be 65%, 62%, 58% and 57% for $Color_{436}$, UV_{365}, UV_{280} and UV_{254}, respectively. The general decreasing trend was detected for all of the UV-vis parameters as could be visualized from the UV-vis spectra (Figure 4.36). While 81% of $Color_{436}$ was removed in 10 minutes of irradiation, 100% removal was achieved after 60 minutes of irradiation period. At the end of 60 minutes of irradiation time, all of the UV-vis parameters *i.e.* $Color_{436}$, UV_{365}, UV_{280}, and UV_{254} expressed almost complete degradation of 30 kDa fraction of humic acid.

4.3.4.2. Fluorescence Spectroscopic Evaluation of 30 kDa Fraction of Humic Acid During Photocatalytic Degradation. Emission scan fluorescence spectra of the oxidized 30 kDa fraction of humic acid were presented in Figure 4.37.

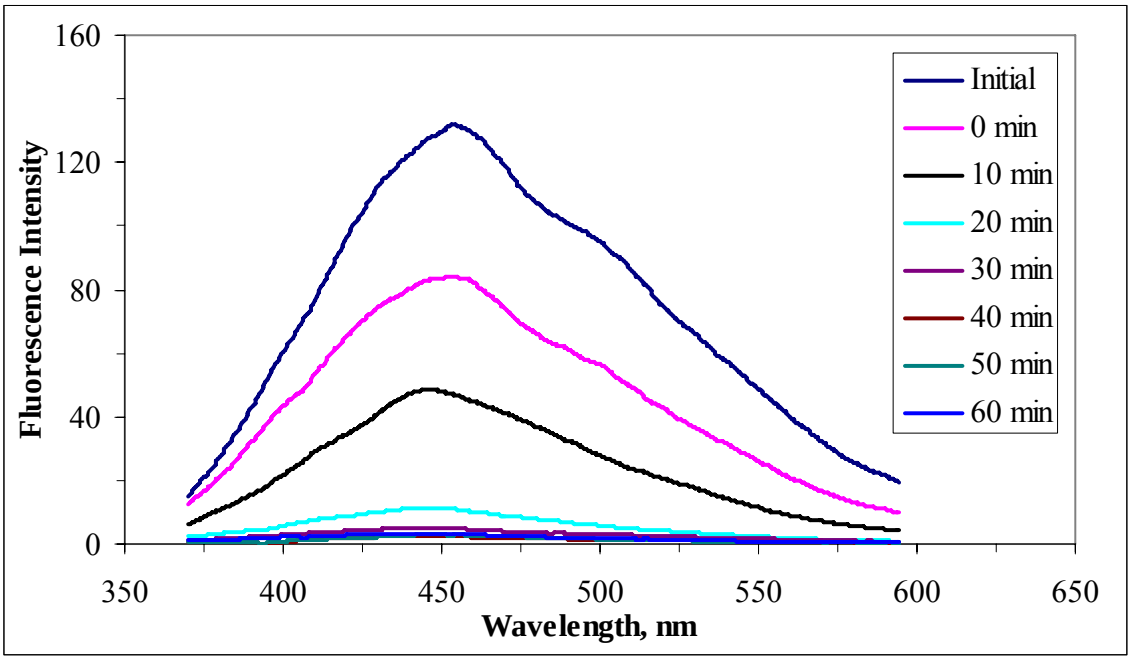

Figure 4.37. Emission scan fluorescence spectra ($FI_{emis\ 350}$) of 30 kDa fraction of humic acid during photocatalytic degradation (Initial represents 30 kDa fraction of humic acid).

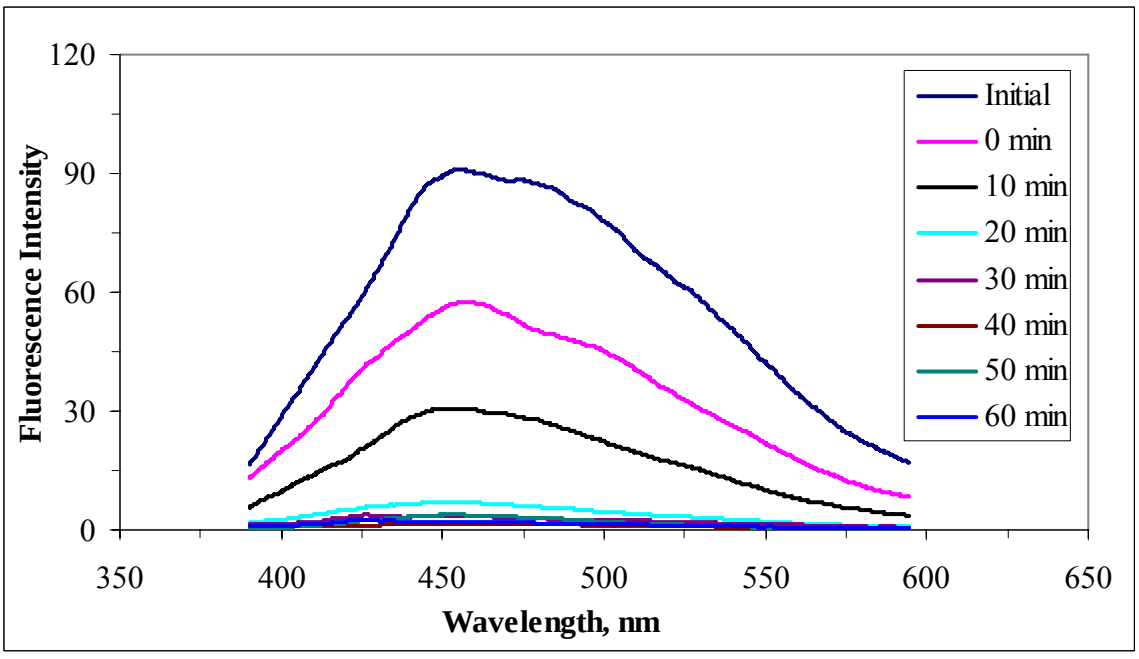

Figure 4.38. Emission scan fluorescence spectra ($FI_{emis\ 370}$) of 30 kDa fraction of humic acid during photocatalytic degradation (Initial represents 30 kDa fraction of humic acid).

Emission scan fluorescence spectra of 30 kDa fraction of humic acid were presented with respect to the applied photocatalytic irradiation time periods. With increased photocatalytic irradiation time, the fluorescence intensities slightly decreased. However, the spectra displayed the same characteristic peak around 450 nm wavelength. After 20 minutes of irradiation time, the characteristic sharp peak of 30 kDa fraction of humic acid recorded at λ_{max} 450 nm completely disappeared.

Moreover, upon comparison of the emission scan fluorescence spectra recorded for all of the humic samples, it could be deduced that the excitation wavelength of 350 nm could be preferred for qualitative purposes. In conclusion, it should be stated that the emission scan fluorescence features could not be considered as significant quantitative parameters for the elucidation of the photocatalytic removal of the humic acid and its molecular size fractions.

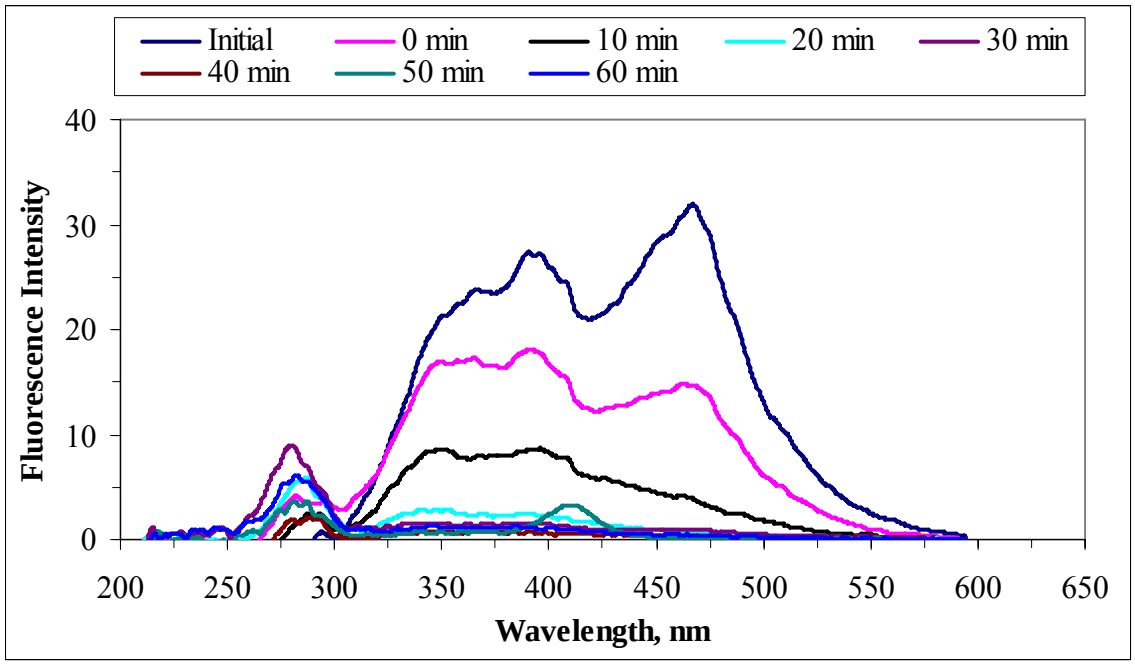

Figure 4.39. Synchronous scan fluorescence spectra of 30 kDa fraction of humic acid during photocatalytic degradation (Initial represents 30 kDa fraction of humic acid).

Synchronous scan fluorescence spectra of 30 kDa fraction of humic acid during photocatalytic degradation were presented in Figure 4.39. Such as raw humic acid, 0.45μm filtered fraction, 100 kDa fraction of humic acid; 30 kDa fraction of humic acid exhibited a similar decreasing trend in terms of fluorescence intensity. Upon irradiation period of 20 minutes, the observed peak at λ_{max} 450 nm started to disappear and the synchronous scan fluorescence spectra showed a featureless regime.

4.3.5. Photocatalytic Degradation of Raw Humic Acid in the Presence of Fe doped TiO_2

In this section, the effect of Fe doping on the TiO_2 photocatalytic degradation of humic acid and its molecular fractions in aqueous medium was investigated and compared to bare TiO_2. In order to evaluate the molecular size effect on photocatalytic degradation of humic acid onto Fe doped TiO_2, experiments were carried out with different molecular size fractions such as 0.45μm filtered fraction, 100 kDa fraction and 30 kDa fraction.

Doping titania with transition metal ions has been tested as a promising way of improving the photocatalytic activity of semiconductor oxides. Particularly, introduction of iron ions in titania has resulted in controversial results with respect to the efficiency of the materials, depending on factors such as the preparation technique, the iron-loading, the temperature of calcination, the iron content, etc. (Litter and Navio, 1996). It was commonly reported that the improvement of photocatalysts was attributed to the Fe^{3+} dopants which can help the separation of photo-generated electrons and holes, and also can absorb and utilize the visible light to photocatalyze the degradation of pollutants (Wei et al., 2007, Yalcin et al, 2010)

4.3.5.1. UV-vis Spectroscopic Evaluation of Raw Humic Acid During Photocatalytic Degradation in the Presence of Fe doped TiO_2. For UV-vis spectral evaluation of raw humic acid, UV-vis absorbance values were recorded in the 200-600 nm wavelength region. As seen in Figure 4.40, the UV-vis spectra of humic acids monotonously decreased with increasing wavelength in a broad and featureless trend as was also observed for the case of the photocatalytic degradation experiments performed using bare TiO_2. The role of adsorptive interactions between the color forming moieties as well as the UV absorbing

centers onto different TiO_2 surfaces could be considered as insignificant due to the observed consistency in decreasing trend of absorbance values with respect to increasing wavelength. Moreover, during photocatalysis the same trend was also observed in UV-vis spectral profiles in relation to the irradiation time.

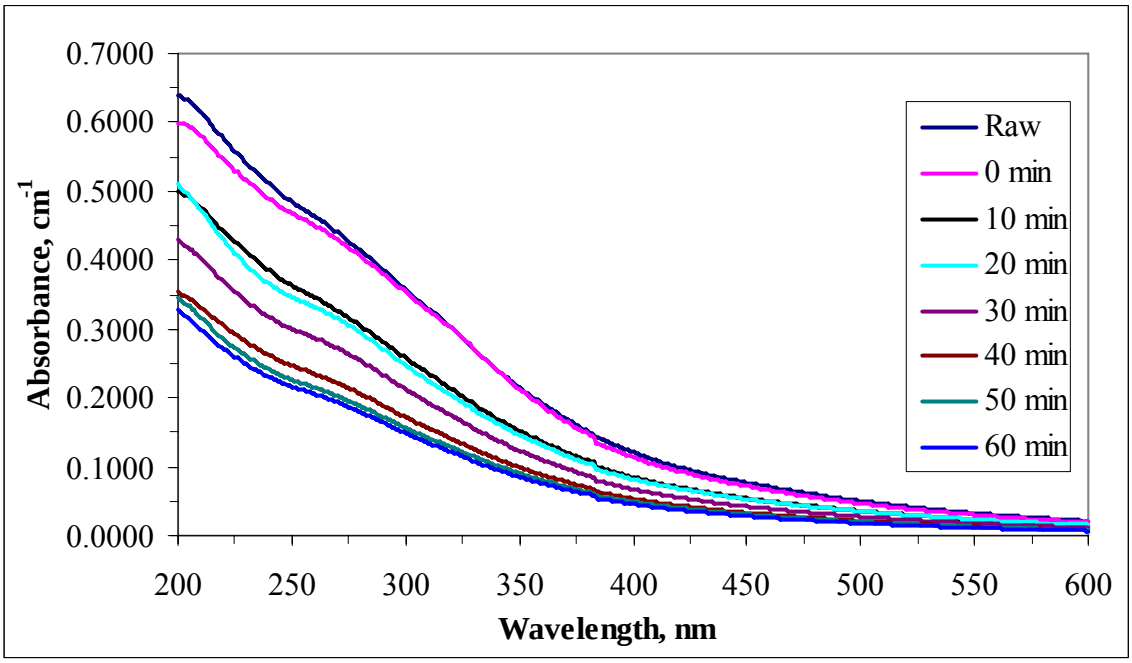

Figure 4.40. UV-vis spectra of raw humic acid during photocatalytic degradation in the presence of Fe doped TiO_2.

Also Figure 4.40 indicated that raw humic acid had the highest absorbance value and 60 minutes of irradiation time had the lowest absorbance value for the spectral wavelength region. When UV-vis spectroscopic profile of the raw humic acid on bare TiO_2 was compared to the UV-vis spectroscopic profile in the presence of Fe doped TiO_2, significantly higher absorbance values could be observed. Furthermore, the photocatalytic degradation of humic acid in the present of Fe doped TiO_2 was evaluated in terms of UV-vis parameters as expressed by $Color_{436}$, UV_{365}, UV_{280} and UV_{254}. The remaining fractions of the specified parameters were displayed with respect to irradiation time (Figure 4.41) Initial adsorptive removal efficiencies of raw humic acid were found to be 6%, 2%, 2% and 3% for $Color_{436}$, UV_{365}, UV_{280} and UV_{254}, respectively. While 29% of $Color_{436}$ was removed in 10 minutes of irradiation, 62% removal was achieved after 60 minutes. The

removal efficiencies followed a basic trend of $Color_{436}$ > UV_{365}> UV_{280} >UV_{254} irrespective of the irradiation time after 60 min. It can be stated that via photocatalysis removal efficiencies of raw humic acid in the presence of Fe doped TiO_2 were comparatively lower compared to the results attained by photocatalytic degradation experiments performed using bare TiO_2.

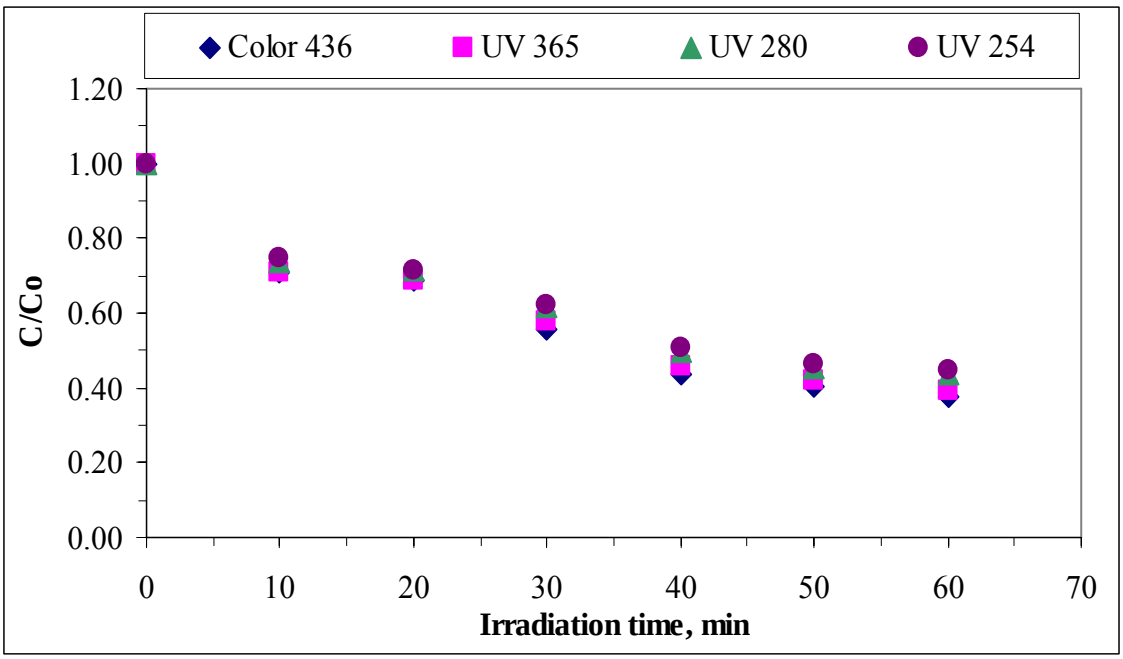

Figure 4.41. Normalized $Color_{436}$, UV_{365}, UV_{280}, and UV_{254} values of raw humic acid with respect to irradiation time in the presence of Fe doped TiO_2.

4.3.5.2. Fluorescence Spectroscopic Evaluation of Raw Humic Acid During Photocatalytic Degradation in the Presence of Fe doped TiO_2. The emission scan fluorescence spectra of the photocatalytically treated humic acid samples were displayed in Figure 4.42 and 4.43. As could be seen in Figure 4.42, a general decreasing trend was attained for the emission scan fluorescence intensities (λ_{exc} = 350 nm) with respect to the irradiation periods. The effect of the excitation wavelength on the fluorescence intensity of raw humic acid could be observed most significantly in the λ_{emis}= 450 nm for both of the excitation wavelengths as 350 and 370 nm. It can be concluded that the fluorescence spectra recorded for the humic acid samples exposed to 10 minutes of irradiation time and 20 minutes of irradiation time in the presence of Fe doped TiO_2 displayed an overlapping trend. Also, it could be

stated that the emission scan fluorescence intensities recorded at 40 minutes, 50 minutes and 60 minutes of irradiation time periods were very close to each other displaying the formation of the oxidized humic moieties with cumulative fluorescent properties. Moreover, the retention of the fluorescence intensity peak at 450 nm wavelength represented that the resulting humic moieties after irradiation for 60 min could still be present in a more complex aromatic structure.

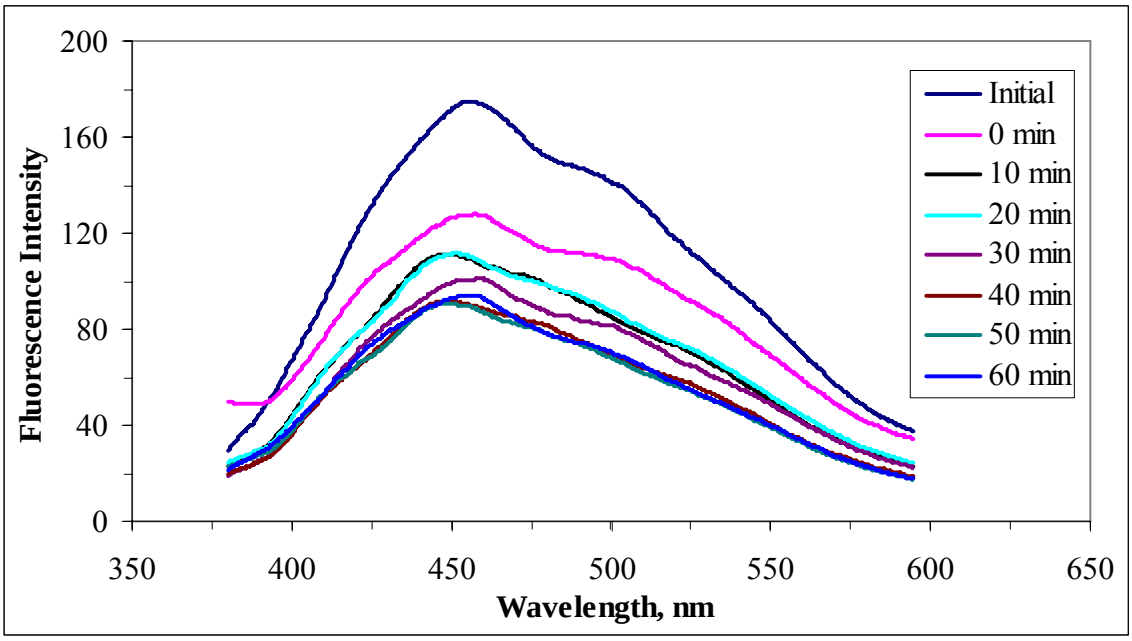

Figure 4.42. Emission scan fluorescence spectra ($FI_{emis\ 350}$) of raw humic acid in the presence of Fe doped TiO_2 during photocatalytic degradation(Initial represents raw humic acid).

Synchronous scan fluorescence spectra were recorded in the excitation wavelength range of 300-600 nm. Synchronous scan fluorescence spectra mode displayed two peak regions at around 390 nm and 470 nm (Figure 4.44). Initial adsorptive removal of raw humic acid at (t= 0) could also be visualized by the synchronous scan fluorescence spectra displaying a quite significant fluorescence intensity increase at around 300-400 nm. The role of the adsorptive interactions would be expressed by the formation of new fluorescent moieties. Moreover, a decreasing trend could be visualized with respect to increasing irradiation period with a characteristic overlapping manner.

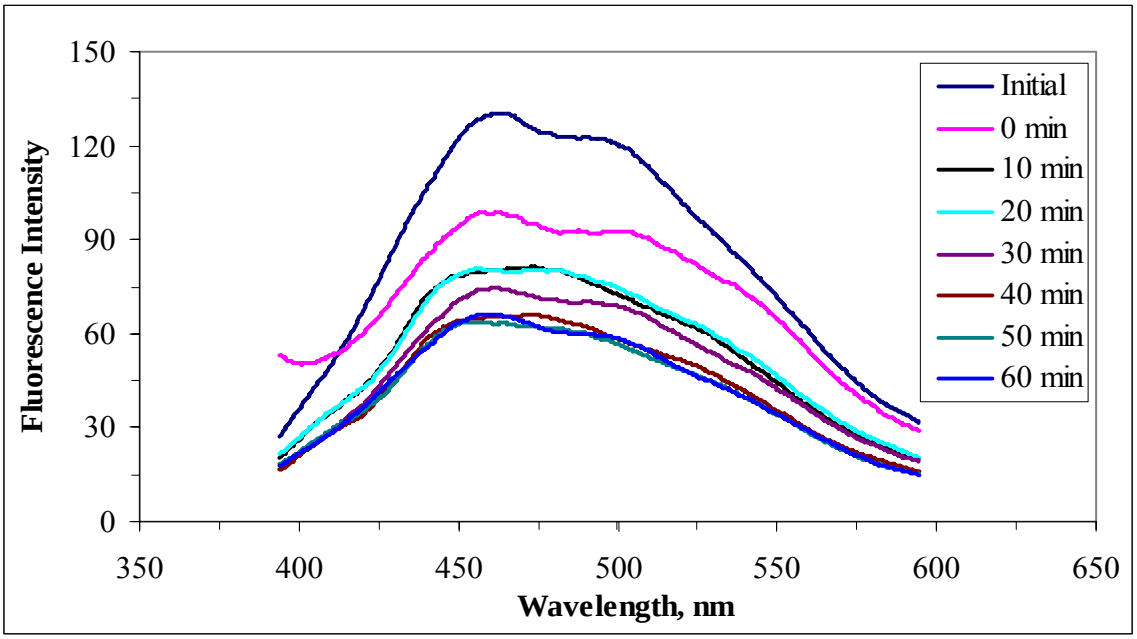

Figure 4.43. Emission scan fluorescence spectra ($FI_{emis\ 370}$) of raw humic acid in the presence of Fe doped TiO_2 during photocatalytic degradation (Initial represents raw humic acid).

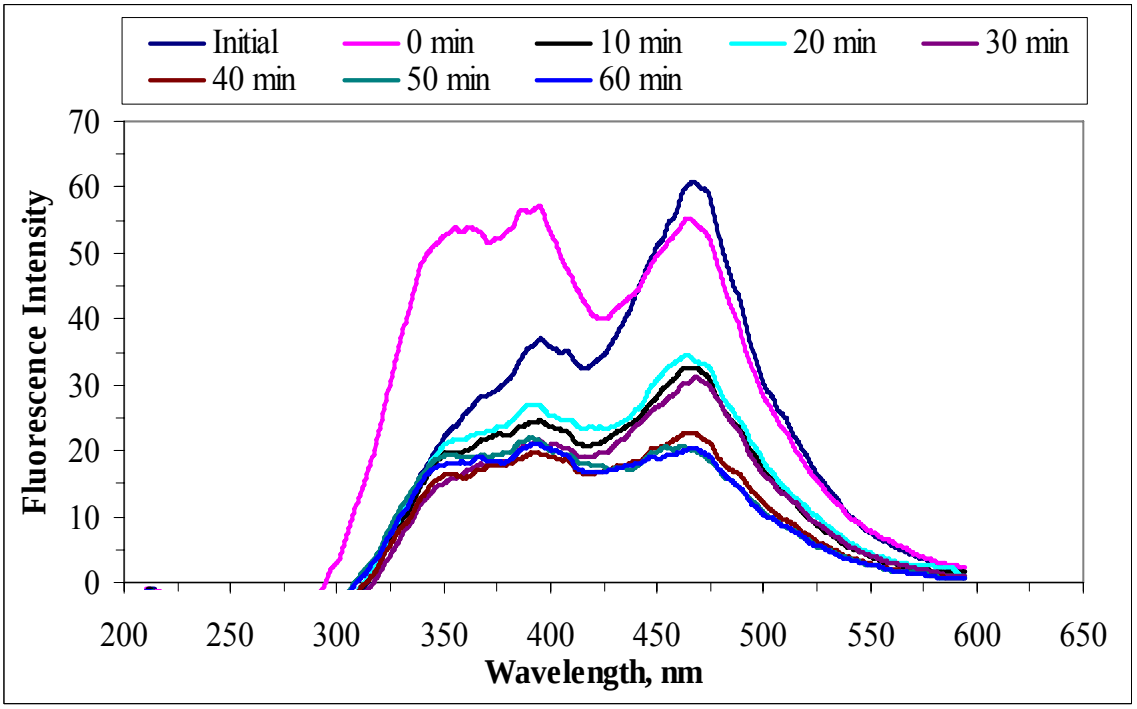

Figure 4.44. Synchronous scan fluorescence spectra of raw humic acid in the presence of Fe doped TiO_2 during photocatalytic degradation (Initial represents raw humic acid).

4.3.6. Photocatalytic Degradation of 0.45µm Filtered Fraction of Humic Acid in the Presence of Fe doped TiO_2

Photocatalytic degradation of 0.45µm filtered fraction of humic acid samples were performed using Fe doped TiO_2 and the resultant solutions were subjected to evaluation by UV-vis spectra and fluorescence spectra recorded in emission scan and synchronous modes.

4.3.6.1. UV-vis Spectroscopic Evaluation of 0.45µm Filtered Fraction of Humic Acid During Photocatalytic Degradation in the Presence of Fe doped TiO_2. The UV-vis spectra of 0.45µm filtered fraction of humic acid monotonously decreased with increasing wavelength. Displaying the same basic pattern of declining trend, a decrease in the absorbance values was observed with the increasing irradiation time during photocatalytic degradation in Figure 4.45. The absorbance values recorded at 50 and 60 minutes of irradiation time were also found to be significantly lower than the absorbance values recorded at other irradiation times at all wavelengths as shown in Figure 4.45. When UV-vis spectroscopic evaluation of the photocatalytic degradation of 0.45µm filtered fraction of humic acid on bare TiO_2 was compared to UV-vis spectroscopic evaluation of the photocatalytic degradation of 0.45µm filtered fraction of humic acid in the presence of Fe doped TiO_2, it was observed that the 0.45µm filtered fraction of humic acid with bare TiO_2 had higher declining trend than with Fe doped TiO_2 for all irradiation times.

Photocatalytic degradation of 0.45µm filtered fraction of humic acids in the presence of Fe doped TiO_2 was also evaluated in terms of UV-vis parameters as expressed by $Color_{436}$, UV_{365}, UV_{280} and UV_{254} (Figure 4.46). Initial adsorptive removal efficiencies of 0.45µm filtered fraction of humic acid were found to be 16%, 13%, 11% and 11% for $Color_{436}$, UV_{365}, UV_{280} and UV_{254}, respectively. The removal percentage for photocatalytic degradation of 0.45µm filtered fraction humic acid in the presence of Fe doped TiO_2 is lower than bare TiO_2 in short irradiation time periods, such as 10 minutes. While 74% removal of $Color_{436}$ and 56% removal of UV_{254} were recorded at the end of 10 minutes of irradiation time in the presence of bare TiO_2, 25% of $Color_{436}$ and 29% removal of UV_{254} were recorded in the presence of Fe doped TiO_2.

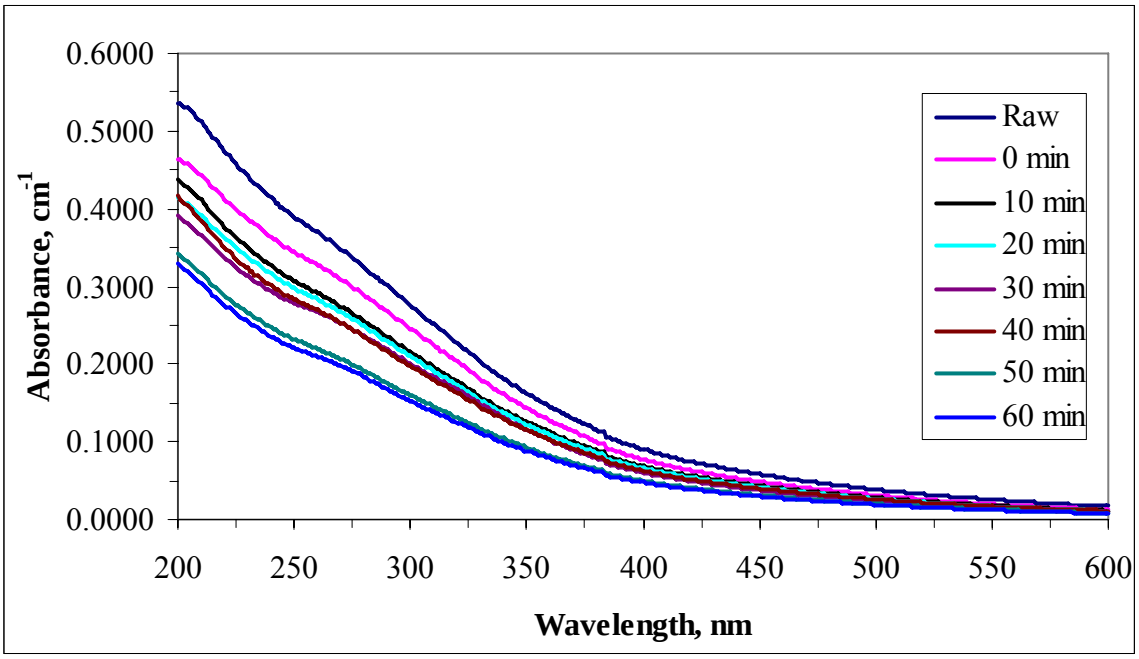

Figure 4.45. UV-vis spectra of 0.45µm filtered fraction of humic acid during photocatalytic degradation in the presence of Fe doped TiO_2.

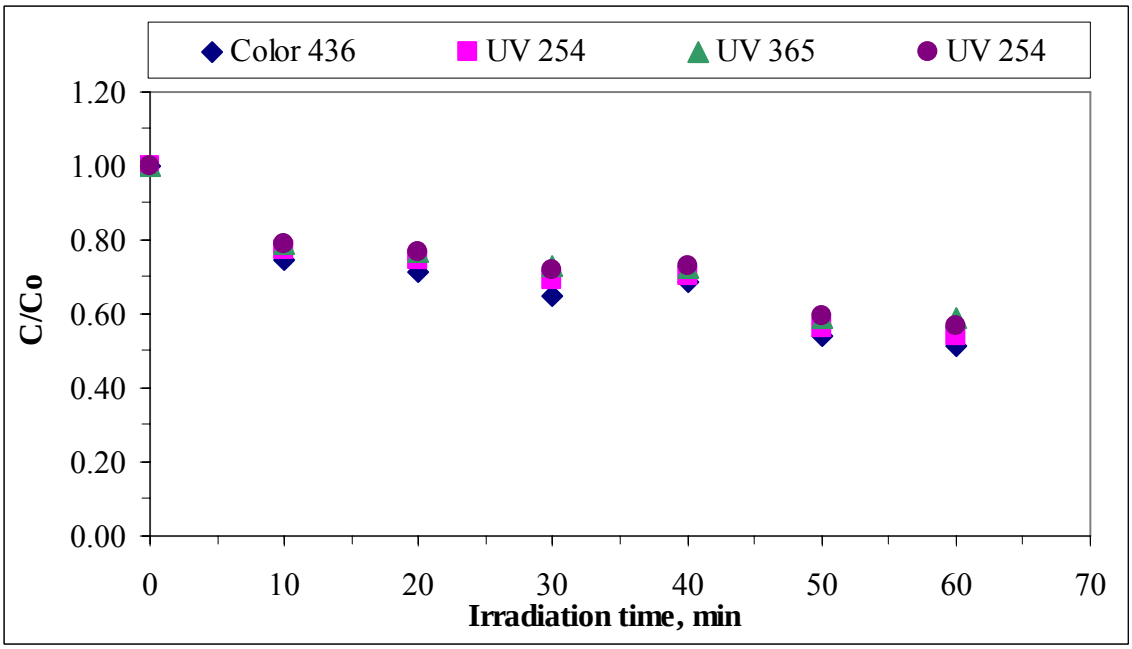

Figure 4.46. Normalized $Color_{436}$, UV_{365}, UV_{280} and UV_{254} values of 0.45µm filtered fraction of humic acid with respect to irradiation time in the presence of Fe doped TiO_2.

4.3.6.2. Fluorescence Spectroscopic Evaluation of 0.45µm Filtered Fraction of Humic Acid During Photocatalytic Degradation in the Presence of Fe doped TiO_2. Emission scan fluorescence spectra of the photocatalytically treated 0.45µm filtered fraction of humic acid in the presence of Fe doped TiO_2 samples were displayed in Figures 4.47 and 4.48. In a similar manner, the fluorescence spectra of the samples were recorded by excitation at 350 and 370 nm causing a major peak at the wavelength of 450 nm.

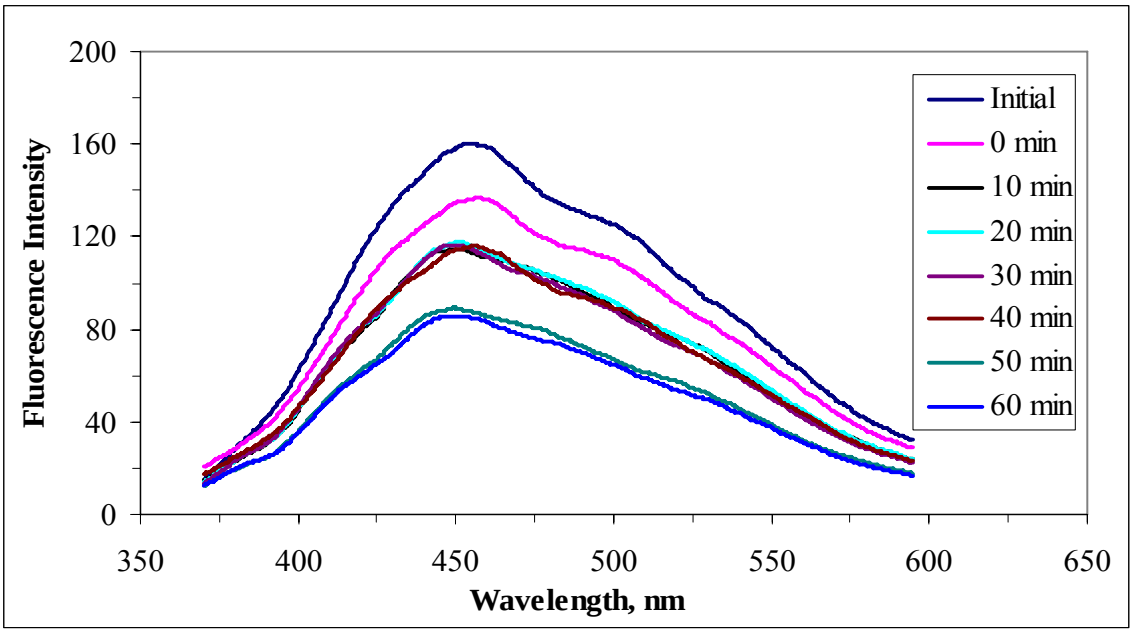

Figure 4.47. Emission scan fluorescence spectra ($FI_{emis\ 350}$) of 0.45µm filtered fraction of humic acid during photocatalytic degradation in the presence of Fe doped TiO_2 (Initial represents 0.45µm filtered fraction of humic acid).

It could be observed that through the excitation of humic moities at wavelengths of 350 nm and 370 caused a major peak in the region of 450 nm as was also recorded for 0.45µm filtered fraction of humic acid in the presence of Fe doped TiO_2. The fluorescence intensities displayed a decreasing trend with respect to increasing irradiation period from time 0 to 60 minutes. The lowest fluorescence intensities were obtained at 60 minutes of irradiation time.

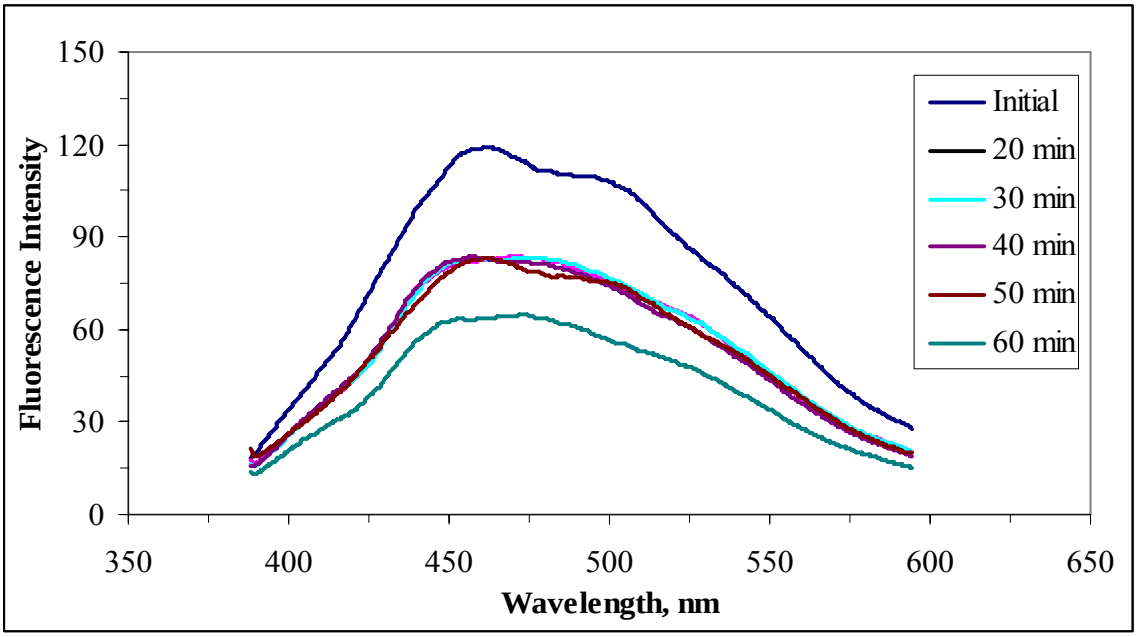

Figure 4.48. Emission scan fluorescence spectra ($FI_{emis\ 370}$) of 0.45µm filtered fraction of humic acid during photocatalytic degradation in the presence of Fe doped TiO_2 (Initial represents 0.45µm filtered fraction of humic acid).

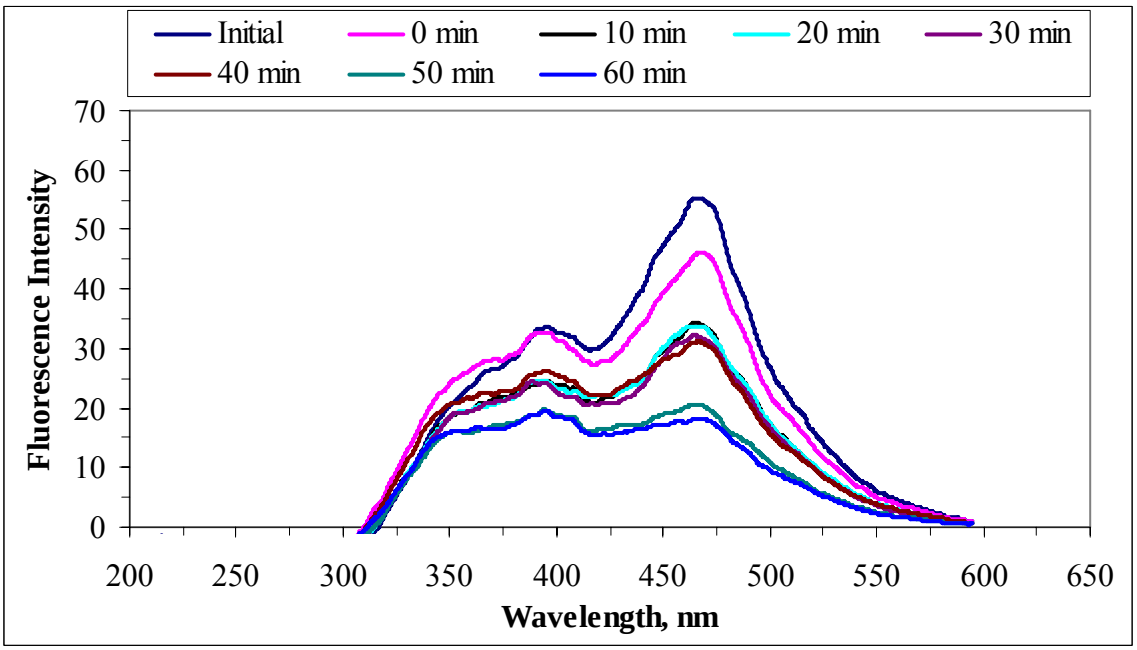

Figure 4.49. Synchronous scan fluorescence spectra of 0.45µm filtered fraction of humic acid during photocatalytic degradation in the presence of Fe doped TiO_2 (Initial represents 0.45µm filtered fraction of humic acid).

Synchronous scan spectra of 0.45μm filtered fraction of humic acid, illustrated by Figure 4.49, gave a major peak around 460 nm. In general, it could be said that the synchronous scan spectra gave decreasing intensities with increasing time radiation retaining the major profile shape. Synchronous scan fluorescence spectra of 0.45 μm filtered fraction of humic acid in the presence of Fe doped TiO_2 did not exhibit similar fluorescence properties in comparison to bare TiO_2. Following increased irradiation time periods, photocatalytically oxidized humic acid moieties in the presence of Fe doped TiO_2 displayed an overlapping trend.

4.3.7. Photocatalytic Degradation of 100 kDa Fraction of Humic Acid in the Presence of Fe doped TiO_2

Photocatalytic degradation of 100 kDa fraction of humic acid samples were performed using Fe doped TiO_2 and evaluated by UV-vis spectra and fluorescence spectra recorded in emission scan and synchronous modes.

4.3.7.1. UV-vis Spectroscopic Evaluation of 100 kDa Fraction of Humic Acid during Photocatalytic Degradation in the Presence of Fe doped TiO_2. In general, the UV-vis spectra of 100 kDa fraction of humic acid in the presence of Fe doped TiO_2 showed a gradually decreasing trend with the respect to wavelength in the 200-600 nm region. As seen in Figure 4.50, the UV-vis spectra of humic acids monotonously decreased with increasing wavelength in a broad and featureless trend irrespective of the irradiation period.

It can be concluded that absorbance values of 100 kDa fraction of humic acid in the presence of Fe doped TiO_2 were very close each other. After 400 nm wavelength, all samples showed a nearly overlapping trend.

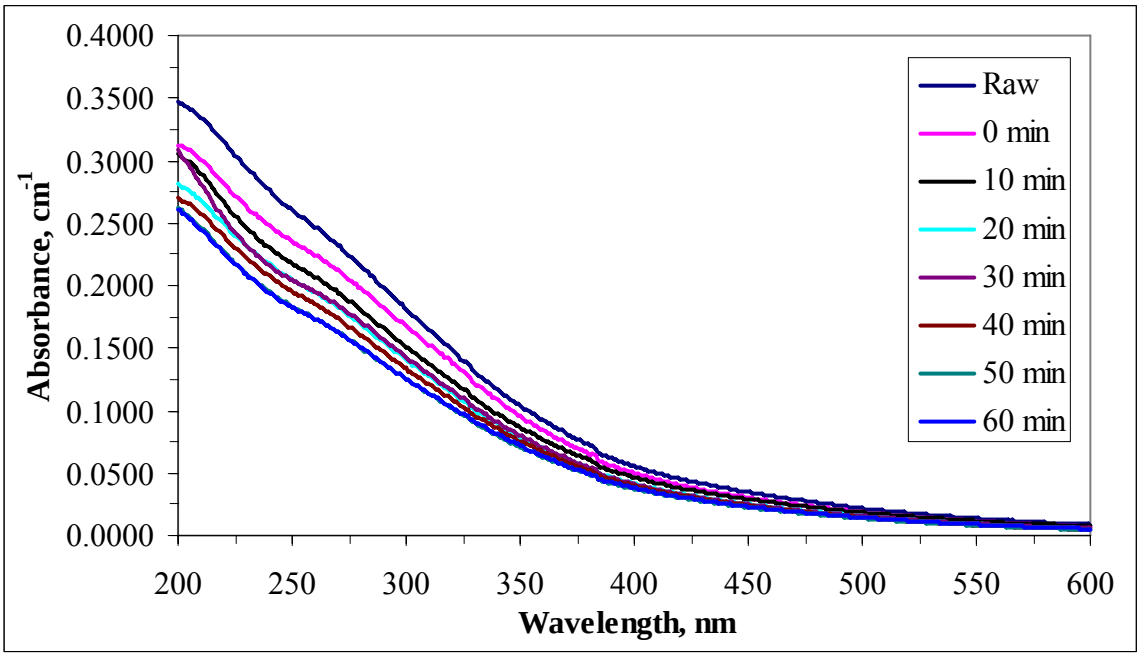

Figure 4.50. UV-vis spectra of 100 kDa fraction of humic acid during photocatalytic degradation in the presence of Fe doped TiO_2.

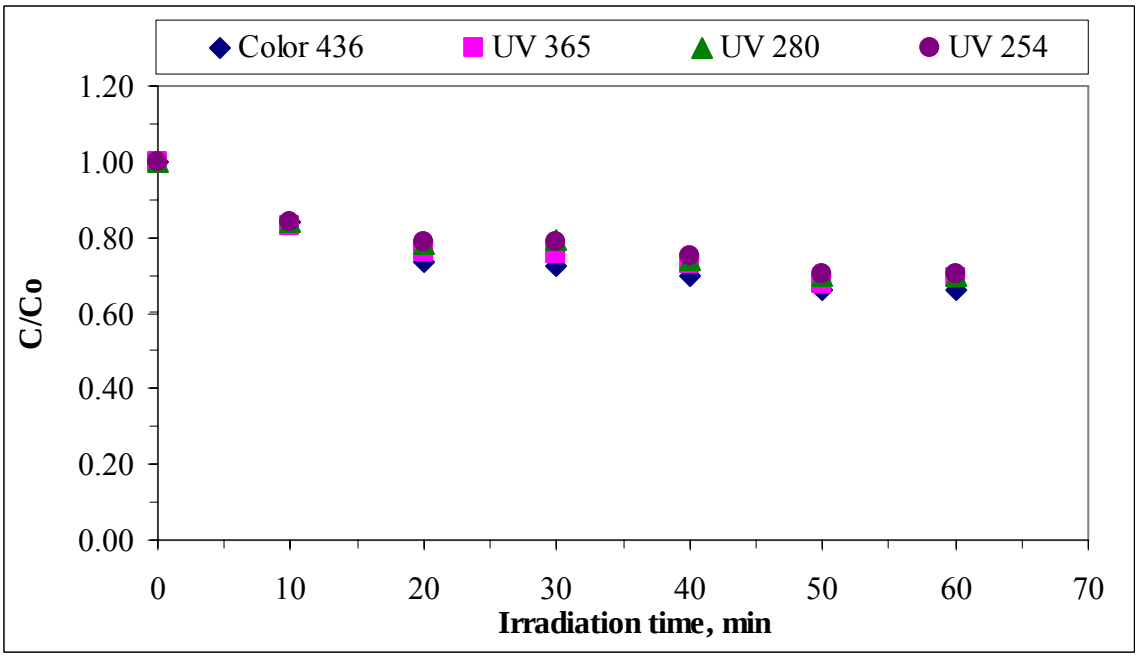

Figure 4.51. Normalized $Color_{436}$, UV_{365}, UV_{280} and UV_{254} values of 100 kDa fraction of humic acid with respect to irradiation time in the presence of Fe doped TiO_2.

Photocatalytic degradation of 100 kDa fraction of humic acid was also evaluated in terms of UV-vis parameters as expressed by $Color_{436}$, UV_{365}, UV_{280} and UV_{254} (Figure 4.51). Initial adsorptive removal of 100 kDa fraction of humic acid in the presence of Fe doped TiO_2 could also be assessed by the specified UV-vis parameters. The initial removal efficiencies were 12%, 9%, 8% and 9% for $Color_{436}$, UV_{365}, UV_{280} and UV_{254}, respectively. Moreover, 34% removal of $Color_{436}$ and 30% removal of UV_{254} were recorded at the end of 60 minutes of photocatalytic treatment. The removal efficiencies followed a basic trend of $Color_{436} > UV_{365} > UV_{280} = UV_{254}$ irrespective of the irradiation time after 60 min. The role of Fe doped TiO_2 could be expressed by the observed comparatively lower removal efficiencies with respect to the results attained using bare TiO_2. The reason could also be attributed to the prevailing surface interactions on the oxide surface in the presence of Fe.

4.3.7.2. Fluorescence Spectroscopic Evaluation of 100 kDa Fraction of Humic Acid During Photocatalytic Degradation in the Presence of Fe doped TiO_2. Emission scan fluorescence spectra of the photocatalytically treated 100 kDa fraction of humic acid in the presence of Fe doped TiO_2 samples were displayed in Figures 4.52 and 4.53. The emission scan fluorescence spectra was scanned in the range of 360-600 nm and 380-600 nm at excitation wavelength of 350 and 370 nm, respectively. The effect of the excitation wavelength on the fluorescence intensity of raw humic acid could also be observed most significantly in the wavelength of 450 nm for both excitation wavelengths of 350 and wavelength of 370 nm. It could be concluded that the fluorescence spectra of the photocatalytically treated 100 kDa fraction of humic acids monotonously decreased with respect to the increasing wavelength. After 30 minutes of irradiation time, the emission fluorescence scan spectra of the photocatalytically oxidized 100 kDa fraction of humic acid displayed a rather smooth fluorescence intensity trend comprised of a broader peak profile and upon further irradiation periods a similar trend was also recorded.

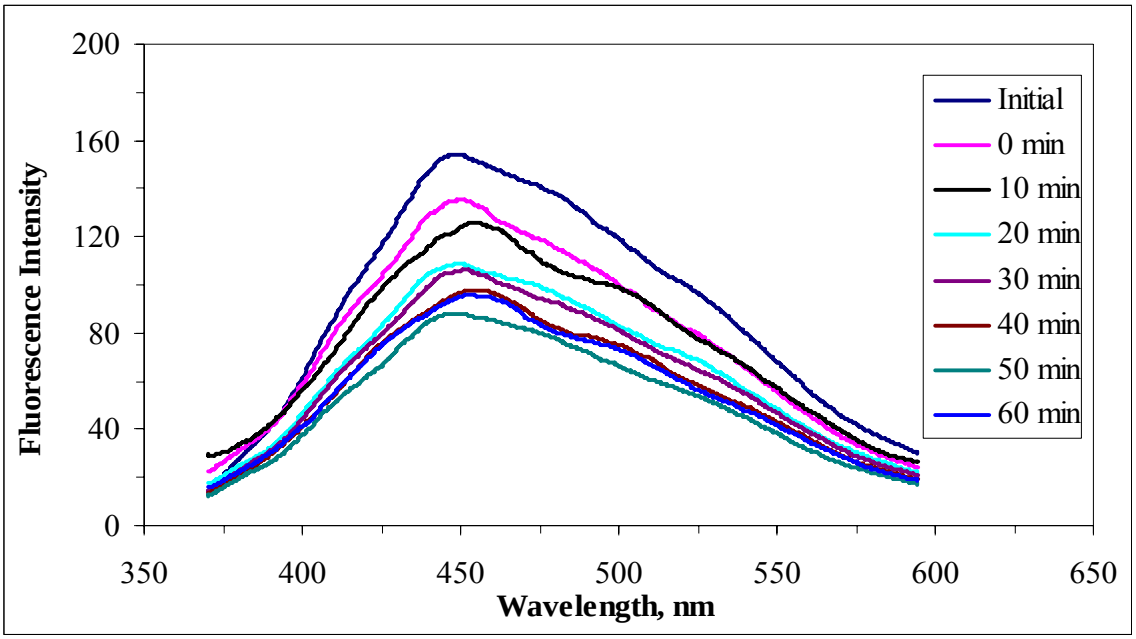

Figure 4.52. Emission scan fluorescence spectra ($FI_{emis\ 350}$) of 100 kDa fraction of humic acid during photocatalytic degradation in the presence of Fe doped TiO_2 (Initial represents 100kDa fraction of humic acid).

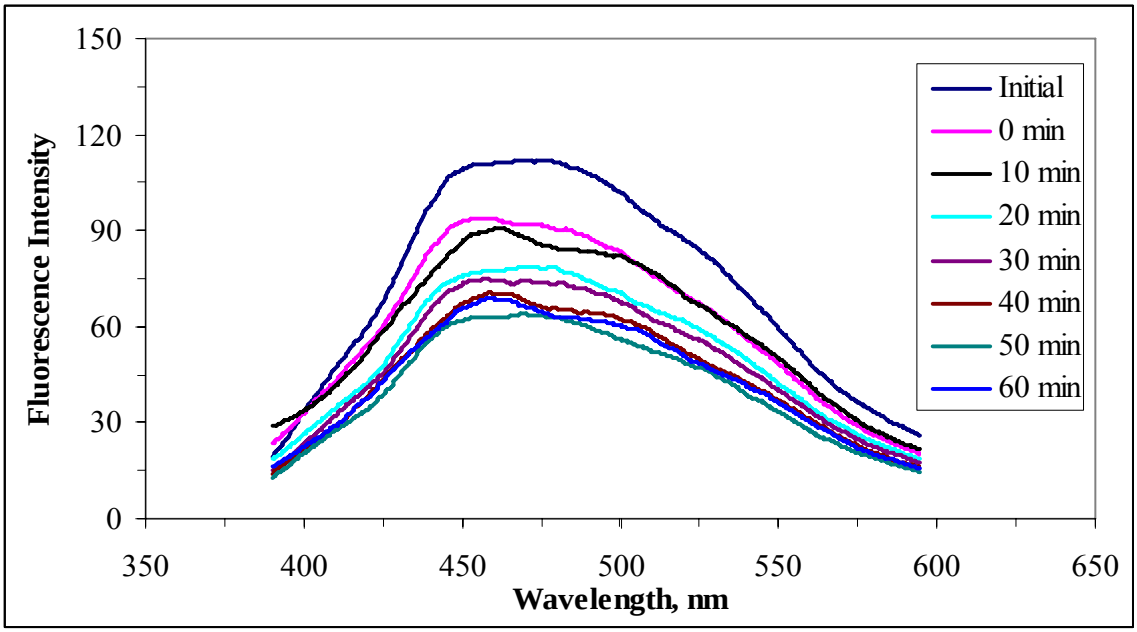

Figure 4.53. Emission scan fluorescence spectra ($FI_{emis\ 370}$) of 100 kDa fraction of humic acid during photocatalytic degradation in the presence of Fe doped TiO_2 (Initial represents 100kDa fraction of humic acid).

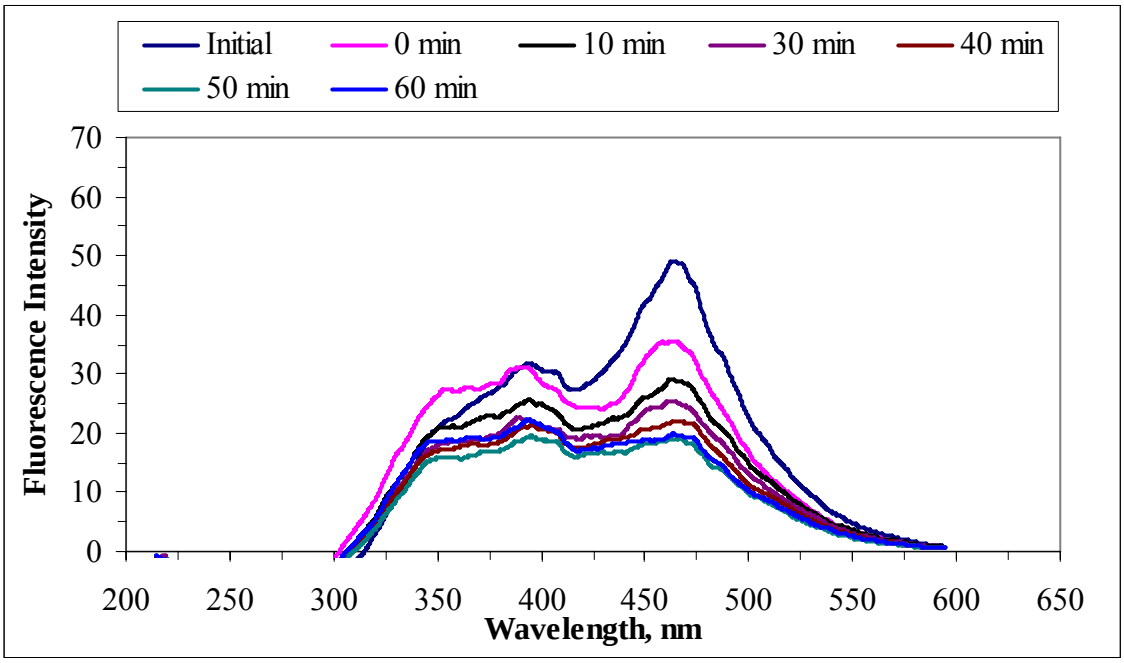

Figure 4.54. Synchronous scan fluorescence spectra of 100 kDa fraction of humic acid during photocatalytic degradation in the presence of Fe doped TiO_2

Synchronous scan fluorescence spectra of the photocatalytically treated 100 kDa fraction of the humic acid were shown in Figure 4.54. After 20 minutes of irradiation time, 100 kDa fraction of humic acid displayed nearly same trend of overlapping spectral profile. Upon irradiation period of 50 min, the evenness observed in the fluorescence spectra acquired in both emission and synchronous scan modes displayed that the photocatalytically oxidized humic moieties exhibited non-reactivity towards Fe doped TiO_2.

4.3.8. Photocatalytic Degradation of 30 kDa Fraction of Humic Acid in the Presence of Fe doped TiO_2

Photocatalytic degradation of 30 kDa fraction of humic acid samples were performed by using Fe doped TiO_2 and evaluated by UV-vis spectra and fluorescence spectra recorded in emission scan and synchronous modes.

4.3.8.1. UV-vis Spectroscopic Evaluation of 30 kDa Fraction of Humic Acid During Photocatalytic Degradation in the Presence of Fe doped TiO_2. UV-vis spectra of 30 kDa fraction of humic acid during photocatalytic degradation were indicated in Figure 4.55.

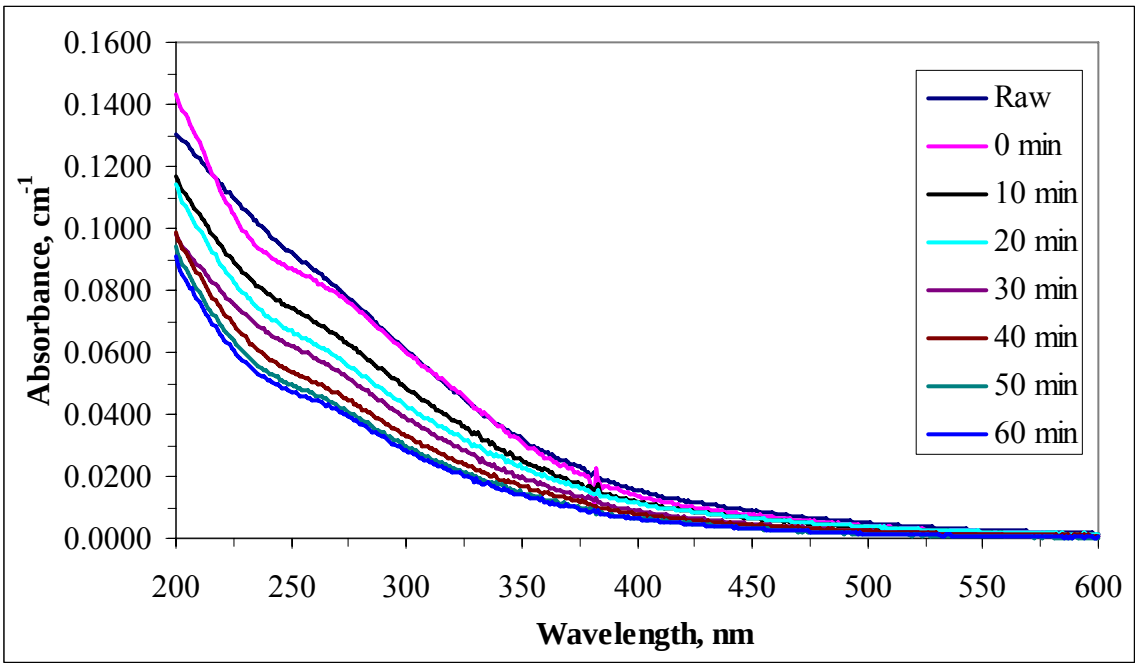

Figure 4.55. UV-vis spectra of 30 kDa fraction of humic acid during photocatalytic degradation in the presence of Fe doped TiO_2 (Initial represents 30 kDa fraction of humic acid).

It could be stated that, the UV-vis spectra of humic acid monotonously decreased with increasing wavelength in a usual manner. Displaying the same basic pattern of declining trend, a decrease in the absorbance values was observed with the increasing irradiation time during photocatalytic degradation of 30 kDa fraction of humic acid. When UV-vis spectroscopic profile of raw humic acid on bare TiO_2 was compared to UV-vis spectroscopic profile in the presence of Fe doped TiO_2, it was observed that the 30 kDa fraction of humic acid in the presence of bare TiO_2 had a similar declining trend with higher absortivities than the ones recorded in the presence of Fe doped TiO_2 for all irradiation times.

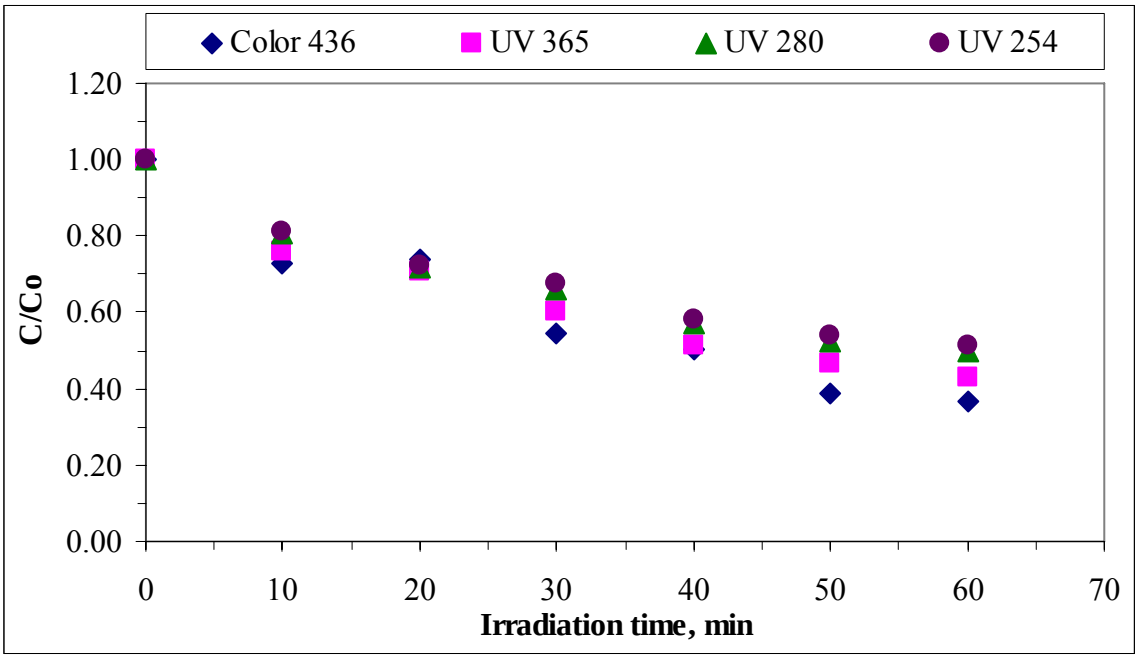

Figure 4.56. Normalized $Color_{436}$, UV_{365}, UV_{280} and UV_{254} values of 30 kDa fraction of humic acid with respect to irradiation time in the presence of Fe doped TiO_2.

Photocatalytic degradation of 30 kDa fraction of humic acid in the presence of Fe doped TiO_2 was also evaluated in terms of UV-vis parameters as expressed by $Color_{436}$, UV_{365}, UV_{280} and UV_{254} (Figure 4.56). Initial adsorptive removal efficiencies of raw humic acid were found to be 16%, 7%, 2% and 5% for $Color_{436}$, UV_{365}, UV_{280} and UV_{254}, respectively.. While 26% of $Color_{436}$ was removed in 10 minutes of irradiation period, 63% removal was achieved after 60 minutes in the presence of Fe doped TiO_2. On the contrary, 81% of $Color_{436}$ was removed in 10 minutes of irradiation period and 100% removal was achieved after 60 minutes of irradiation time in the presence of bare TiO_2. In general, the removal efficiencies followed a basic trend of $Color_{436}>UV_{365}>UV_{280}>UV_{254}$ irrespective of the irradiation time after 60 min.

4.3.8.2. Fluorescence Spectroscopic Evaluation of 30 kDa Fraction of Humic Acid During Photocatalytic Degradation in the Presence of Fe doped TiO_2. Emission scan fluorescence spectra of 30 kDa fraction of humic acid were presented in Figures 4.57 and 4.58. The emission scan fluorescence spectra of 30 kDa fraction of humic acid were presented with respect to the photocatalytic irradiation time.

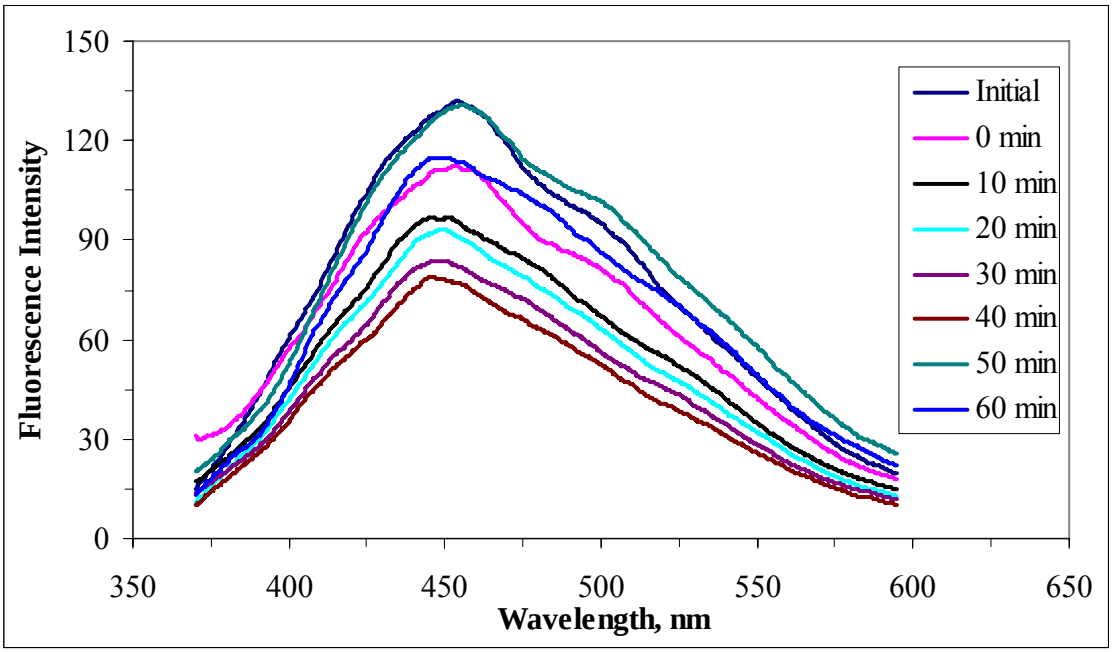

Figure 4.57. Emission scan fluorescence spectra ($FI_{emis\ 350}$) of 30 kDa fraction of humic acid during photocatalytic degradation in the presence of Fe doped TiO_2 (Initial represents 30 kDa fraction of humic acid).

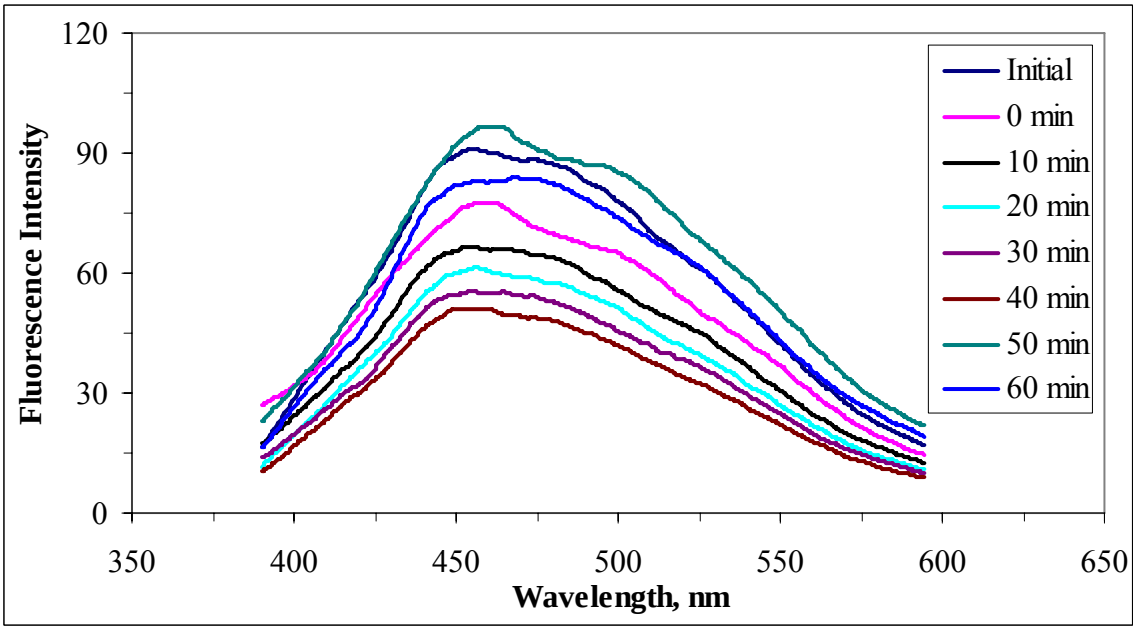

Figure 4.58. Emission scan fluorescence spectra ($FI_{emis\ 370}$) of 30 kDa fraction of humic acid during photocatalytic degradation in the presence of Fe doped TiO_2 (Initial represents 30 kDa fraction of humic acid).

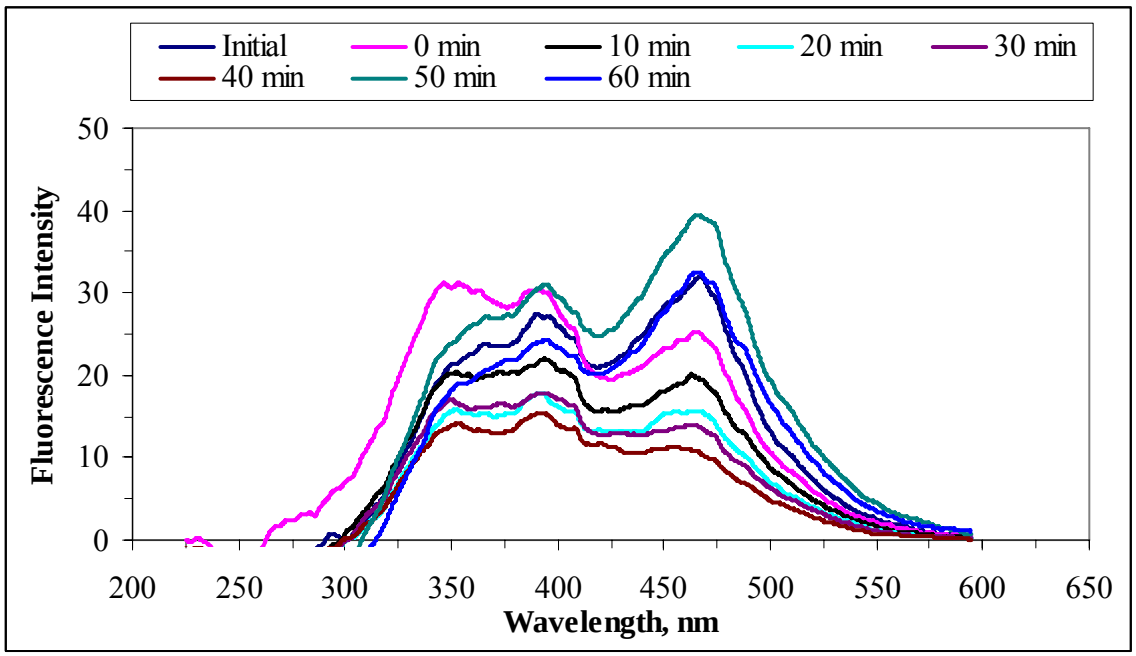

Figure 4.59. Synchronous scan fluorescence spectra of 30 kDa fraction of humic acid during photocatalytic degradation in the presence of Fe doped TiO_2 (Initial represents 30 kDa fraction of humic acid).

With increased photocatalytic irradiation time, the fluorescence intensities slightly decreased. However, both of the scan emission fluorescence spectra recorded kept the same characteristic peak around 450 nm. The synchronous scan fluorescence spectra of 30 kDa fraction of humic acid during photocatalytic degradation in the presence of bare TiO_2 was presented in Figure 4.59. It should also be mentioned that the presented synchronous scan fluorescence spectral patterns displayed a decreasing but inconsistent trend with respect to irradiation time.

It could be concluded that the UV-vis spectra recorded for all of the samples displayed a consistent basic declining pattern irrespective of the irradiation period and photocatalyst type. On the other hand fluorescence spectral profiles exhibited different patterns with respect to both irradiation time and photocatalyst type. Therefore, UV-vis parameters could be used for kinetic evaluation of the photocatalytic degradation of the humic acid and its molecular size fractions whereas fluorescence spectra could only bring a qualitative basis for comparison.

4.3.9. Photocatalytic Degradation of Humic Acid with respect to NPOC

Total organic carbon (TOC) is the amount of carbon bound in an organic compound and is often used as a non-specific indicator of water quality. A typical analysis for TOC measures both the total carbon present as well as the so called "inorganic carbon" (IC), the latter representing the content of dissolved carbon dioxide and carbonic acid salts. Another common variant of TOC analysis involves removing the IC portion first and then measuring the leftover carbon. This method involves purging an acidified sample with carbon-free air or nitrogen prior to measurement, and so is more accurately called non-purgeable organic carbon (NPOC).

4.3.9.1. Photocatalytic Degradation of Raw Humic Acid with respect to NPOC. Photocatalytic degradation of raw humic acid with respect to NPOC was presented in figure 4.60.

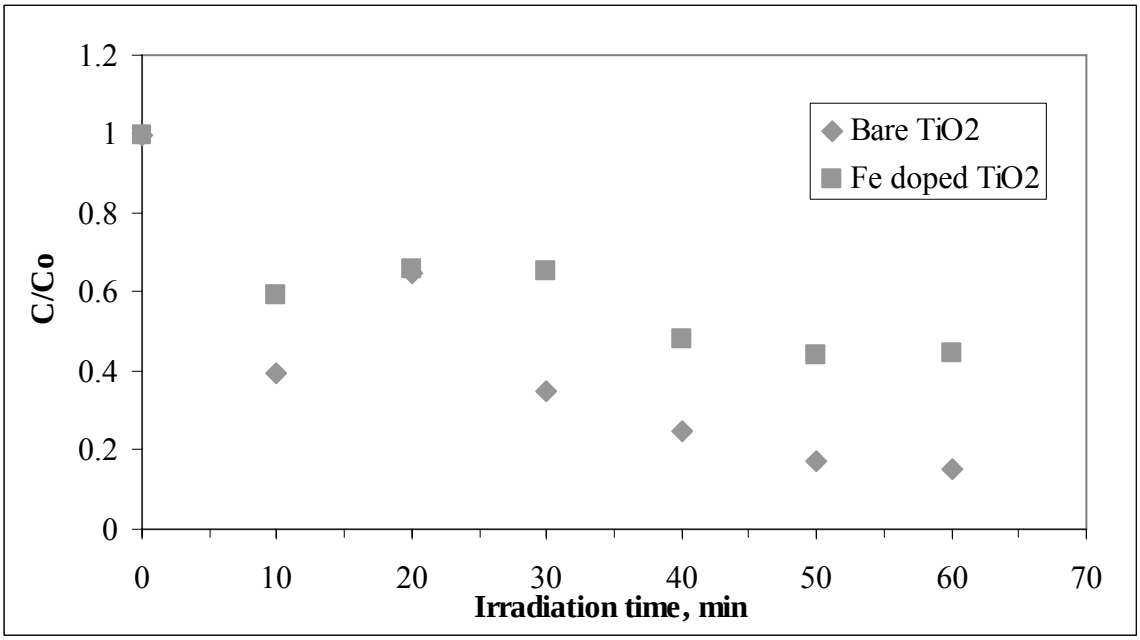

Figure 4.60. Photocatalytic degradation of raw humic acid with respect to NPOC.

Photocatalytic degradation of raw humic acid with respect to NPOC was evaluated in in the presence of bare and Fe doped TiO_2 (Figure 4.60). The initial removal efficiencies were 38% and 22% for bare TiO_2 and Fe doped TiO_2, respectively. 85% removal in the presence of bare TiO_2 and 56% removal in the presence of Fe doped TiO_2 were recorded at

the end of 60 minutes of photocatalytic treatment. The removal efficiencies followed a trend of bare TiO_2 > Fe doped TiO_2.

4.3.9.2. Photocatalytic Degradation of 0.45µm Filtered Fraction of Humic Acid with respect to NPOC. Photocatalytic degradation of 0.45µm filtered fraction of humic acid with respect to NPOC was evaluated in the presence of bare and Fe doped TiO_2 (Figure 4.61).

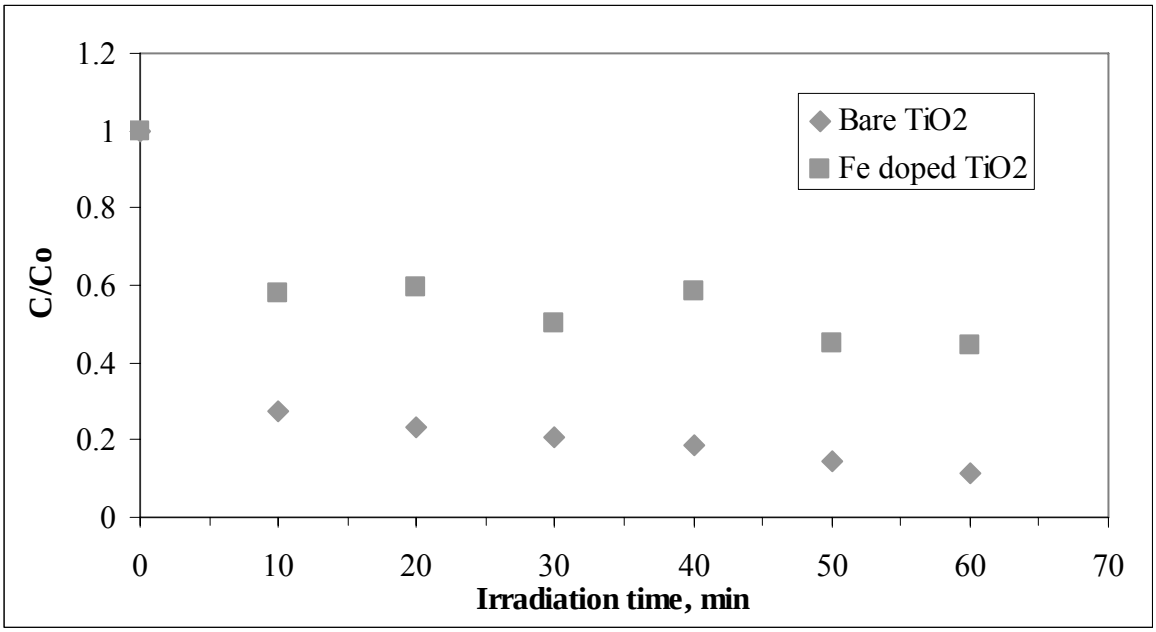

Figure 4.61. Photocatalytic Degradation of 0.45µm Filtered Fraction of Humic Acid with respect to NPOC.

Initial removal efficiencies of 0.45 µm filtered fraction of humic acid with respect to NPOC were 71% and 36%in the presence of bare TiO_2 and in the presence of Fe doped TiO_2, respectively. The removal efficiencies were 72%, 76%, 80%, 81%, 85% and 88% for 10 min, 20 min, 30 min, 40imin, 50min and 60 min, respectively in the presence of bare TiO_2. On the other hand, the removal efficiencies were 42%, 40%, 50%, 41%, 55% and 56% for 10 min, 20 min, 30 min, 40imin, 50min and 60 min, respectively in the presence of Fe doped TiO_2 At the end of 60 minutes of irradiation time, the removal efficiencies followed a trend of bare TiO_2 > Fe doped TiO_2 (Figure 4.61).

4.3.9.3. Photocatalytic degradation of 100 kDa Fraction of Humic Acid with respect to NPOC. Photocatalytic degradation of 100 kDa Fraction of Humic Acid with respect to NPOC was performed in the presence of bare and Fe doped TiO_2 (Figure 4.62).

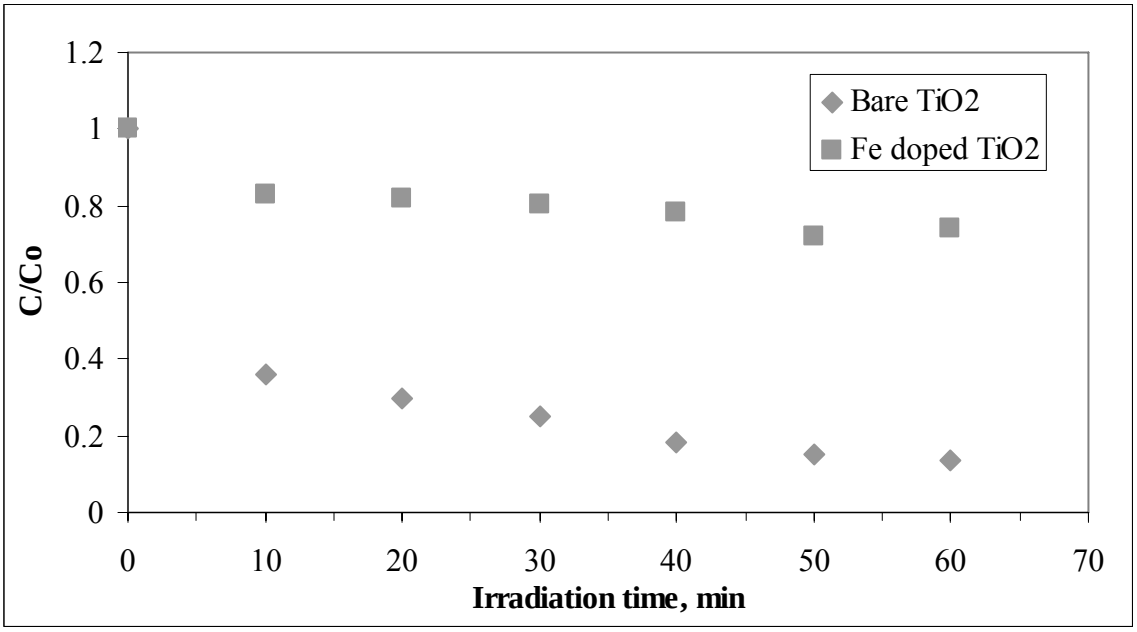

Figure 4.62. Photocatalytic Degradation of 100 kDa Fraction of Humic Acid with respect to NPOC.

Photocatalytic degradation of 100 kDa fraction of humic acid was evaluated in terms of NPOC (Figure 4.62). Initial removal efficiencies of 100 kDa fraction of humic acid were 56% and 23%in the presence of bare TiO_2 and in the presence of Fe doped TiO_2, respectively. 86% removal in the presence of bare TiO_2 and 26% removal in the presence of Fe doped TiO_2 were recorded at the end of 60 minutes of photocatalytic treatment. The removal efficiencies followed a trend of bare TiO_2>Fe doped TiO_2. Removal in the presence of bare TiO2 displayed a faster degradation tendency in comparison to Fe doped TiO_2.

4.3.9.4. Photocatalytic degradation of 30 kDa Fraction of Humic Acid with respect to NPOC. Photocatalytic degradation of 30 kDa Fraction of Humic Acid with respect to NPOC was evaluated in the presence of bare and Fe doped TiO2 (Figure 4.63).

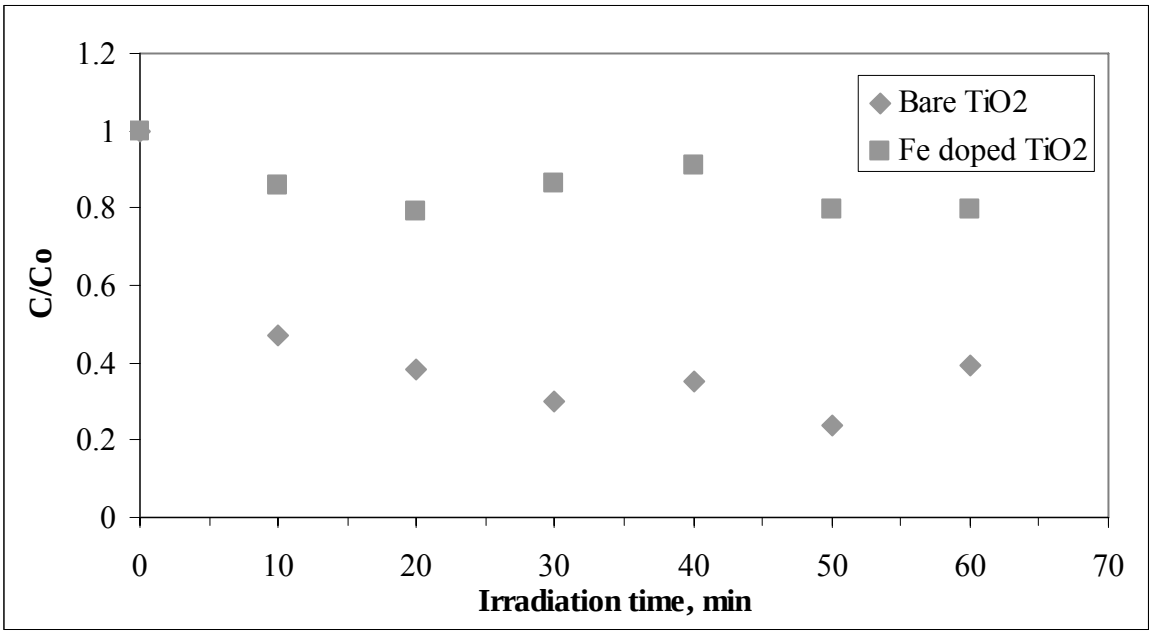

Figure 4.63. Photocatalytic Degradation of 30 kDa Fraction of Humic Acid with respect to NPOC.

Initial removal efficiencies of 100 kDa fraction of humic acid with respect to NPOC were 27% and 8%in the presence of bare TiO_2 and in the presence of Fe doped TiO_2, respectively. 60% removal in the presence of bare TiO_2 and 20% removal in the presence of Fe doped TiO_2 were recorded at the end of 60 minutes of photocatalytic treatment. The removal efficiencies followed a trend of bare TiO_2 > Fe doped TiO_2 (Figure 4.63).

4.4. Comparative Evaluation of the Photocatalytic Degradation of Humic acid and Its Molecular Size Fractions

For comparison purposes, the effect of Fe doping on TiO_2 on the photocatalytic degradation of humic acid and its molecular fractions in aqueous medium was compared to bare TiO_2. The photocatalytic removal efficiencies as expressed for the specified UV-vis parameters for raw, 0. 45µm filtered fraction, 100 kDa fraction and 30 kDa fraction of humic acid at 30 min and 60 min of irradiation times were calculated and given at Table 4.2.

Table 4.2. Removal efficiencies of raw humic acid, 0.45 μm filtered fraction, 100 kDa fraction and 30 kDa fraction of humic in the presence bare TiO_2 and Fe doped TiO_2.

	Removal efficiency, %							
	$Color_{436}$		UV_{365}		UV_{280}		UV_{254}	
	30 min	60 min	30 min	60 min	30 min	60 min	30 min	60 min
Humic acid and molecular size fractions in the presence of bare TiO_2								
Raw	90	96	88	94	83	89	79	88
0.45 μm f.f.*	89	100	85	97	77	92	74	91
100 kDa f.**	81	99	89	97	83	93	74	62
30 kDa f.**	92	100	95	100	94	100	93	99
Humic acid and its molecular size fractions in the presence of Fe doped TiO_2								
Raw	44	62	42	61	39	57	38	56
0.45 μm f.f.*	35	48	31	46	27	41	28	43
100 kDa f.**	28	34	24	31	21	30	21	30
30 kDa f.**	46	63	40	57	34	50	32	49

*filtered fraction, ** fraction

In general, the removal efficiency of humic acid and its molecular size fractions expressed by the specified UV-vis parameters roughly displayed a trend as $Color_{436} \geq UV_{365}$ and $UV_{280} \geq UV_{254}$ both irrespective of the selected irradiation period and the photocatalyst type. The lowest photocatalytic removal was attained for 100 kDa fraction of humic acid in the presence of Fe doped TiO_2 as expressed by UV_{280} and UV_{254}. Complete elimination of the UV-vis parameters were obtained for 30 kDa fraction in the presence of bare TiO_2. However, a retardation effect could be attributed to the use of Fe doped TiO_2 irrespective of the irradiation period and humic acid molecular size fractions.

4.5. Kinetic Evaluation

In relation to the UV-vis and fluorescence spectroscopic characterization of raw and 0.45 µm filtered fraction, 100 kDa fraction and 30 kDa fraction of humic acid, photocatalytic degradation data were also processed using pseudo first order kinetic rate model.

4.5.1. Kinetic model

The generally accepted model for the oxidation of organics to carbon dioxide in the photocatalysis is that the oxygen and organic molecules are adsorbed on the surface of catalyst, and react with photoelectrons to form reactive oxygen species mainly hydroxyl radicals. Then the organic species react with the photoholes either directly or via an adsorbed hydroxide radical intermediate (Abdullah et al., 1990). Moreover from kinetics point of view, photocatalytic degradation of humic substances are known to obey pseudo first order kinetic rate model (Bekbolet et al., 1998; Bekbolet et al., 2002).

Pseudo first order kinetic model is expressed by the following equation;

$$R = - dA/dt = k\ A \qquad (4.1)$$

The terms represent the following meanings;

R: Pseudo first order rate in terms of the specified UV-vis parameters ($m^{-1}\ min^{-1}$)

A: Specified UV-vis parameters (m^{-1})

t: Irradiation time (min)

k: Pseudo first order reaction rate constant (min^{-1}).

The related half life, $t_{1/2}$ (min) values could also be assessed by the Equation (4.2);

$$t_{1/2} = 0.693/k \qquad (4.2)$$

The kinetic model parameters could be successfully used for the comparative evaluation of the photocatalytic degradation data achieved under the specified experimental conditions. According to the data obtained by photocatalytic degradation experiments, pseudo first order reaction rate constants, half-life values, related correlation coefficients of photocatalytic degradation and rates are calculated (R^2 >0.80) and given in respective tables.

4.5.2. Kinetic Modeling of Photocatalytic Degradation of Raw Humic Acid in the Presence of Bare TiO_2

The kinetic evaluation of the experimental data for the photocatalytic degradation of raw humic acid in the presence of bare TiO_2 revealed the following pseudo first order kinetic model parameters for $Color_{436}$, UV_{365}, UV_{280} and UV_{254} as presented in Table 4.3. Pseudo first order degradation rate constants (k, min^{-1}) were found to be $4.74x10^{-2}$, $4.23x10^{-2}$, $3.35x10^{-2}$ and $3.18x10^{-2}$ for the UV-vis parameters specified as $Color_{436}$, UV_{365}, UV_{280} and UV_{254}, respectively.

Table 4.3. Pseudo first order kinetic model parameters for the photocatalytic degradation of raw humic acid in the presence of bare TiO_2.

	First order kinetic model parameters		
Parameter	Rate constant k, min^{-1}	Half-life, $t_{1/2}$, min	Rate, m^{-1} min^{-1}
$Color_{436}$	$4.74x10^{-2}$	15	0.408
UV_{365}	$4.23x10^{-2}$	16	0.766
UV_{280}	$3.35x10^{-2}$	21	1.387
UV_{254}	$3.18x10^{-2}$	22	1.513

The corresponding half life ($t_{1/2}$, min) values were found to be in the range of 15-22 min. Photocatalytic degradation rates (R, m^{-1} min^{-1}) were calculated by using the kinetic rate equation (4.1.) and expressed by the decreasing order of UV_{254} > UV_{280} > UV_{365} > $Color_{436}$. Uyguner and Bekbölet (2005a) reported pseudo first order model reaction rate

constants, k (min^{-1}) for humic acid removal to be decreasing in the order of 2.98 $x10^{-2}$, 2.71$x10^{-2}$, 2.15$x10^{-2}$, 2.01$x10^{-2}$ min^{-1} for the specified UV–vis parameters of $Color_{436}$, UV_{365}, UV_{280} and UV_{254}, respectively. The comparatively lower rate constants could be explained by the composition of the humic acid solution.

4.5.3. Kinetic Modeling of Photocatalytic Degradation of Raw Humic Acid in the Presence of Fe doped TiO_2

The kinetic evaluation of the experimental data for the photocatalytic degradation of raw humic acid in the presence of Fe doped TiO_2 revealed the following pseudo first order kinetic model parameters for $Color_{436}$, UV_{365}, UV_{280} and UV_{254} as presented in Table 4.4. Pseudo first order degradation rate constants (k, min^{-1}) were found to be 1.62$x10^{-2}$, 1.51$x10^{-2}$, 1.37$x10^{-2}$ and 1.33$x10^{-2}$ for the UV-vis parameters specified as $Color_{436}$, UV_{365}, UV_{280} and UV_{254}, respectively.

Table 4.4. Pseudo first order kinetic model parameters for the photocatalytic degradation of raw humic acid in the presence of Fe doped TiO_2

	First order kinetic model parameters		
Parameter	Rate constant k, min^{-1}	Half-life, $t_{1/2}$, min	Rate, m^{-1} min^{-1}
$Color_{436}$	1.62$x10^{-2}$	43	0.1395
UV_{365}	1.51$x10^{-2}$	46	0.2733
UV_{280}	1.37$x10^{-2}$	51	0.5672
UV_{254}	1.33$x10^{-2}$	52	0.6329

The corresponding half life ($t_{1/2}$, min) values were in the range of 43-52 min. Photocatalytic degradation rates (R, m^{-1} min^{-1}) were calculated by using the rate equation (4.1) expressed by removals in the decreasing order of UV_{254} > UV_{280} >UV_{365} > $Color_{436}$. The pseudo first order kinetic parameters displayed considerably higher removal efficiencies for raw humic acid in the presence of bare TiO_2 with respect to raw humic acid in the presence of Fe doped TiO_2. Furthermore, the removal of color forming moieties was

found to be relatively faster than the UV absorbing centers (~ > 15%) as expressed by UV_{280} and UV_{254}.

4.5.4. Kinetic Modeling of Photocatalytic Degradation of 0.45 μm Filtered Fraction of Humic Acid in the Presence of Bare TiO_2

The kinetic evaluation of the experimental data for the photocatalytic degradation of 0.45 μm filtered fraction of humic acid in the presence of bare TiO_2 revealed the following pseudo first order kinetic model parameters for $Color_{436}$, UV_{365}, UV_{280} and UV_{254} as presented in Table 4.5. Pseudo first order degradation rate constants (k, min^{-1}) were found to be $7.71x10^{-2}$, $5.00x10^{-2}$, $3.67x10^{-2}$ and $3.44x10^{-2}$ for the UV-vis parameters specified as $Color_{436}$, UV_{365}, UV_{280} and UV_{254}, respectively.

Table 4.5. Pseudo first order kinetic model parameters for the photocatalytic degradation of 0.45 μm filtered fraction of humic acid in the presence of bare TiO_2.

	First order kinetic model parameters		
Parameter	Rate constant k, min^{-1}	Half-life, $t_{1/2}$, min	Rate, m^{-1} min^{-1}
$Color_{436}$	$7.71x10^{-2}$	9	0.5058
UV_{365}	$5.00x10^{-2}$	14	0.6855
UV_{280}	$3.67x10^{-2}$	19	1.1916
UV_{254}	$3.44x10^{-2}$	20	1.3113

The corresponding half life ($t_{1/2}$, min) values were in the range of 9-20 min. Photocatalytic degradation rates (R, m^{-1} min^{-1}) were calculated by using the rate equation (4.1) expressed by the decreasing order of UV_{254} > UV_{280} > UV_{365} > $Color_{436}$. It can be concluded that 0.45μm filtered fraction of humic acid and raw humic acid indicated similar decreasing order in the presence of bare TiO_2 as presented in Table 4.5 and Table 4.3. The pseudo first order kinetic parameters displayed higher removal efficiencies for 0.45 μm filtered fraction of humic acid than raw humic acid in the presence of bare TiO_2. The enhancement factor could be regarded as 1.6 fold for $Color_{436}$, 1.2 fold for UV_{365}, 1.1 fold

for UV_{280}. Furthermore, the removal of color forming moieties was found to be relatively faster than the UV absorbing centers.

4.5.5. Kinetic Modeling of Photocatalytic Degradation of 0.45 μm Filtered Fraction of Humic Acid in the Presence of Fe doped TiO_2

The kinetic evaluation of the experimental data for the photocatalytic degradation of 0.45 μm filtered fraction of humic acid in the presence of Fe doped TiO_2 revealed the following pseudo first order kinetic model parameters for $Color_{436}$, UV_{365}, UV_{280} and UV_{254} as presented in Table 4.6.

Table 4.6. Pseudo first order kinetic model parameters for the photocatalytic degradation of 0.45 μm filtered fraction of humic acid in the presence of Fe doped TiO_2.

	First order kinetic model parameters		
Parameter	Rate constant k, min^{-1}	Half-life, $t_{1/2}$, min	Rate, m^{-1} min^{-1}
$Color_{436}$	$9.58x10^{-3}$	72	0.0628
UV_{365}	$9.09x10^{-3}$	76	0.1246
UV_{280}	$7.89x10^{-3}$	88	0.2562
UV_{254}	$8.25x10^{-3}$	83	0.3145

Pseudo first order degradation rate constants (k, min^{-1}) were found to be $9.58x10^{-3}$, $9.09x10^{-3}$, $7.89x10^{-3}$ and $8.25x10^{-3}$ for the UV-vis parameters specified as $Color_{436}$, UV_{365}, UV_{280} and UV_{254}, respectively. The corresponding half life ($t_{1/2}$, min) values were in the range of 72-88 min. Photocatalytic degradation rates (R, m^{-1} min^{-1}) were calculated by using the rate equation (4.1) expressed by the decreasing order of $UV_{254} > UV_{280} > UV_{365} > Color_{436}$. Furthermore, the removal of color forming moieties was found to be relatively faster than the UV absorbing centers (~ > 14%) as expressed by UV_{280} and UV_{254}.

4.5.6. Kinetic Modeling of Photocatalytic Degradation of 100 kDa Fraction of Humic Acid in the Presence of Bare TiO_2

The kinetic evaluation of the experimental data for the photocatalytic degradation of 100 kDa fraction of humic acid in the presence of bare TiO_2 revealed the following pseudo first order kinetic model parameters for $Color_{436}$, UV_{365}, UV_{280} and UV_{254} as presented in Table 4.7.

Table 4.7. Pseudo first order kinetic model parameters for the photocatalytic degradation of 100 kDa fraction of humic acid in the presence of bare TiO_2.

	First order kinetic model parameters		
Parameter	Rate constant k, min^{-1}	Half-life, $t_{1/2}$, min	Rate, m^{-1} min^{-1}
$Color_{436}$	$7.17x10^{-2}$	10	0.2825
UV_{365}	$5.78x10^{-2}$	12	0.5029
UV_{280}	$5.24x10^{-2}$	13	1.1313
UV_{254}	$3.01x10^{-2}$	23	0.7669

Pseudo first order degradation rate constants (k, min^{-1}) were calculated as $7.17x10^{-2}$, $5.78x10^{-2}$, $5.24x10^{-2}$ and $3.01x10^{-2}$ for the UV-vis parameters specified as $Color_{436}$, UV_{365}, UV_{280} and UV_{254}, respectively. The corresponding half life ($t_{1/2}$, min) values were in the range of 10-23 min. Photocatalytic degradation rates (R, m^{-1} min^{-1}) were calculated by using the rate equation (4.1) expressed by the decreasing order of $UV_{280} > UV_{254} > UV_{365} > Color_{436}$. The pseudo first order kinetic parameters displayed higher removal efficiencies for 100 kDa fraction of humic acid with respect to both 0.45 μm filtered fraction of humic acid and raw humic acid in the presence of bare TiO_2. The removal of color forming moieties was found to be relatively faster than the UV absorbing centers (~ > 27%) as expressed by UV_{280} and UV_{254}.

4.5.7. Kinetic Modeling of Photocatalytic Degradation of 100 kDa Fraction of Humic Acid in the Presence of Fe doped TiO_2

The kinetic evaluation of the experimental data for the photocatalytic degradation of 100 kDa fraction of humic acid in the presence of Fe doped TiO_2 revealed the following pseudo first order kinetic model parameters for $Color_{436}$, UV_{365}, UV_{280} and UV_{254} as presented in Table 4.8.

Table 4.8. Pseudo first order kinetic model parameters for the photocatalytic degradation of 100 kDa fraction of humic acid in the presence of Fe doped TiO_2.

	First order kinetic model parameters		
Parameter	Rate constant k, min^{-1}	Half-life, $t_{1/2}$, min	Rate, m^{-1} min^{-1}
$Color_{436}$	$6.36x10^{-3}$	108	0.0250
UV_{365}	$5.50x10^{-3}$	126	0.0478
UV_{280}	$5.35x10^{-3}$	130	0.1155
UV_{254}	$5.20x10^{-3}$	133	0.1325

Pseudo first order degradation rate constants (k, min^{-1}) were found to be $6.36x10^{-3}$, $5.50x10^{-3}$, $5.35x10^{-3}$ and $5.20x10^{-3}$ for the UV-vis parameters specified as $Color_{436}$, UV_{365}, UV_{280} and UV_{254}, respectively. The corresponding half life ($t_{1/2}$, min) values were in the range of 108-133 min. Photocatalytic degradation rates (R, m^{-1} min^{-1}) were calculated by using the rate equation (4.1) expressed by the decreasing order of $UV_{280} > UV_{254} > UV_{365} > Color_{436}$. The presence of Fe doped TiO_2 altered the photocatalytic degradation rates of 100 kDa fraction of humic acid with respect to the 0.45 μm filtered fraction of humic acid and raw humic acid. The removal of color forming moieties was found to be relatively faster than the UV absorbing centers (~ > 14%) as expressed by UV_{280} and UV_{254}.

4.5.8. Kinetic Modeling of Photocatalytic Degradation of 30 kDa Fraction of Humic Acid in the Presence of Bare TiO_2

The kinetic evaluation of the experimental data for the photocatalytic degradation of 30 kDa fraction of humic acid in the presence of bare TiO_2 revealed the following pseudo first order kinetic model parameters for $Color_{436}$, UV_{365}, UV_{280} and UV_{254} as presented in Table 4.9.

Table 4.9. Pseudo first order kinetic model parameters for the photocatalytic degradation of 30 kDa fraction of humic acid in the presence of bare TiO_2.

	First order kinetic model parameters		
Parameter	Rate constant k, min^{-1}	Half-life, $t_{1/2}$, min	Rate, m^{-1} min^{-1}
$Color_{436}$	nd*	nd*	nd*
UV_{365}	nd*	nd*	nd*
UV_{280}	$8.70x10^{-2}$	8	0.6438
UV_{254}	$7.23x10^{-2}$	10	0.6500

*not detectable

Pseudo first order degradation rate constants (k, min^{-1}) were found to be $7.93x10^{-2}$ and $8.06x10^{-2}$ for the UV-vis parameters specified as UV_{280} and UV_{254}, respectively. The corresponding half life ($t_{1/2}$, min) values were 8 and 10 min for UV_{280} and UV_{254}. Photocatalytic degradation rates (R, m^{-1} min^{-1}) were calculated by using the rate equation (4.1) expressed by the decreasing order of $UV_{254} > UV_{280}$. The pseudo first order kinetic parameters displayed considerably higher removal efficiencies for 30 kDa fraction of humic acid with respect to 100 kDa fraction of humic acid, 0.45 μm filtered fraction of humic acid and raw humic acid in the presence of bare TiO_2.

4.5.9. Kinetic Modeling of Photocatalytic Degradation of 30 kDa Fraction of Humic Acid in the Presence of Fe doped TiO_2

The kinetic evaluation of the experimental data for the photocatalytic degradation of 30 kDa fraction of humic acid in the presence of Fe doped TiO_2 revealed the following pseudo first order kinetic model parameters for $Color_{436}$, UV_{365}, UV_{280} and UV_{254} as presented in Table 4.10.

Table 4.10. Pseudo first order kinetic model parameters for the photocatalytic degradation of 30 kDa fraction of humic acid in the presence of Fe doped TiO_2.

	First order kinetic model parameters		
Parameter	Rate constant k, min^{-1}	Half-life, $t_{1/2}$, min	Rate, m^{-1} min^{-1}
$Color_{436}$	$1.65x10^{-2}$	42	0.017
UV_{365}	$1.37x10^{-2}$	51	0.036
UV_{280}	$1.14x10^{-2}$	61	0.084
UV_{254}	$1.08x10^{-2}$	64	0.097

Pseudo first order degradation rate constants (k, min^{-1}) were found to be $1.65x10^{-2}$, $1.37x10^{-2}$, $1.14x10^{-2}$ and $1.08x10^{-2}$ for the UV-vis parameters specified as $Color_{436}$, UV_{365}, UV_{280} and UV_{254}, respectively. The corresponding half life ($t_{1/2}$, min) values were in the range of 42-64 min. Photocatalytic degradation rates (R, m^{-1} min^{-1}) were calculated by using the rate equation (4.1) expressed by the decreasing order of $UV_{254} > UV_{280} > UV_{365} > Color_{436}$. The presence of Fe doped TiO_2 displayed a slight decrease in rate constant for 30 kDa fraction of humic acid respect to 0.45 μm filtered fraction of humic acid and raw humic acid.

4.6. Adsorption Studies of Humic Acid and Its Molecular Size Fractions onto Bare TiO_2 and Fe doped TiO_2

In this study, batch adsorption experiments were conducted to elucidate the surface interactions of the molecular size dependent fractions of humic acid solutions onto oxide surfaces. The adsorption experiments were carried out using various molecular size fractions, namely 0.45 μm filtered fraction, 100 kDa fraction, and 30 kDa fraction of 20 mg L^{-1} humic acid solution. Bare TiO_2 and Fe doped TiO_2 in the range of 0.1-1.0 mg mL^{-1} were used as adsorbents. After each run, the humic acid samples were analyzed by UV-vis spectra and fluorescence spectra as well as by the specified UV-vis and fluorescence parameters.

The adsorption of molecules onto a surface is a necessary prerequisite to any surface mediated chemical process. Therefore, the mechanism of binding of humic acids to the TiO_2 surface has to be addressed in order to improve the understanding of photocatalytic degradation. Since, humic substances are anionic polyelectrolytes of low to moderate molecular weight (500–50 000 Da); their charge is primarily due to partially deprotonated carboxylic and phenolic groups. The electrostatic attractions between TiO_2 surface which are assumed to be equally positive and negative at the neutral pH of the solution and the negatively charged humic acid molecule are considered as significant during the course of the adsorption process (Bekbölet et al., 2002). The adsorption of humic acids onto oxide surfaces is explained by surface complexation of functional groups via ligand exchange mechanism. Particularly, the formation of bidentate complexes between two organic ligands in ortho position of an aromatic ring and the surface groups cause a strong chemisorptive binding (Jekel, 1986).

4.6.1. Adsorption of Raw Humic Acid onto Bare TiO_2

In order to investigate the adsorption properties of raw humic acid solution, batch adsorption experiments were carried out with bare TiO_2 in the range of 0.1-1.0 mg mL^{-1}. The spectroscopic properties of raw humic acid were characterized and compared by UV-vis spectroscopy and fluorescence spectroscopy in emission and synchronous scan modes.

4.6.1.1. UV-vis Spectroscopic Evaluation of Raw Humic Acid Adsorption onto Bare TiO_2.

UV-vis absorbance values were measured between 200-600 nm wavelength region.

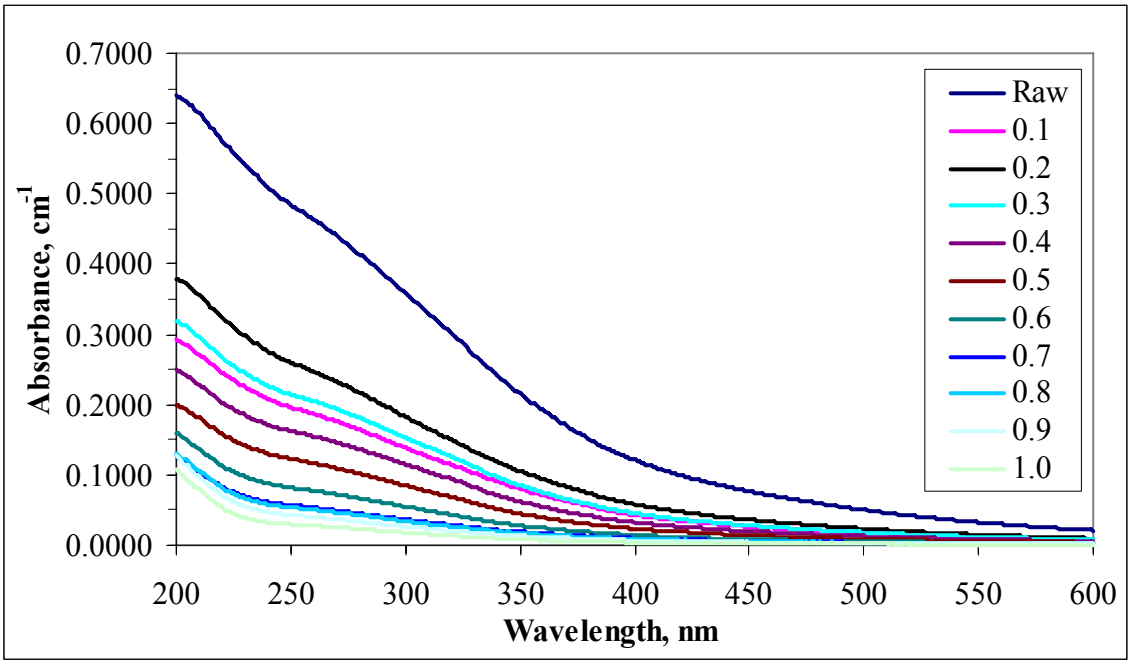

Figure 4.64. UV-vis spectra of raw humic acid adsorption onto bare TiO_2 (legends indicate TiO_2 dosages).

UV-vis spectra of humic substances are commonly broad; they do not exhibit any obvious features and monotonously decrease with increasing wavelength (Schnitzer and Khan, 1972; Traina et al., 1990; Chen et al., 2002; Uyguner and Bekbölet, 2005a). As seen Figure 4.64. UV-vis spectra of the humic acid solutions after adsorption monotonously decreased with increased dosage of TiO_2 (from 0.1 to 1.0 mg mL^{-1}) absorbent. Also, the spectrum of humic acid adsorption onto 0.7 mg mL^{-1} TiO_2 overlapped the recorded spectrum for the adsorption of humic acid onto 0.8 mg mL^{-1} TiO_2. The reason could be attributed to the probable saturation of the surface adsorption sites. Another study supported to this study examined by Degirmenci, (2010) explained that the UV-vis spectra of humic acid adsorption monotonously decreased with increased dosage of TiO_2 (from 0.1 to 1.0 mg mL^{-1}). Besides, it was also noticed that especially for higher TiO_2 loadings, there were no significantly characteristic absorbance recordings after 400 nm wavelength expressing the preferential removal of color forming moieties as shown Figure 4.64.

4.6.1.2. Fluorescence Spectroscopic Evaluation of Raw Humic Acid Adsorption onto Bare TiO_2. Emission scan fluorescence spectra of humic acid samples were displayed in Figures 4.65 and 4.66.

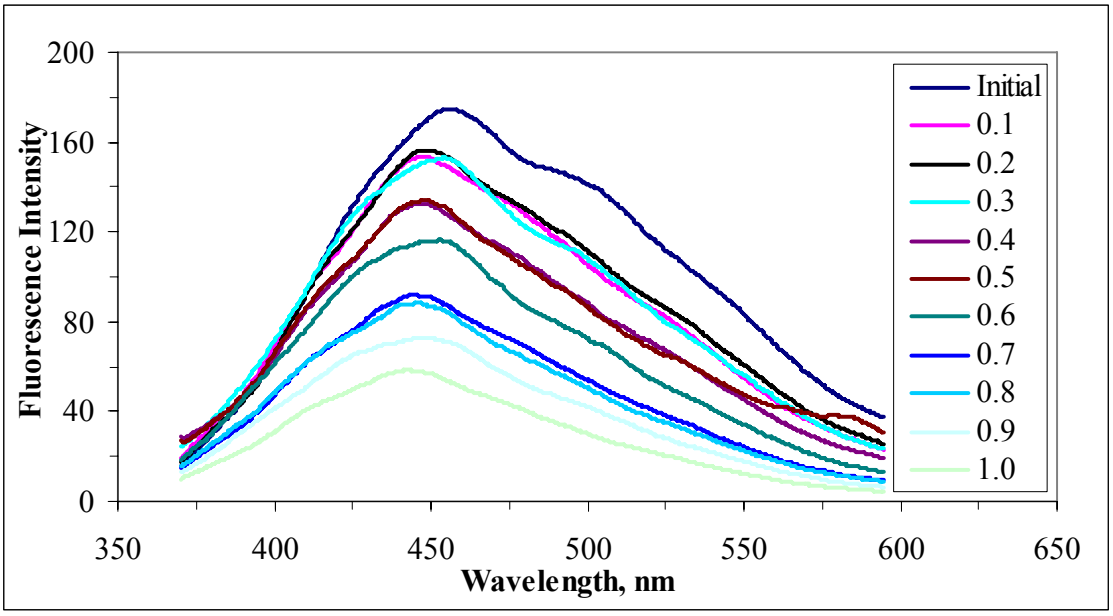

Figure 4.65. Emissions scan fluorescence spectra ($FI_{emis\ 350}$) of raw humic acid adsorption onto bare TiO_2 (where initial represents raw humic acid) (legends indicate TiO_2 dosages).

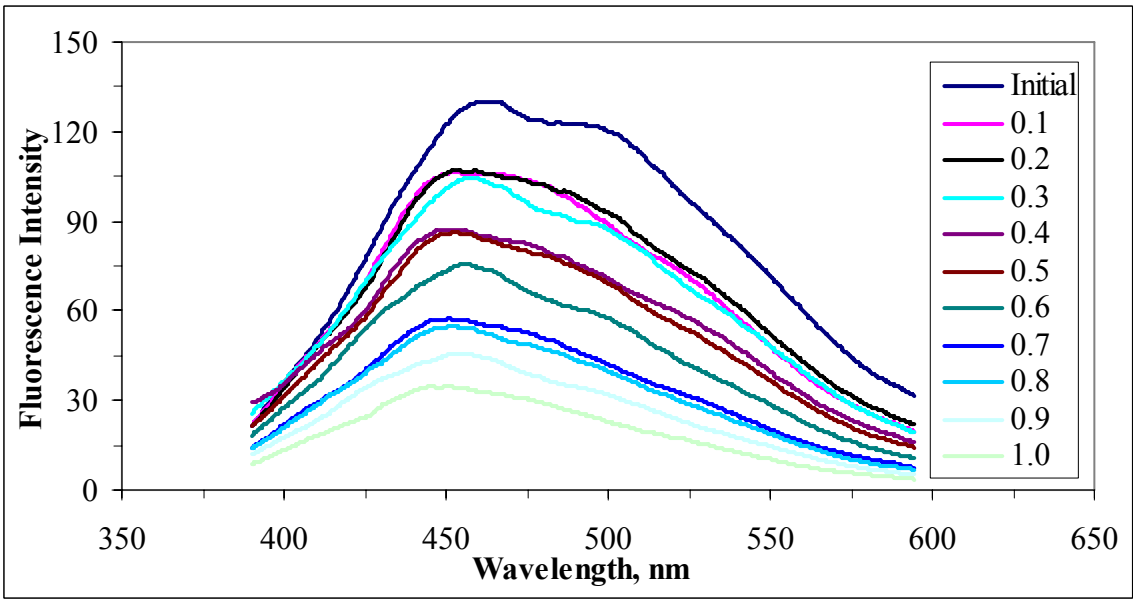

Figure 4.66. Emissions scan fluorescence spectra ($FI_{emis\ 370}$) of raw humic acid adsorption onto bare TiO_2 (where initial represents raw humic acid) (legends indicate TiO_2 dosages).

In a consistent manner, emission scan fluorescence spectra were scanned over the range of 360-600 nm and 380-600 nm at excitation wavelengths of 350 and 370 nm, respectively. The effect of the excitation wavelength on the fluorescence intensity of raw humic acid could be observed most significantly by the peak observed at the wavelength of 450 nm for both of the excitation wavelengths. The maximum fluorescence intensity was observed for initial humic acid and the lowest FI was recorded for raw humic acid in the presence of 1.0 mg mL^{-1} TiO_2 (Figures 4.65 and 4.66). Further, the spectrum of adsorption onto 0.4 mg mL^{-1} TiO_2 overlapped the recorded emission scan spectrum for the adsorption of humic acid onto 0.5 mg mL^{-1} TiO_2.

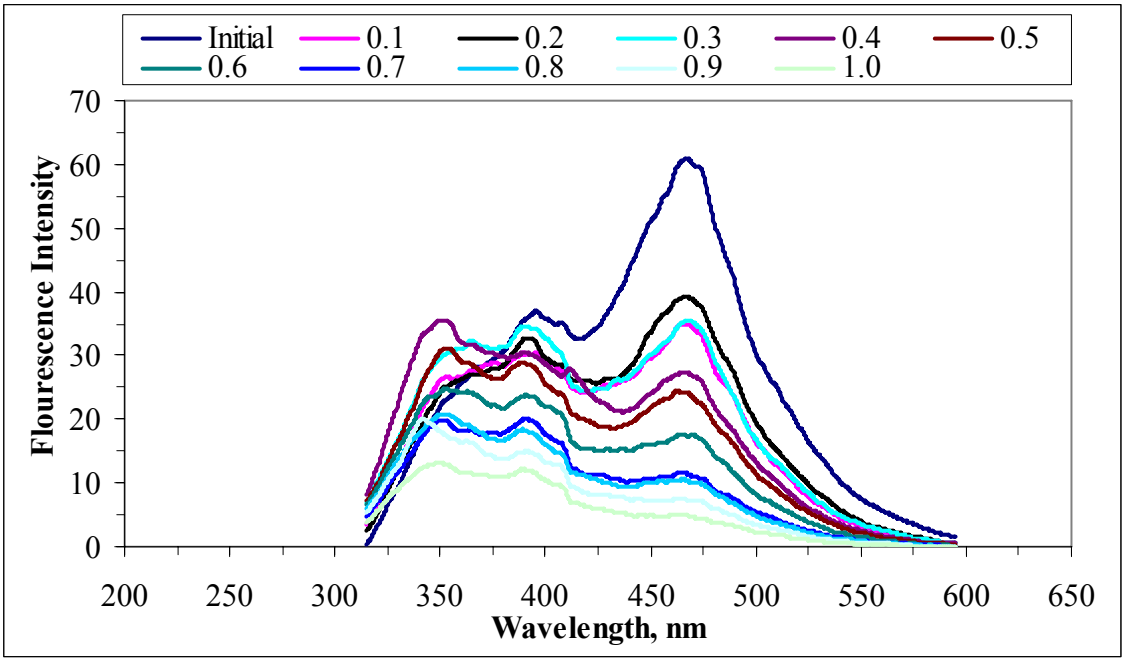

Figure 4.67. Synchronous scan fluorescence spectra of raw humic acid adsorption onto bare TiO_2 (legends indicate TiO_2 dosages).

Synchronous scan fluorescence spectra of raw humic acid adsorption onto bare TiO_2 were displayed in Figure 4.67. Synchronous scan fluorescence spectra for raw humic acid displayed a sharp peak around wavelength of 470 nm. As expected, the lowest fluorescence intensity was recorded for the adsorption of raw humic acid onto 1.0 mg mL^{-1} TiO_2 dose. Adsorption dependent λ_{max} (470 nm) fluorescence intensity displayed a decreasing trend with respect to increased TiO_2 dose.

4.6.1.3. Adsorption Isotherm Modeling of Raw Humic Acid onto Bare TiO_2 Binary System. The adsorption isotherms of the systems as presented by the respective parameters were examined with regard to their representative shapes. The adsorption isotherm shapes are largely determined by the adsorption mechanism, and thus can be used to explain the nature of adsorption (Sposito, 1989). Four basic types (S, L, H, and C) of adsorption isotherms have been recognized and used for identifying the nature of adsorption of solutes from aqueous solutions. Giles et al. (1974) classified sorption isotherms based on their initial slopes and curvatures. They distinguished between high affinity H, Langmuir L, constant partition C and sigmoidal-shaped S isotherm classes.

The adsorption data were evaluated in terms of Freundlich and Langmuir adsorption models. Freundlich adsorption model isotherms were displayed in the following Figures 4.68 and 4.69 for $Color_{436}$ and UV_{254}, respectively. Freundlich adsorption model isotherms for UV_{365} and UV_{280} were presented in Appendix A. It was observed from the Figure 4.68 that C_e values varied between 0.26 – 5.19 m^{-1} for $Color_{436}$ depending on the amount of TiO_2 in the range of 0.1-1.0 mg mL^{-1}. The corresponding values of q_A calculated were found to be in the range of 167 – 684 $m^{-1}g^{-1}$. As presented in Figure 4.69, the equilibrium contents, C_e values varied between 2.91– 30.76 m^{-1} for UV_{254}. The values of q_A calculated to be in the range of 893.6 – 3366 $m^{-1}g^{-1}$ for the corresponding C_e values. The observed trend in the shape of the Freundlich adsorption isotherm expressed a similar surface attraction for both of the parameters. The isotherm could be expressed by an S-type isotherm. Similar trends were obtained for raw humic acid in accordance with the literature (Ülker, 2008). Ülker studied with 50 mg L^{-1} humic acid solution in the presence of bare TiO_2 depending on the amount of TiO_2 in the range of 0.1-1.0 mg mL^{-1}. This study examined that C_e values varied between 8.24-15.6 m^{-1} for $Color_{436}$ depending on the amount of TiO_2 present in solution and the values of q_A calculated to be in the range of 341– 966 $m^{-1}g^{-1}$ for the corresponding C_e values. Furthermore, C_e values varied between 49.8–87.4 m^{-1} for UV_{254} and the values of q_A calculated to be in the range of 1422–3438 $m^{-}g^{-1}$ for the corresponding C_e values.

Langmuir adsorption isotherms of raw humic acid for UV-vis parameters as $Color_{436}$ and UV_{254} were given in Figure 4.70 and Figure 4.71, respectively. The Langmuir isotherms attained for UV_{365} and UV_{280} parameters were presented in Appendix B.

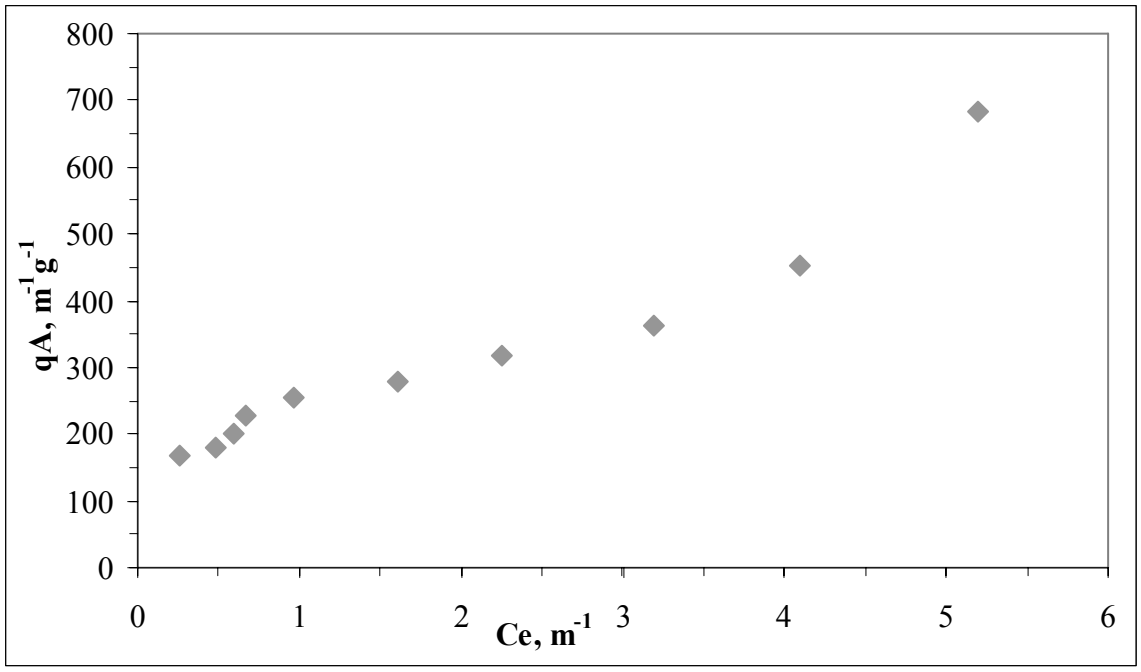

Figure 4.68. Freundlich adsorption isotherm of $Color_{436}$ of raw humic acid onto bare TiO_2.

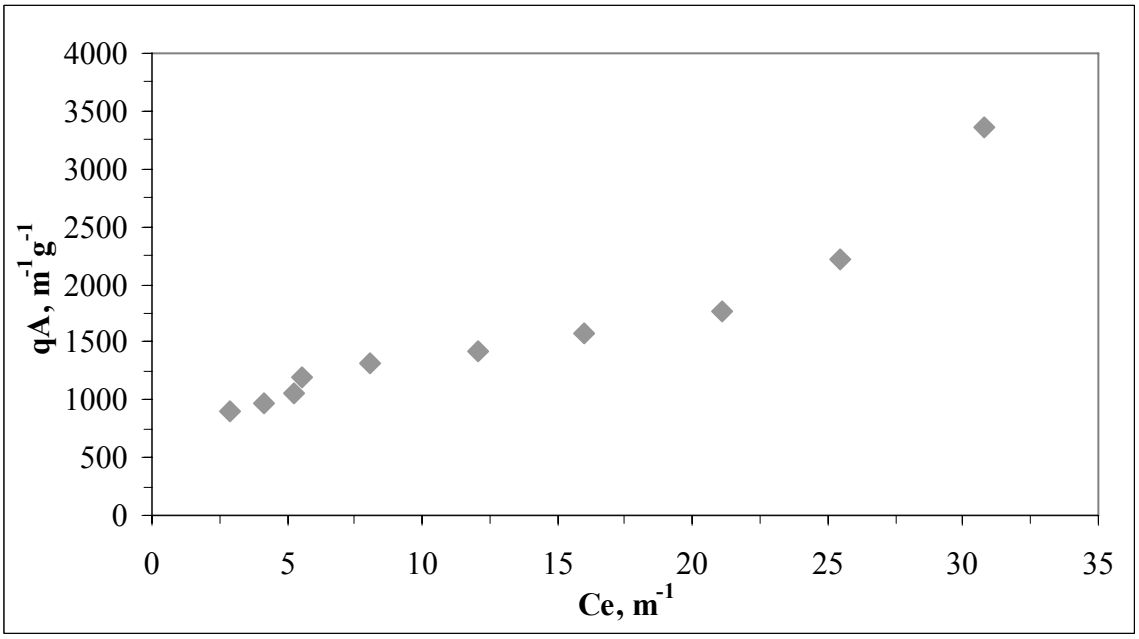

Figure 4.69. Freundlich adsorption isotherm of UV_{254} of raw humic acid onto bare TiO_2.

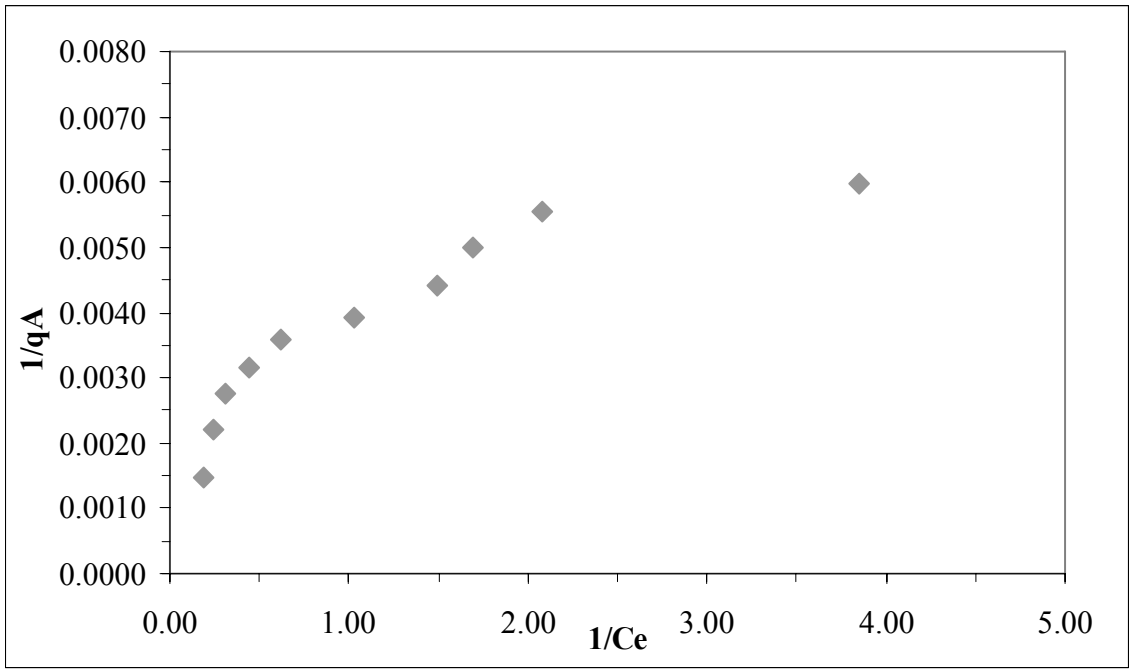

Figure 4.70. Langmuir adsorption isotherm of $Color_{436}$ of raw humic acid onto bare TiO_2.

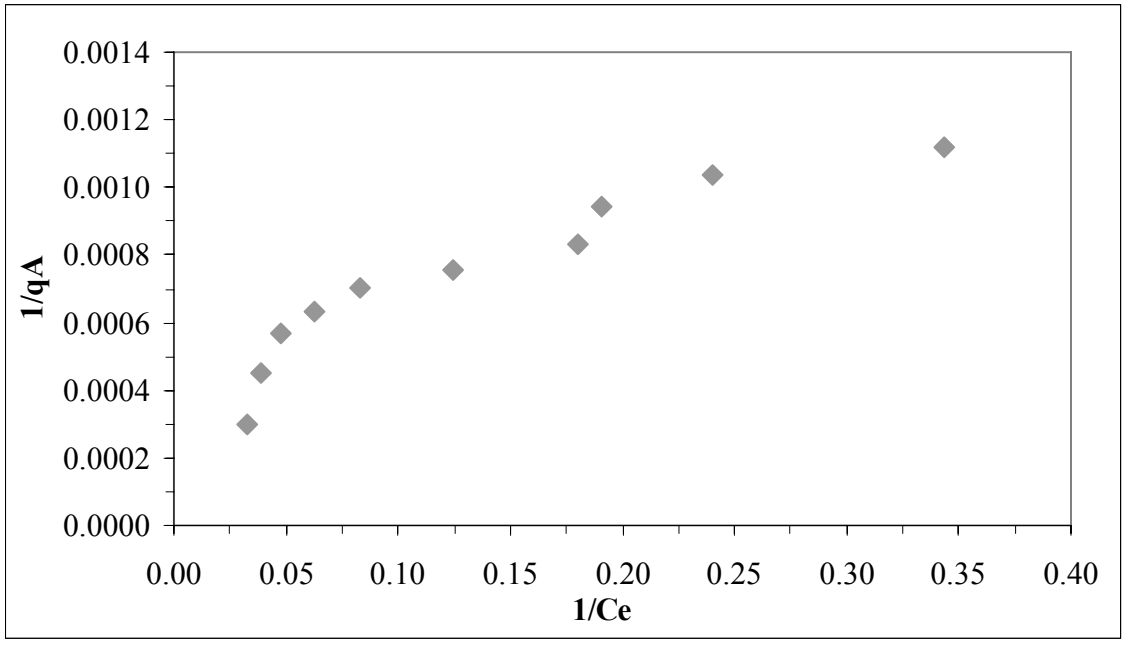

Figure 4.71. Langmuir adsorption isotherm of UV_{254} of raw humic acid onto bare TiO_2.

In order to evaluate the experimental results, the data were fitted to the Freundlich model and Langmuir model. The adsorption capacity, K_f, adsorption strength, 1/n, binding constant, K, and the maximum quantity adsorbable when all adsorption sites were occupied, q_{max}, for the adsorption of raw humic acid onto bare TiO_2 were listed in Table 4.68 and Table 4.69. Adsorption capacity constants were found to be in the order of $Color_{436} < UV_{365} < UV_{254} < UV_{280.}$ Adsorption intensity (1/n) values for UV_{365}, UV_{280} and were found to be very close to each other. Langmuir isotherm binding constants, K, of UV-vis parameters were found to be in the order of $Color_{436} > UV_{365} > UV_{280} > UV_{254}$. On the other hand, q_{max} could be assessed by the order of $UV_{254} > UV_{280} > UV_{365} > Color_{436}$.

Table 4.11. Freundlich and Langmuir Adsorption isotherm model parameters for the adsorption of raw humic acid onto bare TiO_2.

Humic acid Parameter	Freundlich adsorption isotherm model	
	K_f	1/n
$Color_{436}$	257	0.416
UV_{365}	397	0.299
UV_{280}	634	0.294
UV_{254}	501	0.465
Humic acid Parameter	Langmuir adsorption isotherm model	
	q_{max}	K
$Color_{436}$	417	2.180
UV_{365}	769	1.080
UV_{280}	1667	0.333
UV_{254}	2500	0.167

The adsorption of humic acid onto TiO_2 photocatalyst specimens (Degussa P-25 and Hombikat UV-100) was studied comparatively by Bekbolet and coworkers (2002). In their study, the adsorption pattern of humic acid for Degussa P-25 was reported to show an early stage of an S-type isotherm. The lack of an adsorption maximum was explained with surface unsaturation leading to an adsorbate–adsorbate interaction. The results revealed K_f values 0.549 for Degussa P-25 and 0.293 for Hombikat UV-100.

4.6.2. UV-vis Spectroscopic Evaluation of 0.45 µm Filtered Fraction of Humic Acid Adsorption onto Bare TiO_2

In order to investigate the adsorption properties of 0.45 µm filtered fraction of humic acid, batch adsorption experiments were carried out with bare TiO_2 in the range of 0.1-1.0 mg mL^{-1}.

4.6.2.1. UV-vis Spectroscopic Evaluation of 0.45 µm Filtered Fraction of Humic Acid Adsorption onto Bare TiO_2. UV-vis spectra of 0.45 µm filtered fraction of humic acid adsorption onto bare TiO_2 were shown in Figure 4.72.

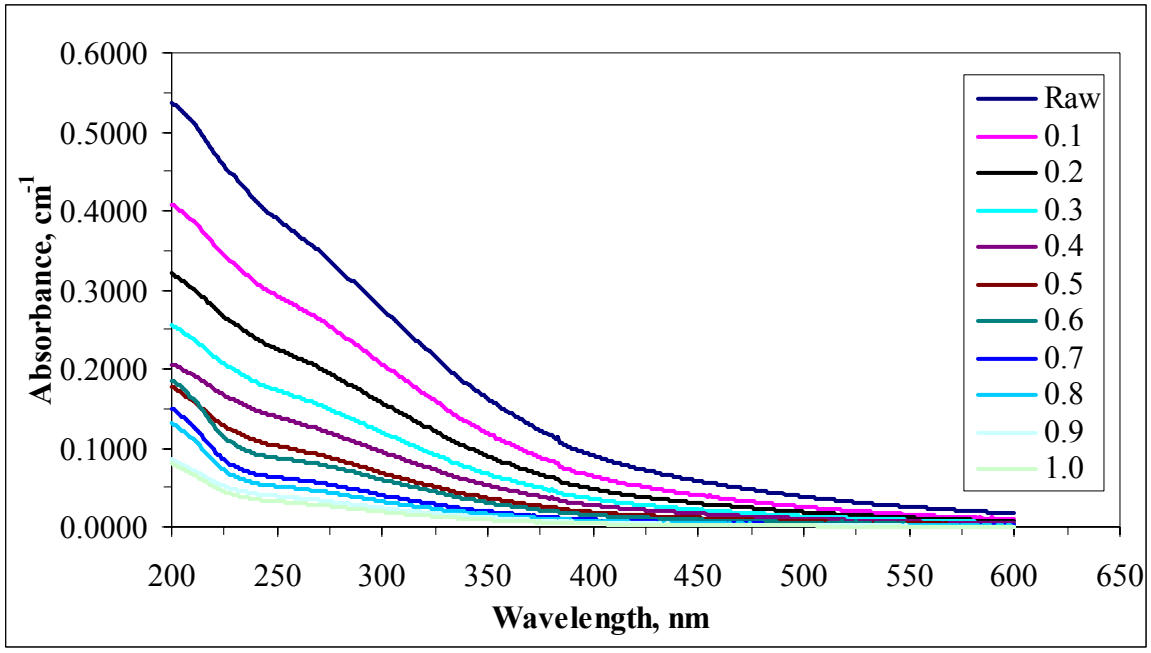

Figure 4.72. UV-vis spectra of 0.45 µm filtered fraction of humic acid adsorption onto bare TiO_2 (legends indicate TiO_2 dosages).

UV-vis spectra of 0.45 µm filtered fraction of humic acid adsorption onto bare TiO_2 were shown in Figure 4.72. It was observed that UV-vis spectra of humic acids monotonously decreased with increasing wavelength as expected. Also, 0.45 µm filtered fraction of humic acid showed the highest trend and raw humic acid with 1.0 mg mL^{-1} TiO_2 gave the lowest absorbance values. Moreover, in the case of 0.9 mg mL^{-1} and 1.0 mg

mL^{-1} TiO_2 doses, the UV-vis spectra followed an overlapping trend. Değirmenci (2010), found a similar result that the spectra of increased amount of TiO_2 exhibited a decreasing trend in terms of UV-vis spectra using spectroscopic analysis.

4.6.2.2. Fluorescence Spectroscopic Evaluation of 0.45 µm Filtered Fraction of Humic Acid Adsorption onto Bare TiO_2. Emission scan fluorescence spectra of humic acid samples were displayed in Figures 4.73 and 4.74. The emission fluorescence spectra was scanned over the range of 360-600 nm and 380-600 nm at excitation wavelengths of 350 and 370 nm, respectively. The adsorption of raw humic acid onto minimum dose, 0.1 mg mL^{-1} TiO_2, gave the highest fluorescence intensity, while highest dose, 1.0 mg mL^{-1} TiO_2 had the lowest fluorescence intensity.

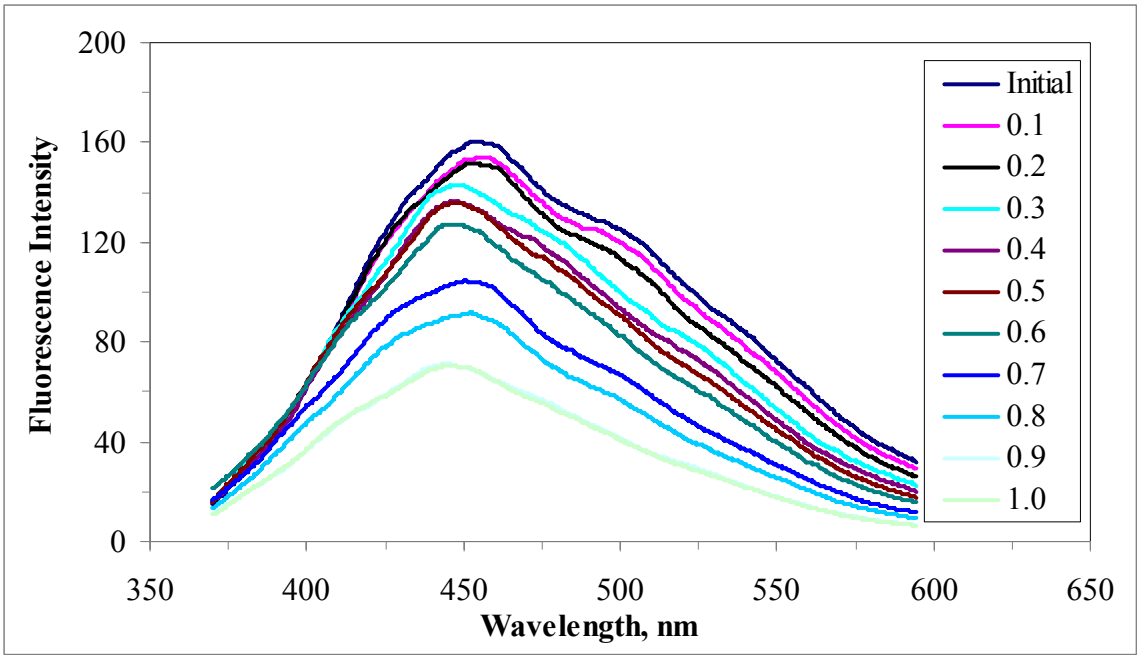

Figure 4.73. Emission scan fluorescence spectra of 0.45µm filtered fraction ($FI_{emis\ 350}$) of humic acid adsorption onto bare TiO_2 (where initial represents 0.45 µm filtered fraction of humic acid) (legends indicate TiO_2 dosages).

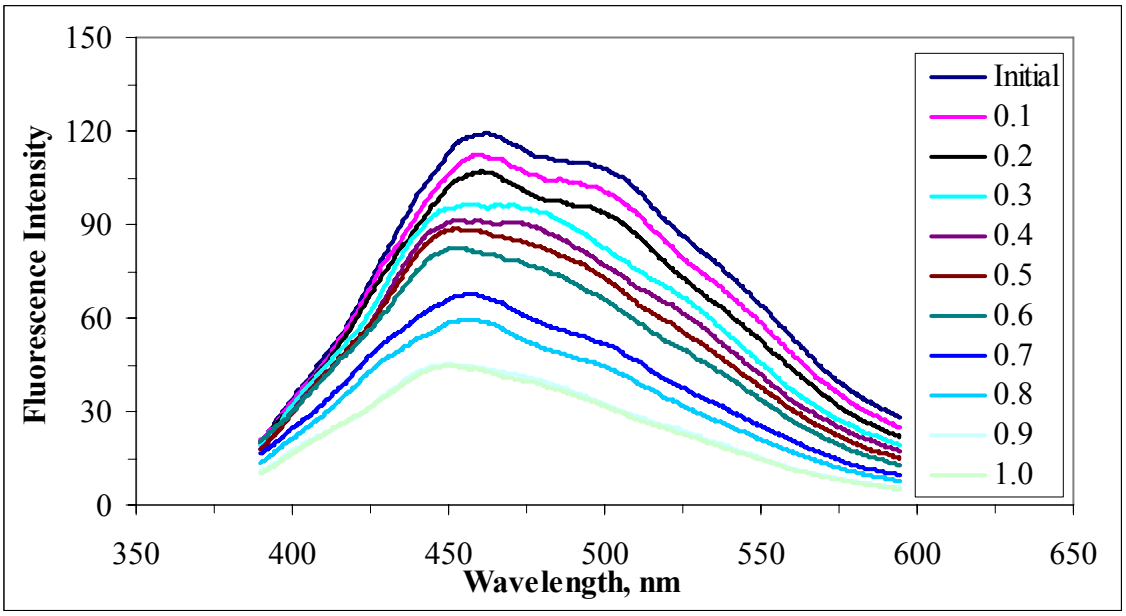

Figure 4.74. Emission scan fluorescence spectra of 0.45µm filtered fraction ($FI_{emis\ 370}$) of humic acid adsorption onto bare TiO_2 (where initial represents 0.45 µm filtered fraction of humic acid) (legends indicate TiO_2 dosages).

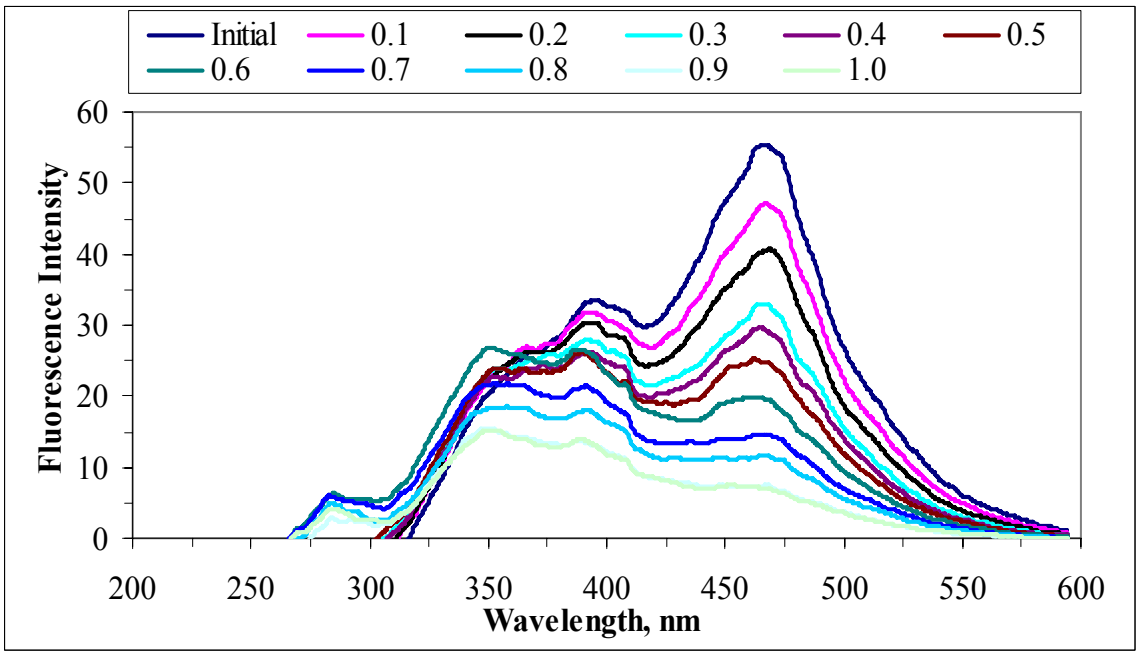

Figure 4.75. Synchronous scan fluorescence spectra of 0.45µm filtered fraction of humic acid adsorption onto TiO_2 (where initial represents 0.45 µm filtered fraction of humic acid) (legends indicate TiO_2 dosages).

It can be seen in Figures 4.73 and 4.74 that the fluorescence spectrum of adsorption onto 0.9 mg mL^{-1} TiO_2 overlapped the recorded emission scan spectrum for the adsorption onto 1.0 mg mL^{-1} TiO_2. As expected, continuously decreasing trend in fluorescence intensity at λ_{max}=450 nm was observed with respect to increasing TiO_2 dose for raw humic acid. Synchronous fluorescence spectra of 0.45µm filtered fraction of humic acid adsorption onto TiO_2 were displayed in Figure 4.75. Two main peaks were observed at 470 and 360 nm wavelengths. The highest fluorescence intensity was observed for adsorption onto raw humic acid with peaks about 470 nm wavelengths. The lowest fluorescence intensity was recorded for the adsorption of 0.45µm filtered fraction of humic acid onto 0.9 and 1.0 mg mL^{-1} TiO_2 dose which were same trend.

4.6.2.3. Adsorption Isotherm Modeling of 0.45 µm Filtered Fraction of Humic Acid onto bare TiO_2 Binary System. In order to evaluate the experimental results, the adsorption data were fitted to Freundlich and Langmuir adsorption models. Freundlich adsorption model isotherms were displayed in Figure 4.76 and Figure 4.77 for $Color_{436}$ and UV_{254}, respectively. Freundlich adsorption model isotherms for UV_{365} and UV_{280} were presented in Appendix A.

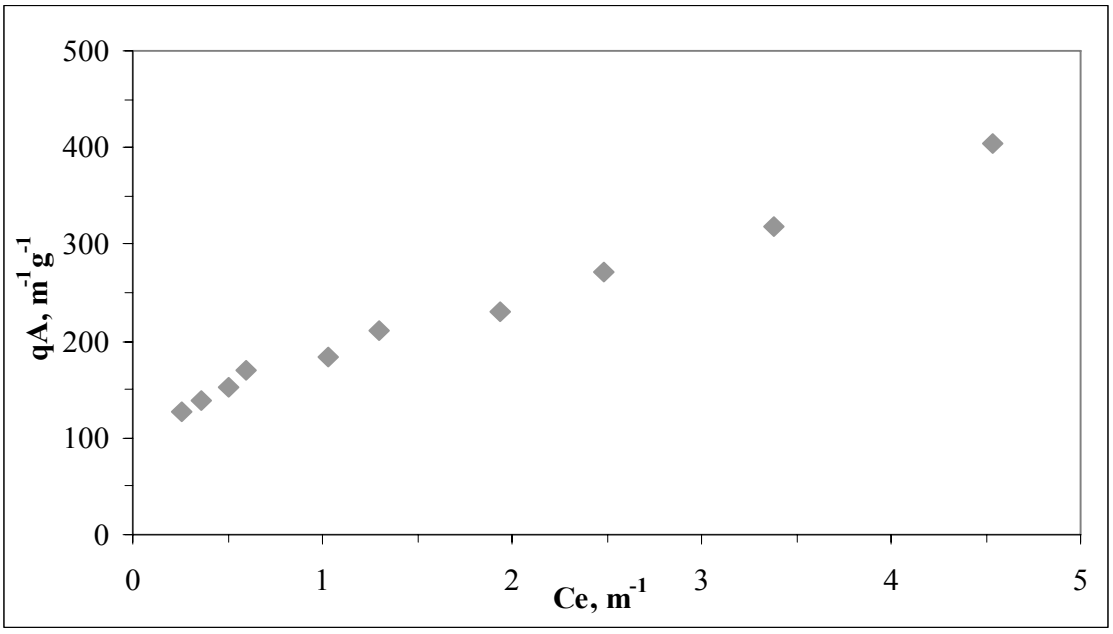

Figure 4.76. Freundlich adsorption isotherm of $Color_{436}$ of 0.45 µm filtered fraction of humic acid onto bare TiO_2.

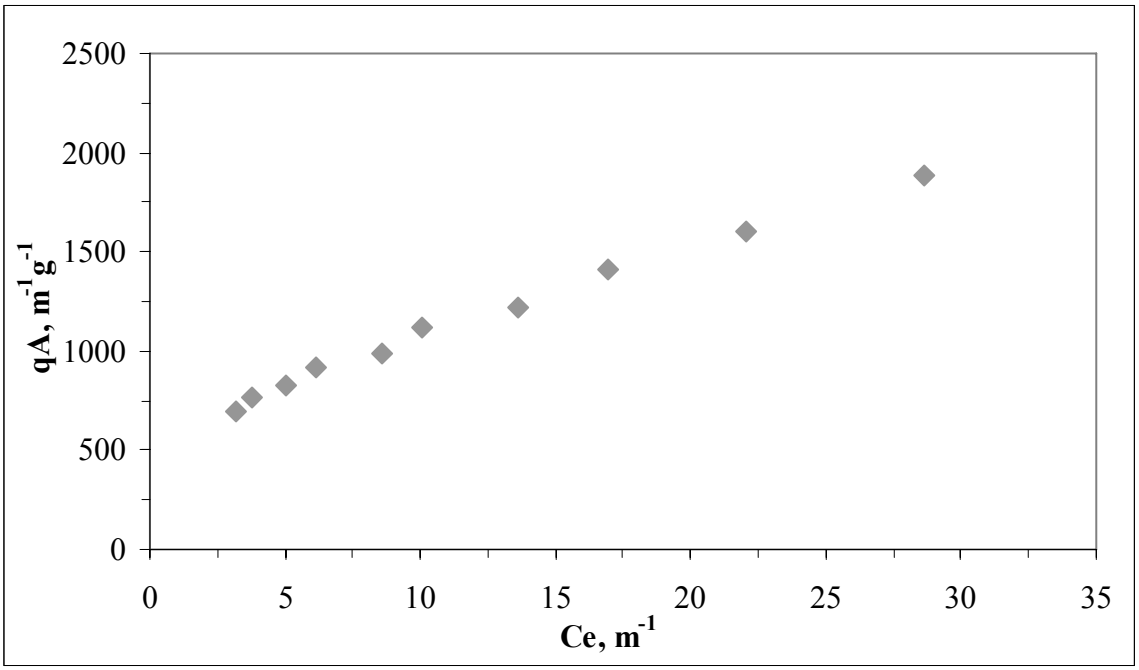

Figure 4.77. Freundlich adsorption isotherm of UV_{254} of 0.45 μm filtered fraction of humic acid onto bare TiO_2.

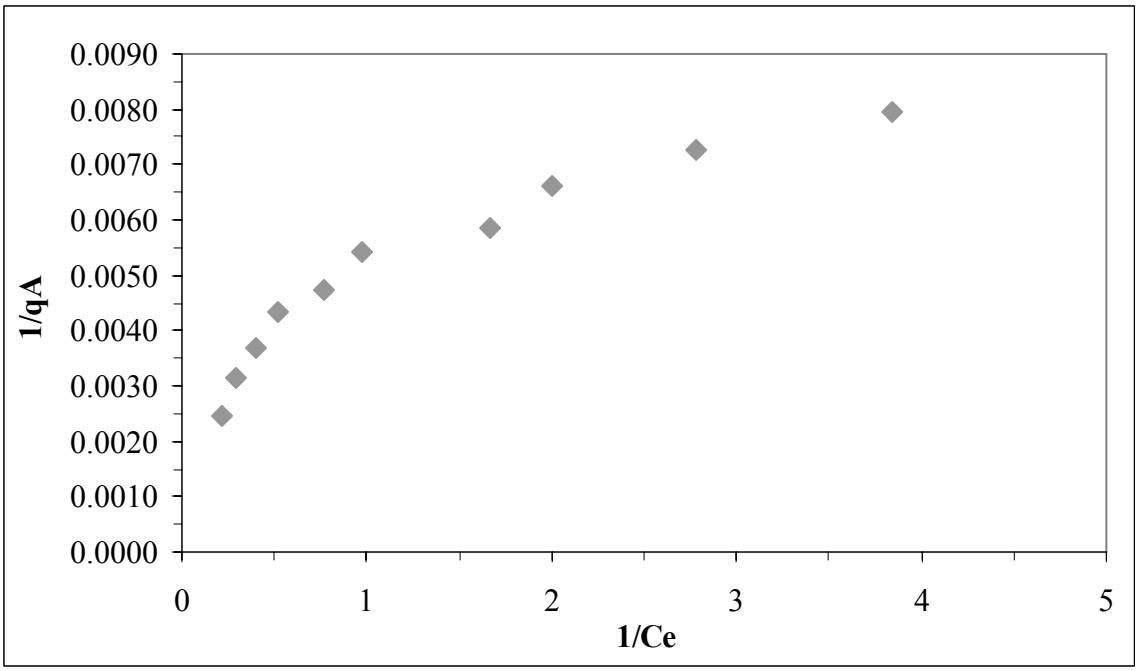

Figure 4.78. Langmuir adsorption isotherm of $Color_{436}$ of 0.45μm filtered fraction of humic acid onto bare TiO_2.

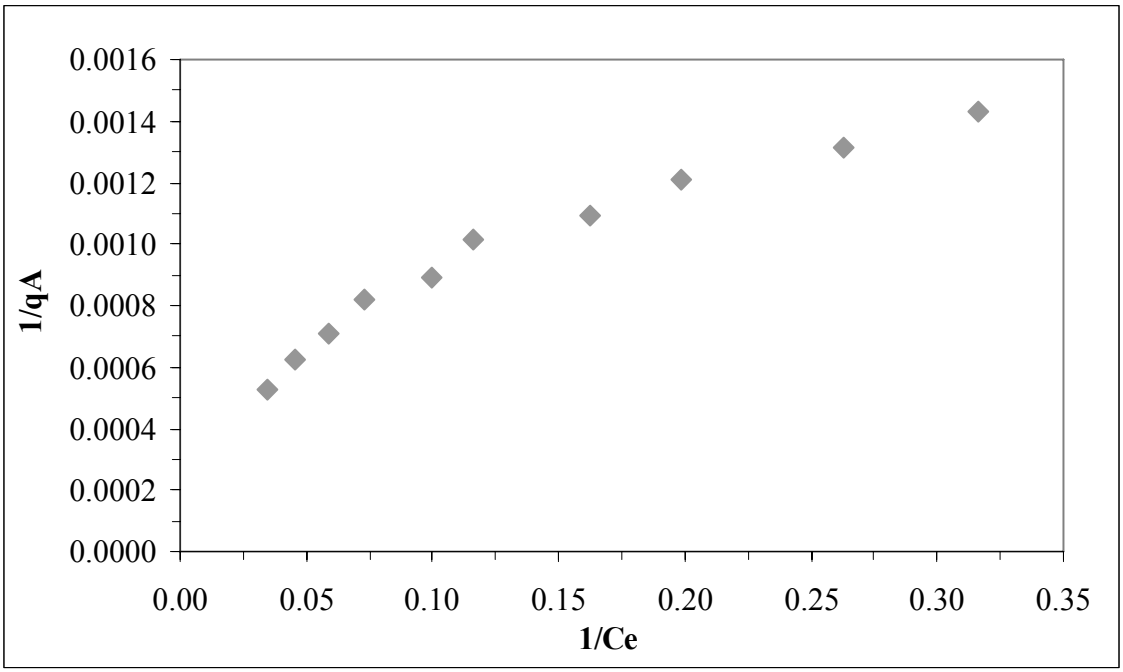

Figure 4.79. Langmuir adsorption isotherm of UV_{254} of 0.45µm filtered fraction of humic acid onto bare TiO_2.

Figure 4.76 indicated that C_e values varied between 0.26 – 4.54 m^{-1} for $Color_{436}$ depending on the amount of TiO_2 present in solution. The values of q_A calculated to be in the range of 126 – 404 $m^{-1}g^{-1}$ for the corresponding C_e values for $Color_{436}$. As could be seen in Figure 4.77, C_e values varied between 3.16 – 28.67 m^{-1} for UV_{254}. The values of q_A calculated to be in the range of 699.2 – 1890 m^{-1} g^{-1} for the corresponding C_e values for UV_{254}. Langmuir adsorption isotherm of 0.45µm filtered fraction of humic acid onto TiO_2 was shown for $Color_{436}$ and UV_{254} in Figures 4.78 and 4.79. Langmuir adsorption model isotherms for UV_{365} and UV_{280} were presented in Appendix B. It could also be stated that the adsorption isotherms showed similar trend both in terms of $Color_{436}$ and UV_{254} parameters and isotherms could be expressed by an L-type isotherm.

In order to evaluate the experimental results, the data were fitted to the Freundlich model and Langmuir model. The adsorption capacity, K_f, adsorption strength, 1/n, , binding constant, K, and the maximum quantity adsorbable when all adsorption sites were occupied, q_{max}, for the adsorption of 0.45µm filtered fraction of humic acid onto TiO_2 were listed in Table 4.12 . According to Table 4.13, adsorption capacity, K_f displayed an

increasing trend as; 199 for $Color_{436}$, 281 for UV_{365}, 392 for UV_{280} and 411 for UV_{254}. The adsorption capacity of color forming moieties could be regarded as comparatively lower than the UV absorbing centers representing a stronger surface interaction with the aromatic moieties rather than the chromophoric groups.

Table 4.12. Freundlich and Langmuir Adsorption isotherm model parameters for the adsorption of 0.45 μm filtered fraction of humic acid onto bare TiO_2.

Humic acid Parameter	Freundlich adsorption isotherm model	
	K_f	1/n
$Color_{436}$	199	0.379
UV_{365}	281	0.392
UV_{280}	392	0.423
UV_{254}	411	0.437
Humic acid Parameter	Langmuir adsorption isotherm model	
	q_{max}	K
$Color_{436}$	303	2.360
UV_{365}	667	0.750
UV_{280}	1429	0.250
UV_{254}	2000	0.167

Adsorption intensity (1/n) values for $Color_{436}$, UV_{365}, UV_{280} and UV_{254} were found to be very close to each other (0.379-0.437). Adsorption intensities for each UV-vis parameter were found to be lower than one, it indicated that the adsorption bond was strong; the capacity tended to be independent of C_e and the isotherm plot approaches the horizontal level. The Langmuir isotherm binding constants, K, of UV-vis parameters were found to be in the order of $Color_{436}$>UV_{365} >UV_{280} >UV_{254}. The maximum quantity adsorbable when all adsorption sites were occupied, q_{max}, could be assessed by the order of UV_{254} > UV_{280} > UV_{365} > $Color_{436}$. It can be concluded that UV_{254} and UV_{280} were found to be close to each other in terms of binding constant. The effect of molecular size fractionation on the sorption properties of humic acid onto TiO_2 studied by Ulker (2008). The adsorption profiles of the selected UV-vis parameters of humic acid displayed various

characteristics that had similar trend as mentioned above. It was found that Ce values varied between 4.2–14.5 m^{-1} for $Color_{436}$ depending on the amount of TiO_2 present in solution and the values of q_A calculated to be in the range of 280 – 774 m^{-1} g^{-1} for the corresponding C_e values.

4.6.3. Adsorption of 100 kDa Fraction of Humic Acid onto Bare TiO_2

In order to investigate the adsorption properties of 100 kDa filtered fraction of humic acid, batch adsorption experiments were carried out with bare TiO_2 in the range of 0.1-1.0 mg mL^{-1}.

4.6.3.1. UV-vis Spectroscopic Evaluation of 100 kDa Fraction of Humic Acid Adsorption onto Bare TiO_2. UV-vis spectra of 100 kDa fraction of humic acid adsorption onto bare TiO_2 were shown in Figure 4.80.

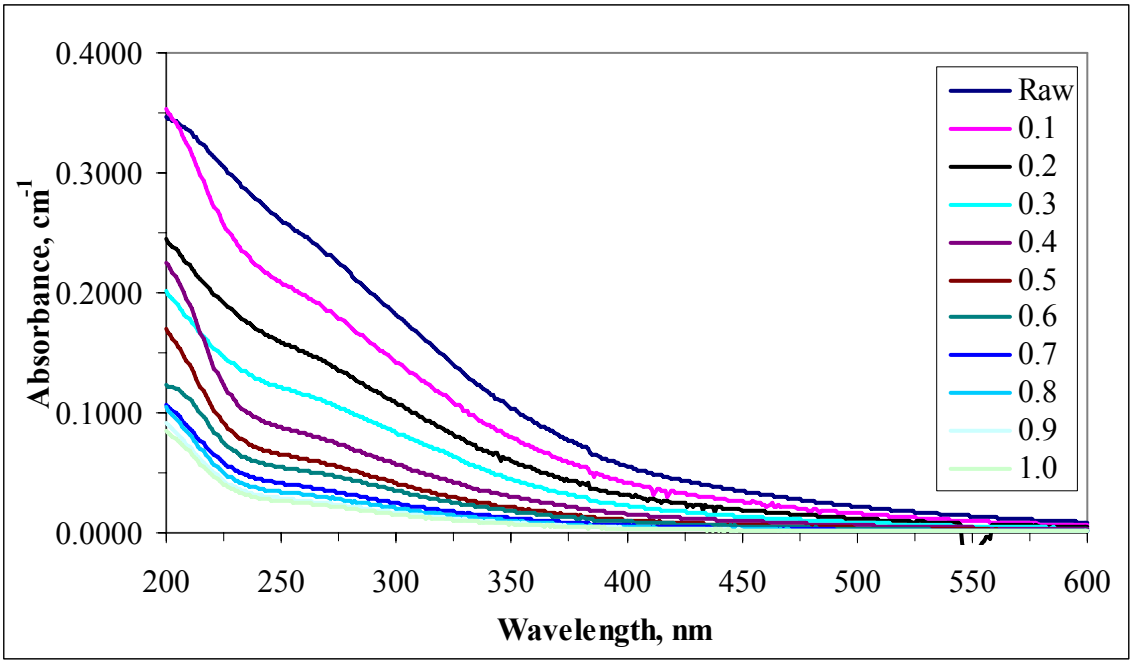

Figure 4.80. UV-vis spectra of 100 kDa fraction of humic acid adsorption onto bare TiO_2 (legends indicate TiO_2 dosages).

The UV-vis absorbance values were measured between 200-600 nm wavelength region. It could be easily seen that the significant decreases were occurred with the addition of increased dose of TiO_2. Further, it was observed that there were no significantly characteristic absorbance recordings for longer wavelengths (λ> 400 nm).

4.6.3.2. Fluorescence Spectroscopic Evaluation of 100 kDa Fraction of Humic Acid Adsorption onto Bare TiO_2. Emission scan fluorescence spectra of 100 kDa fraction of humic acid adsorption onto bare TiO_2 were displayed in Figures 4.81 and 4.82.

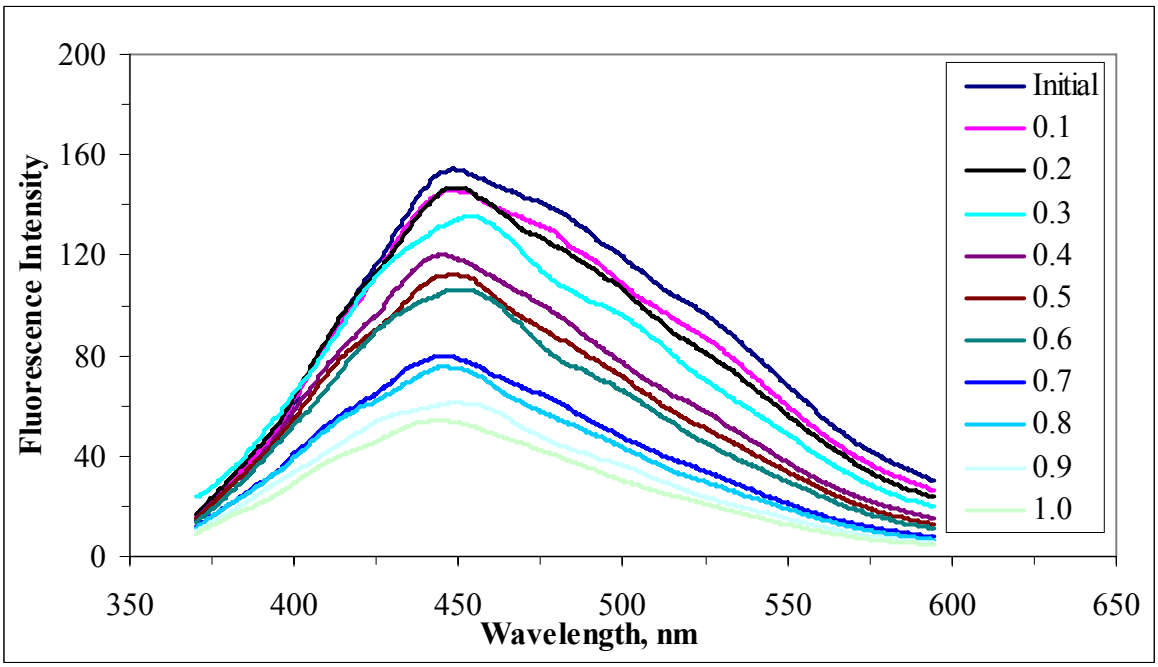

Figure 4.81. Emission scan fluorescence spectra ($FI_{emis\ 350}$) of 100 kDa fraction of humic acid adsorption onto bare TiO_2 (where initial represents 100 kDa fraction of humic acid) (legends indicate TiO_2 dosages).

Emission scan fluorescence spectra were scanned in the range of 360-600 nm and 380-600 nm by excitation at 350 and 370 nm, respectively, which resulted in a continuously decreasing trend in fluorescence intensity at λ_{max}=450 nm with respect to increasing TiO_2 dose for 100 kDa fraction of humic acid. The maximum fluorescence intensity was observed for initial 100 kDa fraction of humic acid and the 100 kDa fraction of humic acid with 1.0 mg mL^{-1} gave minimum fluorescence intensity.

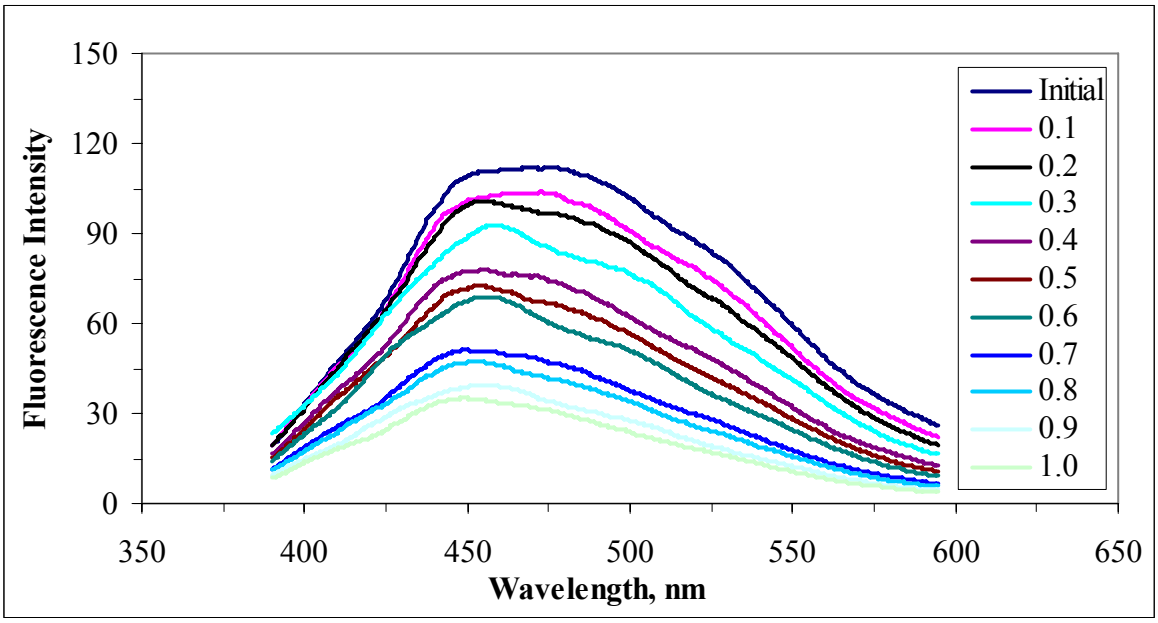

Figure 4.82. Emission scan fluorescence spectra ($FI_{emis\ 370}$) of 100 kDa fraction of humic acid adsorption onto bare TiO_2 (where initial represents 100 kDa fraction of humic acid) (legends indicate TiO_2 dosages).

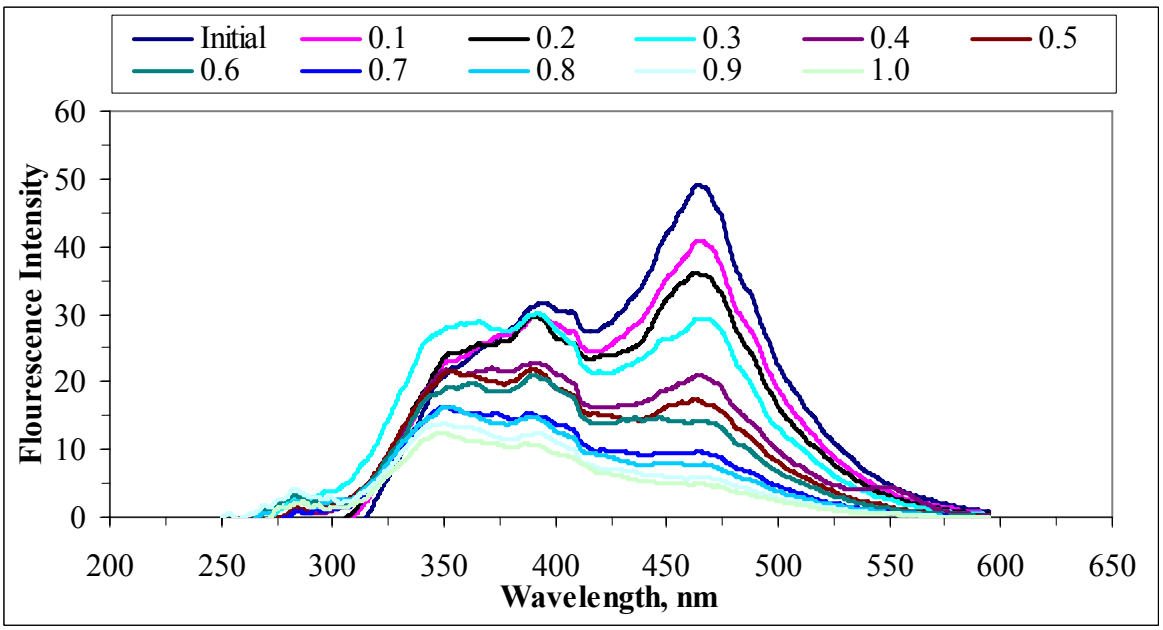

Figure 4.83. Synchronous scan fluorescence spectra of 100 kDa fraction of humic acid adsorption onto bare TiO_2 (where initial represents 100 kDa fraction of humic acid) (legends indicate TiO_2 dosages).

Synchronous scan fluorescence spectra of 100 kDa fraction of humic acid, illustrated by Figure 4.83 gave a major peak around 470 nm. It could be said that the synchronous scan spectra gave decreasing intensity with increasing TiO_2 dose. After adsorption onto 0.7mgL^{-1} of TiO_2, the characteristic sharp peak of for 100 kDa filtered fraction of humic acid at 470 nm wavelength completely disappeared.

4.6.3.3. Adsorption Isotherm Modeling of 100 kDa Fraction of Humic Acid onto Bare TiO_2 Binary System. In order to evaluate the experimental results, the adsorption data were fitted to Freundlich and Langmuir adsorption isotherm models. Freundlich adsorption model isotherms were displayed in Figures 4.84 and 4.85 for $Color_{436}$ and UV_{254}, respectively. Freundlich adsorption model isotherms for UV_{365} and UV_{280} were presented in Appendix A.

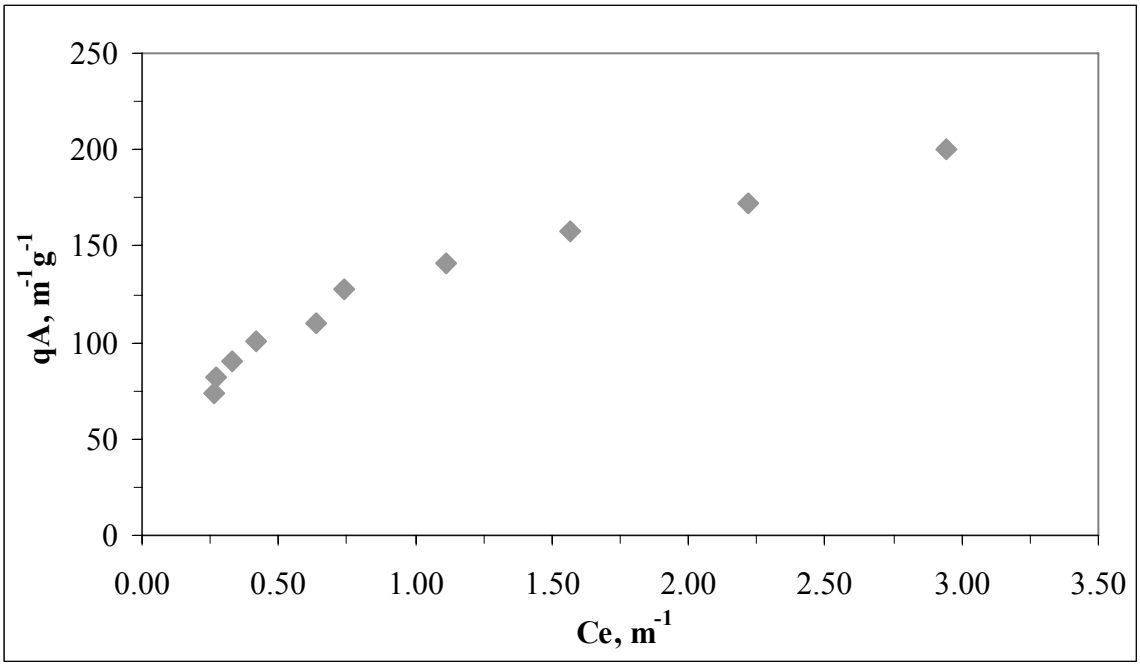

Figure 4.84. Freundlich adsorption isotherm of $Color_{436}$ of 100 kDa fraction of humic acid onto bare TiO_2.

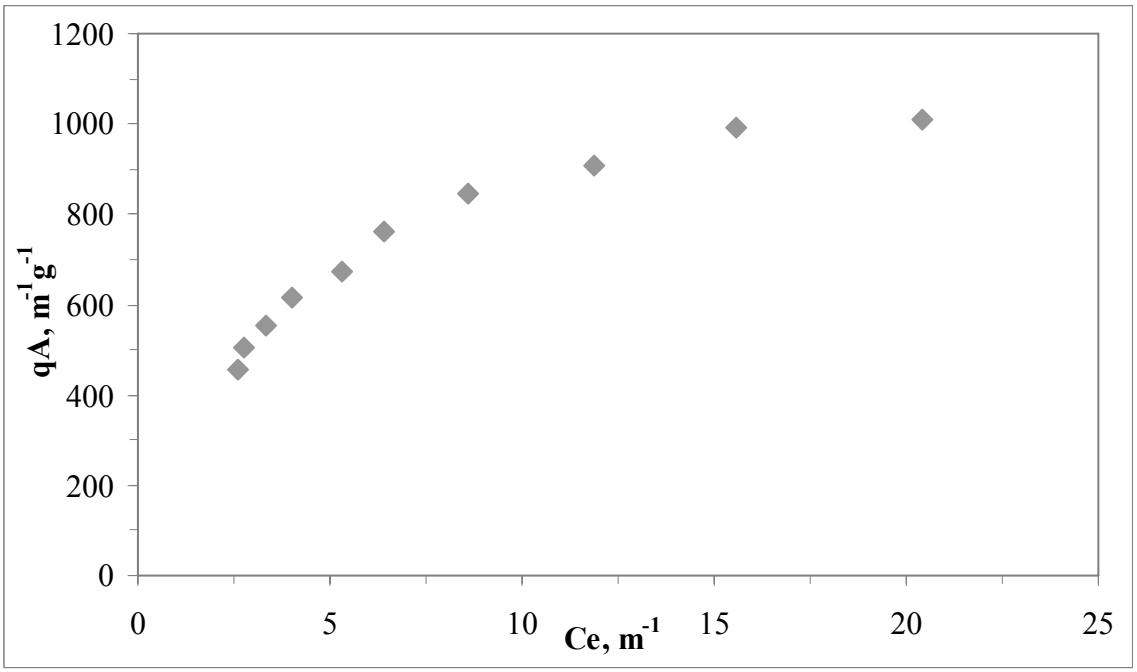

Figure 4.85. Freundlich adsorption isotherm of UV_{254} of 100 kDa fraction of humic acid onto bare TiO_2.

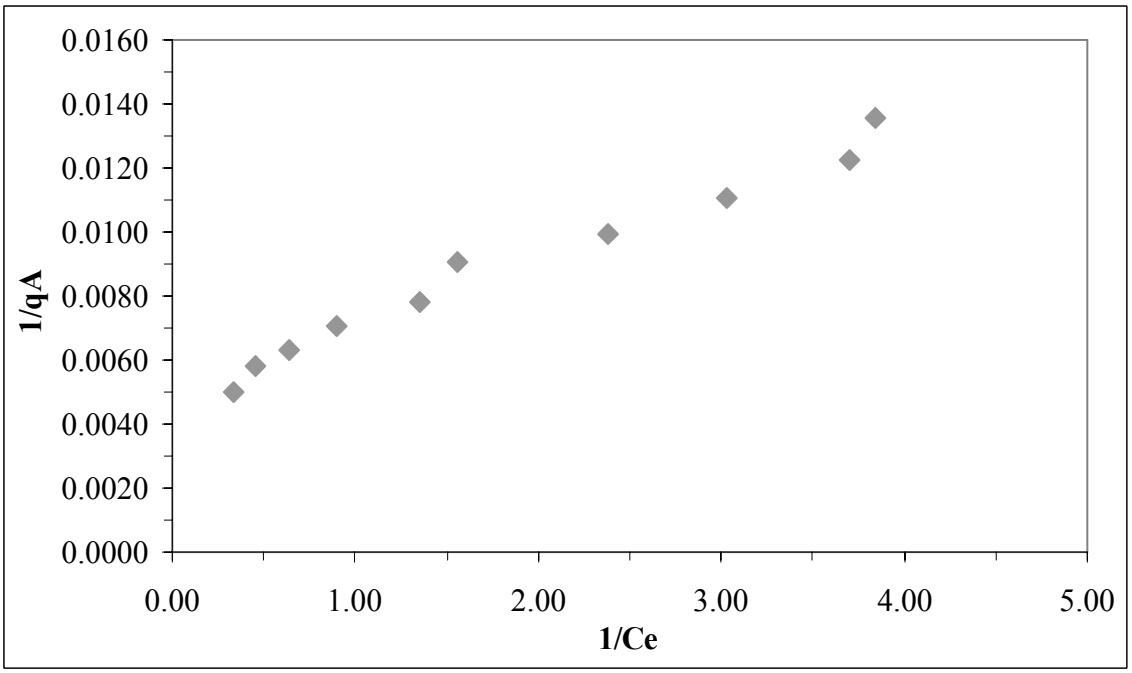

Figure 4.86. Langmuir adsorption isotherm of $Color_{436}$ of 100 kDa fraction of humic acid onto bare TiO_2.

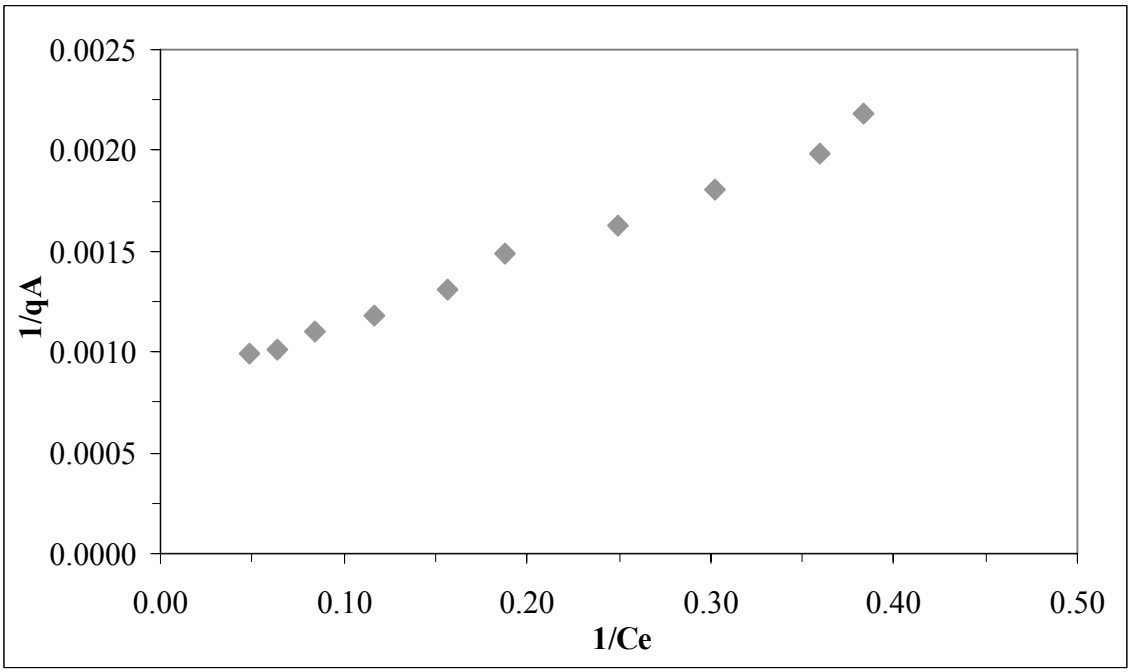

Figure 4.87. Langmuir adsorption isotherm of UV_{254} of 100 kDa fraction of humic acid onto bare TiO_2.

Figure 4.84 indicated that C_e values varied between 0.26–2.94 m^{-1} for $Color_{436}$ depending on the amount of TiO_2 present in solution. The values of q_A calculated to be in the range of 73.6 – 200 $m^{-1}g^{-1}$ for the corresponding C_e values. As could be seen in Figure 4.85, C_e values varied between 2.61–20.43 m^{-1} for UV_{254}. The values of q_A calculated to be in the range of 457.4–1010 $m^{-1}g^{-1}$ for the corresponding Ce values. Langmuir adsorption isotherm of 100 kDa fraction of humic acid onto TiO_2 was shown for $Color_{436}$ and UV_{254} in Figures 4.86 and 4.87. Langmuir adsorption model isotherms for UV_{365} and UV_{280} were presented in Appendix B. It could also be stated that Langmuir isotherm for $Color_{436}$ followed the same pattern with UV_{254}, for the 100 kDa filtered humic acid.

In order to evaluate the experimental results, the data were fitted to the Freundlich model and Langmuir model. The adsorption capacity, K_f, adsorption strength, 1/n, , binding constant, K, and the maximum quantity adsorbable when all adsorption sites were occupied, q_{max}, for the adsorption of 100 kDa fraction of humic acid onto TiO_2 were listed in Table 4.13.

Table 4.13. Freundlich and Langmuir Adsorption isotherm model parameters for the adsorption of 100 kDa fraction of humic acid onto bare TiO_2.

Humic acid Parameter	Freundlich adsorption isotherm model	
	K_f	1/n
$Color_{436}$	134	0.377
UV_{365}	212	0.367
UV_{280}	326	0.376
UV_{254}	349	0.381
Humic acid Parameter	Langmuir adsorption isotherm model	
	q_{max}	K
$Color_{436}$	204	2.33
UV_{365}	435	1.00
UV_{280}	1000	0.323
UV_{254}	1250	0.235

According to Table 4.13, adsorption capacity constants were found to be in the order of $Color_{436} < UV_{365} < UV_{280} < UV_{254}$ .Adsorption intensity (1/n) values for $Color_{436}$, UV_{365}, UV_{280} and UV_{254} were found to be very close to each other. 1/n values were found to be lower than one, it indicated that the adsorption bond was strong; the capacity tended to be independent of C_e. In a recent study by Değirmenci (2010), Freundlich isotherm model for the adsorption of raw humic acid with 20 mg L^{-1} onto TiO_2 in the range of 0.1-1.0 mg mL^{-1} was observed similar trend. It was found that C_e values were changed between 0.17 – 1.98 m^{-1} for $Color_{436}$ depending on the amount of TiO_2 present in solutions and the values of q_A calculated to be in the range of 60.40 - 242 $m^{-1}g^{-1}$ for the corresponding C_e values. Besides, Değirmenci explained C_e values varied between 1.96 – 14.94 m^{-1} for UV_{254}. The values of q_A calculated to be in the range of 374.80 - 1152 $m^{-1}g^{-1}$ for the corresponding C_e values. The Langmuir isotherm binding constants, K, of UV-vis parameters were found to be in the order of $Color_{436}>UV_{365}>UV_{280}>UV_{254}$ as seen in table 4.13. The maximum quantity adsorbable when all adsorption sites were occupied, q_{max}, could be assessed by the order of $UV_{254}>UV_{280}>UV_{365}>Color_{436}$.

4.6.4. Adsorption of 30 kDa Fraction of Humic Acid onto Bare TiO_2

In order to investigate the adsorption properties of 30 kDa filtered fraction of humic acid, batch adsorption experiments were carried out with bare TiO_2 in the range of 0.1-1.0 mg mL^{-1}.

4.6.4.1. UV-vis Spectroscopic Evaluation of 30kDa Fraction of Humic Acid Adsorption onto Bare TiO_2. UV-vis spectra of the 30 kDa fraction of humic acid displayed a decaying trend for all samples in the 200-600 nm wavelength region.

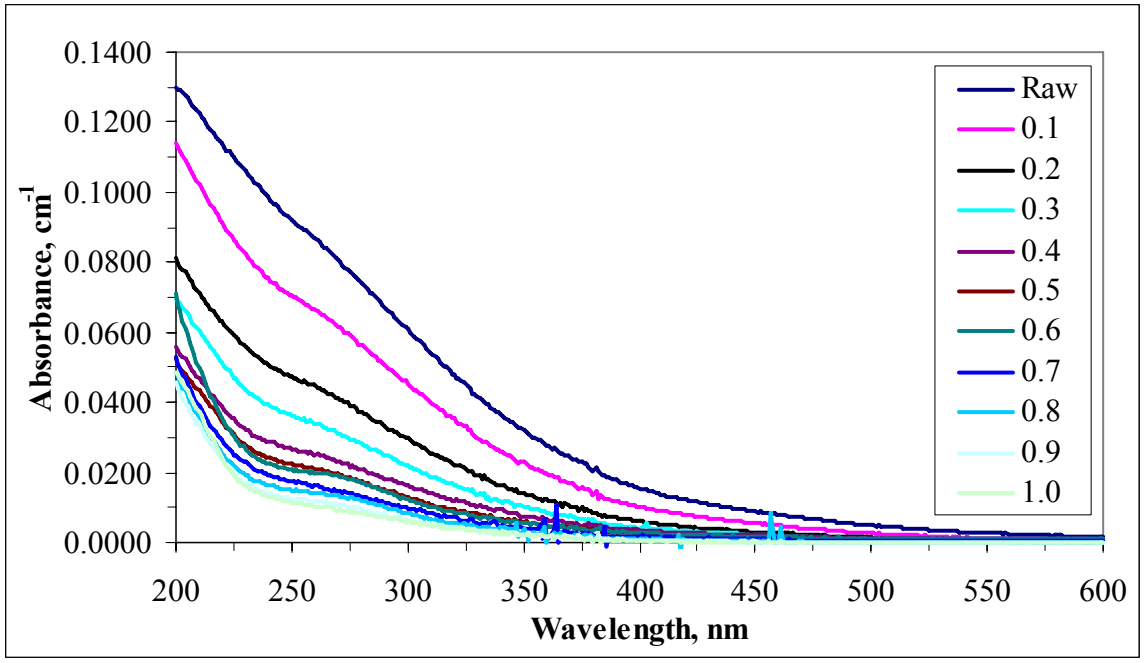

Figure 4.88. UV-vis spectra of 30 kDa fraction of humic acid adsorption onto bare TiO_2 (legends indicate TiO_2 dosages).

It can be seen in Figure 4.88, with increased dosage of TiO_2, the absorbance values showed slightly decrease trend. Further, there were no significantly characteristic absorbance recordings after 350 nm wavelength. It could be easily noticed that UV-vis spectra approached to very low absorbance values while increasing TiO_2 dose.

4.6.4.2. Fluorescence Spectroscopic Evaluation of 30kDa Fraction of Humic Acid Adsorption onto Bare TiO_2. The emission spectra were scanned over the range of 360-600 nm and 380-600 nm at excitation wavelength of 350 and 370 nm, respectively which resulted in a major peak at the wavelength of 450 nm.

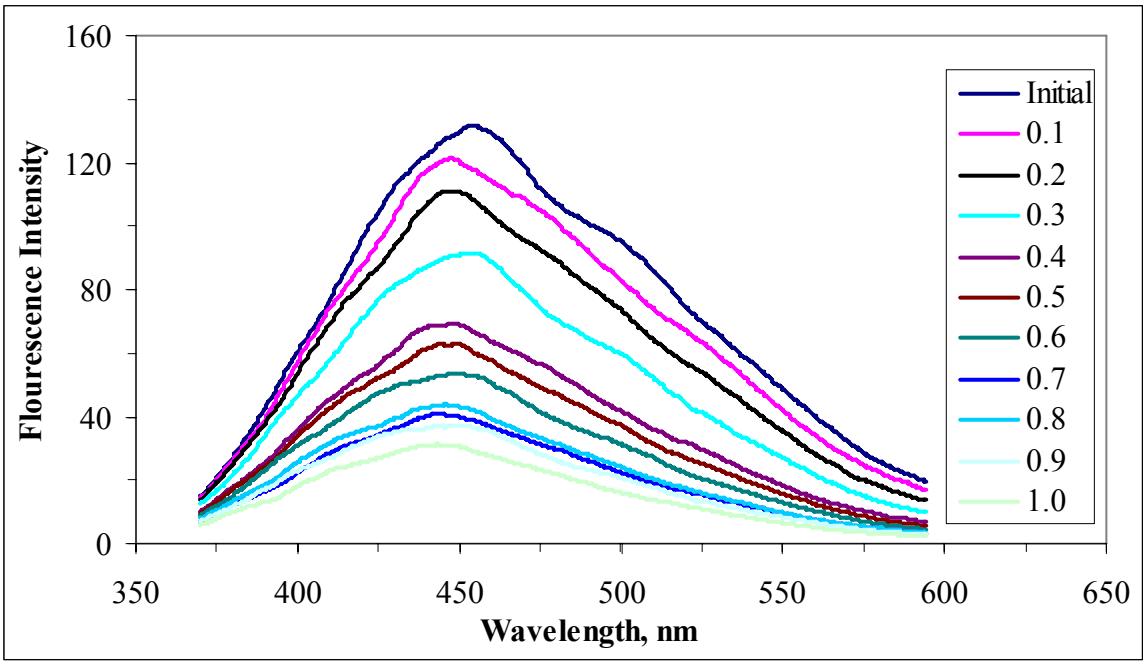

Figure 4.89. Emission scan fluorescence spectra ($FI_{emis\ 350}$) of 30kDa fraction of humic acid adsorption onto bare TiO_2 (where initial represents 30 kDa fraction of humic acid) (legends indicate TiO_2 dosages).

Although TiO_2 dose loading dependent general decreasing trend in fluorescence intensity could be visualized, the maximum fluorescence intensity was observed for adsorption of 30 kDa fraction of humic acid onto lower dose as 0.1 mg mL^{-1} TiO_2. Starting from 0.1 mg mL^{-1} TiO_2 to 1.0 mg mL^{-1} TiO_2 dose, all of the fluorescence intensities were decreased. Also, the spectrum of adsorption onto 0.7 mg mL^{-1} TiO_2 overlapped the recorded emission scan spectrum for the adsorption onto 0.8 mg mL^{-1} TiO_2 (Figure 4.89 and Figure 4.90).

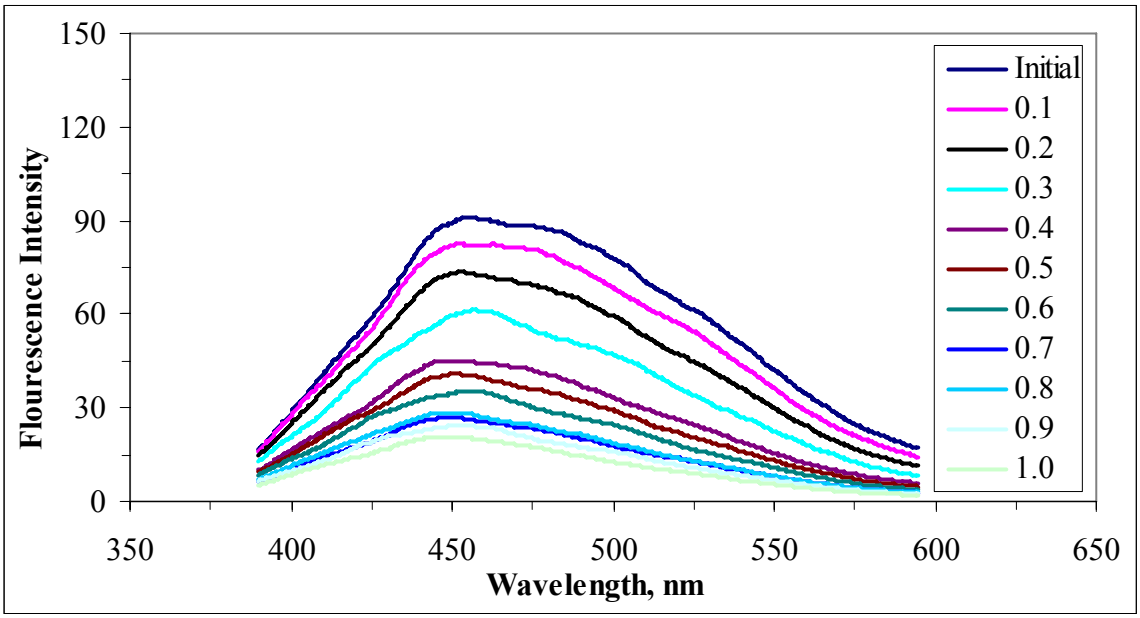

Figure 4.90. Emission scan fluorescence spectra ($FI_{emis\ 370}$) of 30kDa fraction of humic acid adsorption onto TiO_2 (where initial represents 30 kDa fraction of humic acid) (legends indicate TiO_2 dosages).

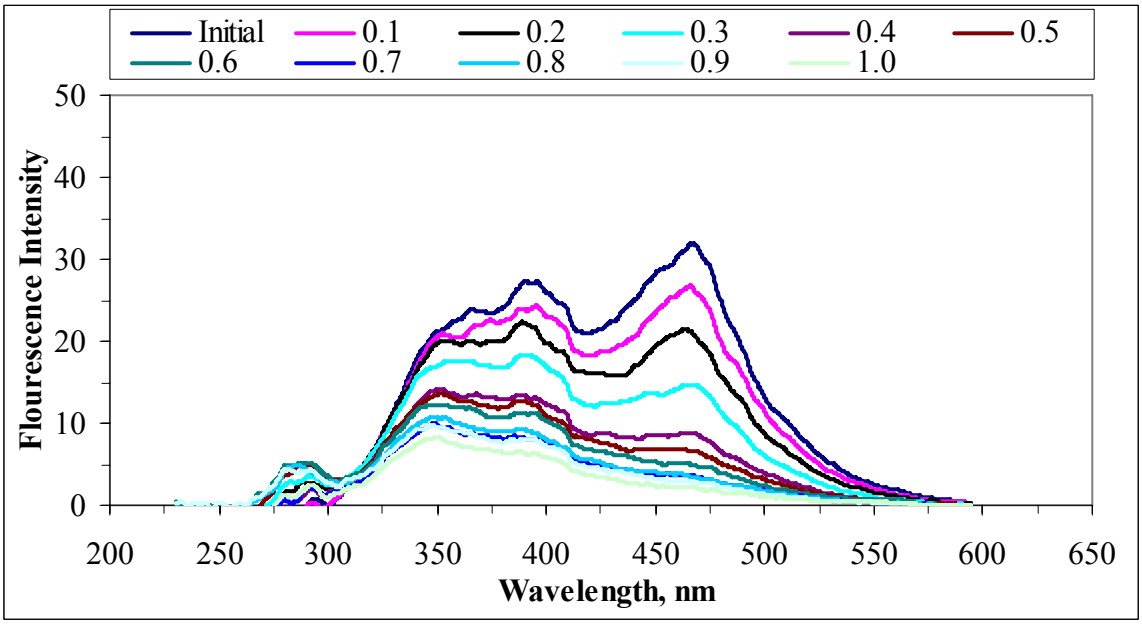

Figure 4.91. Synchronous scan fluorescence spectra of 30 kDa fraction of humic acid adsorption onto bare TiO_2 (where initial represents 30 kDa fraction of humic acid) (legends indicate TiO_2 dosages).

Synchronous fluorescence scan spectra of raw humic acid adsorption onto TiO_2 were displayed in Figure 4.91. Synchronous fluorescence scan spectra was recorded in the excitation wavelength range of 200-600 nm excitation wavelength range which displayed two sharp peak around wavelength of 370 and 470 nm. After dosage with 0.3 mg L^{-1} for TiO_2, the sharp peaks started to disappear. The lowest fluorescence intensity was recorded for the adsorption of raw humic acid onto 1.0 mg mL^{-1} TiO_2 dose. Adsorption dependent λ_{max} (470 nm) fluorescence intensity displayed a decreasing trend with respect to increased TiO_2 dose.

4.6.4.3. Adsorption Isotherm Modeling of 30kDa Fraction of Humic Acid onto Bare TiO_2 Binary System. In order to evaluate the experimental results attained for 30 kDa fraction of humic acid, the adsorption data were fitted to Freundlich and Langmuir adsorption isotherm models.

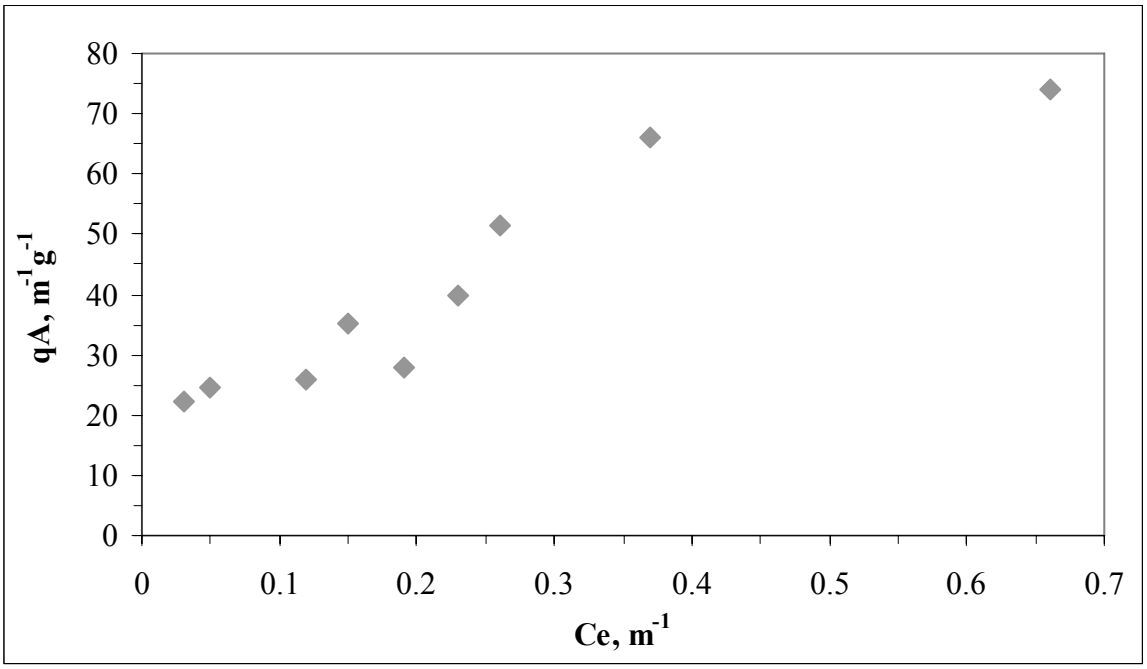

Figure 4.92. Freundlich adsorption isotherm of $Color_{436}$ of 30 kDa fraction of humic acid onto bare TiO_2.

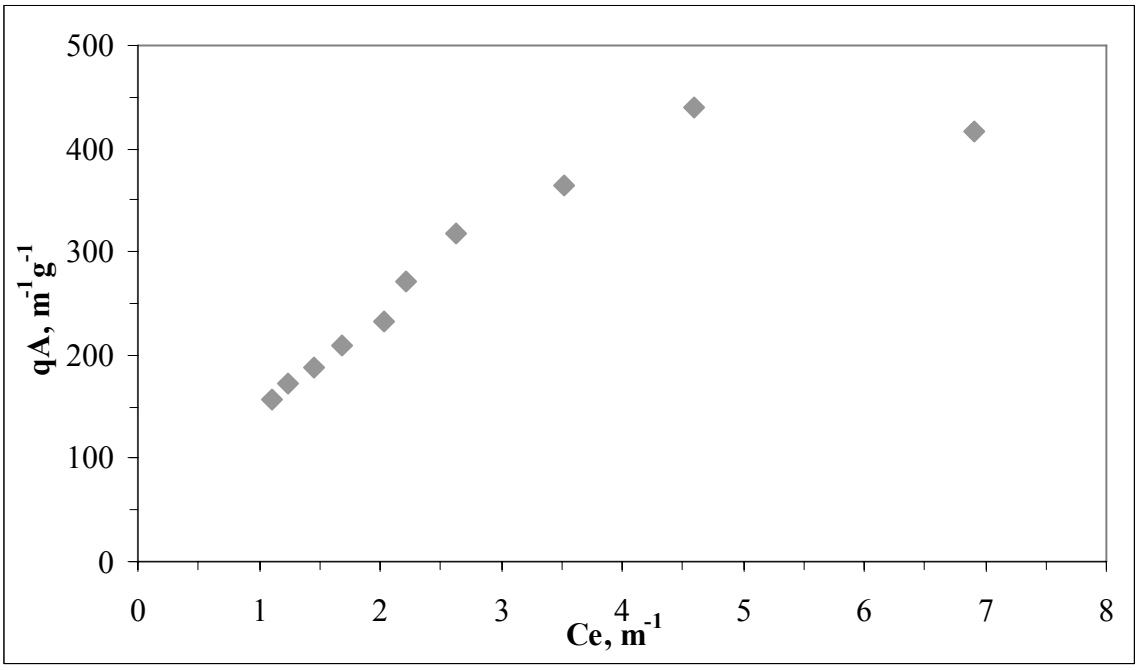

Figure 4.93. Freundlich adsorption isotherm of UV_{254} of 30 kDa fraction of humic acid onto bare TiO_2.

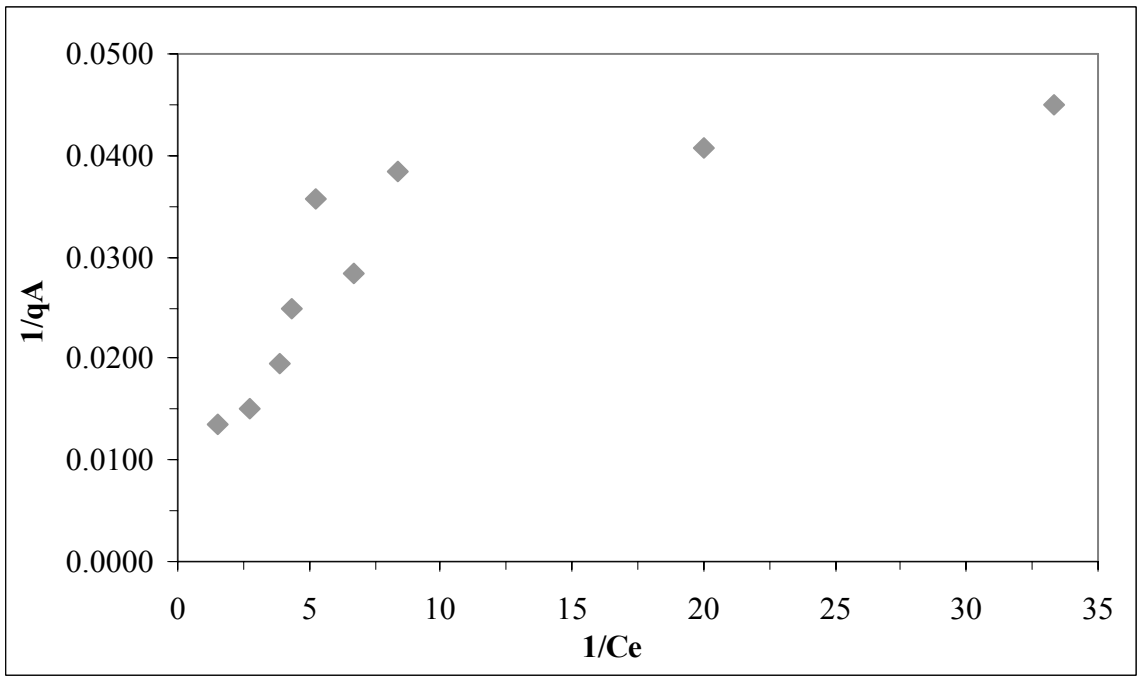

Figure 4.94. Langmuir adsorption isotherm of $Color_{436}$ of 30 kDa fraction of humic acid onto bare TiO_2.

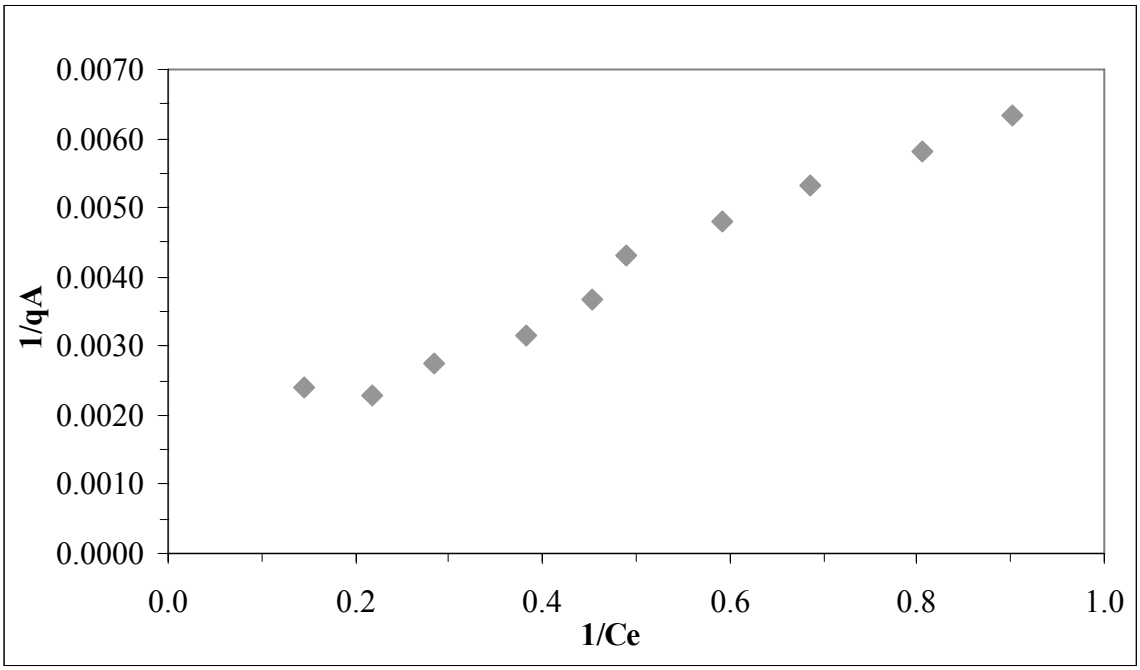

Figure 4.95. Langmuir adsorption isotherm of UV_{254} of 30 kDa fraction of humic acid onto bare TiO_2.

Figure 4.92 indicated that C_e values varied between 0.03–0.66 m^{-1} for $Color_{436}$ depending on the amount of TiO_2 present in solution. The values of q_A calculated to be in the range of 22.2 – 74 m^{-1} g^{-1} for the corresponding C_e values. As could be seen in Figure 4.93, C_e values varied between 1.1–6.91 m^{-1} for UV_{254}. The values of q_A calculated to be in the range of 157.6 – 416 m^{-1} g^{-1} for the corresponding C_e values. The isotherm could be expressed by an S-type isotherm. Langmuir adsorption isotherm of 30 kDa fraction of humic acid onto TiO_2 was shown for $Color_{436}$ and UV_{254} in figure 4.94 and 4.95 Langmuir adsorption model isotherms for UV_{365} and UV_{280} were presented in Appendix B.

In order to evaluate the experimental results, the data were fitted to the Freundlich model and Langmuir model. The adsorption capacity, K_f, adsorption strength, 1/n, binding constant, K, and the maximum quantity adsorbable when all adsorption sites were occupied, q_{max}, for the adsorption of 100 kDa fraction of humic acid onto TiO_2 were listed in Table 4.14.

Table 4.14. Freundlich and Langmuir Adsorption isotherm model parameters for the adsorption 30 kDa fraction of humic acid onto bare TiO_2.

Humic acid Parameter	Freundlich adsorption isotherm model	
	K_f	1/n
$Color_{436}$	79	0.414
UV_{365}	124	0.494
UV_{280}	150	0.592
UV_{254}	156	0.608
Humic acid Parameter	Langmuir adsorption isotherm model	
	q_{max}	K
$Color_{436}$	48	23.15
UV_{365}	167	2.60
UV_{280}	588	0.333
UV_{254}	833	0.211

According to Table 4.14, adsorption capacity constants were found to be in the order of $Color_{436} < UV_{365} < UV_{280} < UV_{254}$. Adsorption intensity (1/n) values for $Color_{436}$, UV_{365}, UV_{280} and UV_{254} were found to be very close to each other. 1/n values were found to be lower than one, it indicated that the adsorption bond was strong; the capacity tended to be independent of C_e. There was approximately 49% difference between the adsorption capacity of $Color_{436}$ and UV_{254}. On the other hand, for the adsorption strength, 1/n, value of UV_{254} was calculated as 32% higher than value of $Color_{436}$. The Langmuir isotherm binding constants, K, of UV-vis parameters were found to be in the order of $Color_{436} > UV_{365} > UV_{280} > UV_{254}$.The maximum quantity adsorbable when all adsorption sites were occupied, q_{max}, could be assessed by the order of $UV_{254} > UV_{280} > UV_{365} > Color_{436}$.

4.6.5. Adsorption of Raw Humic Acid onto Fe doped TiO_2

Adsorption experiments in the presence of Fe doped TiO_2 were conducted by using raw humic acid and its different molecular size fractions, such as 0.45 μm filtered fraction, 100 kDa, and 30 kDa fractions of humic acid solution. TiO_2 loadings were changed in the range of 0.1-1.0 mg mL^{-1}. The spectroscopic properties of raw humic acid were characterized and compared by UV-vis spectroscopy and fluorescence spectroscopy in emission and synchronous scan modes.

4.6.5.1. UV-vis Spectroscopic Evaluation of Raw Humic Acid Adsorption onto Fe doped TiO_2. UV-vis absorbance values were measured between 200-600 nm wavelength region.

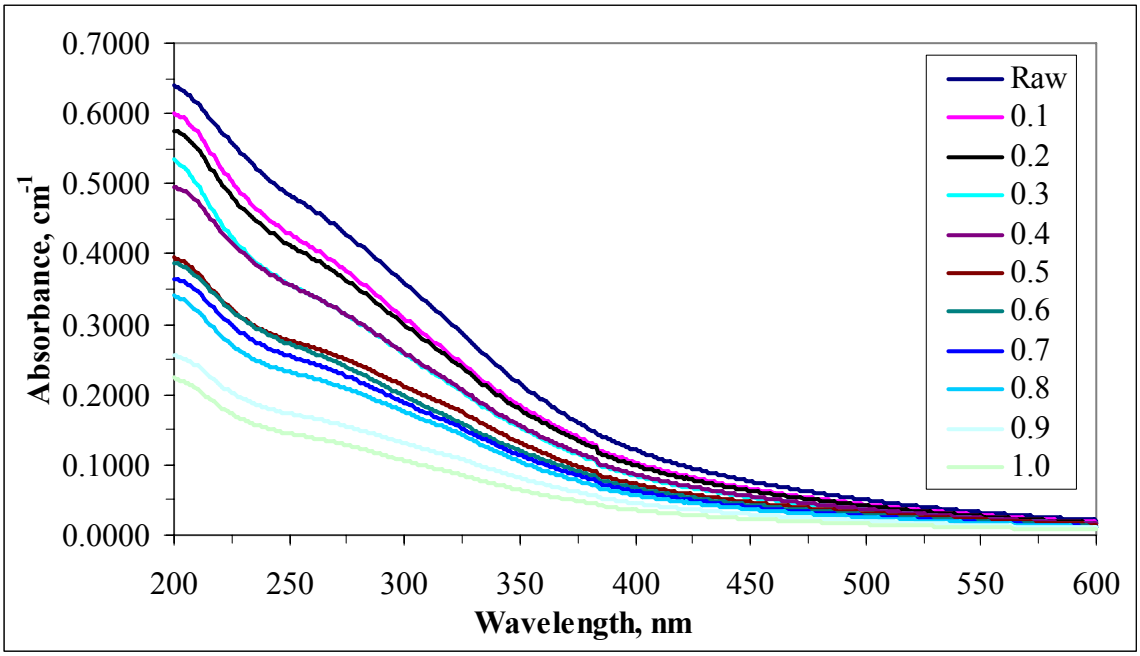

Figure 4.96. UV-vis spectra of raw humic acid adsorption onto Fe doped TiO_2 (legends indicate TiO_2 dosages).

As mentioned before, UV-vis spectra of humic substances are commonly broad; they do not exhibit any obvious features and monotonously decrease with increasing wavelength (Schnitzer and Khan, 1972; Traina et al., 1990; Chen et al., 2002; Uyguner and Bekbölet, 2005a). Figure 4.96 indicated that UV-vis spectra of the humic acid solutions

after adsorption monotonously decreased with increased dosage of TiO_2. Furthermore, UV-vis spectra showed that adsorption onto 0.3 mg mL^{-1} and 0.4 mg mL^{-1} TiO_2 doses have similar trend with declining absorbance recordings. Comparison of the UV-vis spectra of the raw humic acid onto bare TiO_2 indicated the role of Fe and humic interaction with the TiO_2 surface (Figure 4.20 and Figure 4.96). In the presence of bare TiO_2, it was observed that especially for higher TiO_2 loadings, there were no significantly characteristic absorbance recordings after 400 nm wavelength. However, while in the presence of Fe doped TiO_2, UV-vis spectra showed higher absorbance values and had characteristic absorbance recordings for all wavelengths.

4.6.5.2. Fluorescence Spectroscopic Evaluation of Raw Humic Acid Adsorption onto Fe doped TiO_2. Emission scan fluorescence spectra of humic acid samples were displayed in Figures 4.97 and 4.98.

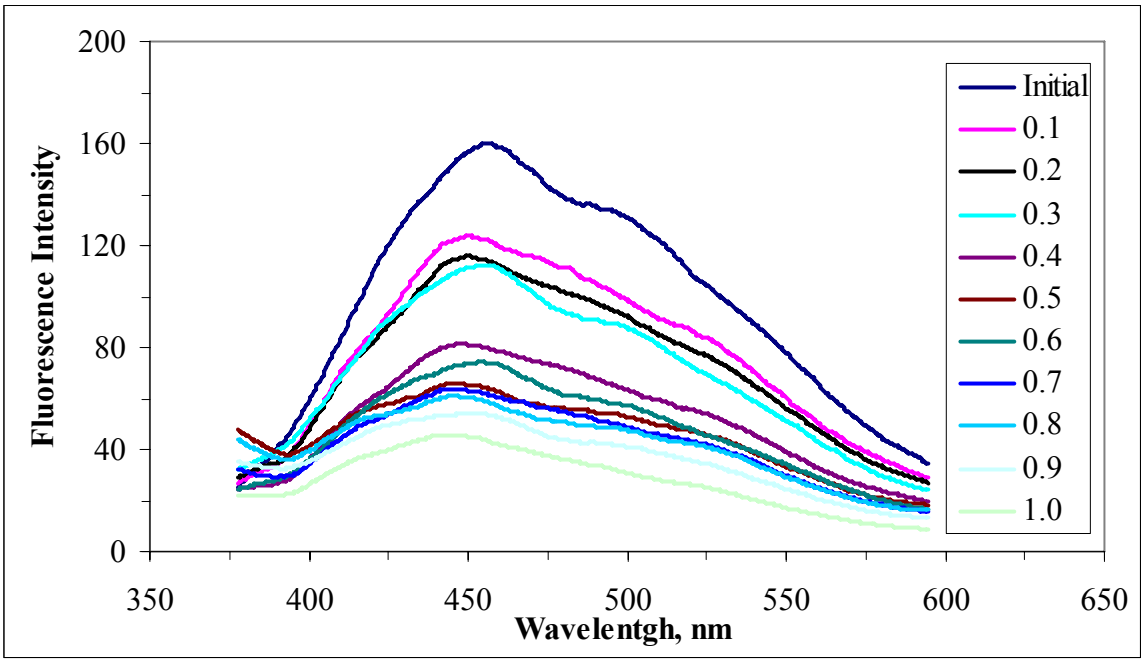

Figure 4.97. Emissions scan fluorescence spectra ($FI_{emis\ 350}$) of raw humic acid adsorption onto Fe doped TiO_2 (where initial represents raw humic acid) (legends indicate TiO_2 dosages).

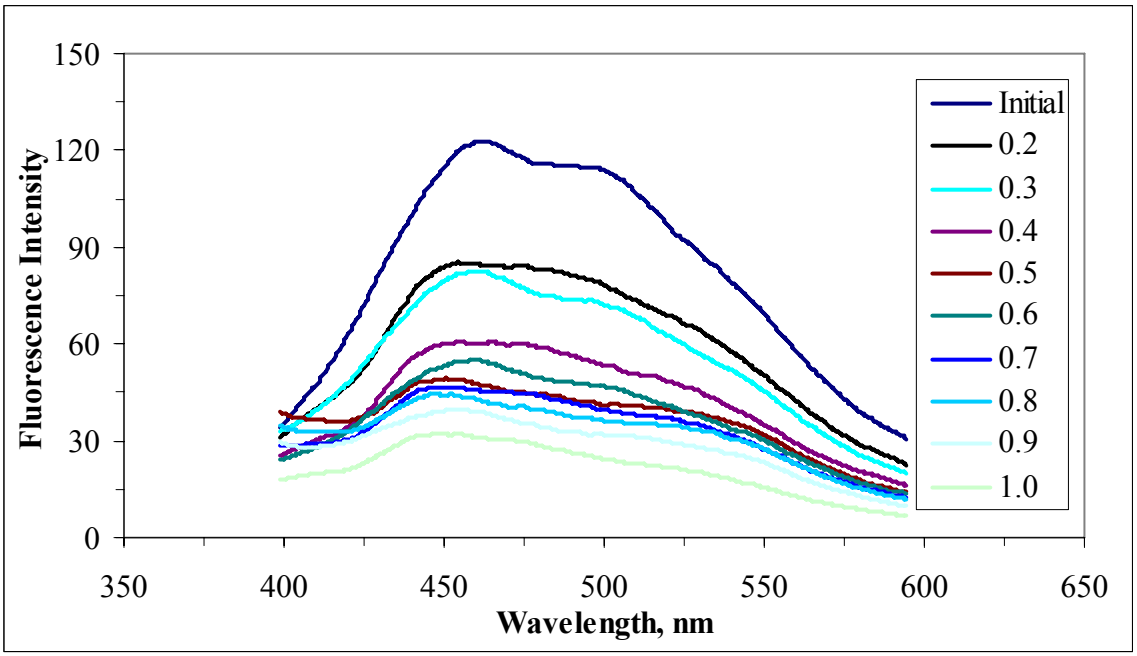

Figure 4.98. Emissions scan fluorescence spectra ($FI_{emis\ 370}$) of raw humic acid adsorption onto Fe doped TiO_2 (where initial represents raw humic acid) (legends indicate TiO_2 dosages).

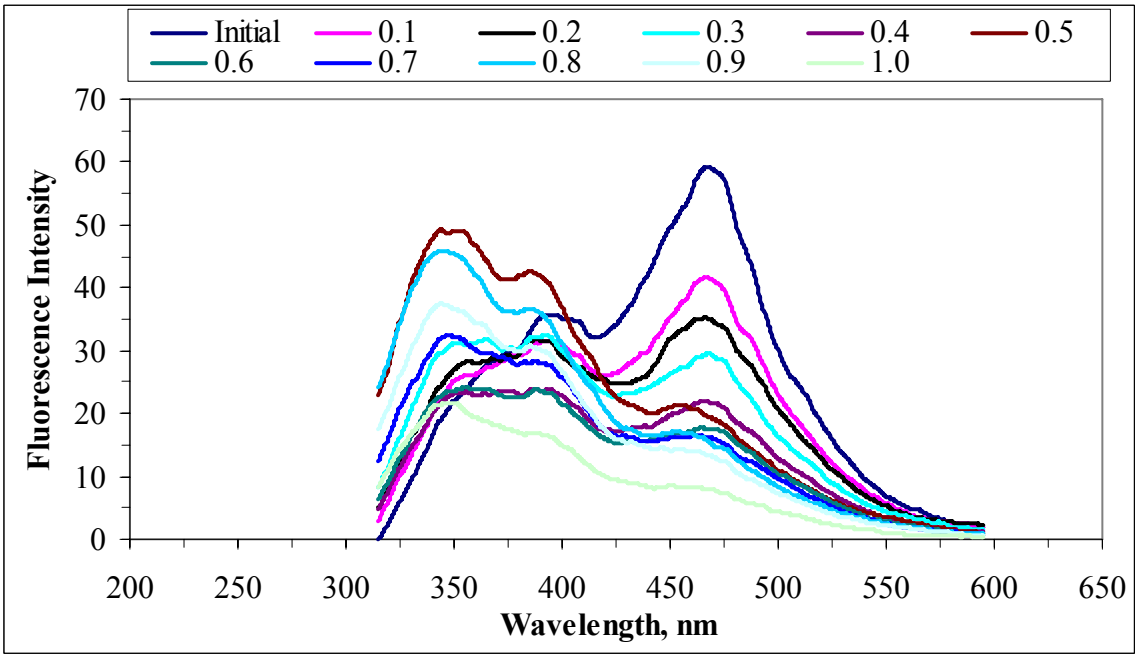

Figure 4.99. Synchronous scan fluorescence spectra of raw humic acid adsorption onto Fe doped TiO_2 (legends indicate TiO_2 dosages).

Emission scan fluorescence spectra were scanned over the range of 375-600 nm and 400-600 nm at excitation wavelengths of 350 and 370 nm, respectively. It could be stated that the excitation wavelength of 350 nm and 370 nm caused a major peak in the region of 450 nm. This peak also recorded for the raw humic acid adsorption onto bare TiO_2 as seen in Figures 4.22 and 4.23. The maximum fluorescence intensity was observed for initial humic acid and the lowest fluorescence intensity was recorded for raw humic acid in the presence of 1.0 mg mL^{-1} TiO_2. The synchronous scan fluorescence spectra recorded for the adsorption of raw humic acid in the presence of Fe doped TiO_2 were shown in Figure 4.99. As expected, the lowest fluorescence intensity was recorded for the adsorption of raw humic acid onto 1.0 mg mL^{-1} TiO_2 dose. Two peaks were observed approximately at 350 and 470 nm wavelength with adsorption of raw humic acid. Adsorption dependent λ_{max} (470 nm) fluorescence intensity displayed a decreasing trend with respect to increased TiO_2 dose.

4.6.5.3. Adsorption Isotherm Modeling of Raw Humic Acid onto Fe doped TiO_2 Binary System. The adsorption data were evaluated in terms of Freundlich and Langmuir adsorption models. Freundlich adsorption model isotherms were displayed in the following Figures 4.100 and 4.101 for $Color_{436}$ and UV_{254}, respectively. The Freundlich adsorption isotherms for UV_{365} and UV_{280} were presented in Appendix A. Figure 4.100 indicated that C_e values varied between 2.6 – 7.43 m^{-1} for $Color_{436}$ depending on the amount of TiO_2 present in solution. The values of q_A calculated to be in the range of 120.2 – 236 $m^{-1}g^{-1}$ for the corresponding C_e values. As presented in Figure 4.101, the equilibrium contents, C_e values varied between 14.22– 42.07 m^{-1} for UV_{254}. The values of q_A calculated to be in the range of 667.4 – 1104 $m^{-1}g^{-1}$ for the corresponding C_e values. Langmuir adsorption isotherms of raw humic acid for UV-vis parameters as $Color_{436}$ and UV_{254} were given in Figure 4.102 and Figure 4.103, respectively. The Langmuir isotherms attained for UV_{365} and UV_{280} parameters were presented in Appendix B.

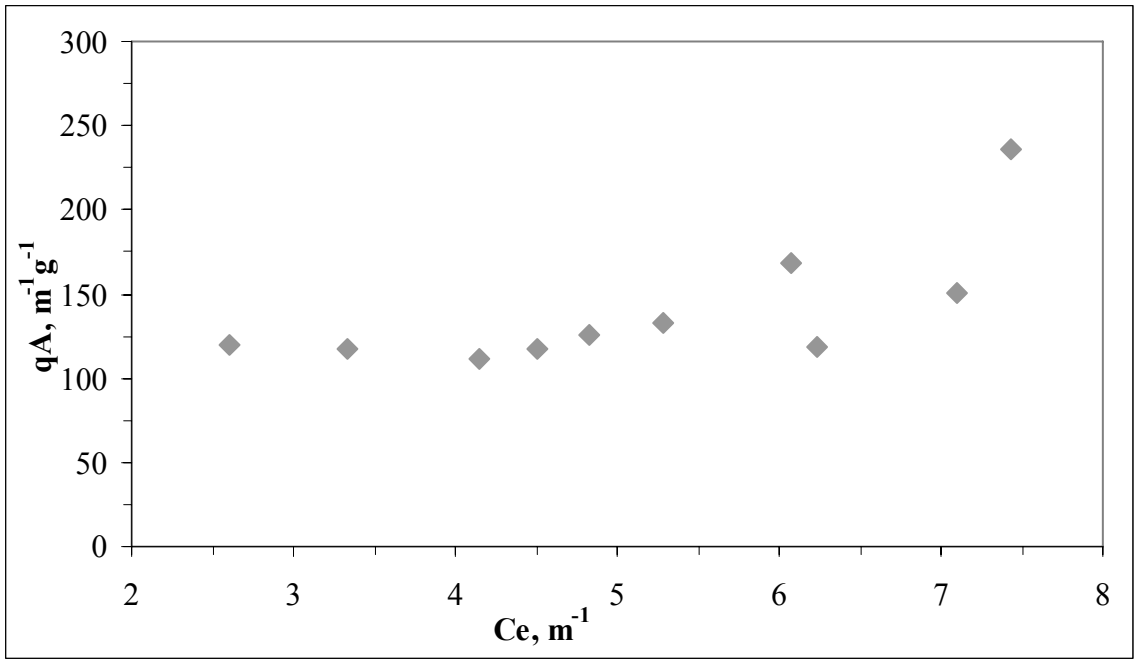

Figure 4.100. Freundlich adsorption isotherm of $Color_{436}$ of raw humic acid onto Fe doped TiO_2.

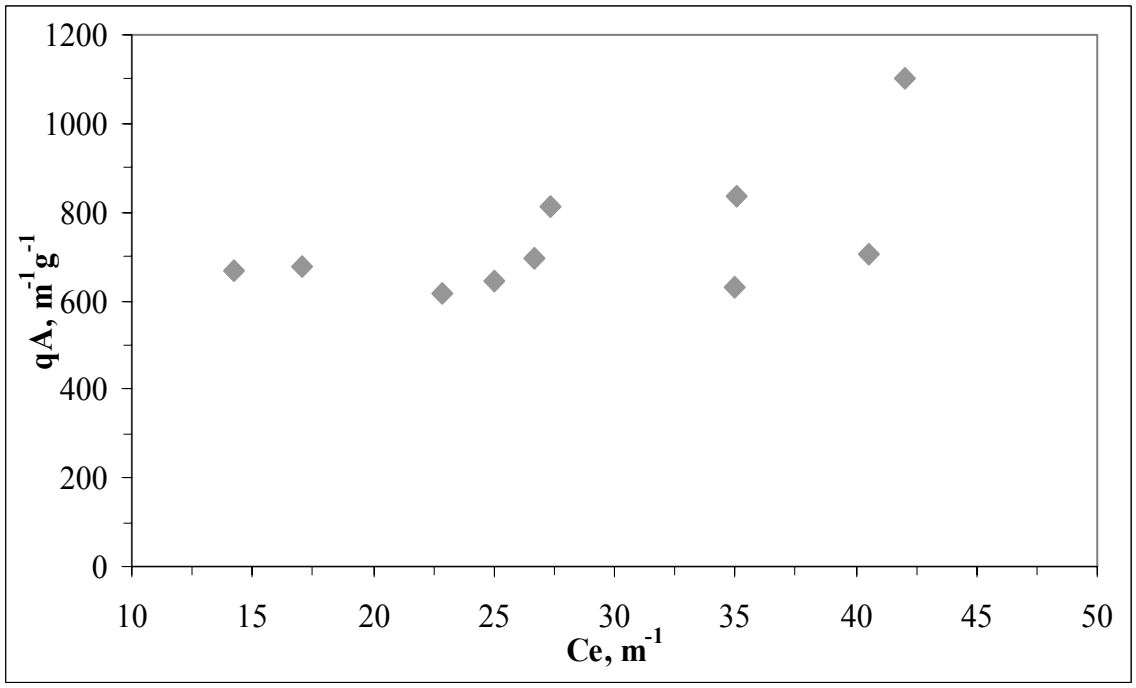

Figure 4.101. Freundlich adsorption isotherm of UV_{254} of raw humic acid onto Fe doped TiO_2.

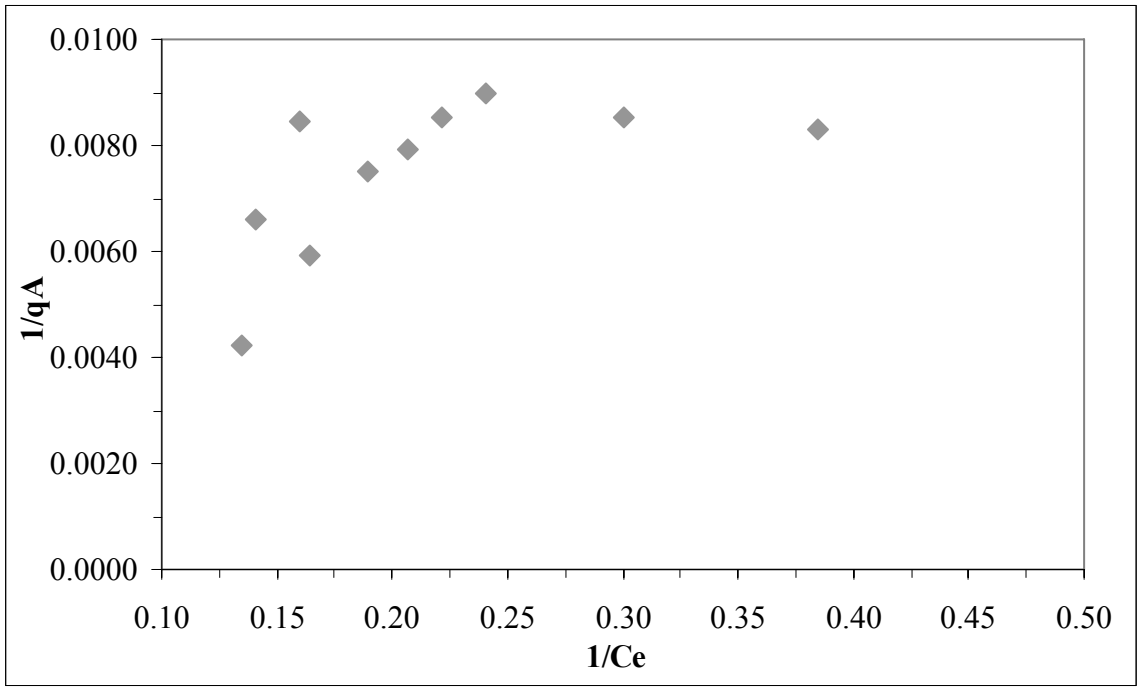

Figure 4.102. Langmuir adsorption isotherm of $Color_{436}$ of raw humic acid onto Fe doped TiO_2.

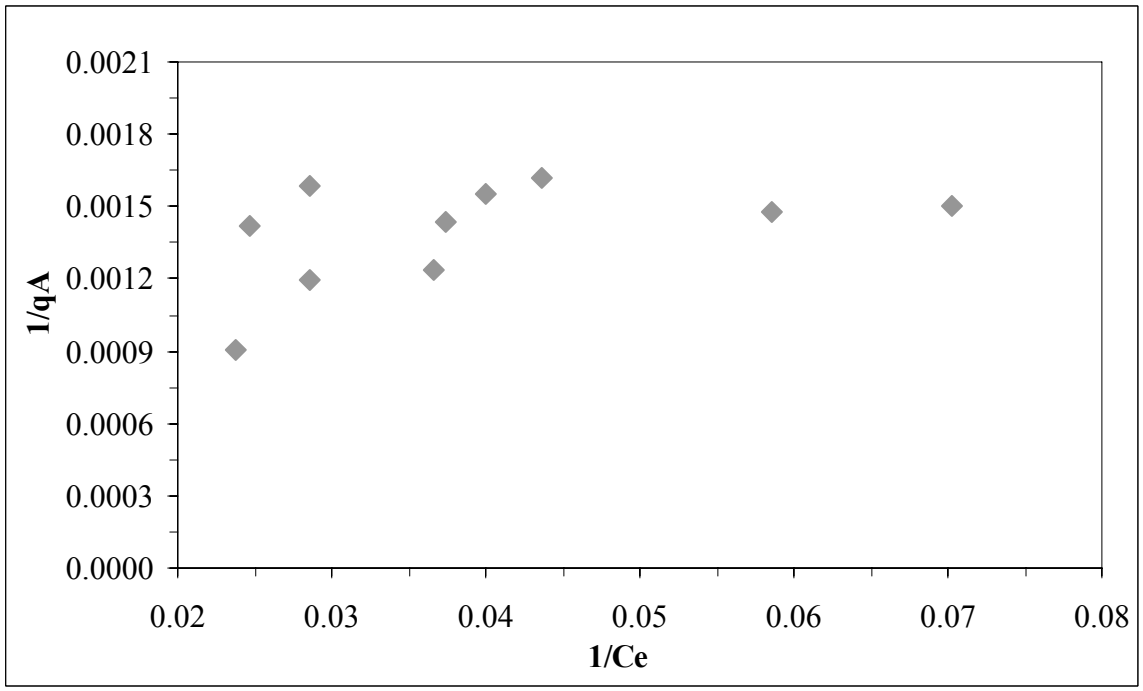

Figure 4.103. Langmuir adsorption isotherm of UV_{254} of raw humic acid onto Fe doped TiO_2.

Adsorption isotherm modeling of raw humic acid onto Fe doped TiO_2 binary system indicated that there was no exact adsorption profile depending on the TiO_2 amounts. The adsorption data for $Color_{436}$ and UV_{254} did not fit to Freundlich and Langmuir isotherm for raw humic acid. Hence, data were evaluated in terms of distribution coefficient.

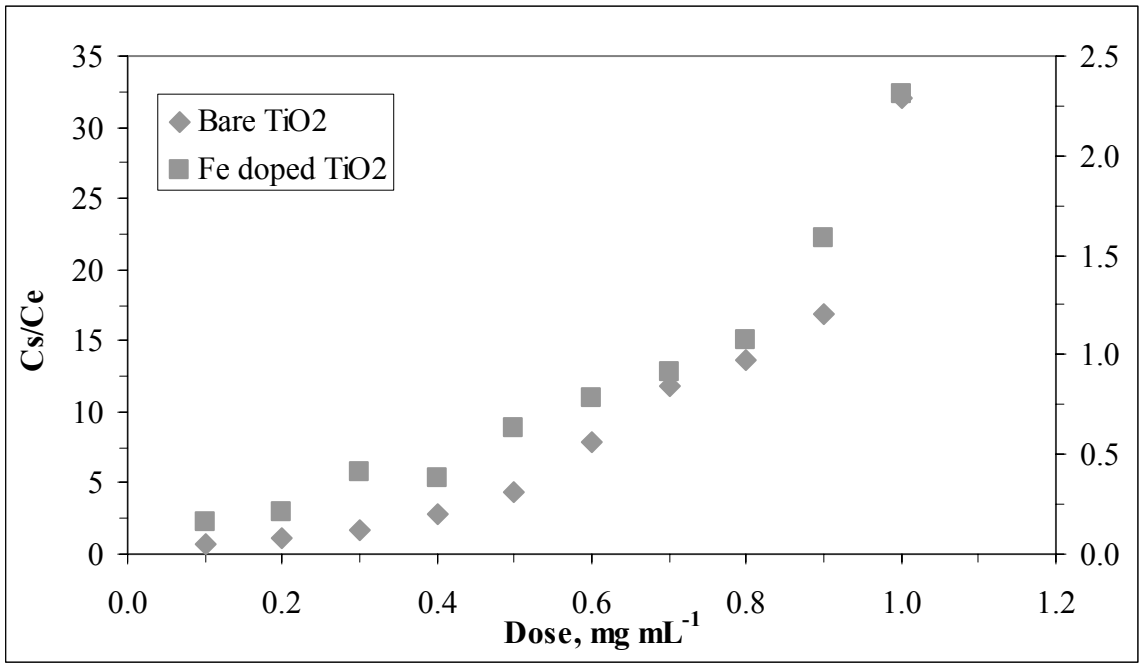

Figure 4.104. Distribution coefficient of $Color_{436}$ of raw humic acid onto bare and Fe doped TiO_2.

Figure 4.104 indicated that C_s/C_e values varied between 0.659 – 32.115 for $Color_{436}$ depending on the amount of TiO_2 present in solution in the presence of bare TiO_2. However, while in the presence of Fe doped TiO_2, C_s/C_e varied between 0.159-2.312. Besides, Figure 4.105 presented similar trend in terms of distribution coefficient both in the presence of bare TiO_2 and in the presence of Fe doped TiO_2. As presented in Figure 4.105, C_s/C_e values varied between 16.83– 44.68 and 5.52-33.37 for UV_{254} in the presence of bare TiO_2 and Fe doped TiO_2, respectively.

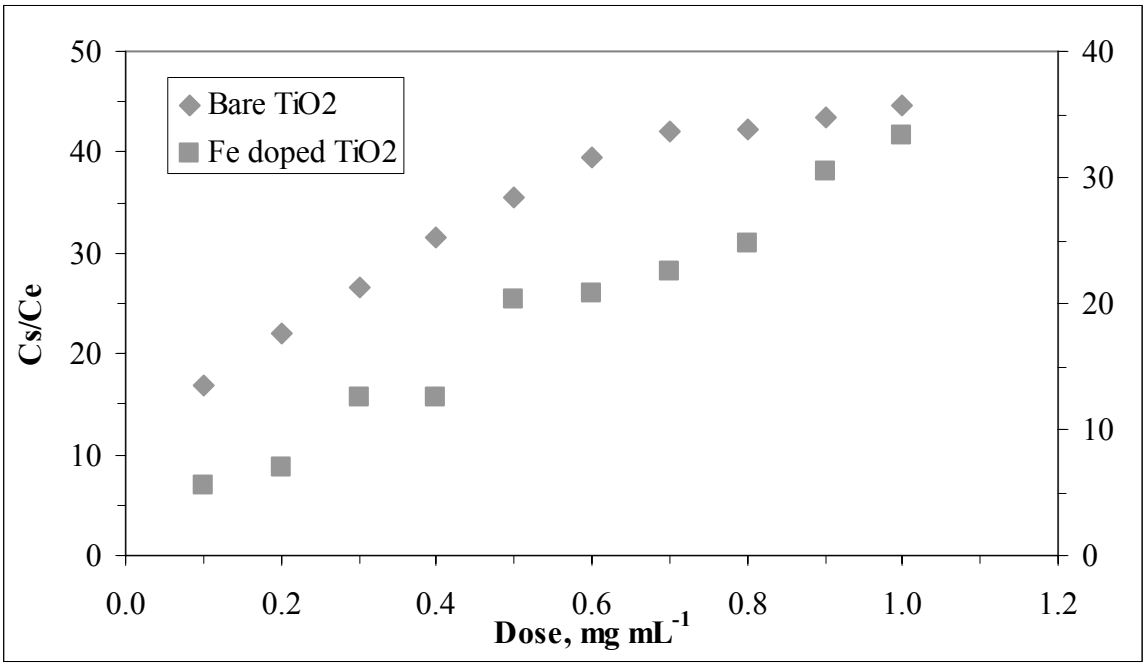

Figure 4.105. Distribution coefficient of UV_{254} of raw humic acid onto bare and Fe doped TiO_2.

4.6.6. Adsorption of 0.45 µm Filtered Fraction of Humic Acid onto Fe doped TiO_2

In order to investigate the adsorption properties of 0.45 µm filtered fraction of humic acid, batch adsorption experiments were carried out with bare TiO_2 in the range of 0.1-1.0 mg mL^{-1}.

4.6.6.1. UV-vis Spectroscopic Evaluation of 0.45 µm Filtered Fraction of Humic Acid Adsorption onto Fe doped TiO_2. UV-vis spectra of 0.45 µm filtered fraction of humic acid adsorption onto Fe doped TiO_2 were shown in Figure 4.106. It was observed that UV-vis spectra of humic acids monotonously decreased with increasing wavelength as expected. As seen in the Figure 4.106, the UV-vis spectra of 0.45 µm filtered fraction of humic acid showed a gradually declining trend with the respect to increasing wavelength in the 200-600 nm region. In the case of 0.1 mg mL^{-1} and 0.2 mg mL^{-1} TiO_2 doses, the UV-vis spectra followed an overlapping trend. The effect of the presence of Fe doped TiO_2 can be observed with higher absorbance in comparison to 0.45 µm filtered fraction of humic acid onto bare TiO_2.

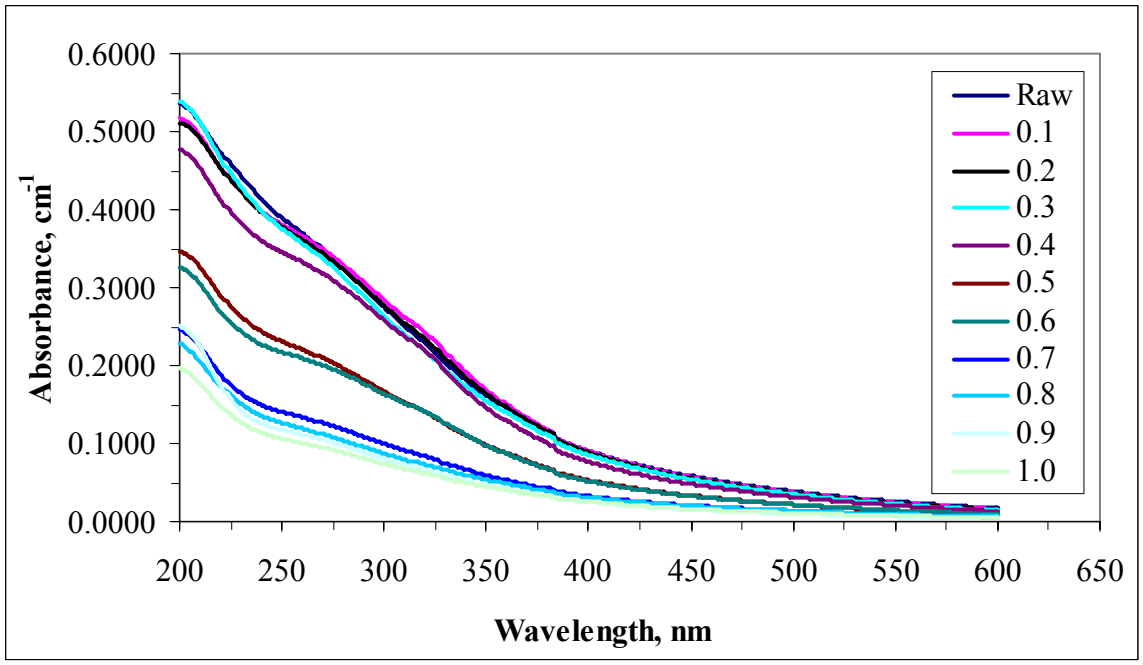

Figure 4.106. UV-vis spectra of 0.45 µm filtered fraction of humic acid onto Fe doped TiO_2 (legends indicate TiO_2 dosages).

4.6.6.2. Fluorescence Spectroscopic Evaluation of 0.45 µm Filtered Fraction of Humic Acid Adsorption onto Fe doped TiO_2 Emission scan fluorescence spectra of 0.45µm filtered fraction of humic acid adsorption onto Fe doped TiO_2 were displayed in Figures 4.107 and 4.108.

It could be stated that the excitation wavelength of 350 nm and 370 nm caused a major peak in the region of 450 nm for 0.45 µm filtered fraction of humic acid in the presence of Fe doped TiO_2. This peak was also recorded for the raw humic acid in the presence of bare TiO_2. The emission scan spectra of fluorescence intensities displayed a declining trend with respect to increasing TiO_2 dose from 0.1 to 1.0 mg mL^{-1}. Upon the adsorption onto 0.8 mg mL^{-1} TiO_2 dose, the peak at 450 nm wavelength was dissappeared and became a linear form. Ülker (2008) investigated that effect of fractionation on the sorption properties of nom onto modified TiO_2 surfaces. This study reported that emission scan fluorescence spectra displayed a decreasing trend in FI at λ_{max} 470 nm with respect to increasing Fe doped TiO_2.

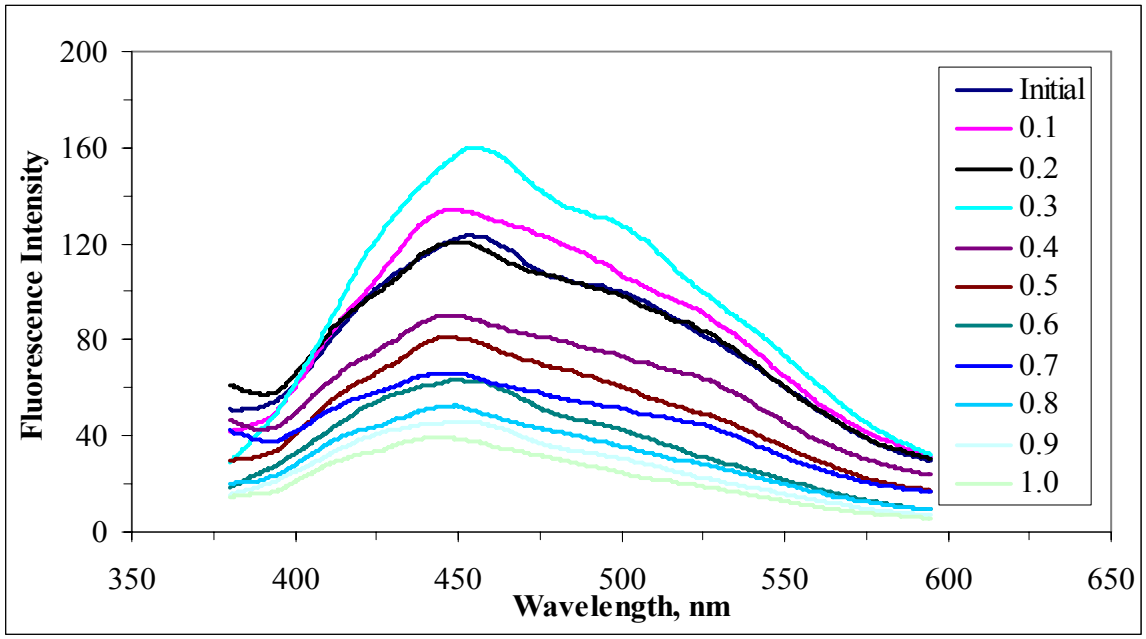

Figure 4.107. Emissions scan fluorescence spectra ($FI_{emis\ 350}$) of 0.45 µm filtered fraction of humic acid adsorption onto Fe doped TiO_2 (where initial represents raw humic acid) (legends indicate TiO_2 dosages).

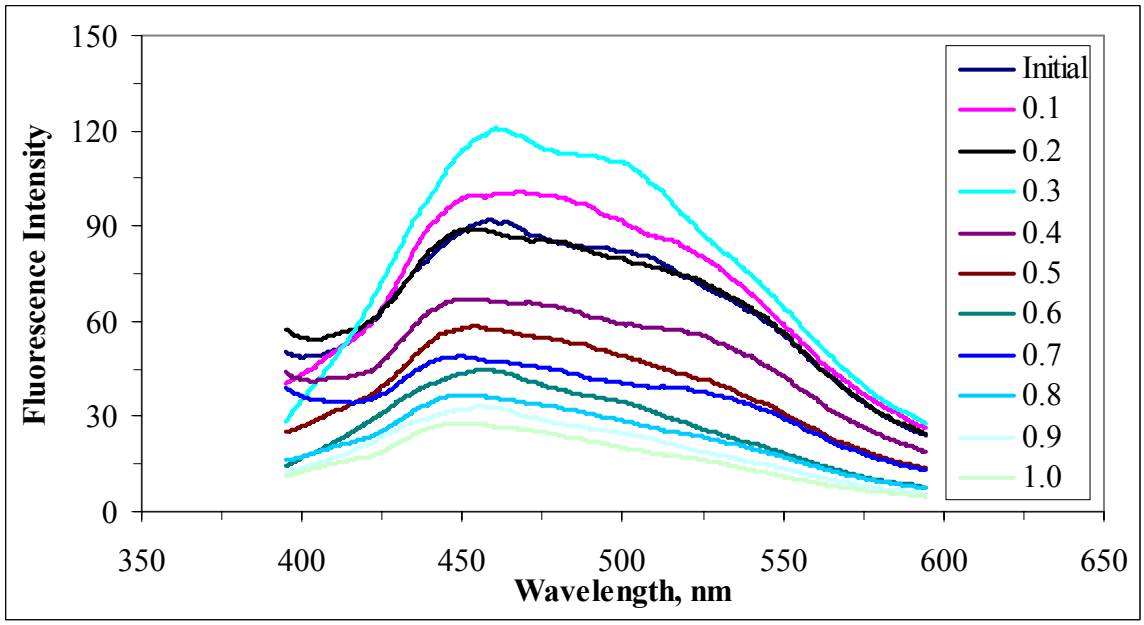

Figure 4.108. Emissions scan fluorescence spectra ($FI_{emis\ 370}$) of 0.45 µm filtered fraction of humic acid adsorption onto Fe doped TiO_2 (where initial represents raw humic acid) (legends indicate TiO_2 dosages).

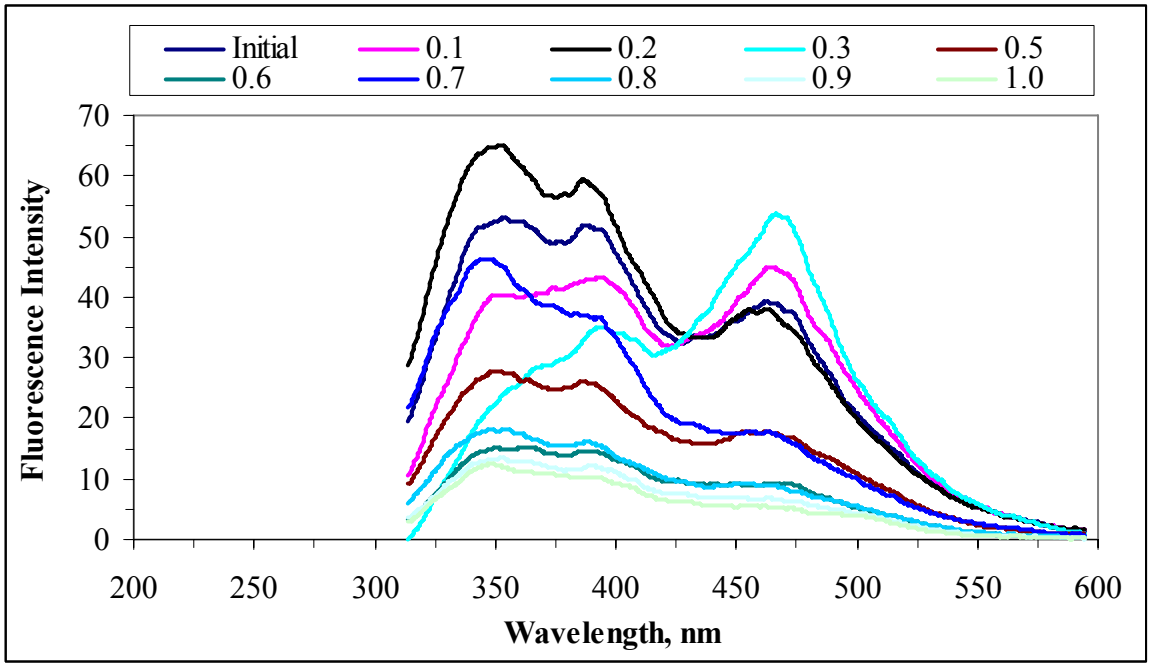

Figure 4.109. Synchronous scan fluorescence spectra of 0.45 µm filtered fraction of humic acid adsorption onto Fe doped TiO_2 (legends indicate TiO_2 dosages).

Synchronous fluorescence spectra of 0.45µm filtered fraction of humic acid adsorption onto Fe doped TiO_2 were displayed in Figure 4.109. Two main peaks were observed at 350 and 475 nm wavelengths. The highest fluorescence intensity was observed for adsorption onto raw humic acid with peaks about 350 nm wavelengths. The lowest fluorescence intensity was recorded for the adsorption of 0.45µm filtered fraction of humic acid onto 0.9 and 1.0 mg mL^{-1} TiO_2 dose which were same trend. As explained in the adsorption studies of humic acid in the presence of bare TiO_2; synchronous scan fluorescence spectra for 0.45 µm filtered fraction of humic acid displayed a sharp peak around wavelength of 470 nm.

4.6.6.3. Adsorption Isotherm Modeling of 0.45 µm Filtered Fraction of Humic Acid onto Fe doped TiO_2 Binary System. In order to evaluate the experimental results, the adsorption data were fitted to Freundlich and Langmuir adsorption models. Freundlich adsorption model isotherms were displayed in Figure 4.110 and Figure 4.111 for $Color_{436}$ and UV_{254}, respectively. Freundlich adsorption model isotherms for UV_{365} and UV_{280} were presented in Appendix A.

Figure 4.110 indicated that C_e values varied between 1.75 – 6.42 m^{-1} for $Color_{436}$ depending on the amount of TiO_2 present in solution. The values of q_A calculated to be in the range of 28 – 122 $m^{-1}g^{-1}$ for the corresponding C_e values for $Color_{436}$. As could be seen in Figure 4.111, C_e values varied between 10.40 – 37.48 m^{-1} for UV_{254}. The values of q_A calculated to be in the range of 87.3– 695.1 m^{-1} g^{-1} for the corresponding C_e values for UV_{254}. Langmuir adsorption isotherm of 0.45µm filtered fraction of humic acid onto TiO_2 was shown for $Color_{436}$ and UV_{254} in figure 4.112 and 4.113. Langmuir adsorption model isotherms for UV_{365} and UV_{280} were presented in Appendix B.

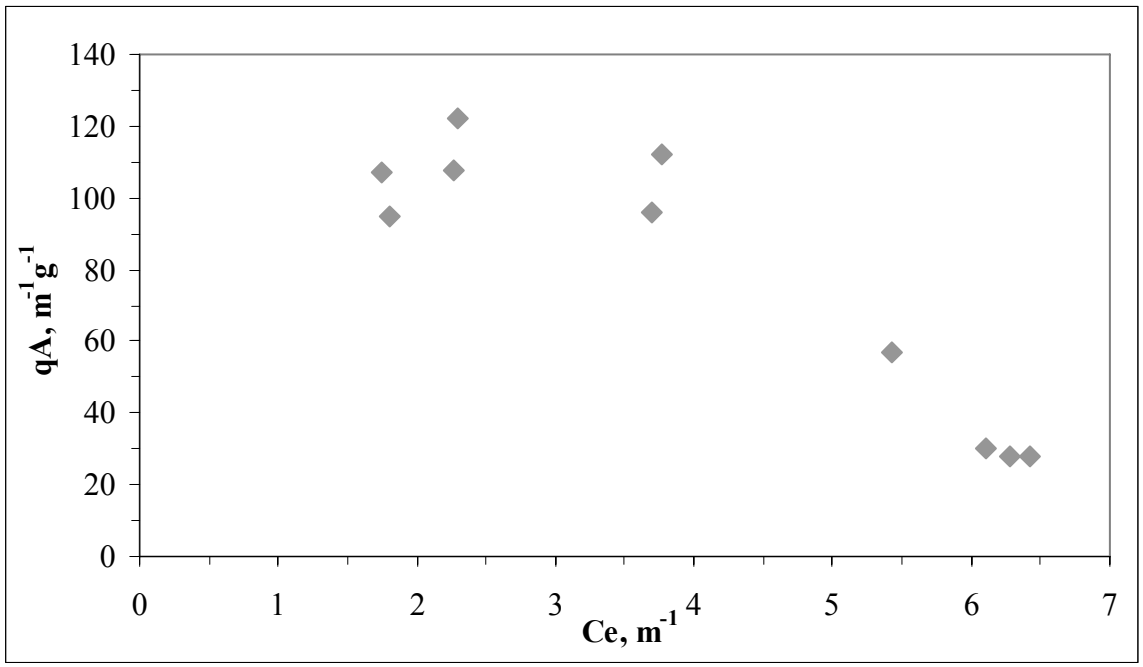

Figure 4.110. Freundlich adsorption isotherm of $Color_{436}$ of 0.45 µm filtered fraction of humic acid onto Fe doped TiO_2.

Adsorption isotherm modeling of 0.45 µm filtered fraction of humic acid onto Fe doped TiO_2 binary system indicated that there was no exact adsorption profile depending on the TiO_2 amounts. The adsorption data for $Color_{436}$ and UV_{254} did not fit to Freundlich and Langmuir isotherm for 0.45 µm filtered fraction of humic acid. Hence, data were evaluated in terms of distribution coefficient.

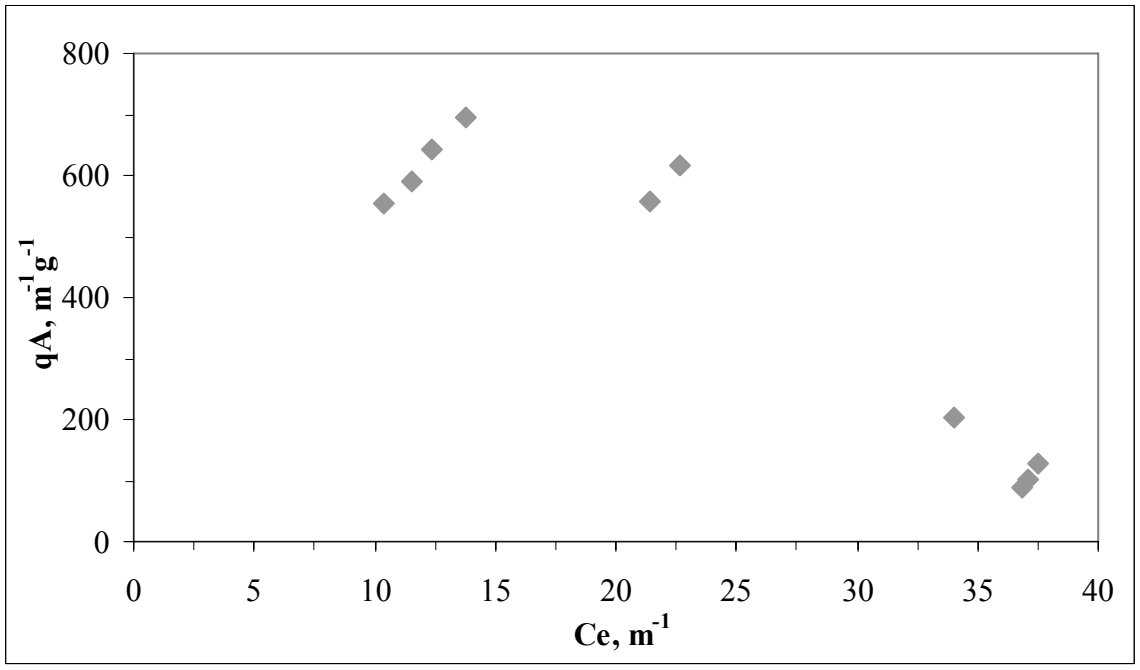

Figure 4.111. Freundlich adsorption isotherm of UV_{254} of 0.45 μm filtered fraction of humic acid onto Fe doped TiO_2.

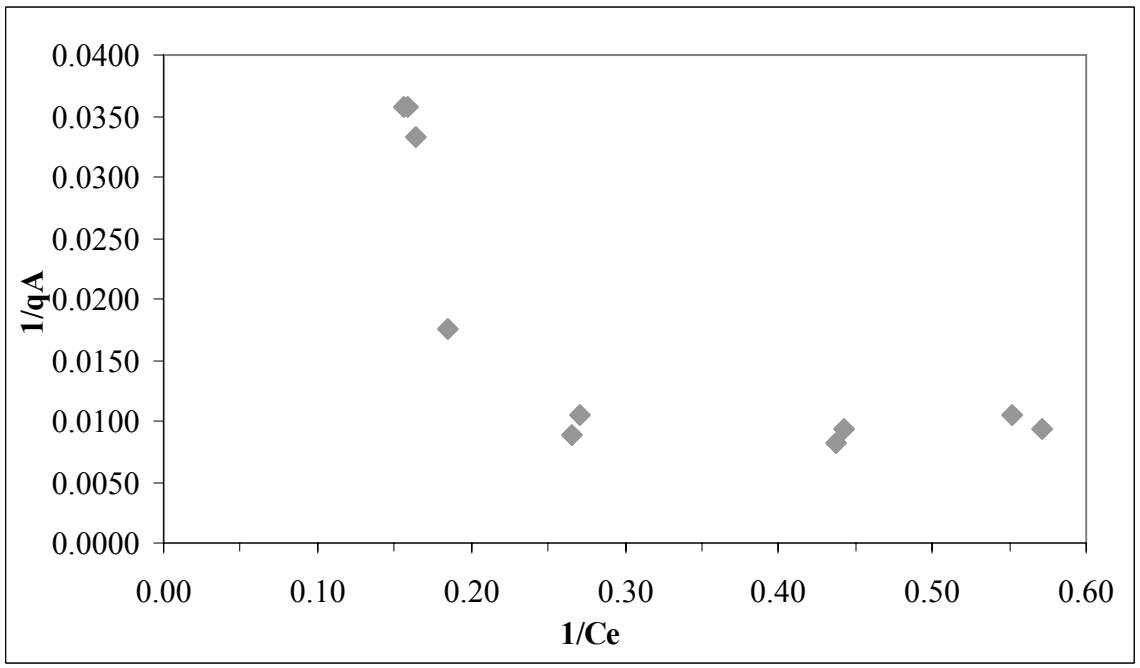

Figure 4.112. Langmuir adsorption isotherm of $Color_{436}$ of 0.45μm filtered fraction of humic acid onto Fe doped TiO_2.

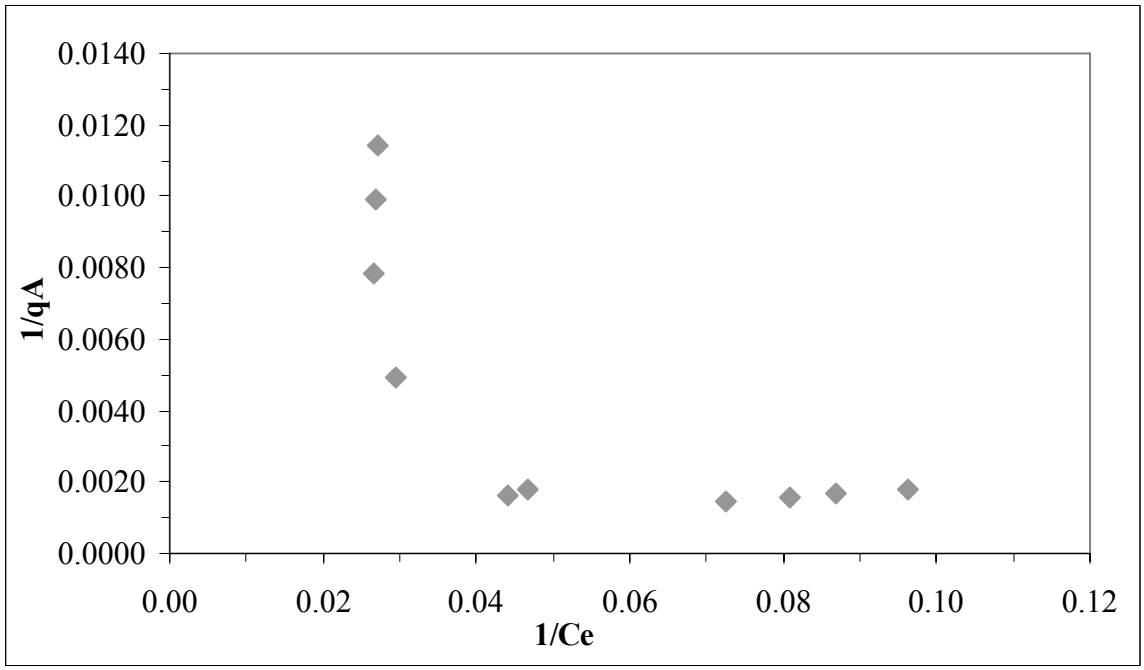

Figure 4.113. Langmuir adsorption isotherm of UV_{254} of 0.45µm filtered fraction of humic acid onto Fe doped TiO_2.

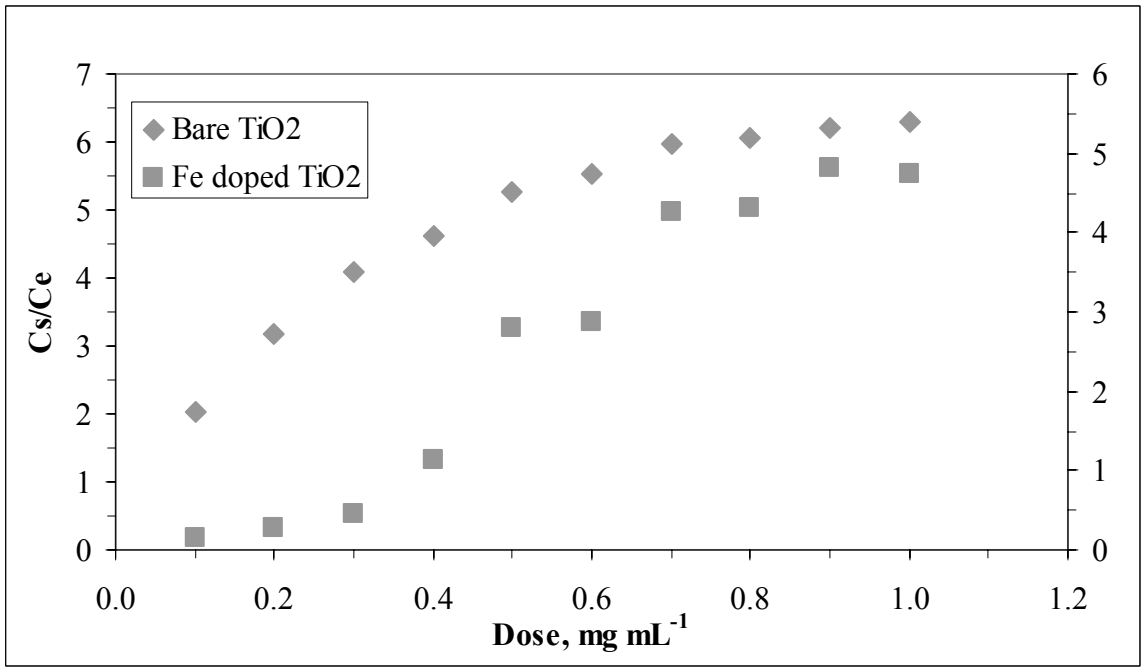

Figure 4.114. Distribution coefficient of $Color_{436}$ of 0.45 µm filtered fraction of humic acid onto bare and Fe doped TiO_2.

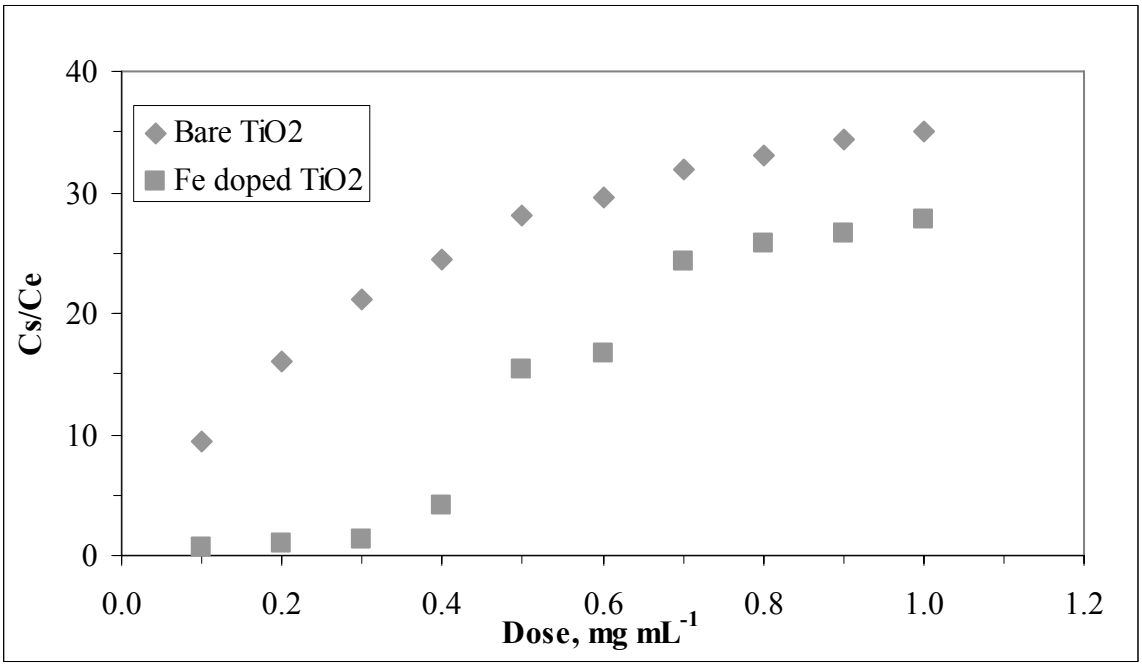

Figure 4.115. Distribution coefficient of UV_{254} of 0.45 μm filtered fraction of humic acid onto bare and Fe doped TiO_2.

As seen in Figure 4.114, C_s/C_e values varied between 2.02-6.30 for $Color_{436}$ depending on the amount of TiO_2 present in solution in the presence of bare TiO_2. However, while in the presence of Fe doped TiO_2, C_s/C_e varied between 0.14-4.81. Figure 4.115 indicated that C_s/C_e values varied between 9.45-34.96 and 0.64 - 27.72 for UV_{254} in the presence of bare TiO_2 and Fe doped TiO_2, respectively.

4.6.7. Adsorption of 100 kDa Fraction of Humic Acid onto Fe doped TiO_2

4.6.7.1. UV-vis Spectroscopic Evaluation of 100 kDa Fraction of Humic Acid Adsorption onto Fe doped TiO_2. UV-vis spectra of 100 kDa fraction of humic acid adsorption onto Fe doped TiO_2 were displayed in Figure 4.116.

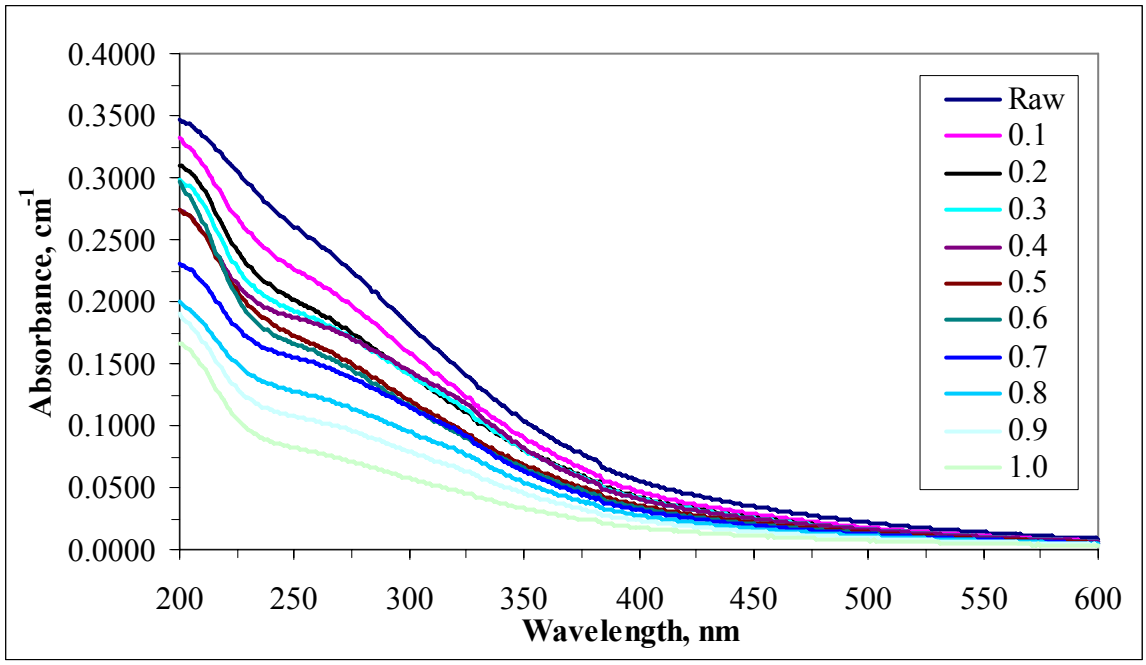

Figure 4.116. UV-vis spectra of 100 kDa fraction of humic acid onto Fe doped TiO_2 (legends indicate TiO_2 dosages).

While raw humic acid shows the highest trend, by the adsorption of raw humic acid onto dose of 0.1 mg mL^{-1} TiO_2, UV-vis spectra displayed a decreasing trend. Moreover, the UV-vis spectra showed that adsorption onto 0.4 mg mL^{-1} and 0.5 mg mL^{-1} TiO_2 doses have similar trend. In the presence of bare TiO_2, it was also observed that especially for higher TiO_2 loadings, there were no significantly characteristic absorbance recordings for longer wavelengths (λ> 400 nm). However, while in the presence of Fe doped TiO_2, it could be easily seen that the slight decreases were occurred with the addition of increased dose of TiO_2 and it was observed that there were significantly characteristic absorbance recordings for longer wavelengths (λ> 400 nm) in comparison to bare TiO_2.

4.6.7.2. Fluorescence Spectroscopic Evaluation of Raw Humic Acid Adsorption onto Bare TiO_2. Emission scan fluorescence spectra of humic acid samples were displayed in Figures 4.117 and 4.118.

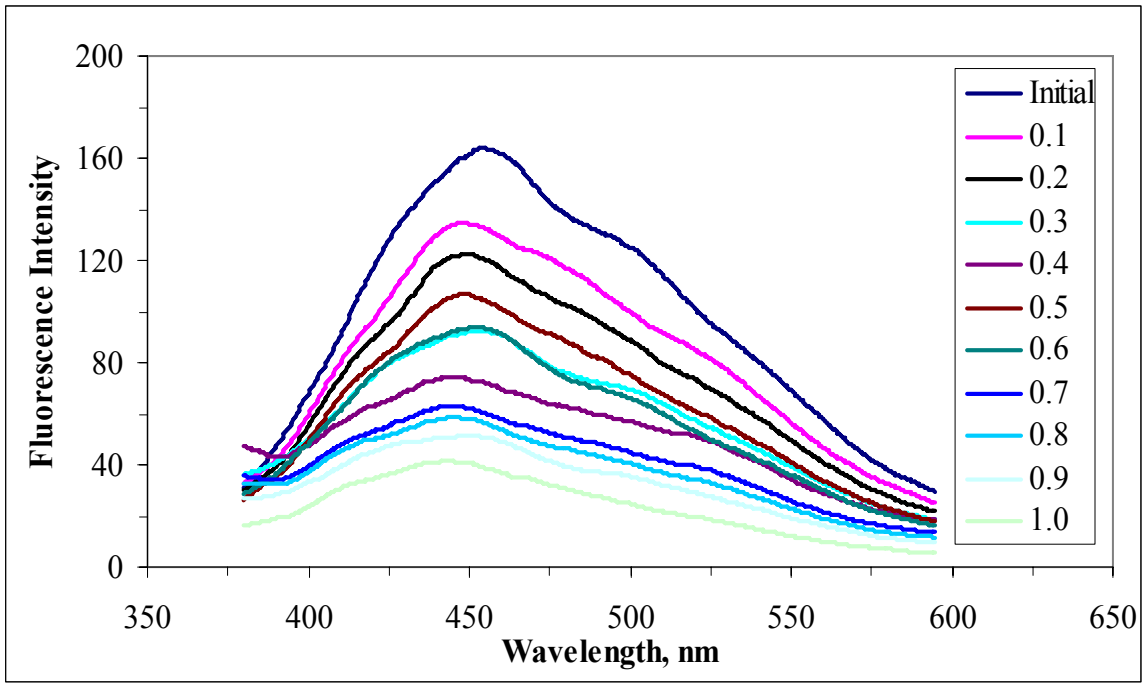

Figure 4.117. Emissions scan fluorescence spectra ($FI_{emis\ 350}$) of 100 kDa fraction of humic acid adsorption onto Fe doped TiO_2 (where initial represents raw humic acid) (legends indicate TiO_2 dosages).

The maximum fluorescence intensity peak was recorded at 450 nm wavelength in accordance with the previously investigated other humic acid such as 0.45 filtered fraction and 100 kDa fraction of humic acid. Starting from adsorption onto 0.1 to 1.0 mg mL^{-1} TiO_2 doses, all of the fluorescence intensities decreased. 100 kDa fraction of humic acid adsorption onto Fe doped TiO_2 exhibited a similar trend between the adsorption doses of 0.3 mg mL^{-1} and 0.6 mg mL^{-1} TiO_2.

Synchronous scan fluorescence spectra of 100 kDa fraction of humic acid, illustrated by Figure 4.118 gave a major peak around 350 nm. It could be said that the synchronous scan fluorescence spectra gave decreasing intensity with increasing TiO_2 dose. After adsorption onto 0.6 mgL^{-1} of TiO_2, the characteristic peak of for 100 kDa filtered fraction of humic acid at 470 nm wavelength completely disappeared. Similar result attained 100 kDa fraction of humic acid adsorption onto bare TiO_2 as seen figure 4.34.

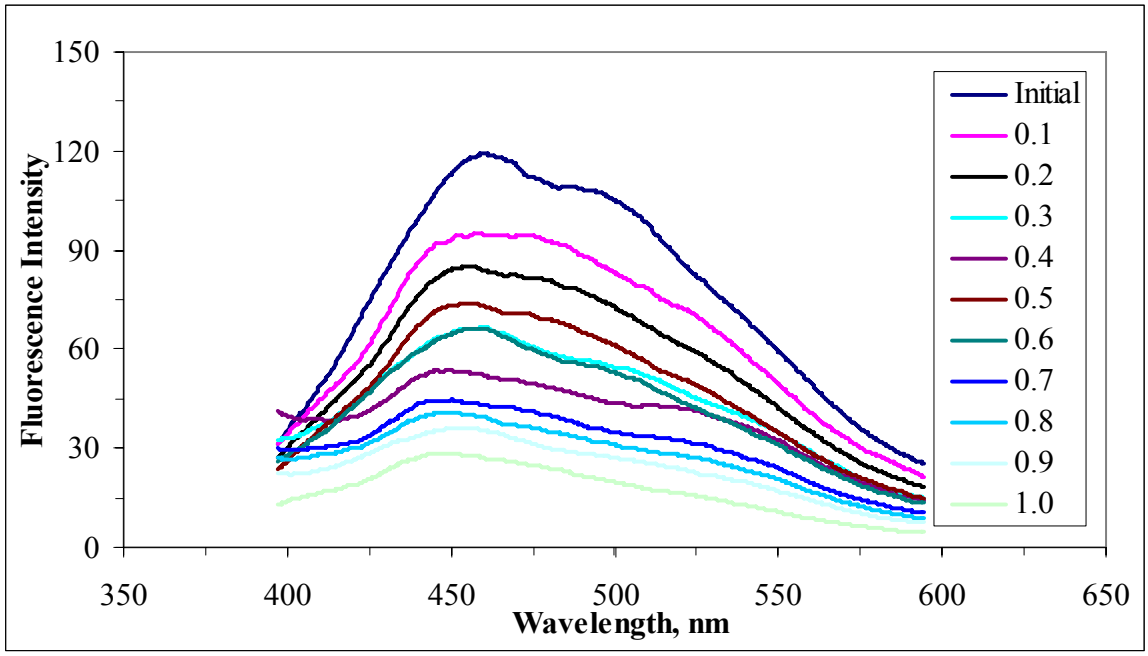

Figure 4.118. Emissions scan fluorescence spectra ($FI_{emis\ 370}$) of 100 kDa fraction of humic acid adsorption onto Fe doped TiO_2 (where initial represents raw humic acid) (legends indicate TiO_2 dosages).

.

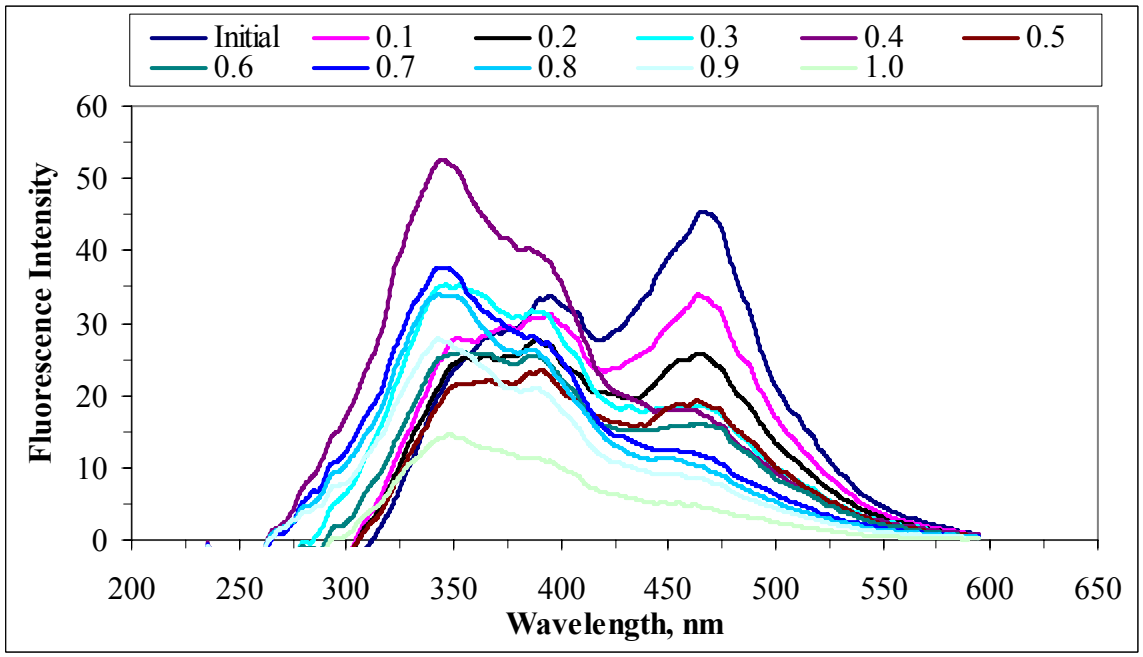

Figure 4.119. Synchronous scan fluorescence spectra of 100 kDa fraction of humic acid adsorption onto Fe doped TiO_2 (legends indicate TiO_2 dosages).

4.6.3.3. Adsorption Isotherm Modeling of 100 kDa Fraction of Humic Acid onto Fe doped TiO_2 Binary System. The adsorption data were evaluated in terms of Freundlich and Langmuir adsorption models. Freundlich adsorption isotherms for $Color_{436}$ and UV_{254} changes of humic acids were given in the Figures 4.120 and 4.121. Freundlich adsorption isotherms for UV_{365} and UV_{280} were presented in Appendix A.

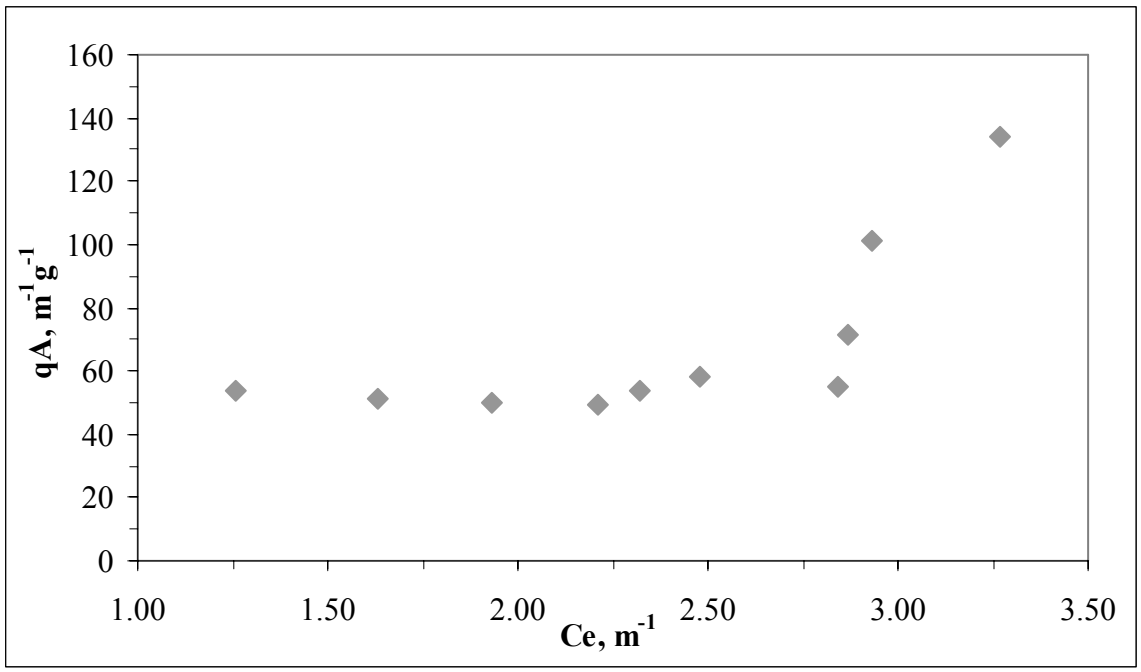

Figure 4.120. Freundlich adsorption isotherm of $Color_{436}$ of 100 kDa fraction of humic acid onto Fe doped TiO_2.

Figure 4.120 indicated that C_e values varied between 1.26 – 3.27 m^{-1} for $Color_{436}$ depending on the amount of TiO_2 present in solution. The values of q_A calculated to be in the range of 49.4 - 134 $m^{-1}g^{-1}$ for the corresponding C_e values. As seen in Figure 4.121, C_e values varied between 8.04 – 22.19 m^{-1} for UV_{254}. The values of q_A calculated to be in the range of 291.1 - 658 $m^{-1}g^{-1}$ for the corresponding C_e values. Langmuir adsorption isotherm of 100 kDa fraction of humic acid onto Fe doped TiO_2 was shown for $Color_{436}$ and UV_{254} in figure 4.122 and 4.123. Langmuir adsorption model isotherms for UV_{365} and UV_{280} were presented in Appendix B.

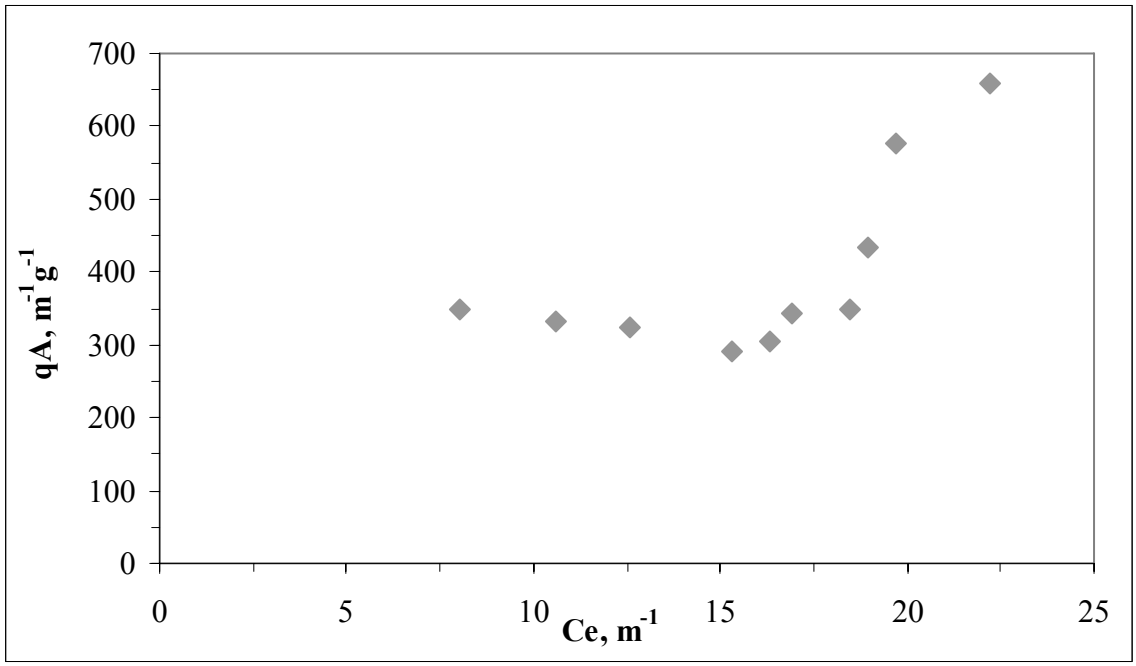

Figure 4.121. Freundlich adsorption isotherm of UV_{254} of 100 kDa fraction of humic acid onto Fe doped TiO_2.

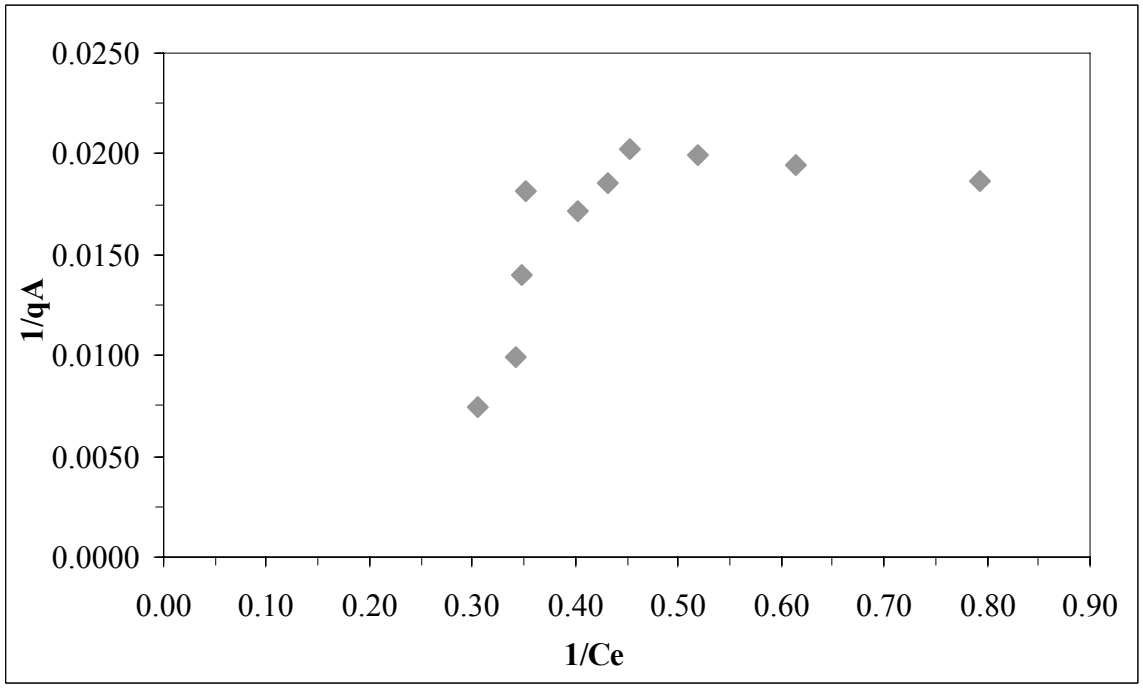

Figure 4.122. Langmuir adsorption isotherm of $Color_{436}$ of 100 kDa fraction of humic acid onto Fe doped TiO_2.

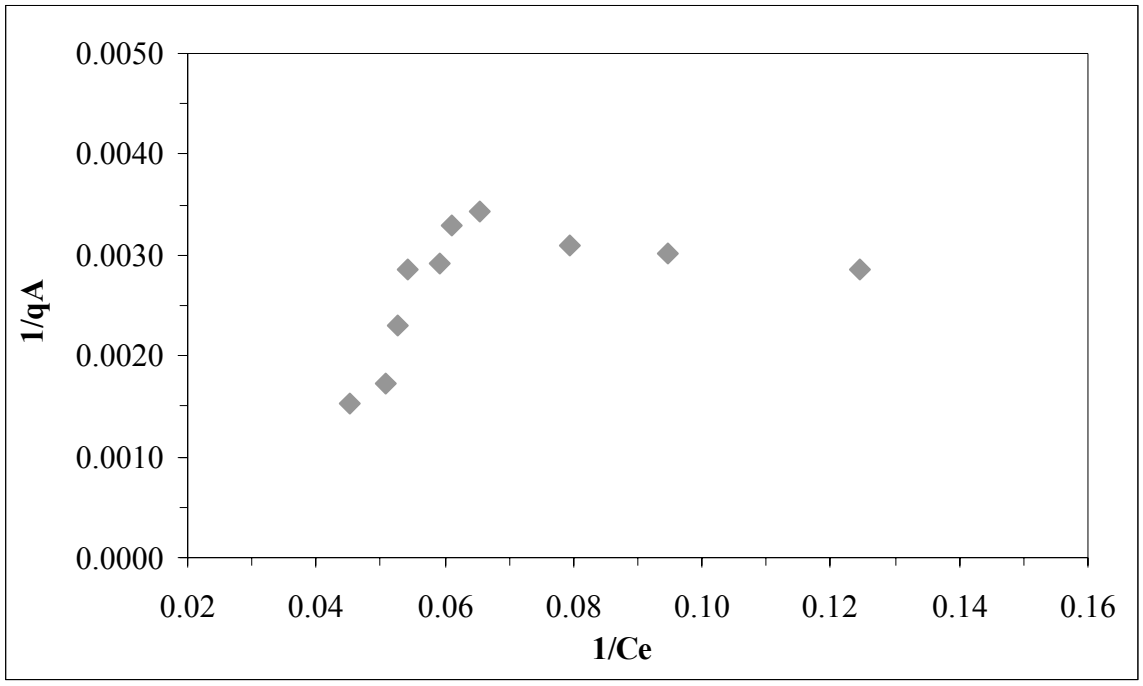

Figure 4.123. Langmuir adsorption isotherm of UV_{254} of 100 kDa fraction of humic acid onto Fe doped TiO_2.

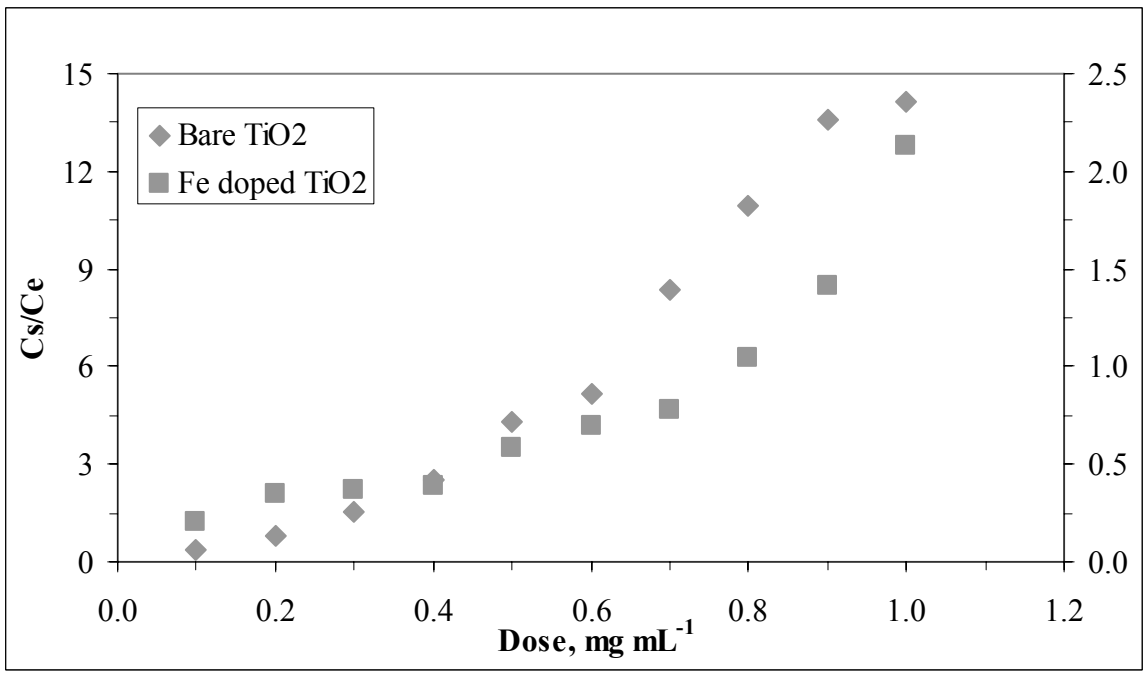

Figure 4.124. Distribution coefficient of $Color_{436}$ of 100 kDa fraction of humic acid onto bare and Fe doped TiO_2.

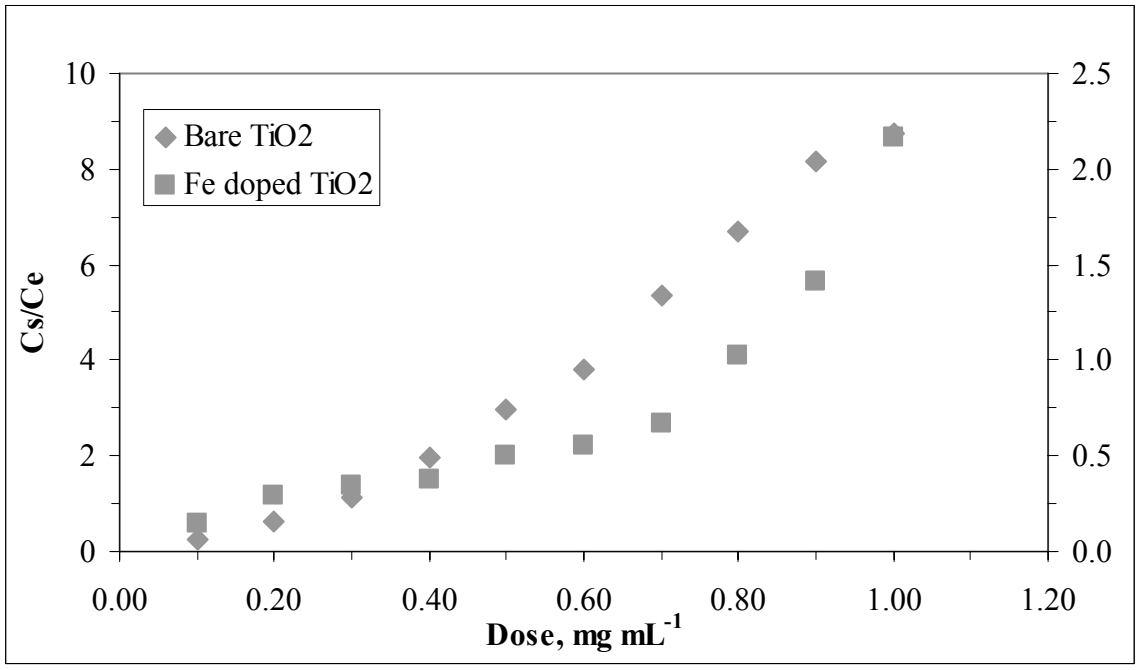

Figure 4.125. Distribution coefficient of UV_{254} of 100 kDa fraction of onto bare and Fe doped TiO_2.

Adsorption isotherm modeling of 100 kDa fraction of humic acid onto Fe doped TiO_2 binary system indicated that there was no exact adsorption profile depending on the TiO_2 amounts. The adsorption data for $Color_{436}$ and UV_{254} did not fit to Freundlich and Langmuir isotherm for 100 kDa fraction of humic acid. Hence, data were evaluated in terms of distribution coefficient.

Figure 4.124 indicated that C_s/C_e values varied between 0.34-14.15 for $Color_{436}$ depending on the amount of TiO_2 present in solution in the presence of bare TiO_2. However, while in the presence of Fe doped TiO_2, C_s/C_e varied between 0.205-2.127. Figure 4.125 presented similar trend in terms of distribution coefficient of $Color_{436}$ and distribution coefficient of UV_{254} in the presence of bare TiO_2 and in the presence of Fe doped TiO_2. As presented in Figure 4.125, C_s/C_e values varied between 0.247-8.762 and 0.148-2.169 for UV_{254} in the presence of bare TiO_2 and Fe doped TiO_2, respectively.

4.6.8. Adsorption of 30 kDa Fraction of Humic Acid onto Fe doped TiO_2

In order to investigate the adsorption properties of 30 kDa filtered fraction of humic acid, batch adsorption experiments were carried out with Fe doped TiO_2 in the range of 0.1-1.0 mg mL^{-1}.

4.6.8.1. UV-vis Spectroscopic Evaluation of 30kDa Fraction of Humic Acid Adsorption onto Fe doped TiO_2. UV-vis spectra of the 30 kDa fraction of humic acid displayed a decaying trend for all samples in the 200-600 nm wavelength region.

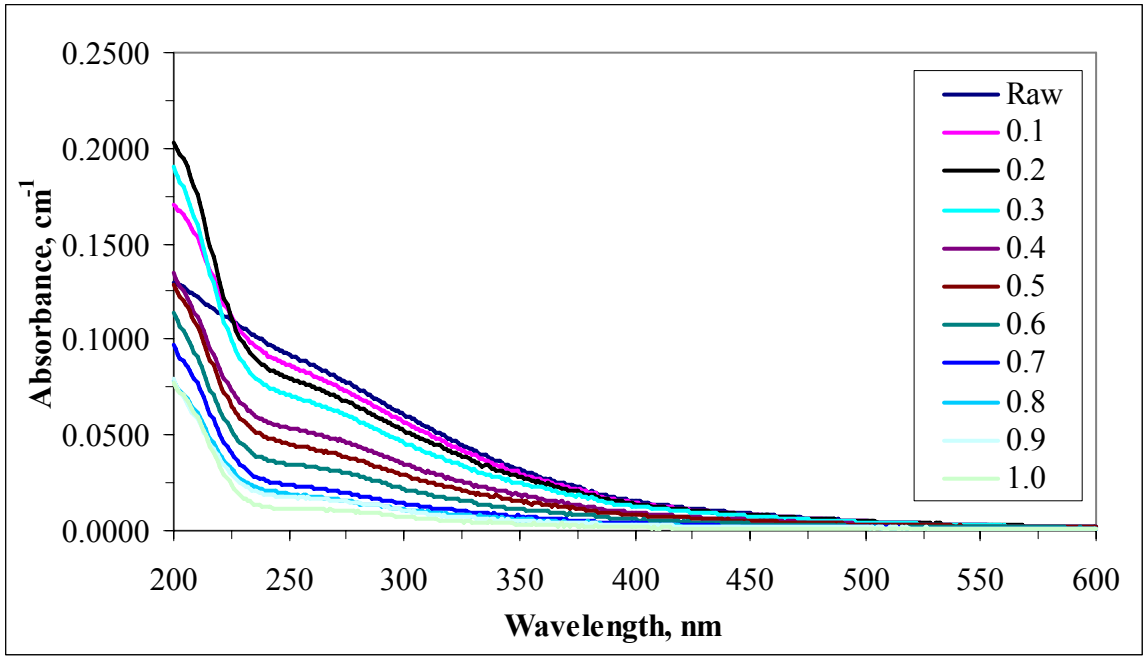

Figure 4.126. UV-vis spectra of 30 kDa fraction of humic acid onto Fe doped TiO_2 (legends indicate TiO_2 dosages).

Considering the initial UV-vis spectral features of the 30 kDa fraction of humic acid, the attained absorbance recordings were significantly lower than the higher molecular weight fractions. Further, there were no significantly characteristic absorbance recordings after 400 nm wavelength. It could be easily noticed that UV-vis spectra approached to very low absorbance values while increasing TiO_2 dose.

4.6.8.2. Fluorescence Spectroscopic Evaluation of 30kDa Fraction of Humic Acid Adsorption onto Fe doped TiO_2. Emissions scan fluorescence spectra were scanned over the range of 360-600 nm and 380-600 nm at excitation wavelength of 350 and 370 nm, respectively which resulted in a major peak at the wavelength of 450 nm. Emission scan fluorescence spectra for 30 kDa fraction of humic acid were shown in Figures 4.127 and 4.128. Initial 30 kDa fraction of humic acid has a peak around 450 nm with relatively high fluorescence intensity. Adsorption of 30 kDa fraction of humic acid onto Fe doped TiO_2 surface with increasing loadings, a gradual decrease in fluorescence intensity became evident in the emission scan fluorescence spectra.

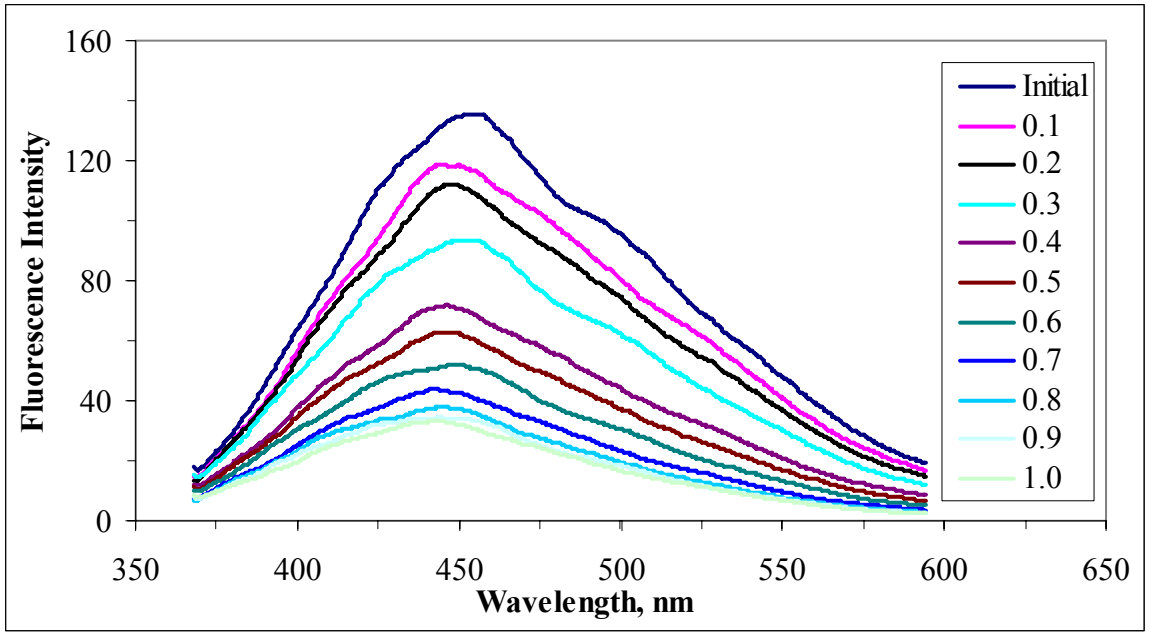

Figure 4.127. Emissions scan fluorescence spectra ($FI_{emis\ 350}$) of 30 kDa fraction of humic acid adsorption onto Fe doped TiO_2 (where initial represents raw humic acid) (legends indicate TiO_2 dosages).

Synchronous scan spectra of 30 kDa fraction of humic acid were shown by Figure 4.129. Synchronous scan fluorescence spectra for 30 kDa fraction of humic acid displayed sharp peaks around wavelength of 380 nm and 470 nm. After adsorption onto higher dosages of TiO_2, the characteristic sharp peaks of 30 kDa fraction of humic acid at 380 nm and 470 nm wavelengths completely disappeared. It was also observed that the trend of 0.9 mg mL^{-1} and 1.0 mg mL^{-1} TiO_2 doses was crossed to each other.

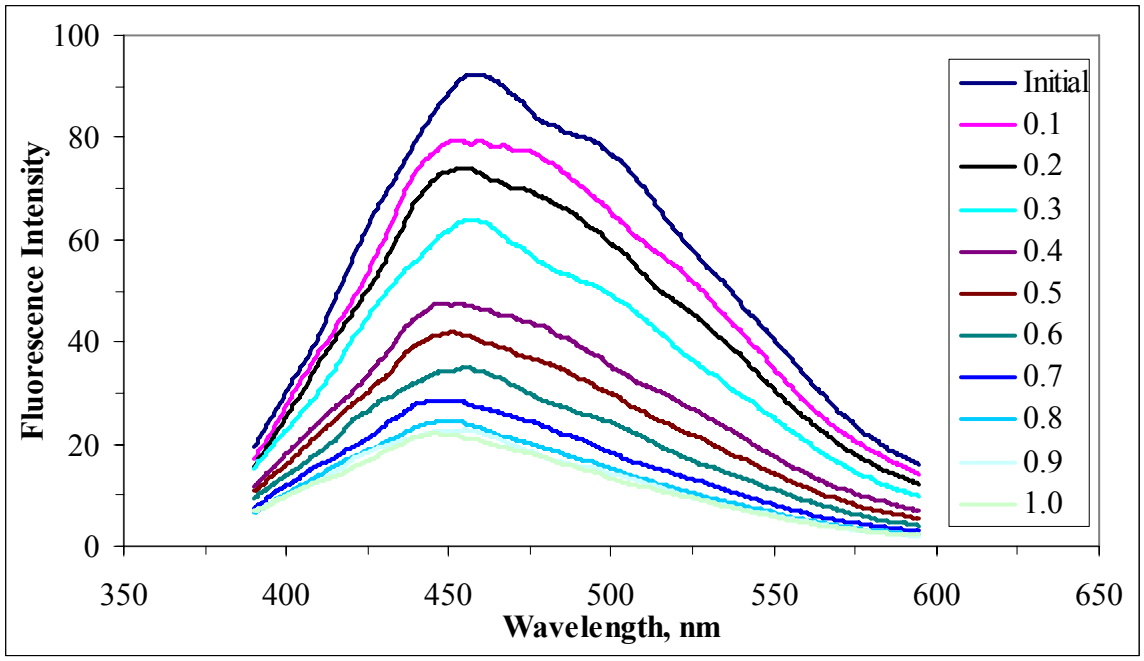

Figure 4.128. Emissions scan fluorescence spectra ($FI_{emis\ 370}$) of 30 kDa fraction of humic acid adsorption onto Fe doped TiO_2 (where initial represents raw humic acid) (legends indicate TiO_2 dosages.

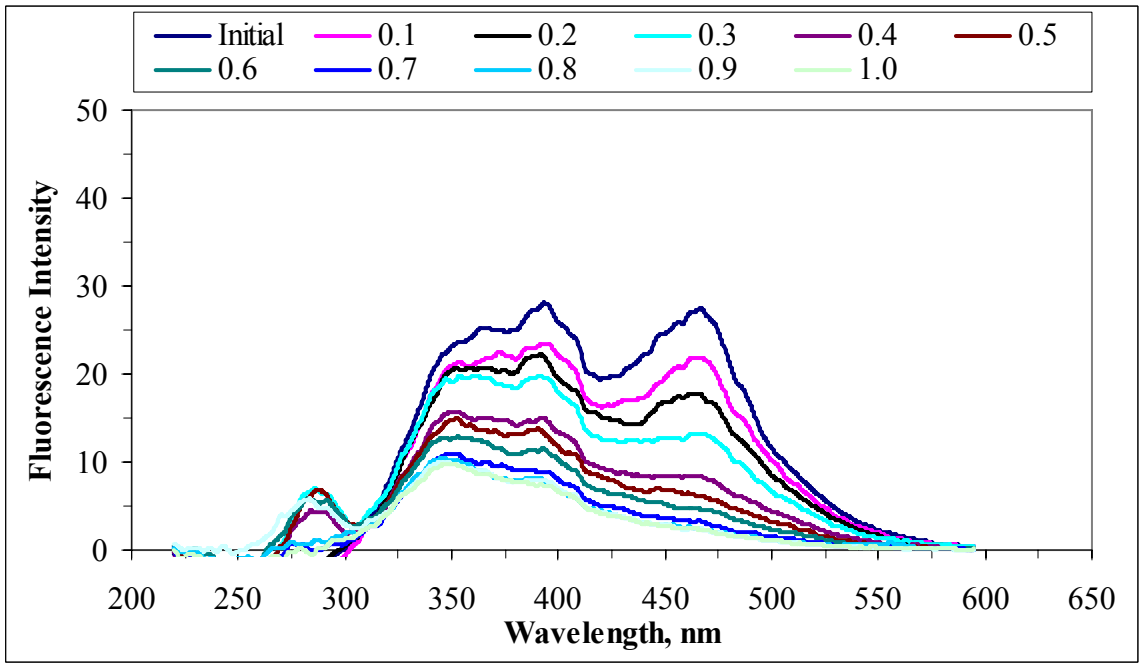

Figure 4.129. Synchronous scan fluorescence spectra of 30 kDa fraction of humic acid adsorption onto Fe doped TiO_2 (legends indicate TiO_2 dosages).

4.6.4.3. Adsorption Isotherm Modeling of 30kDa Fraction of Humic Acid onto Bare TiO_2 Binary System. In order to evaluate the experimental results attained for 30 kDa fraction of humic acid, the adsorption data were fitted to Freundlich and Langmuir adsorption isotherm models.

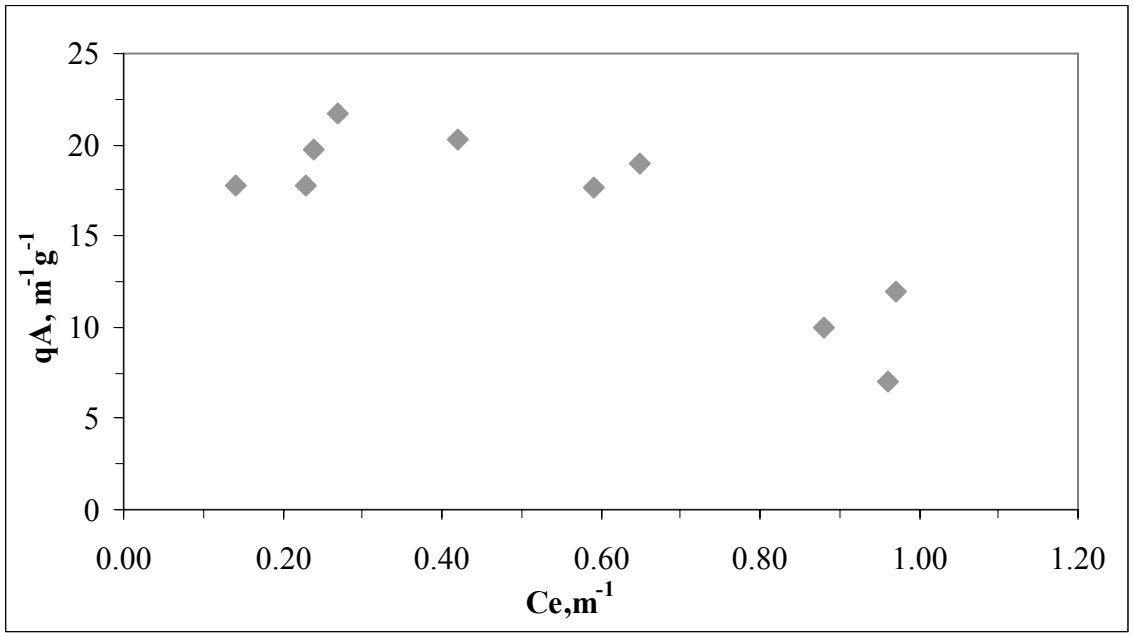

Figure 4.130. Freundlich adsorption isotherm of $Color_{436}$ of 30 kDa fraction of humic acid onto Fe doped TiO_2.

Figure 4.130 indicated that C_e values varied between 0.14-0.97 m^{-1} for $UV_{436.}$ The values of q_A calculated to be in the range of 7-21.7 $m^{-1}g^{-1}$ for the corresponding C_e values. As seen in Figure 4.131, C_e values varied between 1.15-8.49 m^{-1} for $UV_{254.}$ The values of q_A calculated to be in the range of 100-190.3 $m^{-1}g^{-1}$ for the corresponding C_e values. Langmuir adsorption isotherm of 30 kDa fraction of humic acid onto Fe doped TiO_2 was shown for $Color_{436}$ and UV_{254} in Figures 4.132 and 4.133. Langmuir adsorption model isotherms for UV_{365} and UV_{280} were presented in Appendix B.

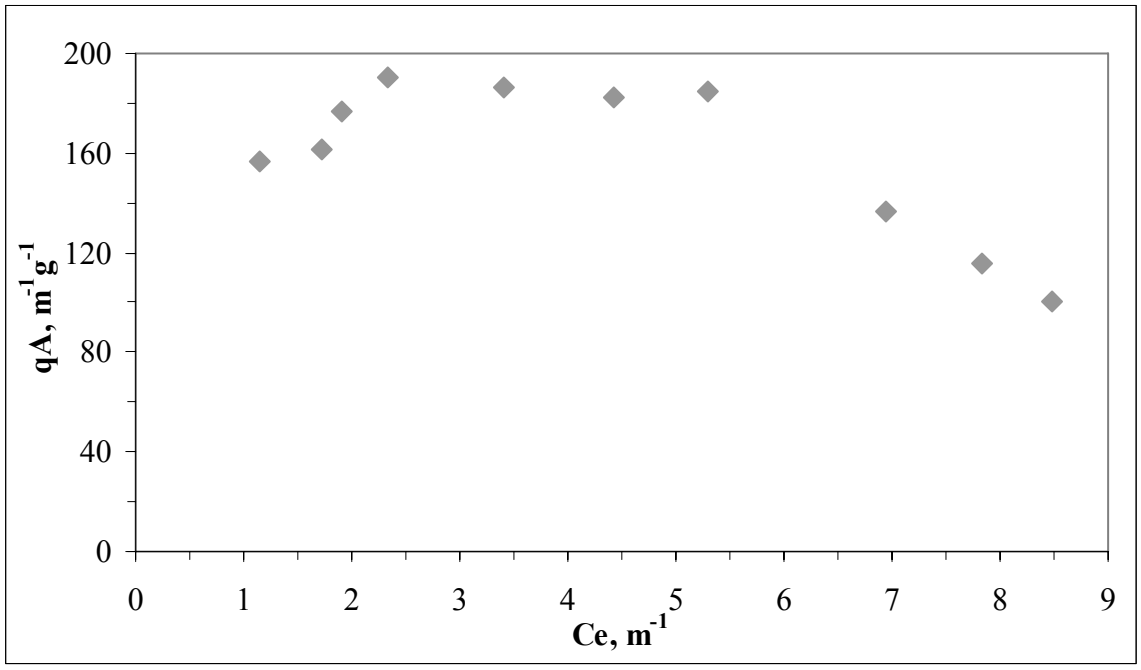

Figure 4.131. Freundlich adsorption isotherm of UV_{254} of 30 kDa fraction of humic acid onto Fe doped TiO_2.

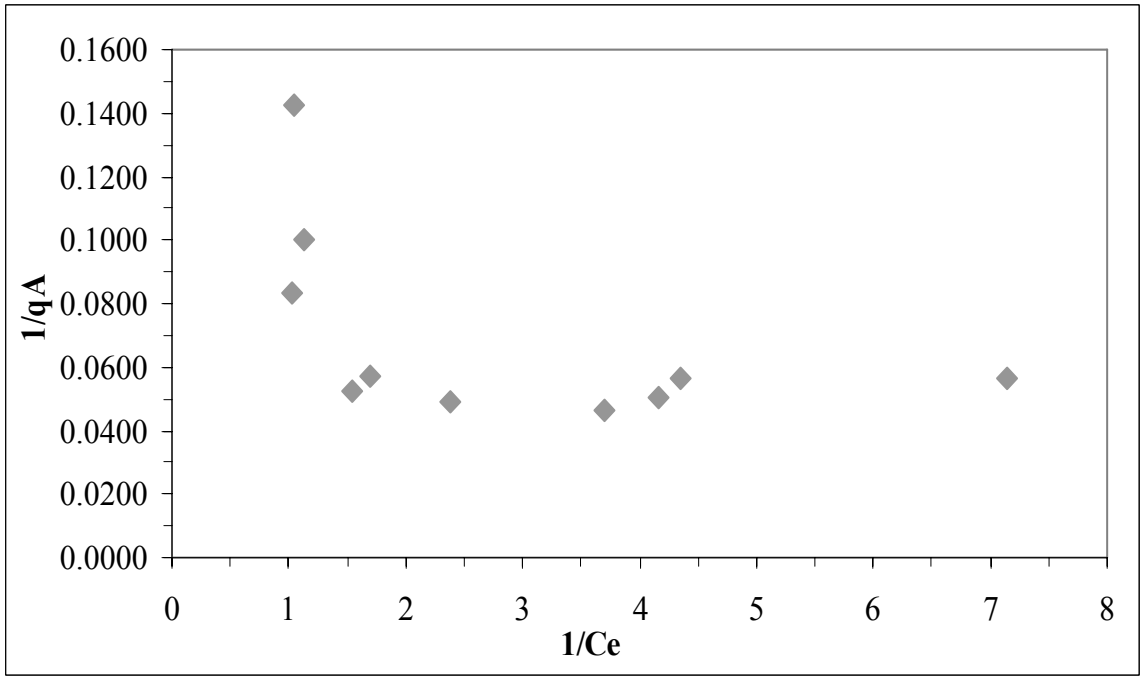

Figure 4.132. Langmuir adsorption isotherm of $Color_{436}$ of 30 kDa fraction of humic acid onto Fe doped TiO_2.

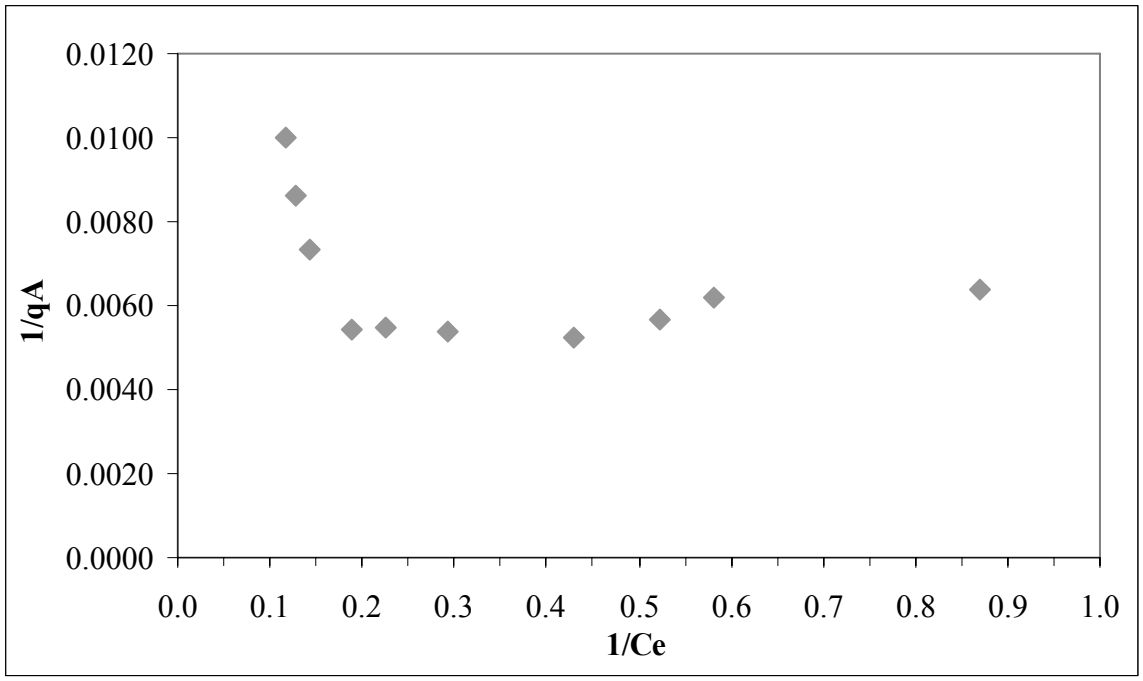

Figure 4.133. Langmuir adsorption isotherm of UV_{254} of 30 kDa fraction of humic acid onto Fe doped TiO_2.

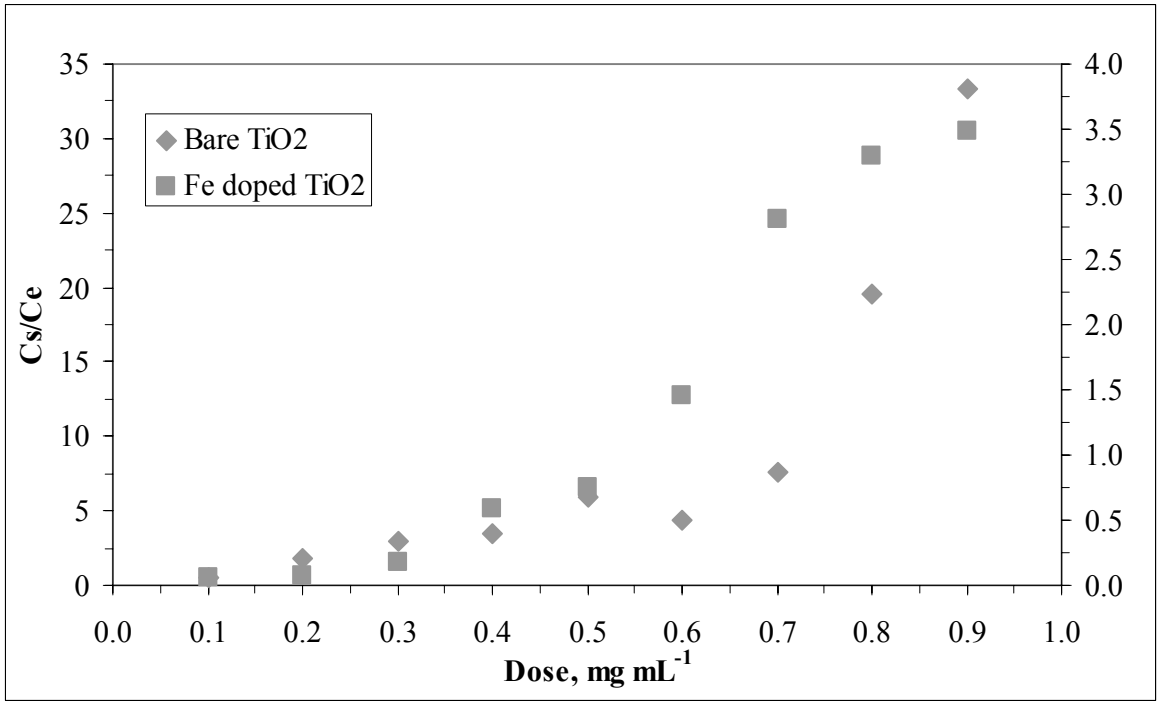

Figure 4.134. Distribution coefficient of $Color_{436}$ of 30 kDa fraction of humic acid onto bare and Fe doped TiO_2.

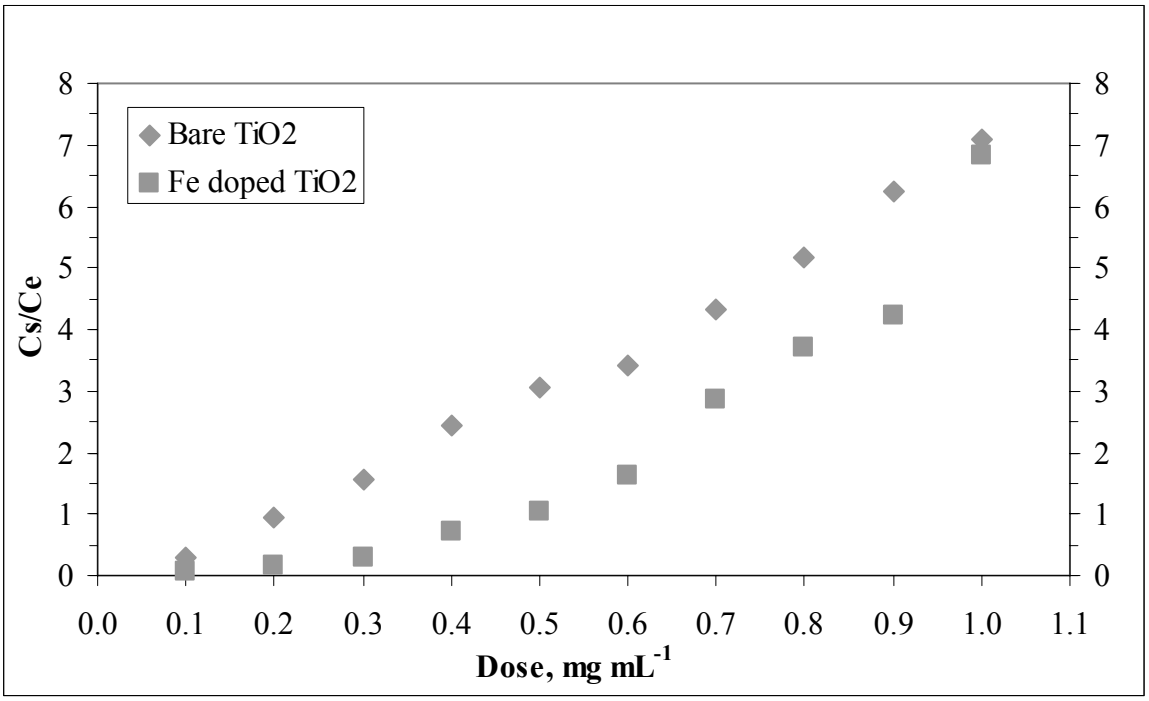

Figure 4.135. Distribution coefficient of UV_{254} of 30 kDa fraction of humic acid onto bare and Fe doped TiO_2.

Adsorption isotherm modeling of 30 kDa fraction of humic acid onto Fe doped TiO_2 binary system indicated that there was no exact adsorption profile depending on the TiO_2 amounts. The adsorption data for $Color_{436}$ and UV_{254} did not fit to Freundlich and Langmuir isotherm for 30 kDa fraction of humic acid. Hence, data were evaluated in terms of distribution coefficient.

Figure 4.134 indicated that C_s/C_e values varied between 0.56-33.33 for $Color_{436}$ depending on the amount of TiO_2 present in solution in the presence of bare TiO_2. However, while in the presence of Fe doped TiO_2, C_s/C_e varied between 0.062-3.478. As presented in Figure 4.135, C_s/C_e values varied between 0.301-7.10 and 0.059-6.817 for UV_{254} in the presence of bare TiO_2 and Fe doped TiO_2, respectively.

4.6.5. Adsorption of Humic Acid onto Bare TiO_2 and Fe doped TiO_2 with respect to NPOC

In order to investigate the adsorption properties of raw humic acid solution, batch adsorption experiments evaluated in terms of NPOC.

4.6.5.1. Adsorption of Raw Humic Acid onto Bare TiO_2 and Fe doped TiO_2 with respect to NPOC. Adsorption of humic acid with respect to NPOC was evaluated in the presence of bare and Fe doped TiO_2.

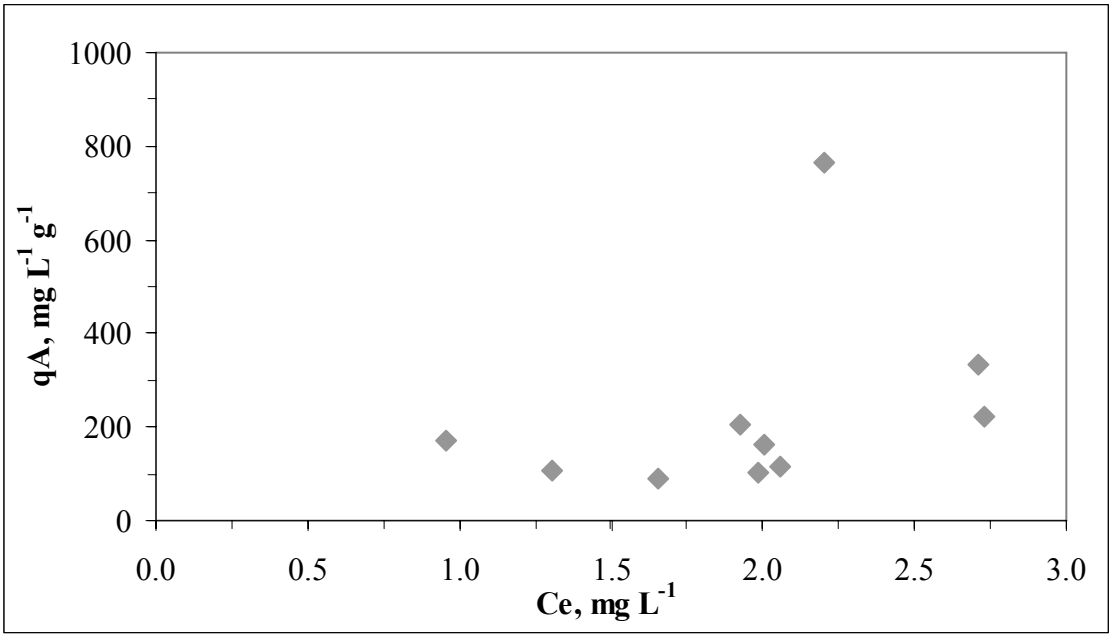

Figure 4.136. Adsorption of raw humic acid onto bare TiO_2 with respect to NPOC.

Figure 4.136 indicated that adsorption of raw humic acid onto bare TiO_2 with respect to NPOC. As could be seen in Figure 4.136, C_e values varied between 1.305-2.707 mg L^{-1}.The values of q_A calculated to be in the range of 87.7-766.8 mg L^{-1} g^{-1} for the corresponding C_e values. Adsorption of raw humic acid in the presence of Fe doped TiO_2, C_e values varied between 1.546-5.914 mg L^{-1}. The values of q_A calculated to be in the range of 25-127.2 mg L^{-1} g^{-1} for the corresponding C_e values (Figure 4.137).

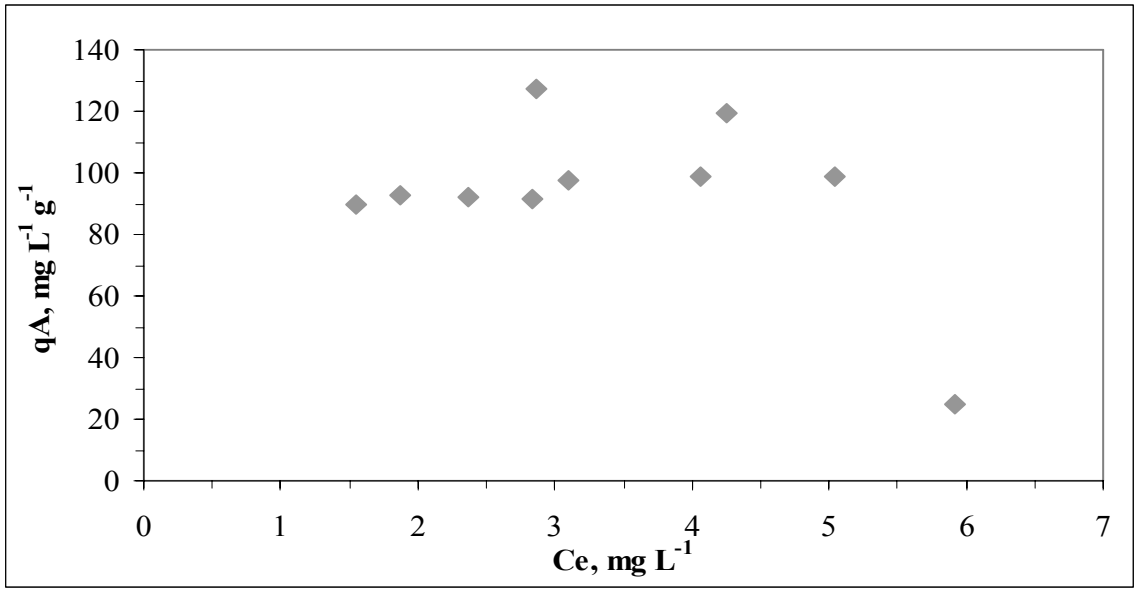

Figure 4.137. Adsorption of raw humic acid onto Fe doped TiO_2 with respect to NPOC.

4.6.5.2. Adsorption of 0.45 μm Filtered Fraction of Humic Acid onto Bare TiO_2 and Fe doped TiO2 with respect to NPOC. Adsorption of 0.45 μm filtered fraction of humic acid with respect to NPOC was evaluated in the presence of bare and Fe doped TiO_2.

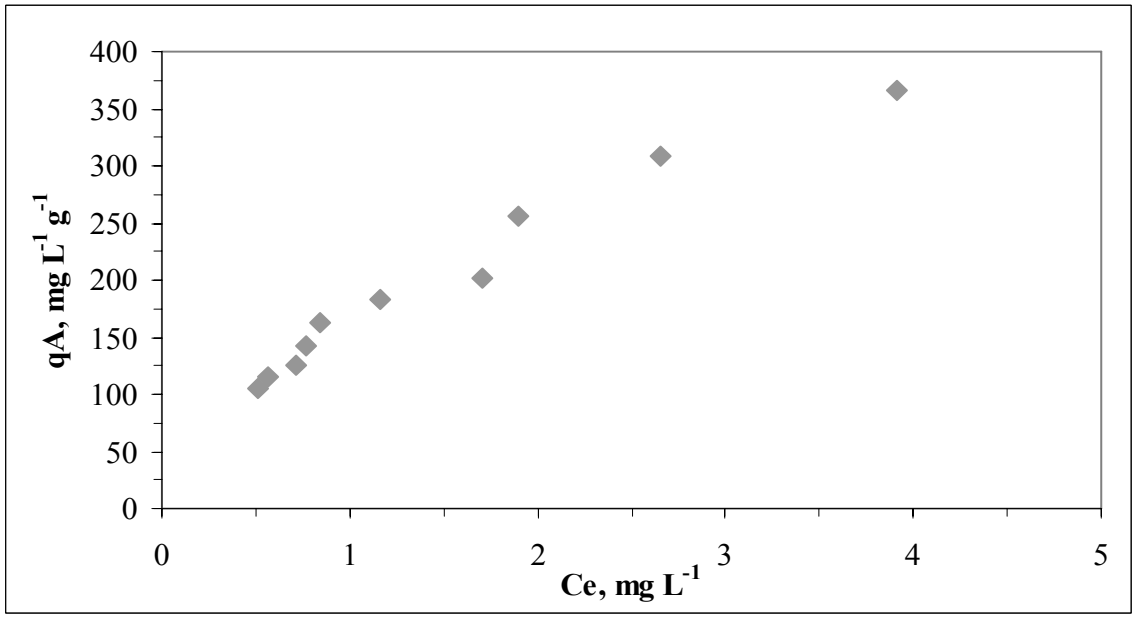

Figure 4.138. Adsorption of 0.45 μm filtered fraction of humic acid onto bare TiO_2 with respect to NPOC.

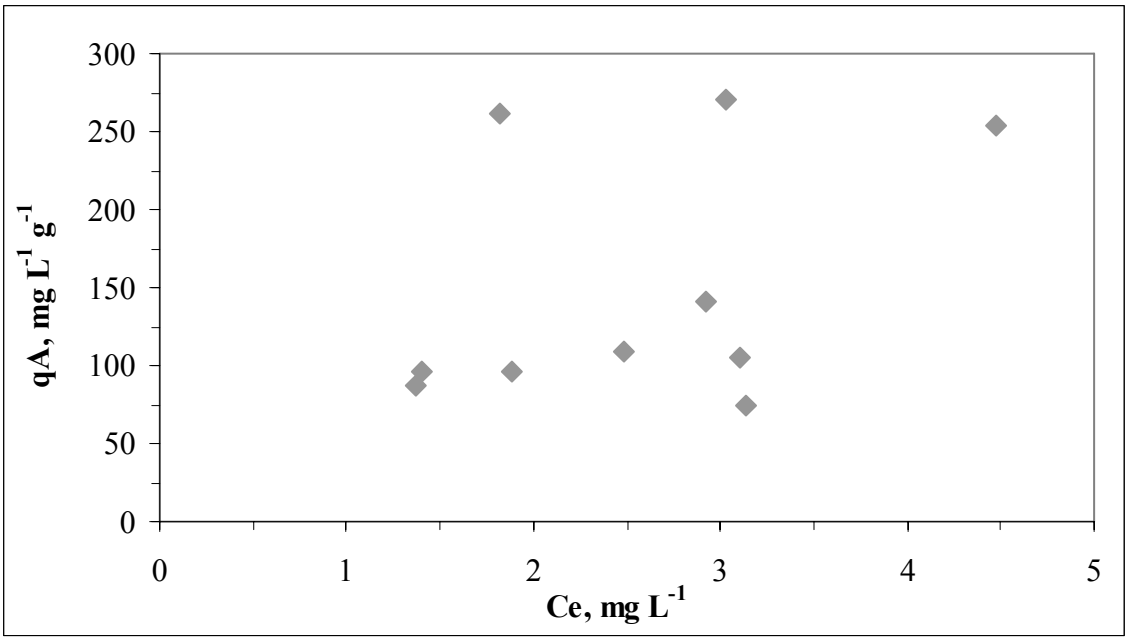

Figure 4.139. Adsorption of 0.45 μm filtered fraction of humic acid onto Fe doped TiO_2 with respect to NPOC.

As could be seen in Figure 4.138, C_e values varied between 0.517–3.911 mg L^{-1}. The values of q_A calculated to be in the range of 125.6–365.6 mg L^{-1} g^{-1} for the corresponding C_e values. In the presence of Fe doped TiO_2, C_e values varied between 1.371–4.472 mg L^{-1}. The values of q_A calculated to be in the range of 74.3–270.6 mg L^{-1} g^{-1} for the corresponding C_e values (Figure 4.139).

4.6.5.3. Adsorption of 100 kDa Fraction of Humic Acid onto Bare TiO_2 and Fe doped TiO2 with respect to NPOC. Adsorption of 100 kDa Fraction of Humic Acid with respect to NPOC was evaluated in the presence of bare and Fe doped TiO_2.

Figure 4.140 indicated that, C_e values varied between 0.391–2.349 mg L^{-1}. The values of q_A calculated to be in the range of 50.7–116.1 mg L^{-1} g^{-1} for the corresponding C_e values. Adsorption of 100 kDa fraction of humic acid in the presence of Fe doped TiO_2, C_e values varied between 1.069–2.651 mg L^{-1}. The values of q_A calculated to be in the range of 27.7–76.2 mg L^{-1} g^{-1} for the corresponding C_e values (Figure 4.141).

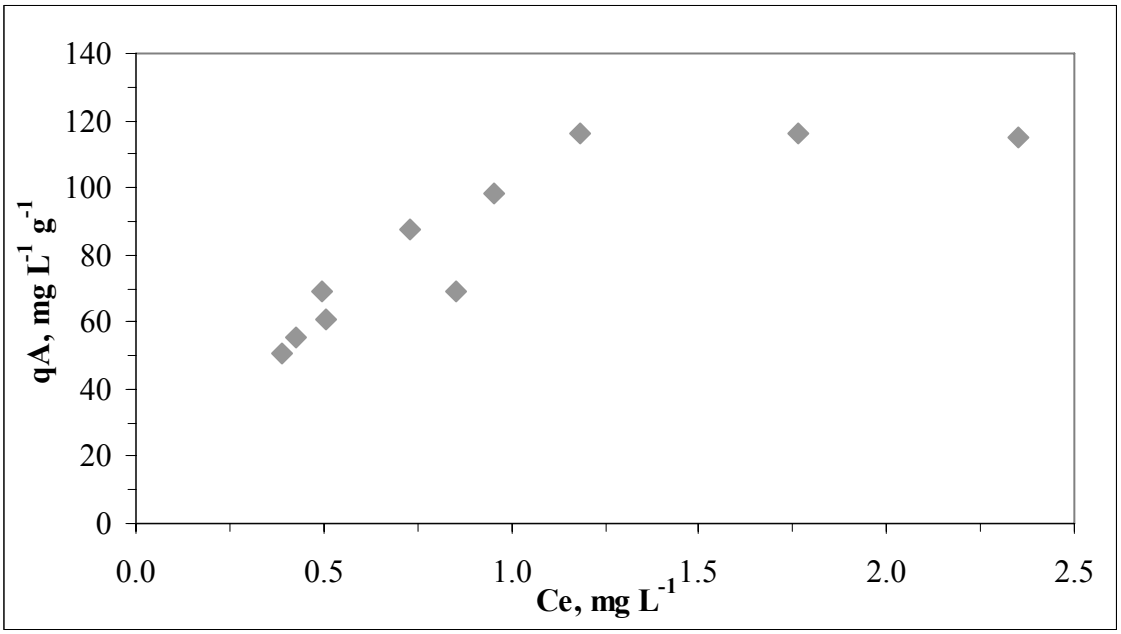

Figure 4.140. Adsorption of 100 kDa fraction of humic acid onto bare TiO_2 with respect to NPOC.

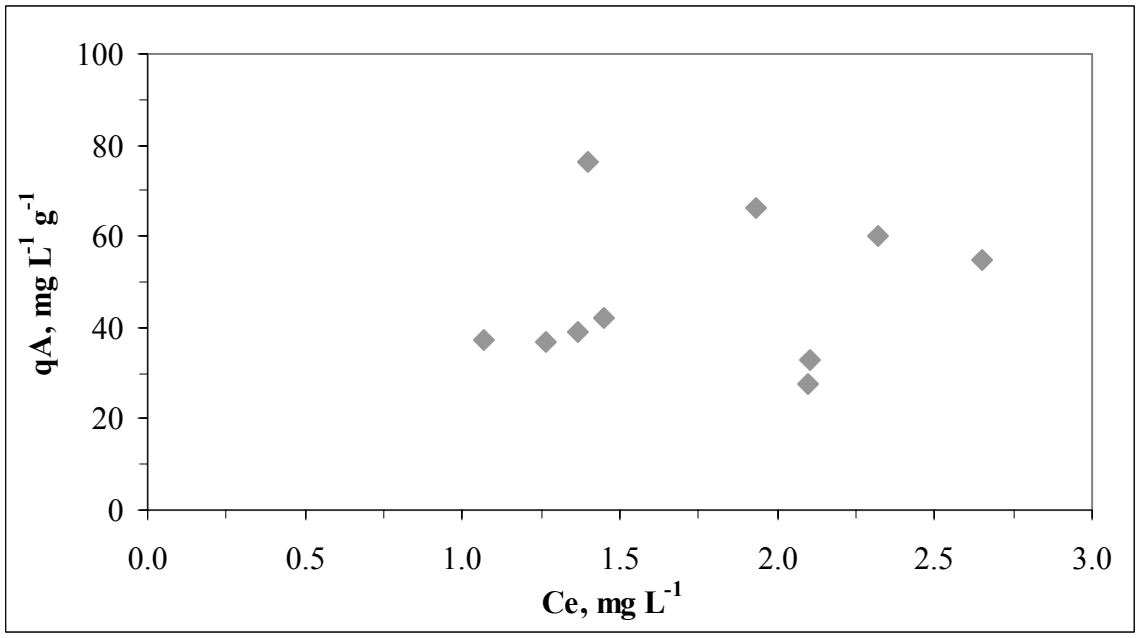

Figure 4.141. Adsorption of 100 kDa Fraction of Humic Acid onto Fe doped TiO_2 with respect to NPOC.

4.6.5.3. Adsorption of 30 kDa Fraction of Humic Acid onto Bare TiO_2 and Fe doped TiO_2 with respect to NPOC. Adsorption of 30 kDa Fraction of Humic Acid with respect to NPOC was evaluated in the presence of bare and Fe doped TiO_2.

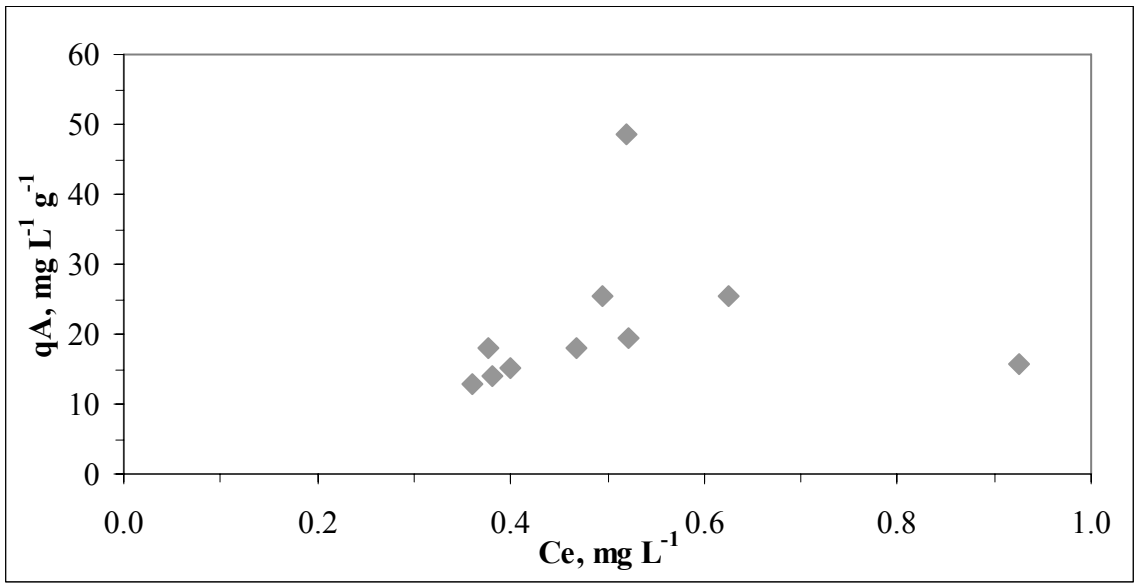

Figure 4.142. Adsorption of 30 kDa fraction of humic acid onto bare TiO_2 with respect to NPOC.

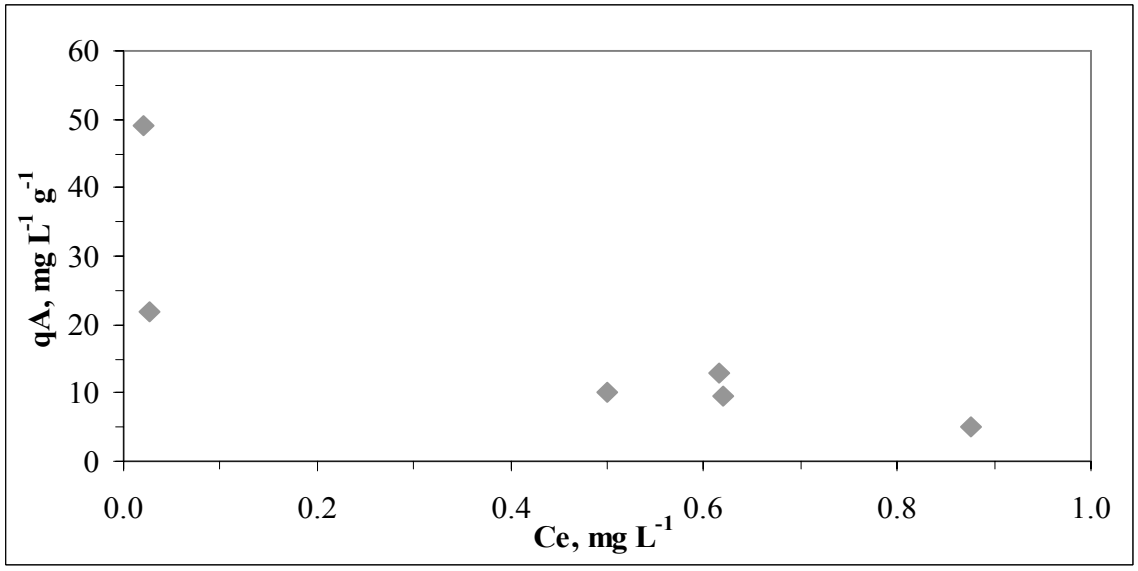

Figure 4.143. Adsorption of 30 kDa fraction of humic acid onto Fe doped TiO_2 with respect to NPOC.

Figure 4.142. indicated that adsorption of 30 kDa fraction of humic acid onto bare TiO_2 with respect to NPOC. As could be seen in Figure 4.142, C_e values varied between 0.359–0.926 mg L^{-1}.The values of q_A calculated to be in the range of 12.9–48.6mg L^{-1} g^{-1} for the corresponding C_e values. In the presence of Fe doped TiO_2, C_e values varied between 0.022–0.876 mg L^{-1}. The values of q_A calculated to be in the range of 5.1–49.2 mg L^{-1} g^{-1} for the corresponding C_e values (Figure 4.143).

5. CONCLUSIONS

The main objective of this research is to investigate the effect of Fe doping on TiO_2 on the photocatalytic degradation of humic acid and its molecular size fractions in aqueous medium in comparison to the use of bare TiO_2. Adsorption experiments were conducted to elucidate the surface interactions of the molecular size fractions of humic acid solutions onto oxide surfaces. The photocatalytic and adsorption experiments were carried out using various molecular size fractions, namely raw, 0.45 μm filtered fraction, 100 kDa filtered fraction, and 30 kDa filtered fraction of humic acid solution. The results of adsorption experiments were evaluated using appropriate adsorption isotherms. The spectroscopic properties of each size fraction were characterized and compared by UV-vis spectroscopy and fluorescence spectroscopy in emission and synchronous scan modes. UV–vis parameters were described in terms of the absorbance values measured at the selected wavelengths as follows: absorbance values at 436 nm as $Color_{436}$, 365 nm as UV_{365}, 280 nm as UV_{280} and 254 nm as UV_{254} and the emission scan fluorescence spectra was scanned in the range of 360-600 nm and 380-600 nm at excitation wavelength of 350 and 370 nm, respectively. Moreover, synchronous scan fluorescence spectra was recorded in the range of 200-600 nm excitation wavelength region.

Photocatalytic degradation data were processed using pseudo first order kinetic model. Photocatalytic degradation rates (R, m^{-1} min^{-1}) were attained in a decreasing order of $UV_{254} > UV_{280} > UV_{365} > Color_{436}$ for raw, 0.45 μm filtered fraction, 100 kDa fraction and 30 kDa fraction of humic acid in the presence of bare TiO_2. In the presence of Fe doped TiO_2, photocatalytic degradation rate orders were found to be same to degradations profile of humic acid in the presence of bare TiO_2.

For raw humic acid, the removal of color forming moieties was found to be faster (~ > 29%) than the UV absorbing centers as expressed by UV_{280} and UV_{254} in the presence of bare TiO_2. The presence of Fe doped TiO_2 altered the pseudo first order kinetic model rate constants of raw humic acid for all of the specified parameters and the removal of color

forming moieties was found to be relatively faster than the UV absorbing centers (> 15%) as expressed by UV_{280} and UV_{254}.

For 0.45 μm filtered fraction of humic acid, the removal of color forming moieties was observed faster (~ > 55%) than the UV absorbing centers. The pseudo first order kinetic parameters displayed higher removal efficiencies for 0.45 μm filtered fraction of humic acid than raw humic acid in the presence of bare TiO_2. The enhancement factor could be regarded as 1.6 fold for $Color_{436}$, 1.2 fold for UV_{365}, 1.1 fold for UV_{280}. Photocatalytic degradation rates (R, m^{-1} min^{-1}) were calculated by using the rate equation expressed by the decreasing order of $UV_{254} > UV_{280} > UV_{365} > Color_{436}$ in the presence of bare TiO_2. Same order attained in the presence of Fe doped TiO_2.

For 100 kDa fraction of humic acid, the removal of color forming moieties was found to be relatively faster (~ > 27%) than the UV absorbing centers. The pseudo first order kinetic parameters displayed considerably higher removal efficiencies for 100 kDa fraction of humic acid with respect to both 0.45 μm filtered fraction of humic acid and raw humic acid. The presence of Fe doped TiO_2 changed the photocatalytic degradation rates of 100 kDa fraction of humic acid with respect to 0.45 μm filtered fraction of humic acid and raw humic acid. Photocatalytic degradation rates (R, m^{-1} min^{-1}) were calculated by using the rate equation expressed by the decreasing order of $UV_{280} > UV_{254} > UV_{365} > Color_{436}$ both in the presence of bare TiO_2.

For 30 kDa fraction of humic acid, the pseudo first order kinetic parameters displayed considerably higher removal efficiencies for 30 kDa fraction of humic acid with respect to 100 kDa fraction of humic acid, 0.45 μm filtered fraction of humic acid and raw humic acid in the presence of bare TiO_2. The presence of Fe doped TiO_2 displayed a slight decrease in rate constant for 30 kDa fraction of humic acid respect to 100 kDa fraction of humic acid, 0.45 μm filtered fraction of humic acid and raw humic acid. Photocatalytic degradation rates (R, m^{-1} min^{-1}) were calculated by using the rate equation expressed by the decreasing order of $UV_{254} > UV_{280} > UV_{365} > Color_{436}$ in the presence Fe doped TiO_2.

The adsorption experiments were conducted with different molecular size fractions such as raw, 0.45 μm filtered fraction, 100 kDa fraction and 30 kDa fraction of Aldrich humic acid solution in the presence of bare TiO_2 and in the presence of Fe doped TiO_2. The adsorption data were fitted Freundlich and Langmuir adsorption models.

Freundlich adsorption model parameters showed some changes as;

In the presence of bare TiO_2, K_f values changed as raw > 0.45 μm filtered fraction > 100 kDa > 30 kDa for $Color_{436}$. Same order attained for UV_{254}. The overall evaluation of 1/n could be expressed by the range of 0.294 - 0.608. Adsorption intensity (1/n) values which were lower than 1, expressing the adsorption bond was strong and the capacity tended to be independent of C_e. In the presence of Fe doped TiO_2, Adsorption isotherm modeling of humic acid onto Fe doped TiO_2 binary system indicated that there was no exact adsorption profile depending on the TiO_2 amounts. The adsorption data for specific parameters did not fit to Freundlich isotherm. Hence, data were evaluated in terms of distribution coefficient.

Langmuir adsorption model parameters showed some changes as;

In the presence of bare TiO_2, the maximum quantity adsorbable when all adsorption sites were occupied, q_{max} values changed as raw > 0.45 μm filtered fraction > 100 kDa > 30 kDa for $Color_{436}$. q_{max} values changed as raw > 0.45 μm filtered fraction > 100 kDa > 30 kDa for UV_{254}. For binding constant, K, the order observed as 30 kDa > 0.45 μm filtered fraction > 100 kDa > raw for $Color_{436}$. K values changed as 100 kDa > 30 kDa > 0.45 μm filtered fraction = raw for UV_{254}. In the presence of Fe doped TiO_2, adsorption isotherm modeling of humic acid onto Fe doped TiO_2 binary system indicated that there was no exact adsorption profile depending on the TiO_2 amounts. The adsorption data for specific parameters did not fit to Langmuir isotherm. Hence, data were evaluated in terms of distribution coefficient.

REFERENCES

Aiken, G. R., McKnight, D. M., Wershaw, R. L., MacCarthy, P. (Eds.), 1985. Humic Substances in Soil, Sediment and Water, John Wiley and Sons, Inc., U.S.A.

Ambrus, Z., Balazs, N., Alapi, T., Wittmann, G., Sipos, P., Dombi, A., Mogyorosi, K., 2008. Synthesis, structure and photocatalytic properties of Fe(III) doped TiO_2 prepared from $TiCl_3$. Applied Catalysis B: Environmental, 81, 27–37.

Bekbolet, M., Balcioglu, I., 1996. Photocatalytic degradation kinetics of humic acid in aqueous TiO_2 dispersions: The influence of hydrogen peroxide and bicarbonate ion. Water Science and Technology, 34, 73–80.

Bekbolet, M., Cecen, F., Ozkosemen, G., 1996. Photocatalytic oxidation and subsequent adsorption characteristic of humic acids. Water Science and Technology, 34, 65-72.

Bekbolet, M., Ozkosemen, G., 1996. A preliminary investigation on the photocatalytic degradation of a model humic acid. Water Science and Technology, 33, 189-194.

Bekbolet, M., Suphandag, A. S., Uyguner, C. S., 2002. An investigation of the photocatalytic efficiencies of TiO_2 powders on the decolorisation of humic acids. Journal of Photochemistry and Photobiology A: Chemistry, 148, 121-128.

Bouras, P., Stathatos, E., Lianos, P., 2007. Pure versus metal-ion-doped nanocrystalline titania for photocatalysis. Applied Catalysis B: Environmental, 73, 51–59.

Braun**,** A.M., Oliveros, E., 1997. How to evaluate photochemical methods for water treatment. Water Science and Technology**,** 35, 17-23.

Buffle, J., 1988. Complexation Reactions in Aquatic Systems; Analytical Approach. Chichester, John Wiley and Sons, Inc, U.S.A.

Cabaniss, S. E., Shuman, M. S., 1988. Copper binding by dissolved organic matter: I. Suwannee river fulvic acid equilibria. Geochimica et Cosmochimica Acta, 52, 185–193.

Canela, M. C., Alberici, R. M., Sofia, R. C. R., Eberlin, M. N., Jardim, W. F., 1999. Destruction of malodorous compunds using heterogeneous photocatalysis. Environmental Science and Technology, 33, 2788-2792.

Carneiro, J. O., Teixeira, V., Portinha, A., Magalhaes, A., Coutinho, P., Tavares, C. J., Newton, R., 2007. Iron-doped photocatalytic TiO_2 sputtered coatings on plastics for self-cleaning applications. Materials Science and Engineering B, 138, 144–150.

Carp, O., Huisman, C. L., Reller, A., 2004. Photoinduced reactivity of titanium dioxide. Solid State Chemistry, 32, 33–177.

Chen, J., Gu, B., LeBoeuf, P. H., Dai, S., 2002. Spectroscopic characterization of the structural and functional properties of natural organic matter fractions. Chemosphere, 48, 59-68.

Chin, Y. P., Aiken, G., O'Loughlin, E., 1994. Molecular weight, polydispersity and spectroscopic properties of aquatic humic substances. Environmental Science and Technology, 28, 1853-1858.

Chin, Y. P., Traina, S. J., Swank, C. R., Backhus, D., 1998. Abundance and properties of dissolved organic matter in pore waters of a fresh water wetland. Limnology and Oceanography, 43, 1287-1296.

Cho, Y., and Choi, W., 2002. Visible light-induced reactions of humic acids on TiO_2. Journal of Photochemistry and Photobiology A: Chemistry, 148, 129-135.

Choi , W., Temrin, A., Hoffmann, M. R.,1994. The role of metal ion dopants in quantum-sized TiO_2: Correlation between photoreactivity and charge carrier recombination dynamics. Journal of Physical Chemistry, 98, 13669–13679.

Choudhry, G.G., 1981. Humic substances: Photophysical, photochemical and free radical characteristics. Environmental Chemistry, 4, 261-295.

Chun, H., Yizhong, W., Hongxiao, T., 2000. Destruction of phenol aqueous solution by photocatalysis or direct photolysis. Chemosphere, 41, 1205-1209.

Cong, Y., Zhang, J., Chen, F., Anpo, M., He, D., 2007. Preparation, photocatalytic activity, and mechanism of nano-TiO_2 co-doped with nitrogen and iron (III). Journal of Physical Chemistry C, 111, 10618-10623.

Daßler, A., Feltz, A., Jung, J., Ludwig, W., Kaiserberger, E., 1988. Characterization of rutile and anatase powders by thermal analysis. Journal of Thermal Analysis and Calorimetry, 33, 803-809.

Davis, R. J., Gainer, J. L., O'Neal, G., Wu, I.W., 1994. Photocatalytic decolorization of wastewater dyes. Water Environmental Research, 66, 50-53.

Davis, W. M., Eriekson, C. L., Johnston, C. T., Delfino, J. J., Porter, J. E., 1999. Quantitative Fourier transform infrared spectroscopic investigation of humic substance functional group composition. Chemosphere, 38, 2913–2928.

Değirmenci E., 2010., Assesment of Molecular Size Distribution Effects on the Nonselective Oxidation of Trace Metal Humic Acid Binary System., M. S. Thesis, Bogazici University.

D'Orazio, V., Loffredo, E., Brunetti, G., Senesi, N., 1999. Trillate adsorption onto humic acids of different origin and nature. Chemosphere, 39, 183-198.

Fettig. J.,1999. Removal of humic substances by adsorption/ion exchange. Water Science and Technology, 40, 173 -182.

Gaffney J. S., Marley N.A., Clark S. B. (Eds.). 1996. Humic and fulvic acids: Isolation, Structure, and Environmental Role, ACS Symposium Series, USA.

Gaya, U. M., Abdullah, A. H., 2008. Heterogeneous photocatalytic degradation of organic contaminants over titanium dioxide: A review of fundamentals, progress and problems. Journal of Photochemistry and Photobiology C: Photochemistry Reviews, 9, 1–12.

Giles, C. H., MacEwan, T. H., Nakhwa, S. N., Smith, D., 1960. Studies in adsorption. A system classification of solution adsorption isotherms and its use in diagnosis of adsorption and in measurement of specific surface areas of solids. Journal of Chemical Society, 3973-3993.

Goslan, E. H., Voros, S., Banks, J., Wilson, D., Hillisd, P., Campbell, A.T., Parsons, S.A., 2004. A model for predicting dissolved organic carbon distribution in a reservoir water using fluorescence spectroscopy. Water Research, 38, 783–791.

Graham, N .J .D., 1999. Removal of humic substances by oxidation/biofiltration processes -A review. Water Science and Technology, 40, 141-148.

Greenwood, N. N., Earnshaw, A., 1997. Chemistry of the Elements, Second Edition, Butterworth-Heinemann, Oxford.

Gu, B., Schmitt, J., Chen, Z., Liang, L., McCarthy, J. F., 1995. Adsorption and desorption of different organic matter fractions on iron oxide. Geochimica et Cosmochimica Acta, 59, 219-229.

Hamerski, M., Grzechulska, J., Morawski, A. W., 1999. Photocatalytic purification of soil contaminated with oil using modified TiO_2 powders. Solar Energy, 66, 395–399.

Haque, M. M., Muneer, M., 2007. Photodegradation of norfloxacin in aqueous suspensions of titanium dioxide. Journal of Hazardous Materials, 145, 51-57.

Hautala, K., Peuravuori, J., Pihlaja, K., 2000. Measurement of aquatic humus content by spectroscopic analyses. Water Research , 34, 246–258.

Heijman, S. G. J., Van Paassen, A. M., Van der Meer, W. G. J., Hopman, R., 1999. Adsorptive removal of natural organic matter during drinking water treatment. Water Science and Technology, 40, 183-190.

Hesse, S., Kleiser, G., Frimmel, F. H., 1999. Characterization of refractory organic substances (ROS) in water treatment. Water Science and Technology, 40, 1-7.

Hoffmann, M. R., Martin, S. T., Choi, W., Bahnemann, D., 1995. Environmental applications of semiconductor photocatalysis. Chemical Reviews, 95, 69-96.

Huck, P. M., 1999. Development of a framework for quantifying the removal of humic substances by biological filtration. Water Science and Technology, 40, 149-156.

Khan, E., Babcock, R. W., Viriyavejakul, S., Suffet, I. H., Stenstorm, M. K., 1998. Biodegradable dissolved organic carbon for indication wastewater reclamation plant performance and treated wastewater quality. Water Environmental Research, 70, 1033–1040.

Kim, B. R., Podsiadlik, D. H., Kalis, E. M., Hartlund J. L and Gaines, W. A., 1998, Photochemical destruction of cyanide in landfill leachate. Journal of Environmental Engineering, 124, 1108-1112.

Kim, H. C., Yu M. J., 2005. Characterization of natural organic matter in conventional water treatment processes for selection of treatment processes focused on DBPs control. Water Research, 39, 4779–4789.

Kopal, L. K., Riemsdijk, V. H., Kinniburgi, D. G., 2001. Humic matter and contaminants. General aspects and modeling metal ion binding. Pure and Applied Chemistry, 12, 2005–2016.

Litter, M. I., Navio, J. A., 1996. Photocatalytic properties of iron-doped titania semiconductors. Journal of Photochemistry and Photobiology A: Chemistry, 3, 171-181.

Liu, S., Chen, Y., 2009. Enhanced photocatalytic activity of TiO_2 powders doped by Fe unevenly. Catalysis Communications, 10, 894–899.

Ma, H., Allen, H. E., Yin, Y., 2001. Characterization of isolated fractions of dissolved organic matter from natural waters and a wastewater effluent. Water Research, 35, 985–996.

Malato, S., Blanco, J. A., Vidal, A., Diego, A. O., Maldonado, M. I., Aceres, J. C., Gernjak, W., 2003. Applied studies in solar photocatalytic detoxification: An Overview. Solar Energy, 75, 329-336.

Matilainen, A., Gjessing, E. T. , Lahtinen ,T., Hed, L., Bhatnagar, A., Sillanpää, M., 2011. An overview of the methods used in the characterization of natural organic matter (NOM) in relation to drinking water treatment. Chemosphere, 83, 1431-1442.

Maurice, P. A., Pullin, M. J., Cabaniss, S. E., Zhou, Q., Namjesnik-Dejanovic, K., Aiken, G. R., 2002. A comparison of surface water natural organic matter in raw filtered water samples, XAD, and reverse osmosis isolates. Water Research, 36, 2357–2371.

Muneer, M., Bahnemann, D., 2002. Semiconductor-mediated photocatalysed degradation of two selected pesticide derivatives, Terbacil and 2,4,5-Tribromoimidazole, in aqueous suspension. Applied Catalysis B: Environmental, 36, 95-111.

Nadeem, M., Mahmood, A., Shahid, S. A., Shah, S S.,. Khalid, A. M., McKay, G., 2006. Sorption of lead from aqueous solution by chemically modified carbon adsorbents, Journal of Hazardous Materials, 138, 604–613.

Ohlenbusch, G., Hesse, S., Frimmel, F.H.,1998. Effects of ozone treatment on the soil organic matter on contaminated sites. Chemosphere, 37, 1557-1569.

Ollis, D.F., Pelizzetti, E., Serpone, N., 1991. Destruction of water contaminants. Environmental Science and Technology, 25, 1523-1529.

O'Melia, C. R., Becker W. C., Au, K. K., 1999. Removal of humic substances by coagulation. Water Science and Technology, 40, 47 - 54.

Ødegaard, H., Eikebrokk, B., Storhaug, R., 1999. Processes for the removal of humic substances from water – an overview based on Norwegian experiences. Water.Science and Technology, 40, 37-46.

Palmer, F. L., Eggins, B. R., Coleman, M. H., 2002. The effect of operational parameters on the photocatalytic degradation of humic acid. Journal of Photochemistry and Photobiology A: Chemistry, 148, 137–143.

Peuravuori, J., Koivikko, R., Pihlaja, K., 2002. Characterization, differentiation and classification of aquatic humic matter separated with different sorbents: Synchronous scanning fluorescence spectroscopy. Water Research, 36, 4552-4562.

Rajeshwar, K., 1995. Photoelectrochemistry and environment. Journal of Applied Electrochemitry, 25, 1067-1082.

Rajeshwar, K., Chenthamarakshan, C. R., Goeringer, S., Djukic, M., 2001. Titania-based heterogeneous photocatalysis. Materials, mechanistic issues, and implications for environmental remediation. Pure and Applied Chemistry, 73, 1849-1860.

Rakhshandeh, P. D., Heterogeneous Photocatalytic Activity of Transition-Metal Cation Impregnated TiO_2, M.S. Thesis, Boğaziçi University, 1993.

Rivero, C., Senesi, N., Paolini, J., D'Orazio, V., 1998. Characteristics of humic acids of some Venezuelan soils. Geoderma, 81, 227-239.

Sawyer, C. N., McCarty, P. L., Parkin, G. F.,2003. Chemistry for Environmental Engineering and Science, McGraw-Hill, U.S.A.

Schnitzer, M., Khan, S. U., 1972. Humic Substances in the Environment, Marcel Dekker Inc, New York.

Schulten, H. R., Plage, B., Schnitzer, M., 1993. A chemical structure for humic substances. Naturwissenschaften, 78, 311–312.

Selcuk, H., Bekbolet, M., 2008. Photocatalytic and photoelectrocatalytic humic acid removal and selectivity of TiO_2 coated photoanode. Chemosphere, 73, 854-858.

Senesi, N., 1990. Molecular and quantitative aspects of the chemistry of fulvic acid and its interactions with metal ions and organic chemicals Part II: The fluorescence spectroscopy approach. Analytica Chimica Acta, 232, 77-106.

Senesi, N., 1993. Inorganic substances in soil and water: natural constituents and their influences on contaminant behavior; Beck, A. J., Jones, K. C., Hayes, M. H. B., Mingelgrin, U., Eds.; The Royal Society of Chemistry: Cambridge, pp 74-77.

Serpone, N., 1995. Brief introductory remarks on heterogeneous photocatalysis. Solar Energy Materials Solar Cells, 38, 369-379

Serpone, N., 1997. Relative photonic efficiencies and quantum yields in heterogeneous photocatalysis. Journal of Photochemistry and Photobiolology A, 104, 1-12.

Siddiqui, M. S., Amy, G. L., Murphy, B. D., 1997. Ozone enhanced removal of natural organic matter from drinking water sources, Water Research, 31, 3098-3106.

Shiga, A., Tsujiko, A., Yae, S., Nakato, Y., 1998. High photocurrent quantum yields at short wavelengths for nanocrystalline anatase-type TiO_2 film electrodes compared with those for rutile type. Bulletin of the Chemical Society of Japan, 71, 2119.

So, W. W., Park S. B., Kim K. J., Shin C. H. and Moon S. J., 2001. The crystalline phase stability of titania particles prepared at room temperature by the sol-gel method. Journal of Materials Science, 36, 4299-4305.

Sposito, G., 1989. The Chemistry of Soils, Oxford University Press, New York.

Stevenson, F. J., 1982. Humus Chemistry: Genesis, Composition, Reactions, Wiley and Sons, New York.

Stevenson, F. J., 1994. Humus Chemistry: Genesis, Composition, Reactions, Second Edition, John Wiley and Sons, New York.

Stir, M., Traykova, T., Nicula, R., Burkel, E., Baehtz, C., Knapp, M., Lathe, C., 2003. In situ high-pressure and high-temperature diffraction experiments on pure and Ag-doped TiO_2 nanopowders. Nuclear Instruments and Methods in Physics B, 199, 59-63.

Suffet, I. H., MacCarthy, P., 1989. Aquatic Humic Substances: Influence on Fate and Treatment of Pollutants, Advances in Chemistry Series 219, American Chemical Society, Washington DC.

Suphandag, S. A., 1998. Adsorption Capacity of Natural Organic Matter on Semiconductor Powders, M. S. Thesis, Bogazici University.

Suphandag, S. A., 2006. Evaluation of Natural Organic Matter-Metal Oxide Adsorption Isotherms Under Influential Structural Concepts, Ph.D. Thesis, Bogazici University.

Suri, R. P. S., Liu, J., Hand, D. W., Crittenden, J. C., Perram, D. L., Mullins, M. E., 1993. Heterogeneous photocatalytic oxidation of hazardous organic contaminants in water. Water Environmental Research, 65, 665-673.

Thakur, R. S., Chaudhary R., Singh, C., 2010. Fundamentals and applications of the Photocatalytic treatment for the removal of industrial organic pollutants and effects of operational parameters: A review. Journal of Renewable and Sustainable Energy 2, 042701.

Thomsen, M., Lassen, P., Dobel, S., Hansen, P. E., Carlsen, L., Mogensen, B.B., 2002. Characterisation of humic materials of different origin: a multivariate approach for quantifying the latent properties of dissolved organic matter. Chemosphere, 49, 1327–1337.

Thurman, E. M., Wershaw, R. L., . Malcolm, R. L., Pinckney, D. J., 1982. Molecular size of aquatic humic substances. Geochemistry, 4, 27–35.

Tong, T., Zhang, J., Tian, B., Chen, F., He, D., 2008. Preparation of Fe^{3+} doped TiO_2 catalysts by controlled hydrolysis of titanium alkoxide and study on their photocatalytic activity for methyl orange degradation. Journal of Hazardous Materials, 155, 572–579.

Traina, S. J., Novak, J. and Smeck, N. E., 1990. An ultraviolet absorbance method of estimating the percent aromatic carbon content of humic acids, Journal of Environmental Quality, 19, 151-153.

Uyguner, C. S., Bekbolet, M., 2004b. Evaluation of humic acid, chromium (VI) and TiO_2 ternary system in relation to adsorptive interactions. Applied Catalysis B, Environmental, 49, 267-275.

Uyguner, C. S., 2005. Elucidation of the photocatalytic Removal Pathways of Humic Substances: Progress Towards Mechanistic Explanations, Ph.D. Thesis, Bogazici University.

Uyguner, C. S., Bekbolet, M., 2005a. Evaluation of humic acid photocatalytic degradation by UV–vis and fluorescence spectroscopy. Catalysis Today, 101, 267–274.

Uyguner, C. S., Bekbolet, M., 2005b. A comparative study on the photocatalytic degradation of humic substances of various origins. Desalination, 176, 167-176.

Uyguner, C. S., Bekbolet, M., 2007. Contribution of metal species to the heterogeneous photocatalytic degradation of natural organic matter. International Journal of Photoenergy. Article ID 23156, 8 pages.

Uyguner, C. S., Suphandag, S. A., Kerc, A., Bekbolet, M., 2007. Evaluation of adsorption and coagulation characteristics of humic acids preceded by alternative advanced oxidation techniques. Desalination, 210, 183-193.

Uyguner, C. S., Bekbolet, M., 2010. TiO_2-assisted photocatalytic degradation of humic acids: effect of copper ions. Water Science and Technology, 2581-2590.

Ulker, Y., 2008. Effect of Fractionation on the Sorption Properties of NOM onto Modified TiO_2 Surface, M. S. Thesis, Bogazici University.

Wang, Y., 2000. Solar photocatalytic degradation of eight commercial dyes in TiO_2 suspension. Water Research, 34, 990-994.

Wang, G. S., Hsieh S. T., Hong C. S., 2000. Destruction of humic acid in water by UV light-catalyzed oxidation with hydrogen peroxide. Water Research, 34, 3882–3887.

Wei, Z., Xi, B., Zhao Y., Wang, S., Liu, H., Jiang, Y., 2007. Effect of inoculating microbes in municipal solid waste composting on characteristics of humic acid Life Science College, Northeast Agriculture University, Harbin 150030, China.

Yalçın,Y., Kılıç, M., Çınar Z., 2010. Fe^{3+} doped TiO2: A combined experimental and computational approach to the evaluation of visible light activity. Applied Catalysis B: Environmental, 99, 469–477.

Yamashita, H., Harada, M., Misaka, J., Takeuchi, M., Neppolian, B., M, Anpo., 2003. Photocatalytic degradation of organic compounds diluted in water using visible light-responsive metal ion-implanted TiO_2 catalysts: Fe ion implanted TiO_2. Catalysis Today, 84, 191–196.

Zhang, X., Zhou, M., Lei, L., 2006. Co-deposition of photocatalytic Fe doped TiO_2 coatings by MOCVD. Catalysis Communications, 7, 427–431.

Zhang, Z., Maggard, P.A., 2007. Investigation of photocatalytically-active hydrated forms of amorphous titania. Journal of Photochemistry and Photobiolology A, 186, 8–13.

Zhu, J., Zheng, W., He, B., Zhang, J., Anpo, M., 2004. Characterization of Fe TiO_2 photocatalysts synthesized by hydrothermal method and their photocatalytic reactivity for photodegradation of XRG dye diluted in water. Journal of Molecular Catalysis A: Chemical, 216, 35–43.

Zhu, J.F., Chen, F., Zhang, J.L., Chen, H.J., Anpo, M., 2006. Fe^{3+} TiO2 photocatalysts prepared by combining sol-gel method with hydrothermal treatment and their characterization. Journal of Photochemistry and Photobiology A: Chemistry, 180, 196-204.

APPENDIX A

Freundlich Adsorption Isotherms of Humic Acids

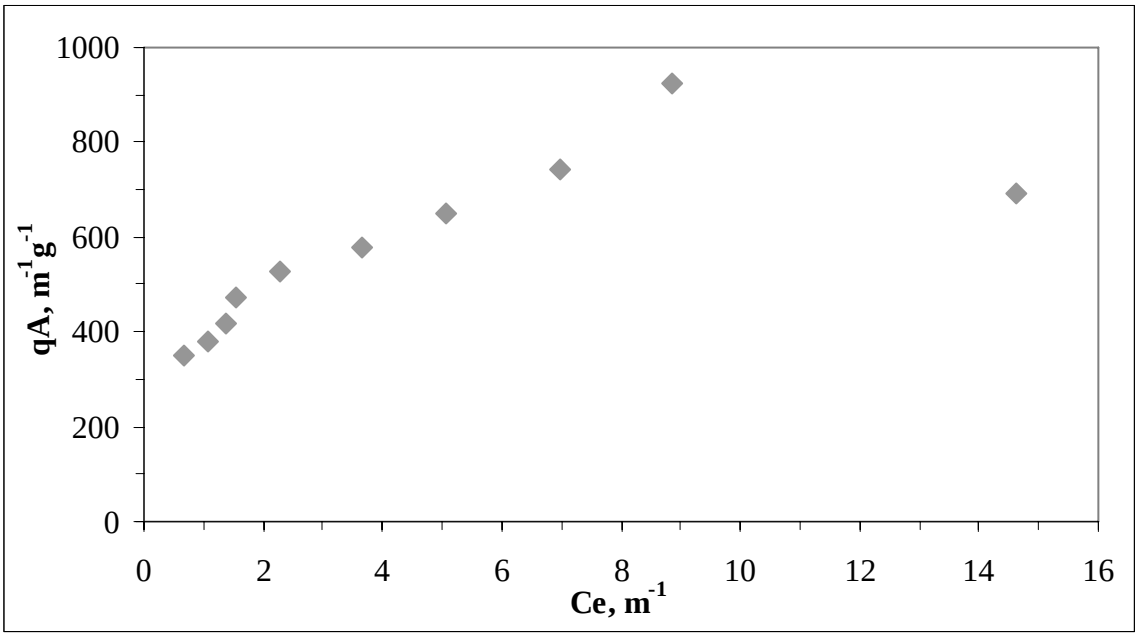

Figure A.1. Freundlich adsorption isotherm of UV_{365} of raw humic acid onto bare TiO_2

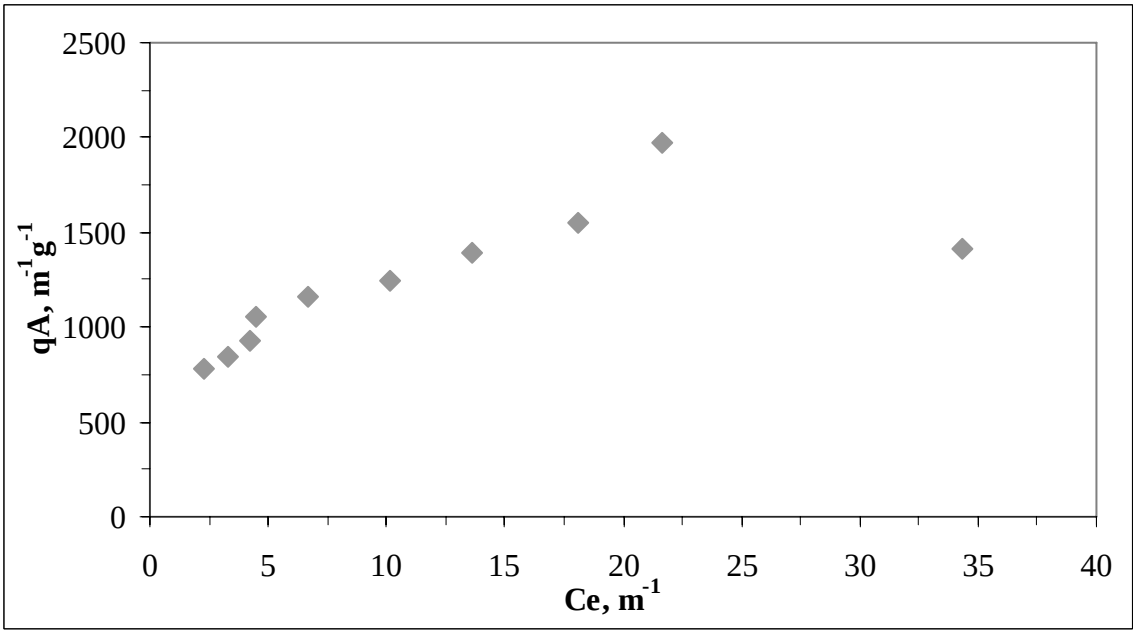

Figure A.2. Freundlich adsorption isotherm of UV_{280} of raw humic acid onto bare TiO_2

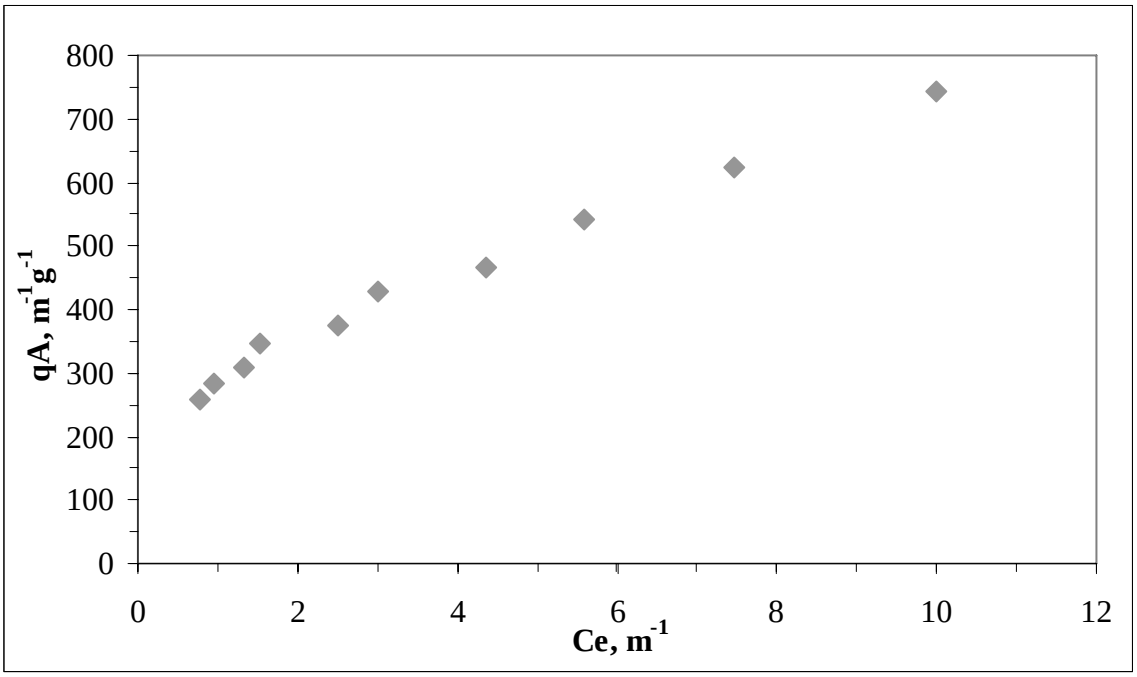

Figure A.3. Freundlich adsorption isotherm of UV_{365} of 0.45µm filtered fraction of humic acid onto bare TiO_2

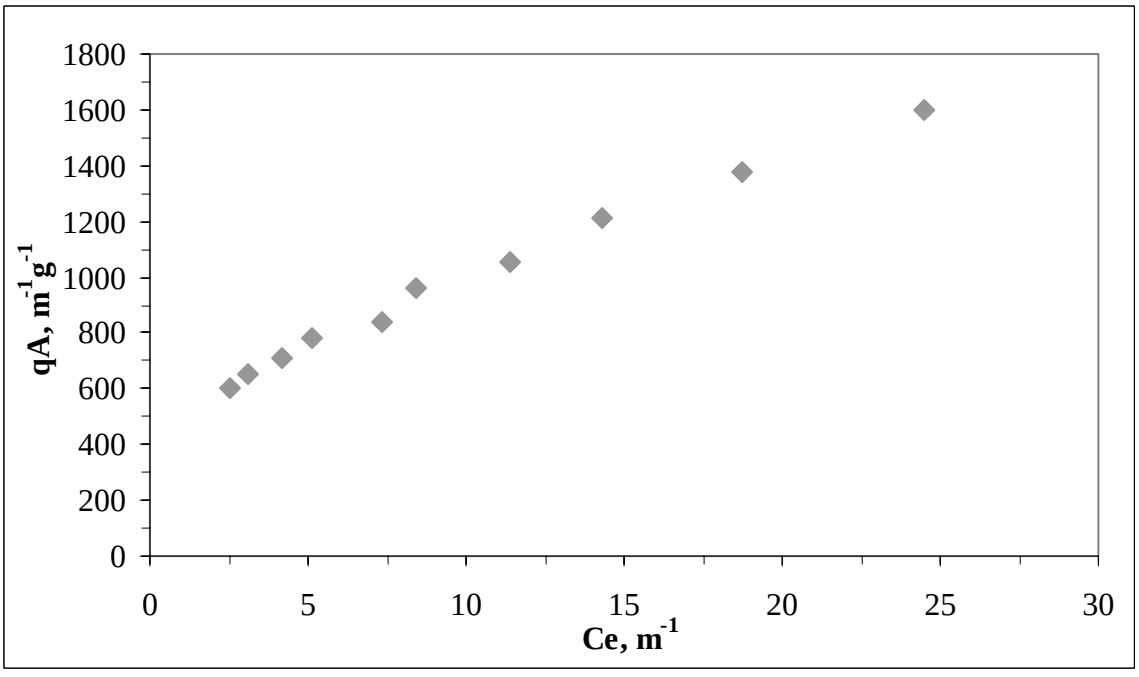

Figure A.4. Freundlich adsorption isotherm of UV_{280} of 0.45µm filtered fraction of humic acid onto bare TiO_2

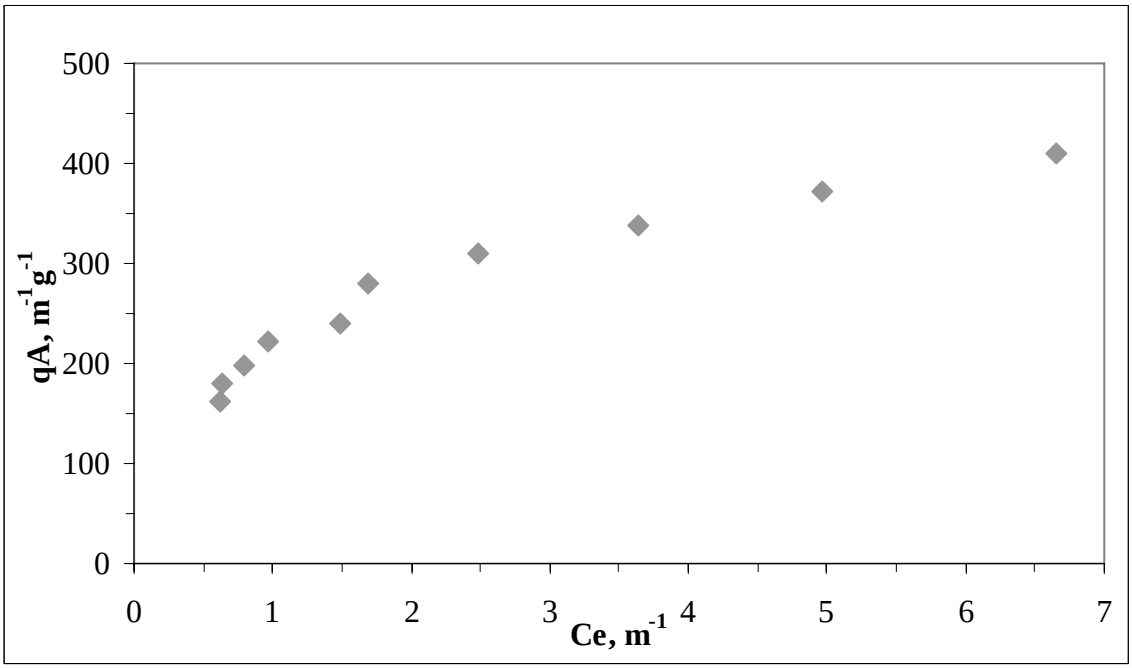

Figure A.5. Freundlich adsorption isotherm of UV_{365} of 100 kDa fraction of humic acid onto bare TiO_2

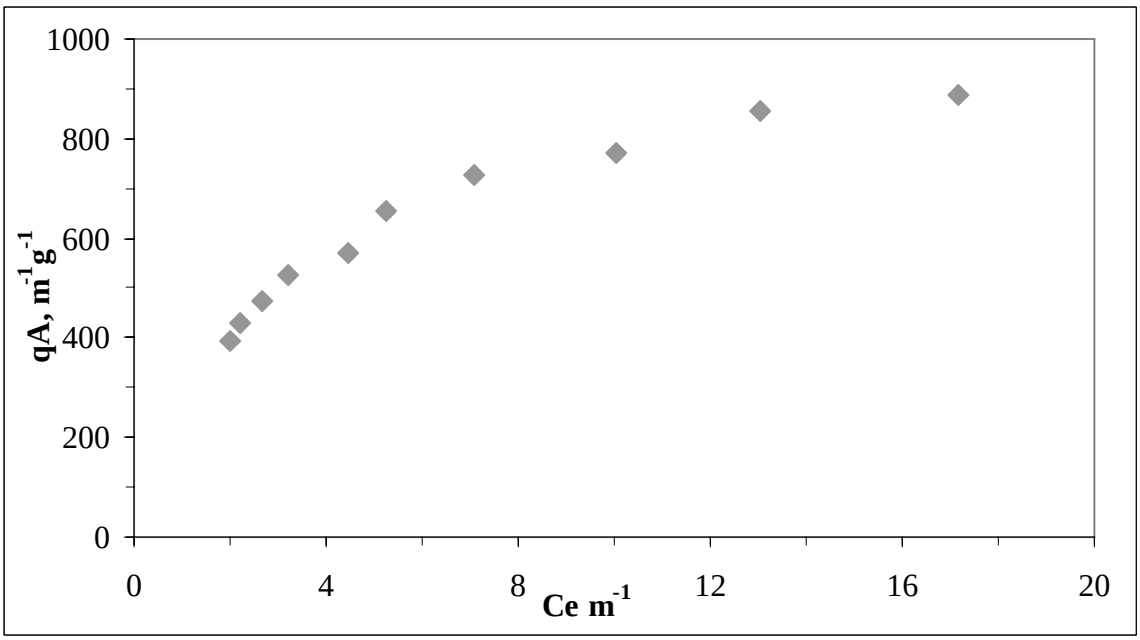

Figure A.6. Freundlich adsorption isotherm of UV_{280} of 100 kDa fraction of humic acid onto bare TiO_2

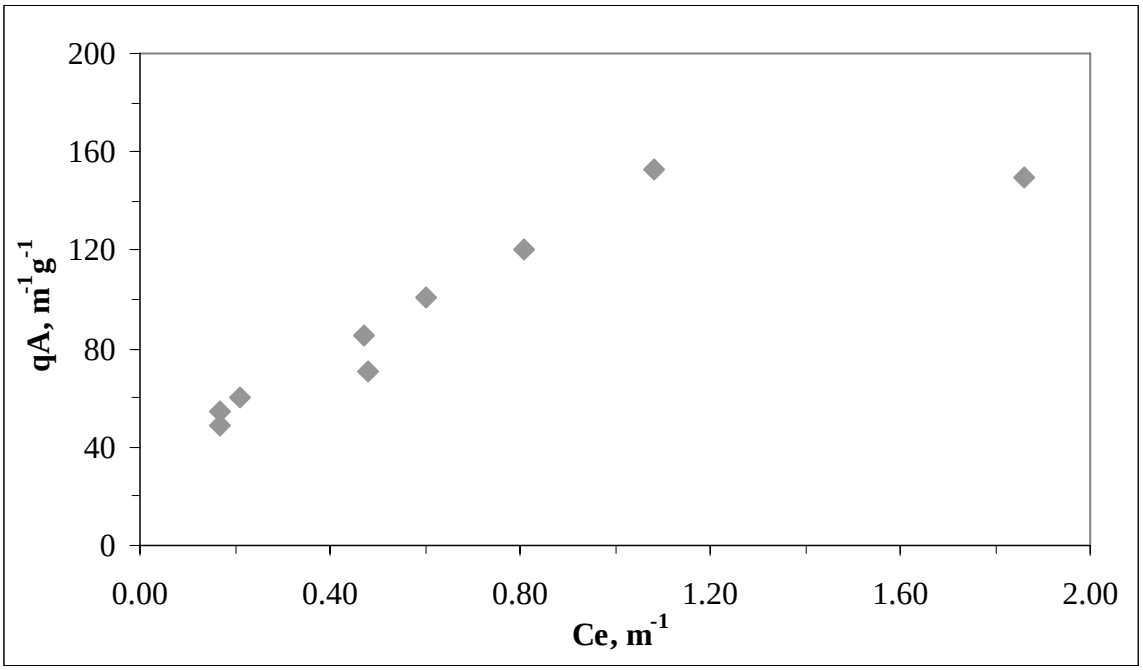

Figure A.7. Freundlich adsorption isotherm of UV_{365} of 30 kDa fraction of humic acid onto bare TiO_2

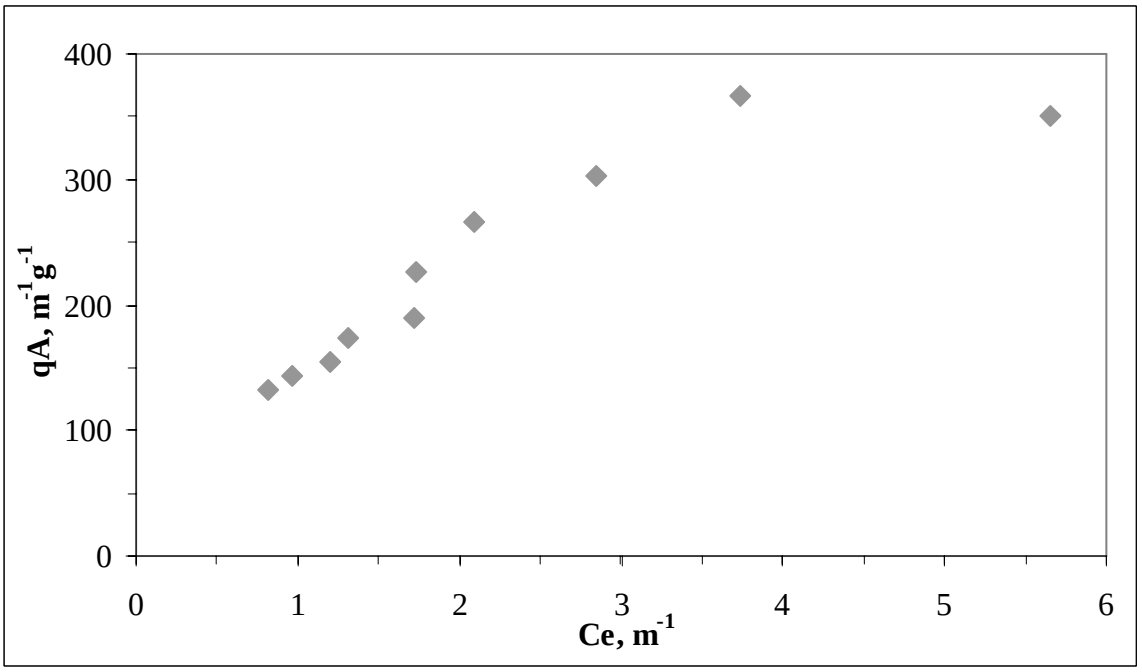

Figure A.8. Freundlich adsorption isotherm of UV_{280} of 30 kDa fraction of humic acid onto bare TiO_2

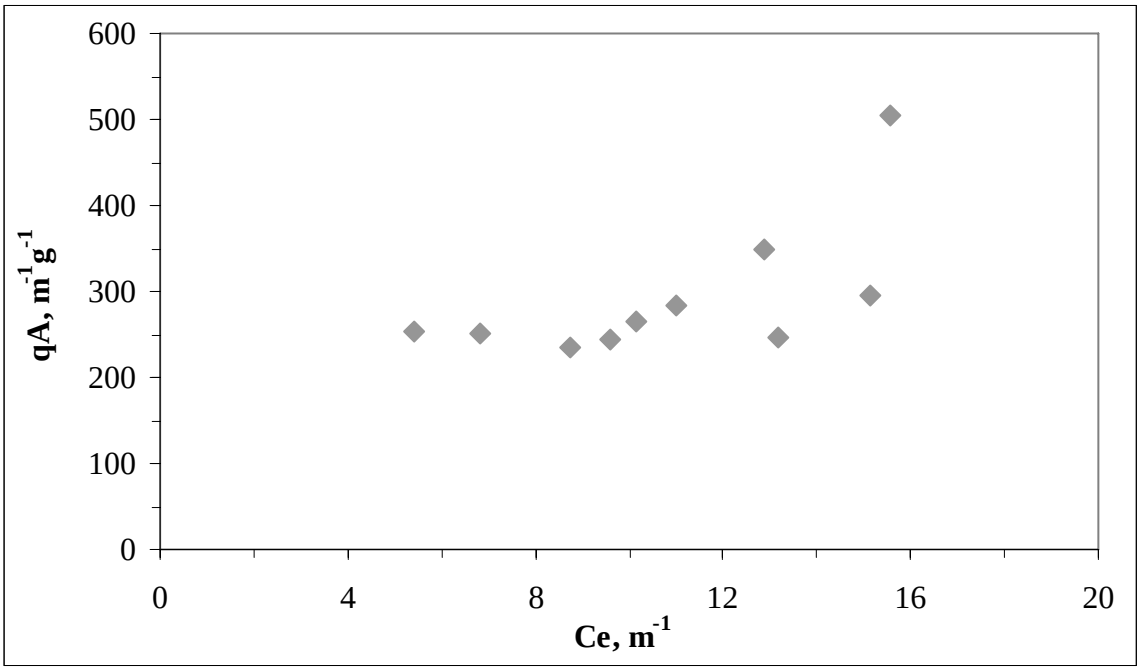

Figure A.9. Freundlich adsorption isotherm of UV_{365} of raw humic acid onto Fe doped TiO_2

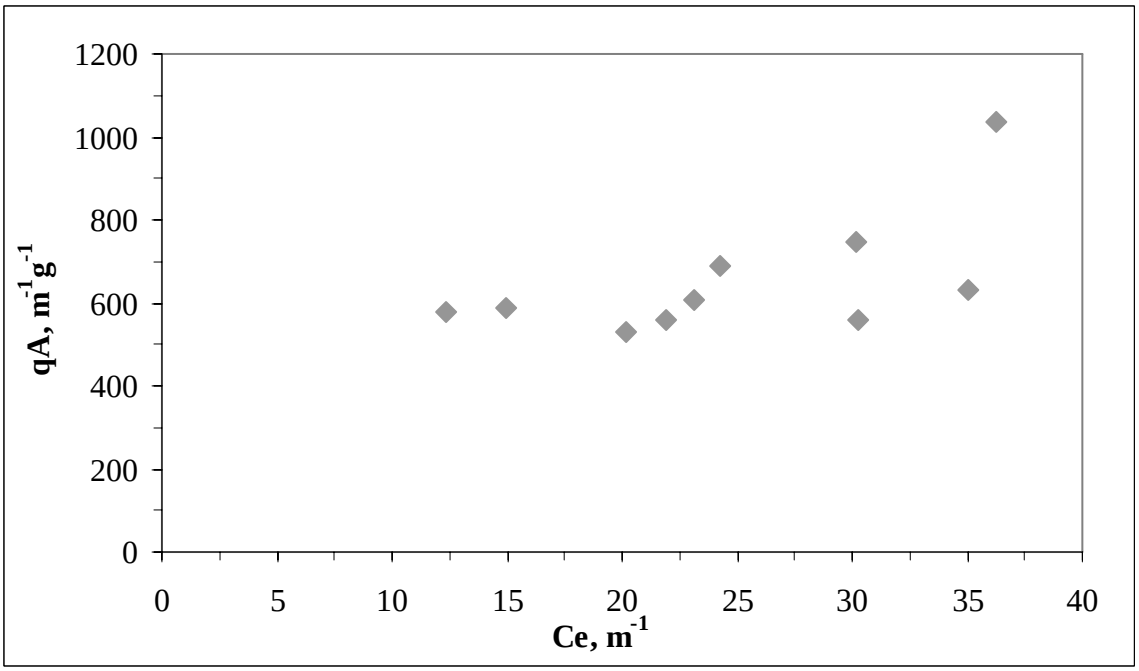

Figure A.10. Freundlich adsorption isotherm of UV_{280} of raw humic acid onto Fe doped TiO_2

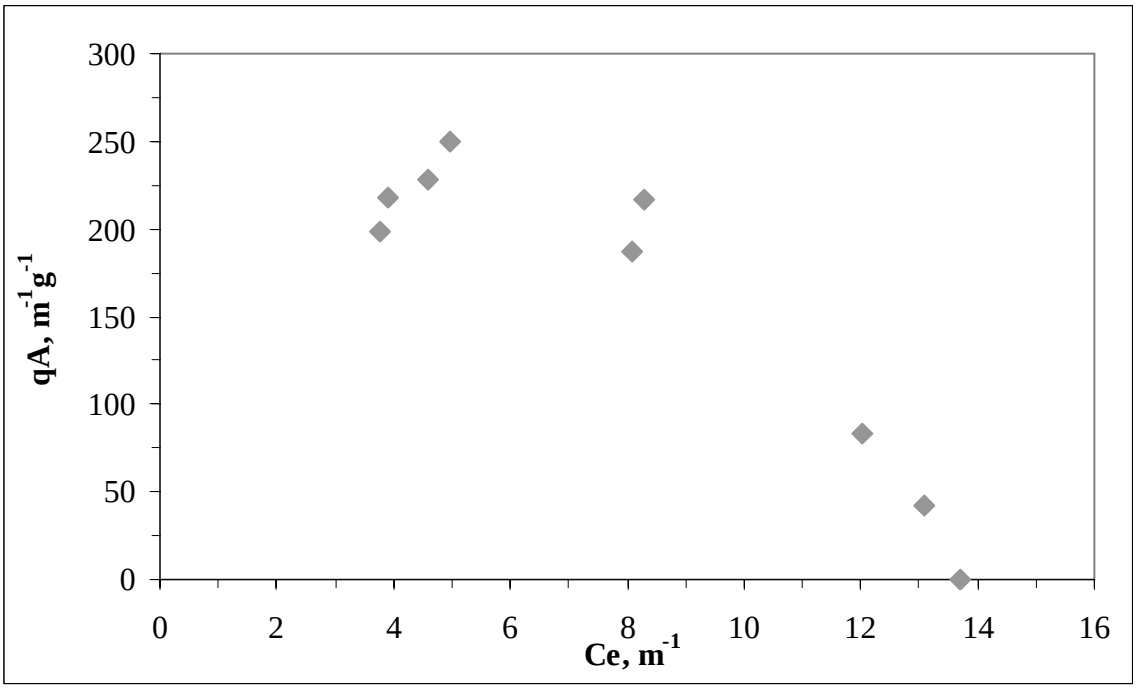

Figure A.11. Freundlich adsorption isotherm of UV_{365} of 0.45µm filtered fraction of humic acid onto Fe doped TiO_2

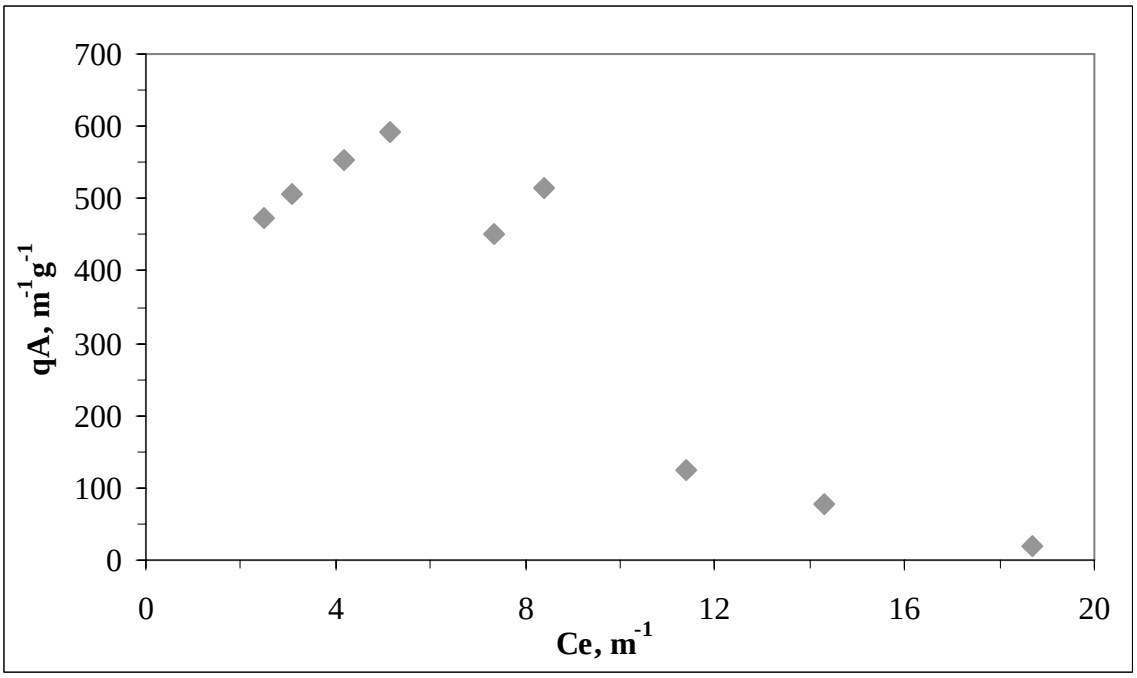

Figure A.12. Freundlich adsorption isotherm of UV_{280} of 0.45µm filtered fraction of humic acid onto Fe doped TiO_2

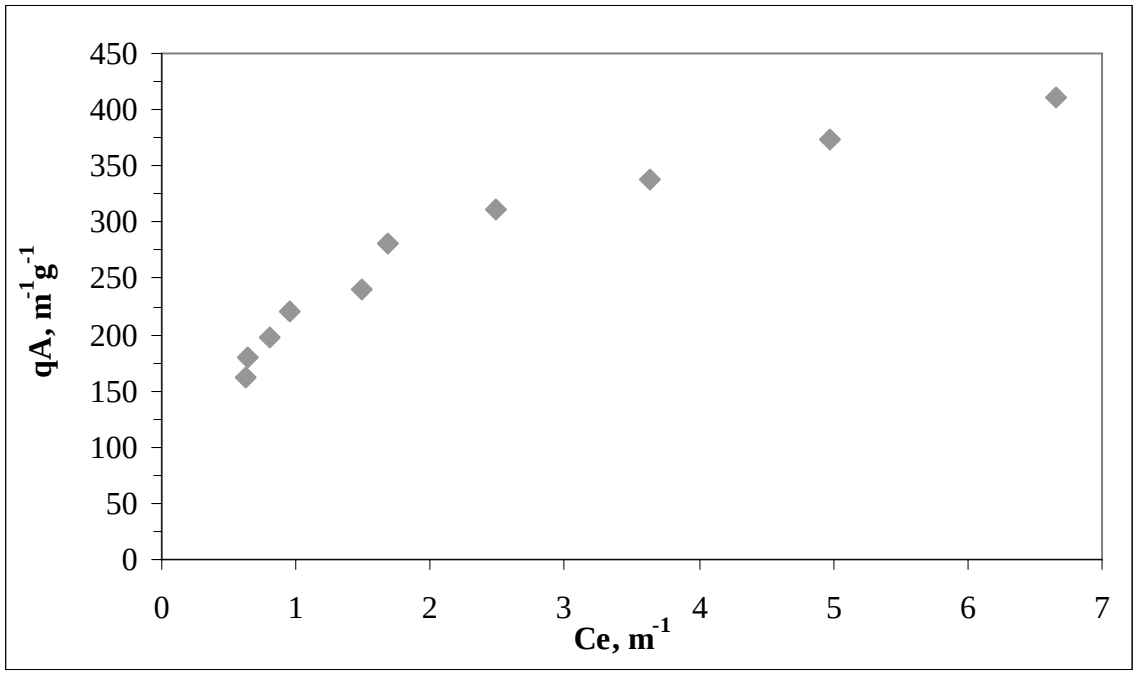

Figure A.13. Freundlich adsorption isotherm of UV_{365} of 100 kDa fraction of humic acid onto Fe doped TiO_2

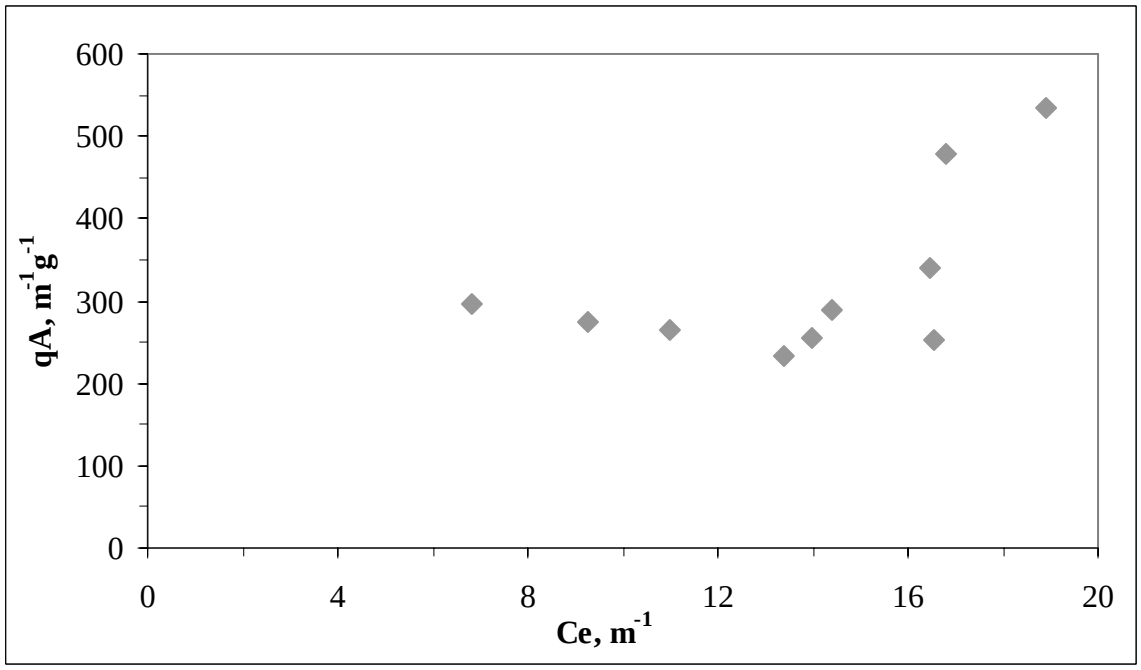

Figure A.14. Freundlich adsorption isotherm of UV_{280} of 100 kDa fraction of humic acid onto Fe doped TiO_2

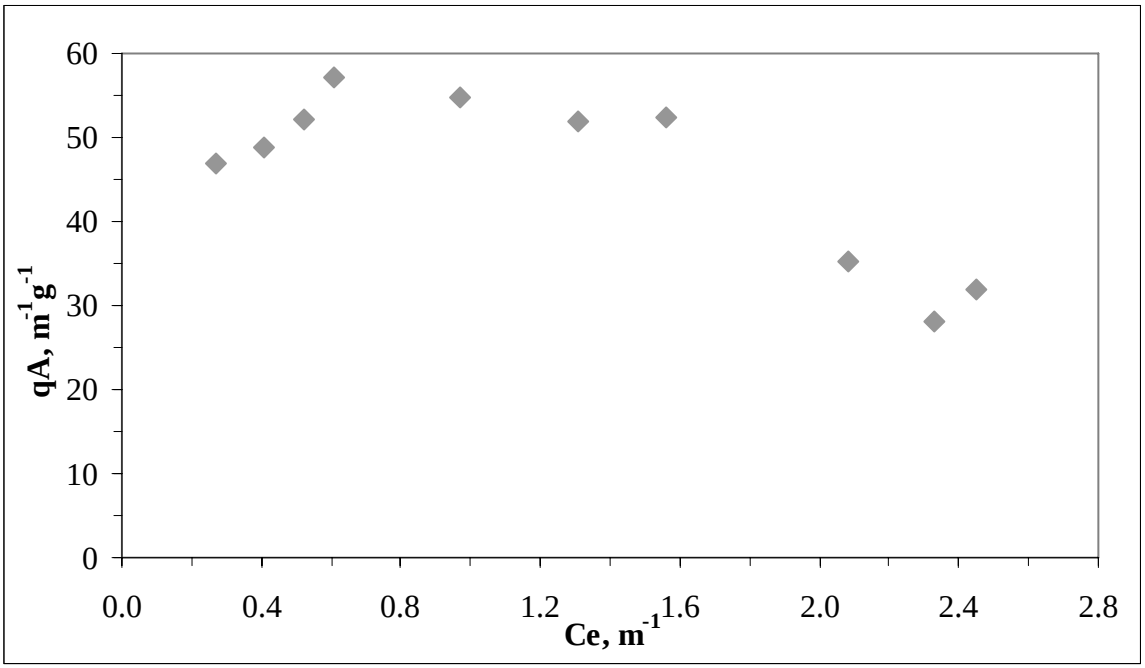

Figure A.15. Freundlich adsorption isotherm of UV_{365} of 30 kDa fraction of humic acid onto Fe doped TiO_2

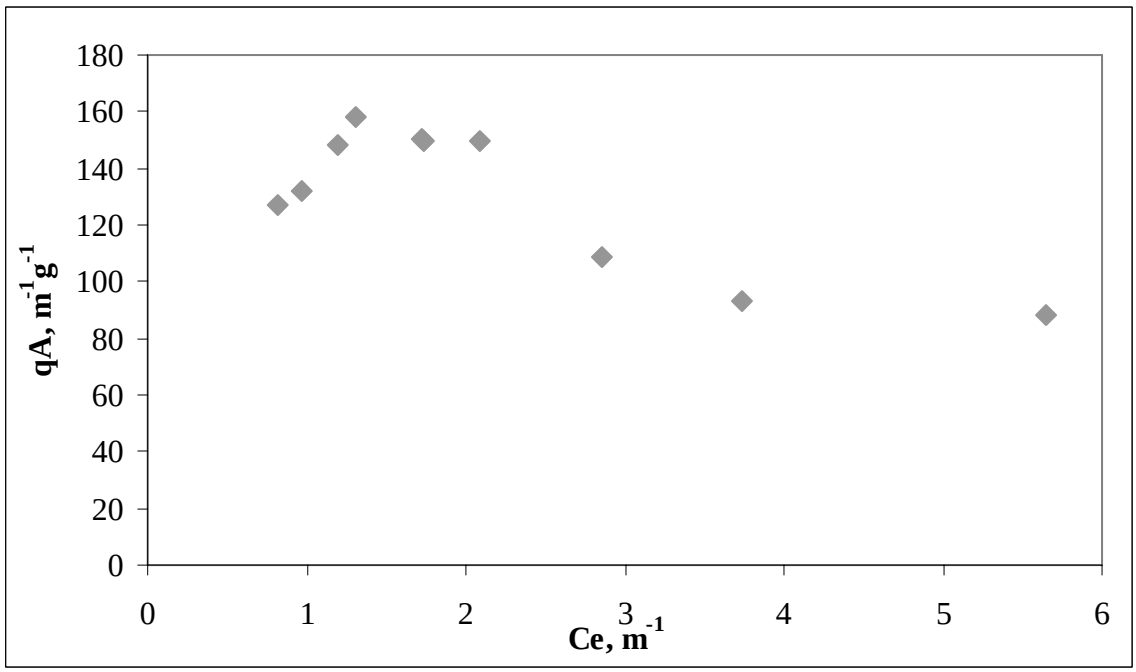

Figure A.16. Freundlich adsorption isotherm of UV_{280} of 30 kDa fraction of humic acid onto Fe doped TiO_2

APPENDIX B

Langmuir Adsorption Isotherms of Humic Acids

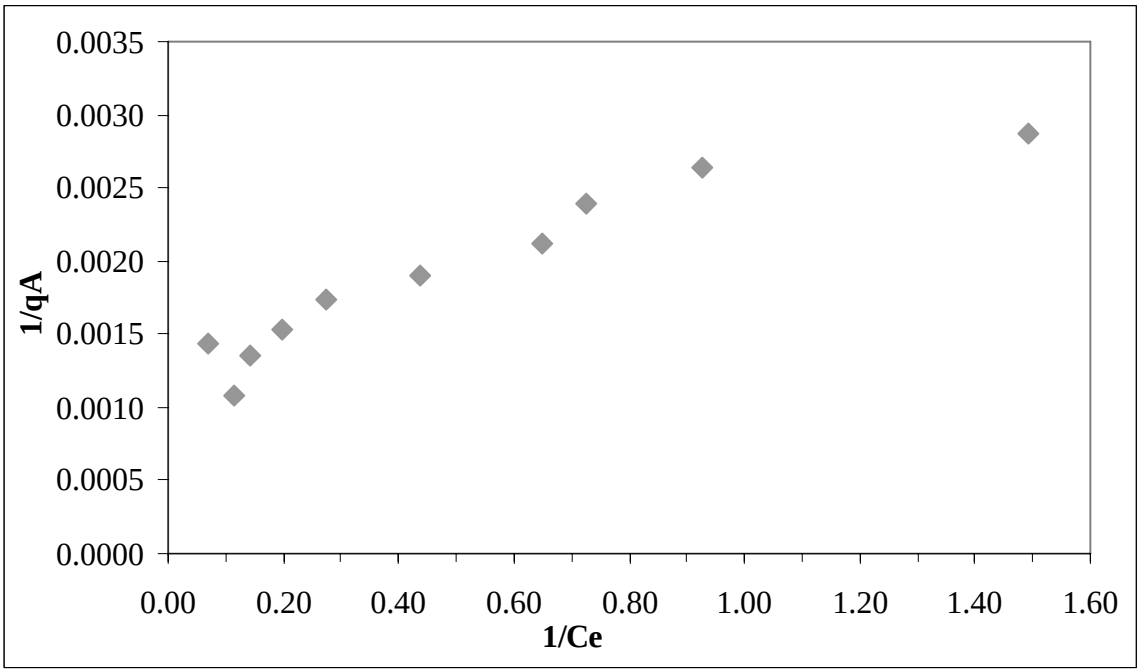

Figure B.1. Langmuir adsorption isotherm of UV_{365} of raw humic acid onto bare TiO_2

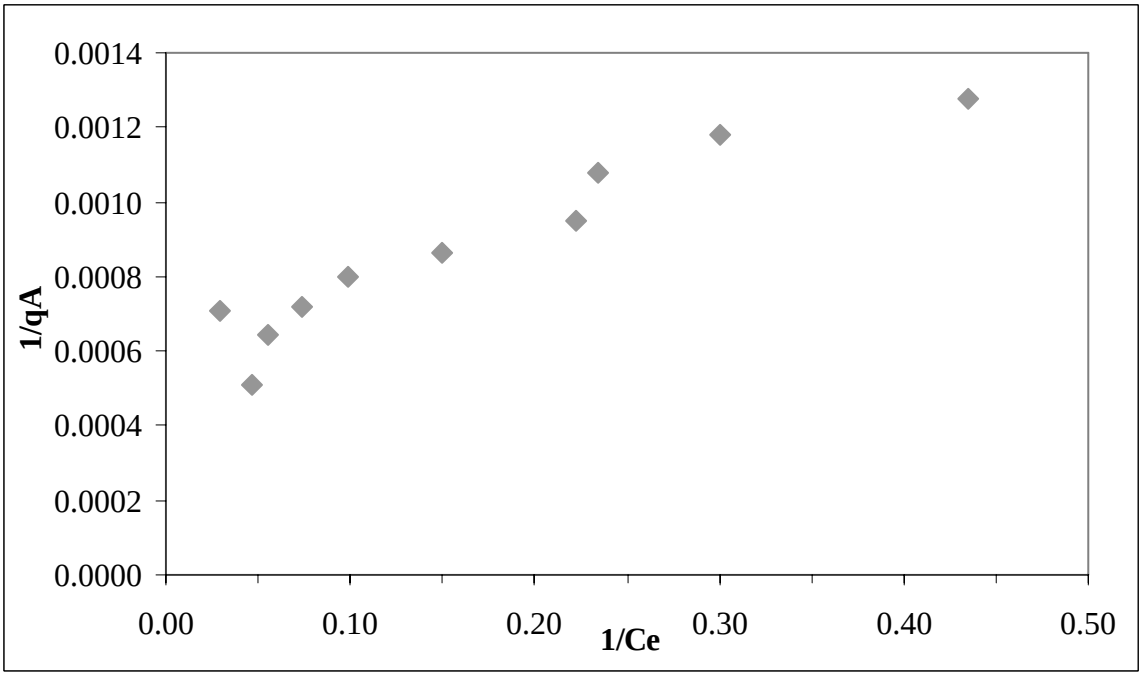

Figure B.2. Langmuir adsorption isotherm of UV_{280} of raw humic acid onto bare TiO_2

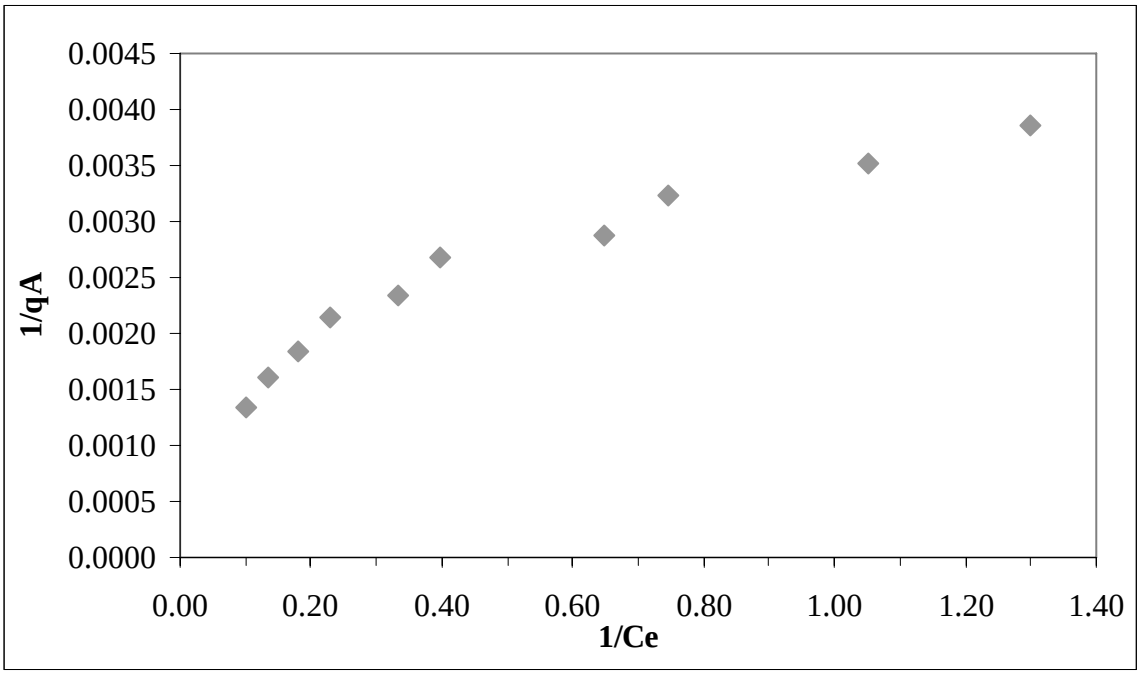

Figure B.3. Langmuir adsorption isotherm of UV_{365} of 0.45µm filtered fraction of humic acid onto bare TiO_2

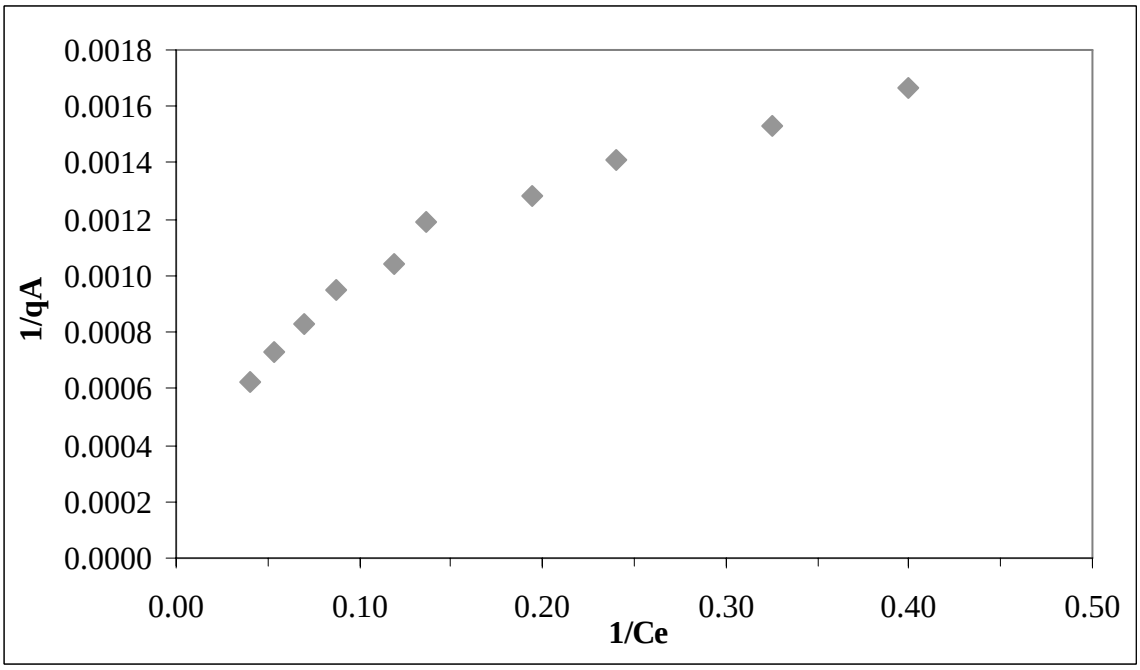

Figure B.4. Langmuir adsorption isotherm of UV_{280} of 0.45µm filtered fraction of humic acid onto bare TiO_2

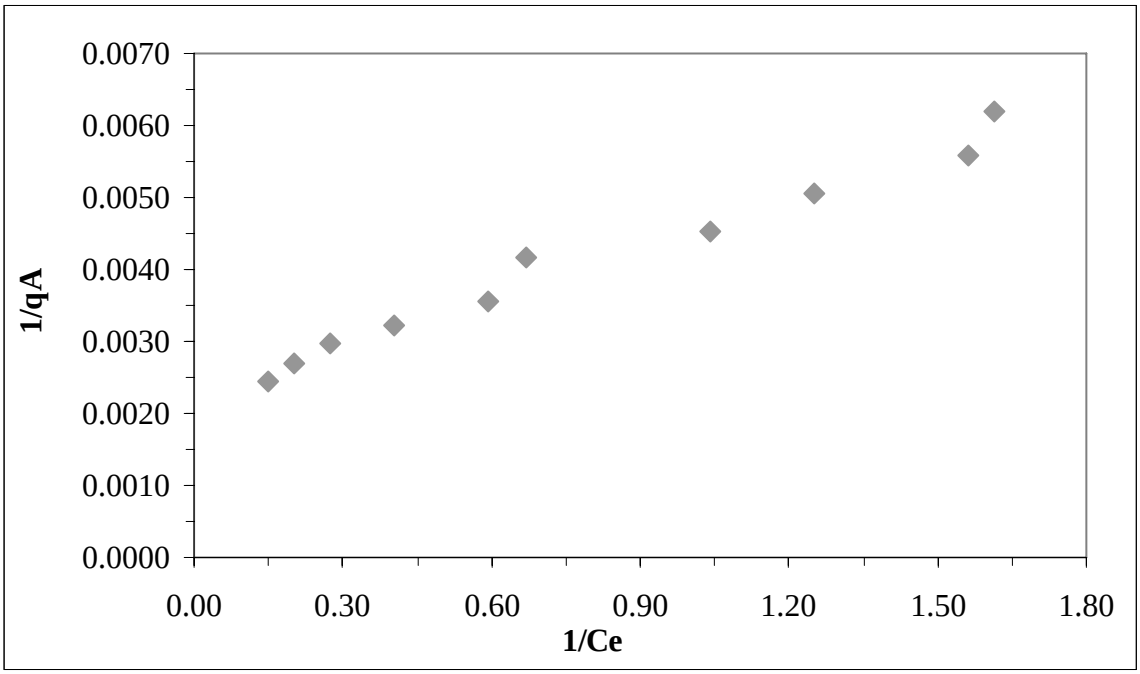

Figure B.5. Langmuir adsorption isotherm of UV_{365} of 100 kDa fraction of humic acid onto bare TiO_2

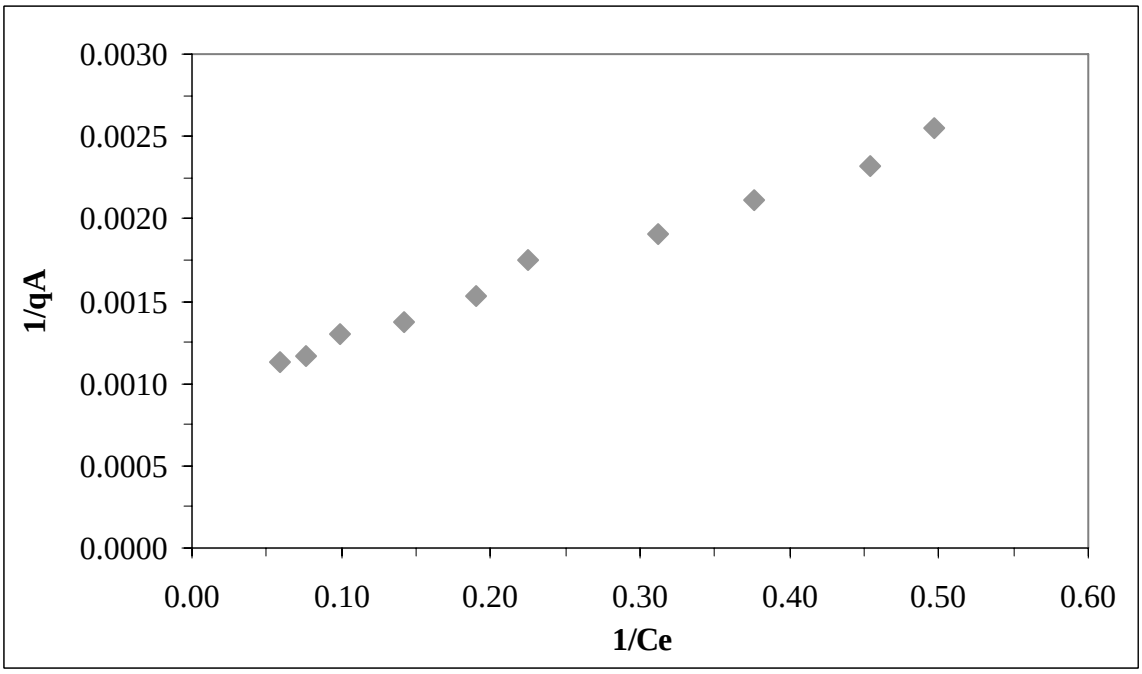

Figure B.6. Langmuir adsorption isotherm of UV_{280} of 100 kDa fraction of humic acid onto bare TiO_2

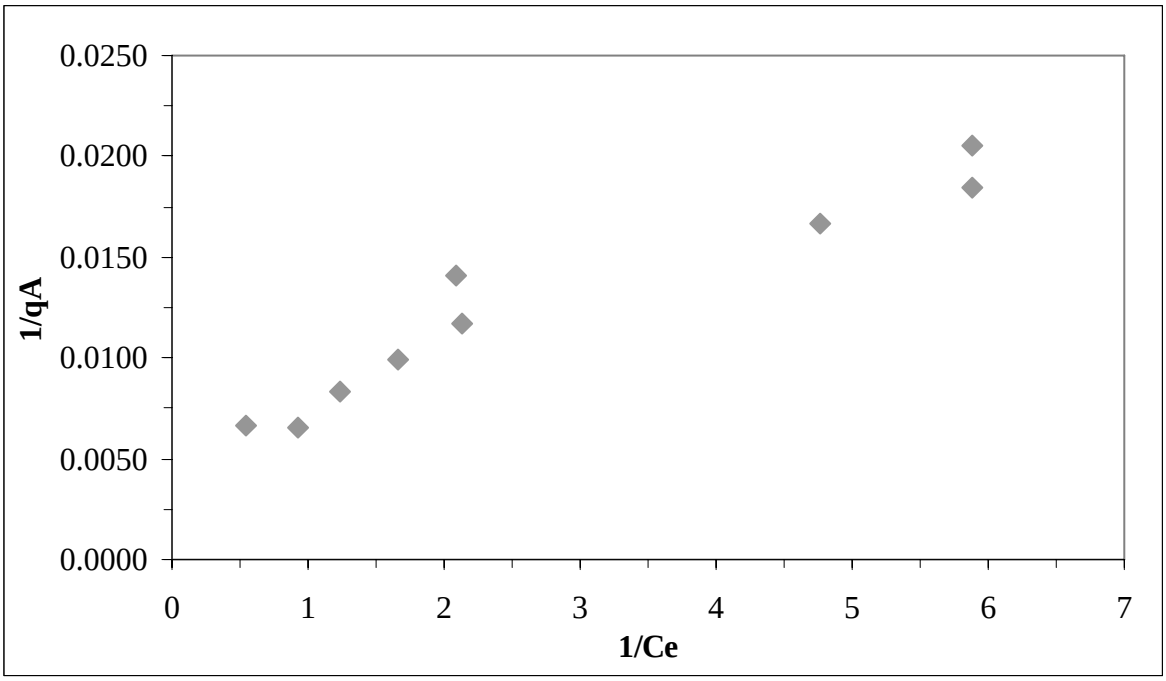

Figure B.7. Langmuir adsorption isotherm of UV_{365} of 30 kDa fraction of humic acid onto TiO_2

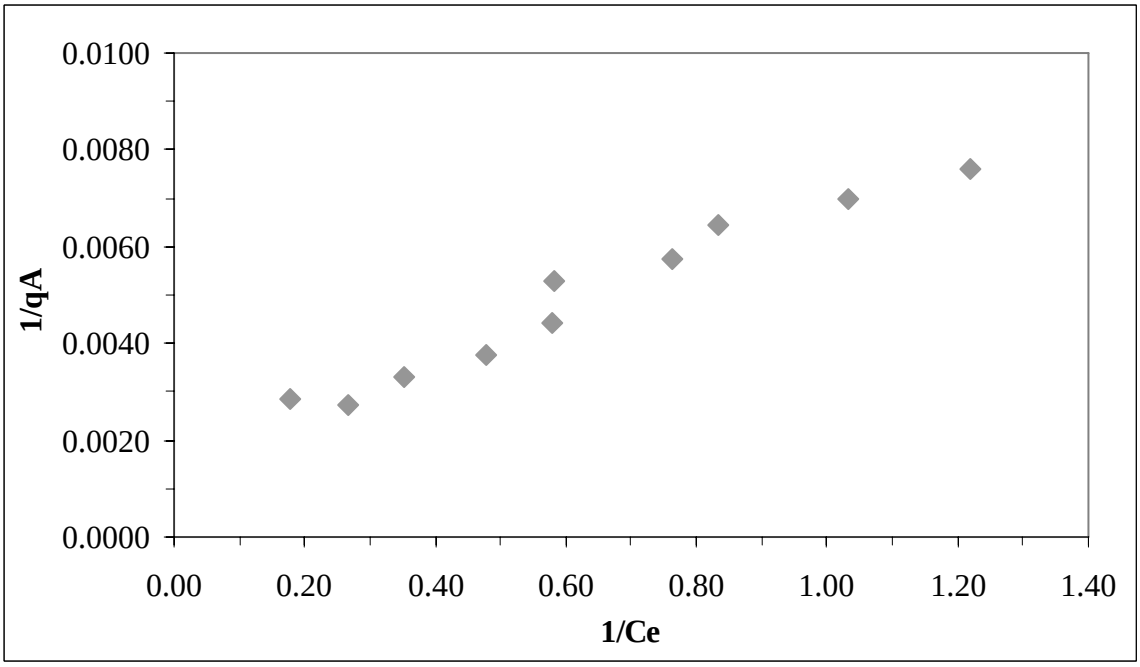

Figure B.8. Langmuir adsorption isotherm of UV_{280} of 30 kDa fraction of humic acid onto TiO_2

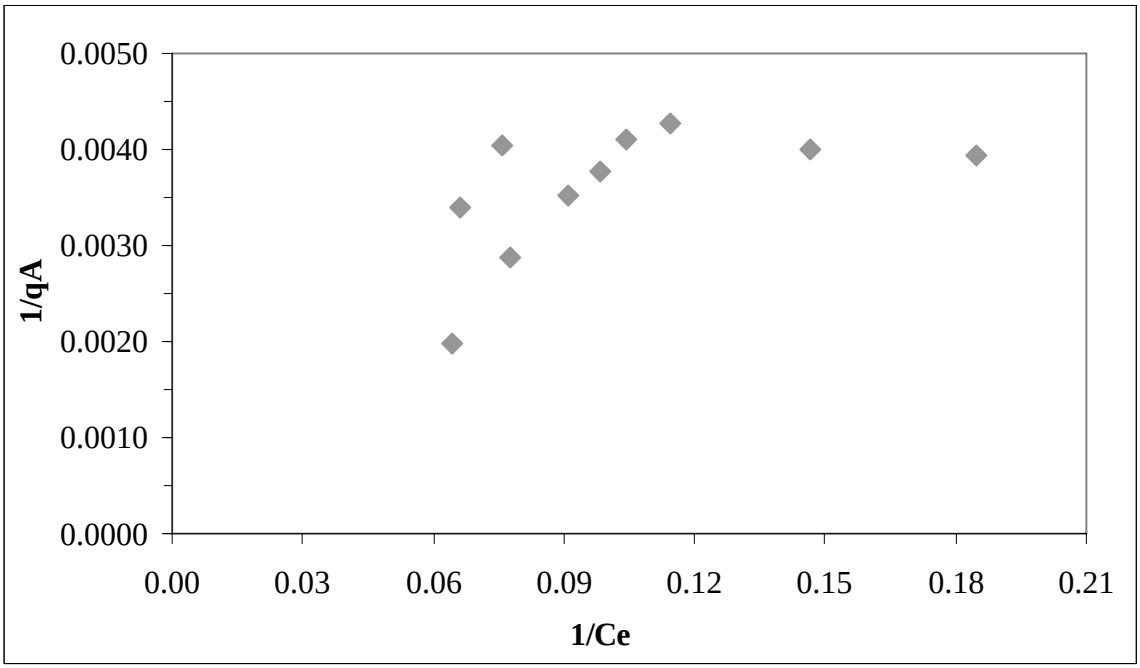

Figure B.9. Langmuir adsorption isotherm of UV_{365} of raw humic acid onto Fe doped TiO_2

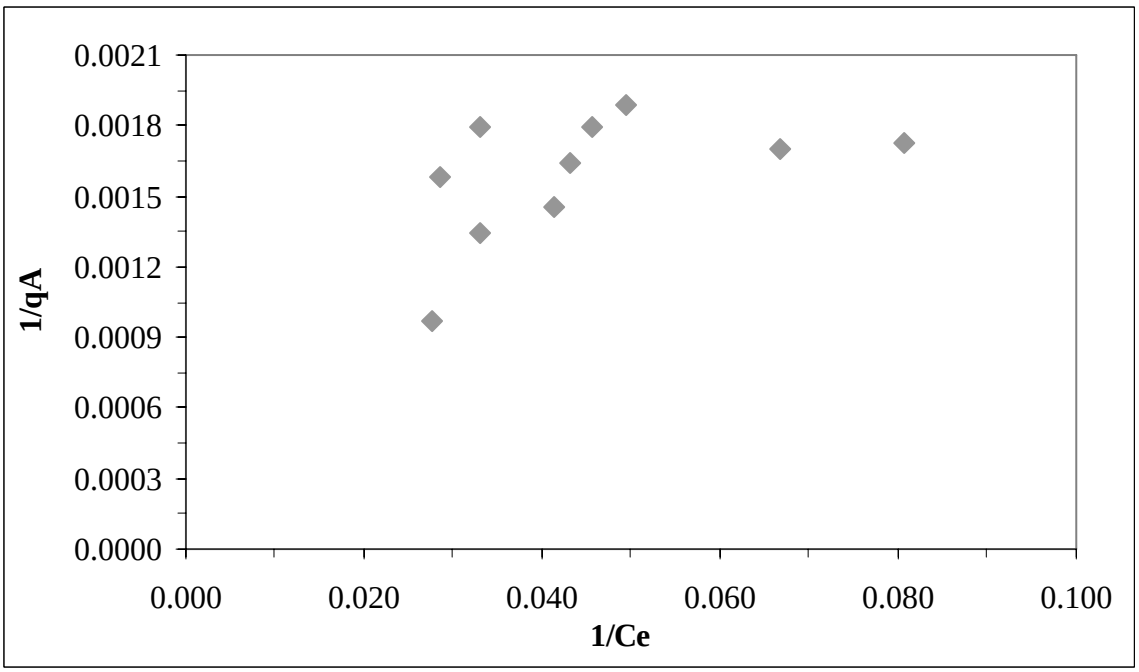

Figure B.10. Langmuir adsorption isotherm of UV_{280} of raw humic acid onto Fe doped TiO_2

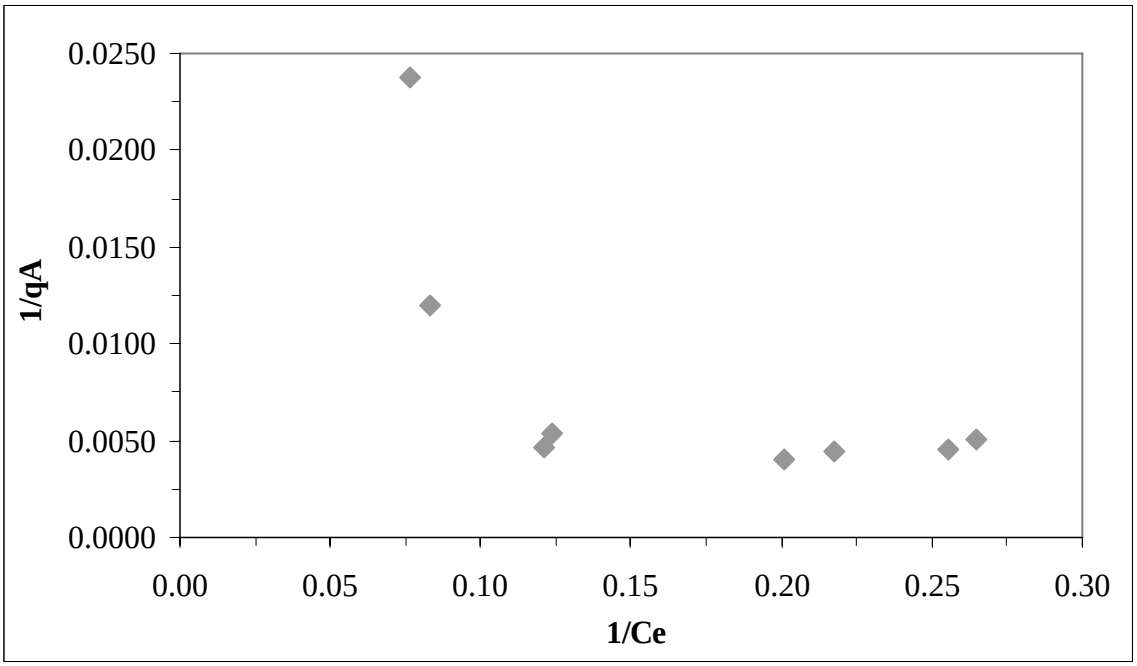

Figure B.11. Langmuir adsorption isotherm of UV_{365} of 0.45µm filtered fraction of humic acid onto Fe doped TiO_2

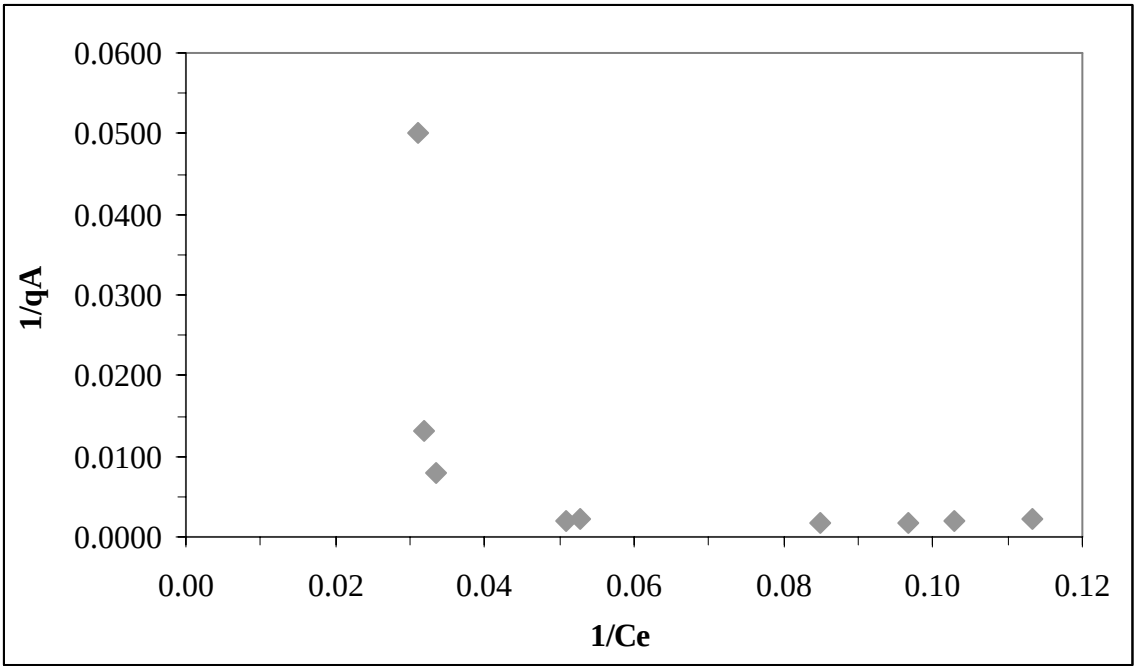

Figure B.12. Langmuir adsorption isotherm of UV_{280} of 0.45µm filtered fraction of humic acid onto Fe doped TiO_2

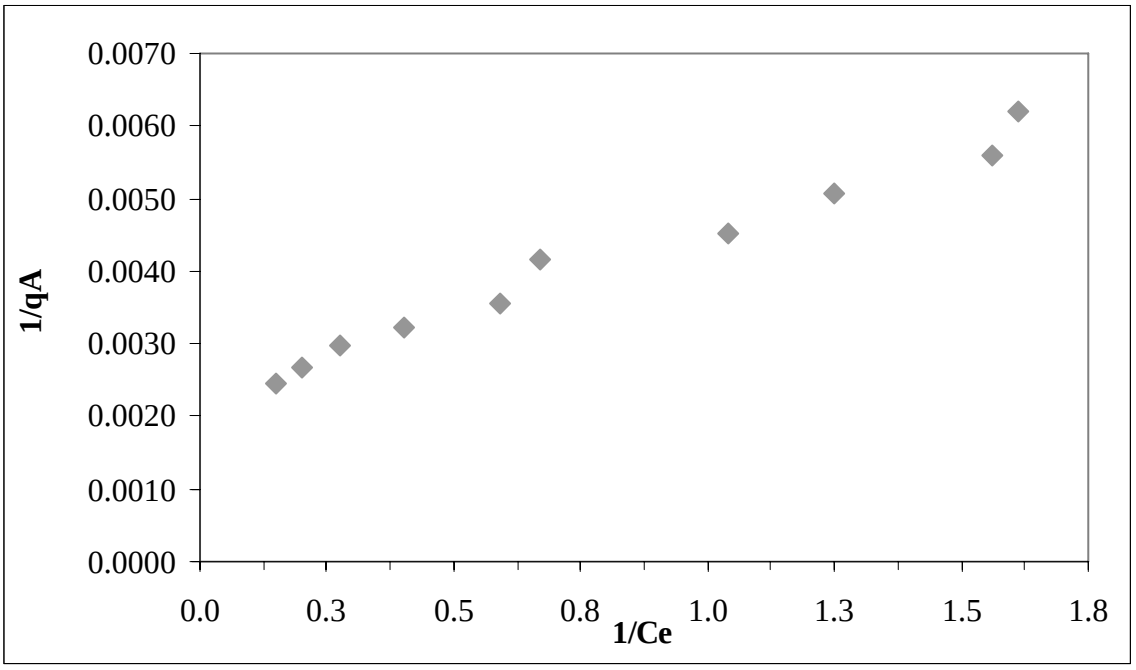

Figure B.13. Langmuir adsorption isotherm of UV_{365} of 100 kDa fraction of humic acid onto Fe doped TiO_2

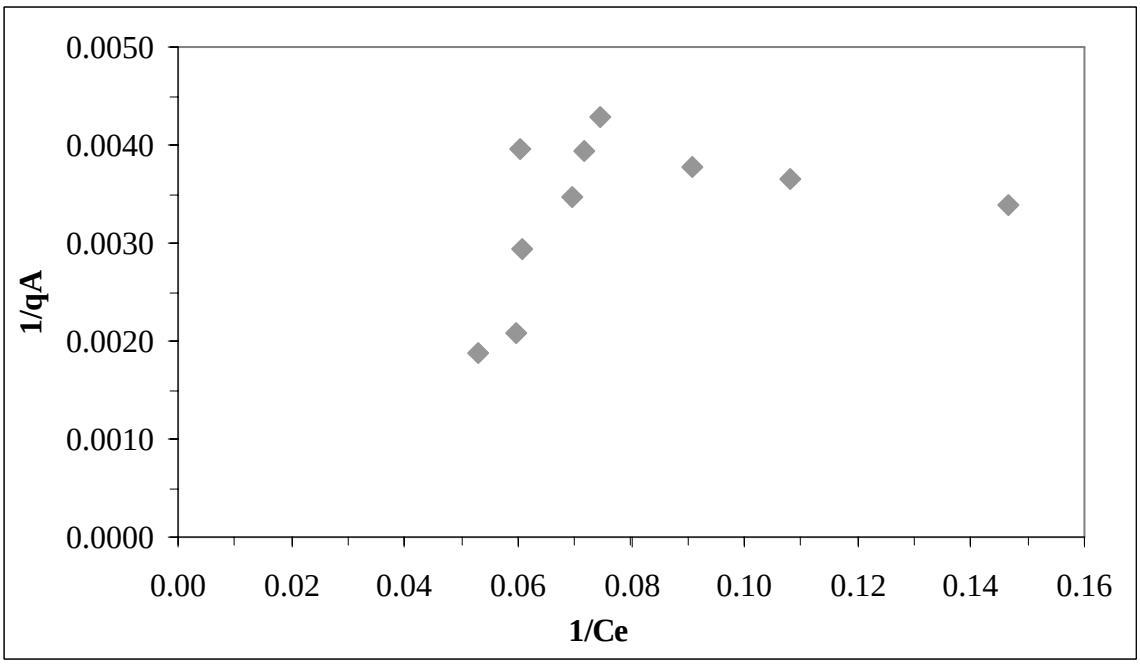

Figure B.14. Langmuir adsorption isotherm of UV_{280} of 100 kDa fraction of humic acid onto Fe doped TiO_2

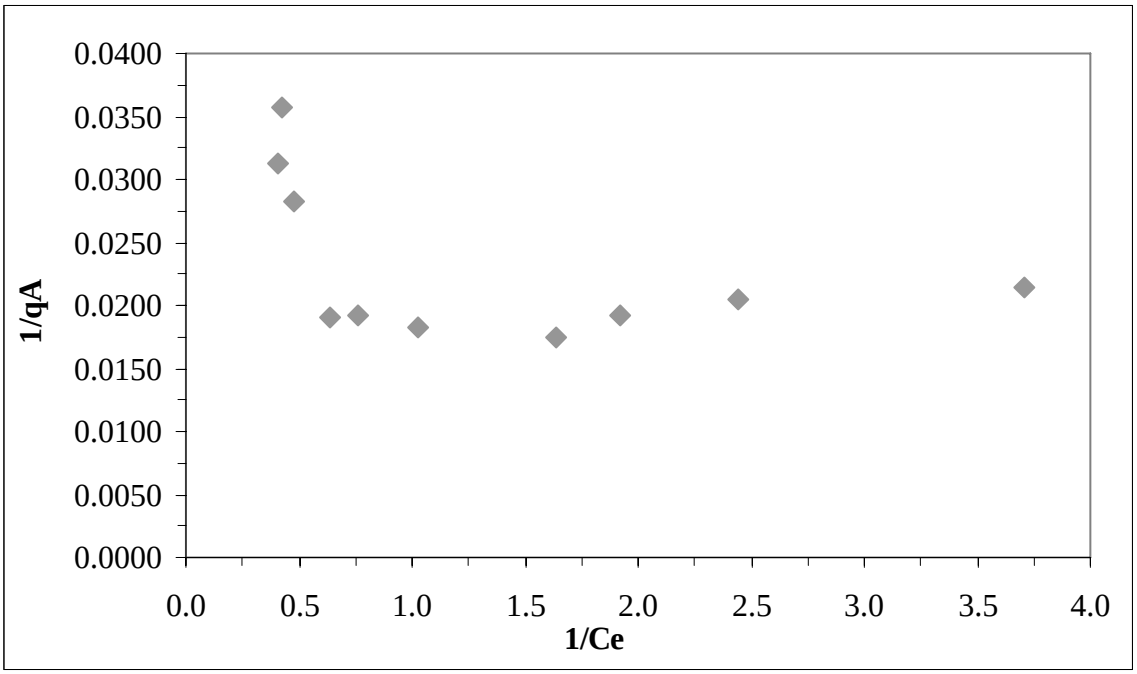

Figure B.15. Langmuir adsorption isotherm of UV_{365} of 30 kDa fraction of humic acid onto Fe doped TiO_2

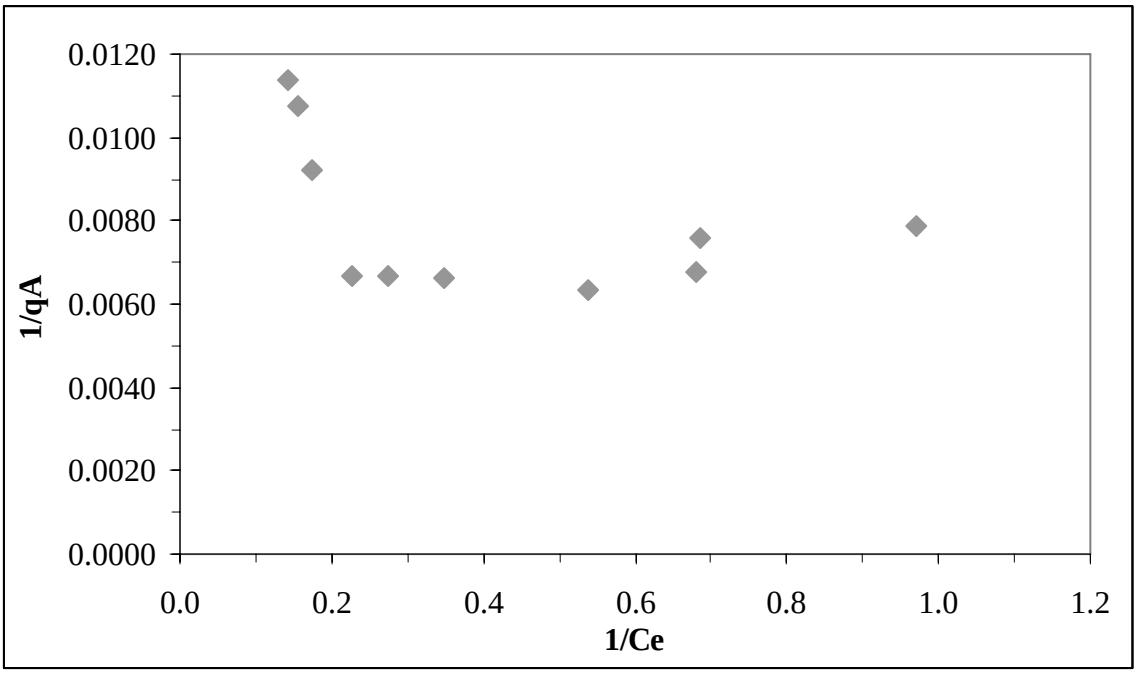

Figure B.16. Langmuir adsorption isotherm of UV_{280} of 30 kDa fraction of humic acid onto Fe doped TiO_2